

## DOTTORATO DI RICERCA IN INGEGNERIA CIVILE, CHIMICA, AMBIENTALE E DEI MATERIALI Ciclo 37

Settore Concorsuale: 09/D2 - SISTEMI, METODI E TECNOLOGIE DELL'INGEGNERIA CHIMICA E DI PROCESSO

Settore Scientifico Disciplinare: ING-IND/24 - PRINCIPI DI INGEGNERIA CHIMICA

ANALYSIS AND OPTIMIZATION OF LOW-EMISSION TECHNOLOGIES: THE CASES OF CHEMICAL LOOPING DRY REFORMING AND ADSORPTIVE VAPOR RECOVERY

Presentata da: Mattia Boscherini

Coordinatore Dottorato Supervisore

Enrico Sassoni Ferruccio Doghieri

**Co-supervisore** 

Matteo Minelli

#### Abstract

Global warming due to greenhouse gases emissions by human activities has become a critical concern for the future of our civilization on this planet. The ever-increasing levels of carbon dioxide in the atmosphere are causing evident dramatic effects on Earth's climate, with destruction of ecosystems, increase in extreme climate events and their following dramatic and negative consequences on human health, economy and society. As such, novel environmentally sustainable low emission processes need to be developed to replace conventional industrial processes. In particular, hydrogen and syngas demand to be used in the energy and industrial sector has seen a dramatic rise in the last years, which is expected to keep increasing at remarkable rate with the further growth of industrial activities, but its conventional production process, steam reforming and coal gasification, utilize mainly nonrenewable fossil sources as their feedstock and are associated with high carbon dioxide emissions. As such, new approaches to these processes are needed to achieve greater sustainability. In this elaborate first part, an extensive review of current and novel hydrogen and syngas production technologies is provided. The key aspects of each technology are reported, discussing their advantages, disadvantages and technology readiness levels, with a further focus on the chemical looping technology utilizing solid oxygen carriers to substitute direct contact between gaseous reactants and simplify product current post treatment and separation. For the chemical looping approach, the state of the art of oxygen carrier development is discussed, with focus on the use of cerium dioxide based carriers. Cerium dioxide provides excellent performance in terms of stability over multiple reaction cycles and product selectivity. The review work is then followed by the presentation of experimental results for methane conversion on four different oxygen carriers: a natural chromite mineral, pure cerium dioxide, a 50% mol mixture of cerium and copper oxide and a mixture of 30 %w alumina in cerium dioxide. While the chromite and cerium-copper oxide carriers proved inadequate for syngas production due to excessive aggregation and low selectivity, the alumina-cerium dioxide carrier showed enhanced conversion, selectivity and yield compared to the pure cerium dioxide carrier, with yields of 2.9±0.5 and 1.5±0.3 mmol/gCeO<sub>2</sub> for H<sub>2</sub> and CO and 41±6% average methane conversion when regenerating in 3% vol oxygen, and yields of 2.80±0.01 and 1.35±0.04 mmol/gCeO<sub>2</sub> for H<sub>2</sub> and CO, with average coke formation of 0.7±0.4 mmol/gCeO<sub>2</sub> per partial oxidation step and 31.6±0.3% average methane conversion when regeneration of the carrier was carried out in 15% CO2 feed. Cerium dioxide carriers demonstrated low coke formation, especially once process time duration was optimized to 20 min for the studied process conditions (10% mol CH<sub>4</sub> flow, 1 NL/min, 950 °C), which coincides with carrier conversion around 40% at temperature of 950 °C. A first attempt at modeling the chemical looping reforming process using kinetic data retrieved from the literature was carried out implementing a model on Aspen Adsorption<sup>TM</sup> software. While the qualitative results of simulation match the behavior observed in the experimental tests, the lack of quantitative agreement points to the need to dedicate further research in understanding process mechanisms and obtaining accurate data for process simulation.

Other than greenhouse gases emissions, toxic emissions are also a critical concern for process sustainability. In particular, volatile organic compounds are persistent environmental pollutants that are greatly associated to severe health consequences upon exposure, with a significant number of such substances being potent carcinogens. Oil refineries, and in particular leakages and fugitive emissions from oil storage tanks are a severe source of hydrocarbon volatile organic compounds, causing severe risk for the workers and the population around such plants, as well as a threat to the surrounding environment. These emissions are also a severe economic problem, causing significant losses of valuable products, also compounded by the cost of the damage caused by the emissions themselves. As such, it is necessary to deal with these emissions in order to avoid negative consequences and prevent economic losses. In the second part of the present elaborate, the main technologies available for abatement of volatile organic compounds are discussed, with a greater focus on adsorption. Adsorption, especially if followed by absorption to complete recovery, allows to obtain high degree of abatement in a wide concentration range. However, the design of multicomponent adsorption processes is a complex phenomenon which is only limitedly discussed in literature for this application. In the present elaborate, an extensive review of literature data for adsorption of hydrocarbons is performed for zeolite, activated carbon and silica adsorbents. Then, an Aspen Adsorption<sup>TM</sup> simulation is performed to assess the behavior of an activated carbon adsorption column with different designs on the performance of the purification. Bed height and diameter were shown to play the greatest role in determining column performance, with a power law relationship between each parameter value and concentration at the end of 30 days of continuous operation. Regeneration pressure was shown to have instead an exponential effect, while purge flowrate effect was negligible in the range investigated. The work in adsorption simulation was carried out in collaboration with Duemme Engineering, Bologna.

## **Table of contents**

ABSTRACT	1
TABLE OF CONTENTS	3
FIGURE INDEX	5
TABLE INDEX	7
INTRODUCTION	8
PART 1: CHEMICAL LOOPING FOR SYNGAS PRODUCTION: EXPERIMENTAL AND NUMERICAL STUDY OF THE I PROCESS USING SOLID OXYGEN CARRIERS FOR METHANE CONVERSION WITH A FOCUS ON CERIUM OXIDE	
1.1-Hydrogen and syngas in the chemical and energy sector	
1.1.1-Hydrogen and syngas demand	
1.1.2-Hydrogen and syngas production: the colors of hydrogen	
1.1.2.1-Hydrogen and syngas production from fossil sources	
Reforming of gaseous and liquid hydrocarbons: grey hydrogen	
Steam reforming (SR)	
Partial oxidation (PO)	
Dry reforming (DR)	
Combined reforming and oxidation strategies	
Integration of CCUS technologies: blue hydrogen	
Methane decomposition (MD): turquoise hydrogen	
Thermal methane decomposition (TMD) and thermocatalytic methane decomposition (TCMD)	
Plasma driven methane decomposition (PD-MD)	
1.1.2.2-Hydrogen and syngas production from biomass and biogas: green hydrogen	
Biogas reforming	
Biomass gasification	
Hydrogen production from biofermentation (BF)	
1.1.2.3-Other hydrogen production sources	30
Hydrogen production from water	31
Hydrogen production from hydrogen sulfide	34
Naturally available hydrogen: white hydrogen	36
1.1.2.4-Final remarks on hydrogen and syngas production technologies	38
1.2-Overcoming the limits of conventional syngas production by reforming processes: the chemical looping approach	45
1.2.1-Chemical looping conversion of methane	
1.2.2-Selection of oxygen carrier	
Copper oxides	
Ni oxides	
Iron oxides	
Perovskites	49
Hexaaluminates	
Cerium dioxide	
1.2.3-Looping configuration: fixed vs fluidized bed	61
1.2.3.1-Fixed bed	_
1.2.3.2-Fluidized bed	
1.2.4-Final remarks on chemical looping reforming	63

cerium dioxide oxygen carrier in and modelling activity	
1.3.2-Materials and methods	
1.3.2.1-Material preparation	
1.3.2.2-Thermogravimetric Analysis (TGA)	
1.3.2.3-Chemical Looping Tests	
1.3.2.4-Numerical elaboration of data	
1.3.2.5-Mathematical model and simulation of the chemical looping process	71
1.3.3-Results and discussion	
1.3.3.1-Comparison of oxygen carrier activity	
1.3.3.2-TGA investigation of cerium dioxide	81
1.3.3.3-Optimization of reaction time for reforming on CeO <sub>2</sub>	
1.3.3.4-XRD and SEM analysis of the tested oxygen carriers	91
1.3.3.5-Results of numerical simulation	95
1.3.4-Conclusion and future perspectives	97
FOR CAPTURE OF FUEL STORAGE TANK VOCS VAPORS USING ASPEN ADSORPTION™ SOF  2.1- Incidence and harmful effects of exposure to VOCs in refineries	
2.2-Vapor recovery units	
2.2.1-Condensation/cryogenic separation	
2.2.2-Membrane separation	
2.2.3-Absorption	
2.2.4-Adsorption	
2.2.5-Combined approaches	
2.2.6-Final remarks on Vapor Recovery Units and separation technology	107
2.3-Numerical simulation of multicomponent adsorption of VOCs on activated carbon so	lvent for the treatment of
oil storage tank emissions	109
2.3.1-Scope of the activity	
2.3.2-Material and methods	
2.3.2.1-Literature review of adsorption data for VOCs	
2.3.2.2-Mathematical model and simulation of the adsorption process	
2.3.5-Results and discussion	
2.3.5.1-Results of literature search of adsorption data	
2.3.5.2-Simulation of adsorption	
2.3.6-Conclusion and future perspectives	131
GENERAL CONCLUSIONS	134
APPENDIX: DESCRIPTION OF ASPEN ADSORPTION MODELS FOR CLR AND PSA	136
LISTS OF MATHEMATICAL SYMBOLS	139
	143
LIST OF ACRONYMS	1-3
LIST OF ACRONYMS	

## Figure index

Figure 1: monthly Average CO₂ atmospheric concentration measurements (part per million) taken at the Mauna Lo Observatory of the Scripps Institute of Oceanography, starting from year 1959 up to August 2024. Image taken fror Scripps Institute of Oceanography website [10]
Figure 2: interannual variation of the annual total non-methane VOC (NMVOC) emissions during 2000–2019. (a, on NMVOC emissions according to region; (b, d) emissions according to sector. Numbers in panels (a, b) represent the relative rate of change in NMVOC emissions during 2000–2019. Percentage values within panels (c, d) indicate the
proportions of regional and sectoral emissions in the global annual total emissions for 2000–2019, respectively ECEurope=Eastern and Central Europe), LATIN =Latin America, NAME=Northern Africa and the Middle East, ROA=Res
of Asia, ROW=Rest of the World), SSA=Sub-Saharan Africa, WEurope=Western Europe, AGR=agriculture, ENE=energ production, IND=industry, TRA=transportation, RCO=residential, commercial, and other, SLV=solvent, WST=waste
SHP=international shipping [29]1
Figure 3: prospected growth of the syngas market in the U.S.A. by production technology in years 2020-2030 [51]1 Figure 4: perspective of global hydrogen use: estimated growth by sector over the 2019-2030 period in the Net Zer Emissions by 2050 scenario (NZE). "Other" includes buildings and biofuels upgrading. 2024e = estimate for 2024. The estimated value for 2024 is a projection based on trends observed until June 2024 [43]
Figure 5: simplified scheme of a typical steam reforming process1
Figure 6: typologies of gasifier [137]: updraft gasifier (a); downdraft gasifier (b); fluidized bed gasifier (c); entraine gasifier (d); plasma gasifier (e)2
Figure 7: schemes of processes for water electrolysis [215]: A-WE (a); PEM-WE (b); SOFC-WE (c); AEM-WE (d). GDL=Ga Diffusion Layer, PTL= Proton Transfer Layer3
Figure 8: chemical looping processes for methane conversion: combustion (a); partial oxidation (b); steam reformin (c); dry reforming (d)4
Figure 9: the fluorite structure of cerium dioxide [354]
Figure 10: phase diagram of cerium oxides in function of temperature and oxygen content [373]: complete diagram (a detail of the area in the red rectangle, atomic O content 55 to 70% (b). G=gas phase, L=liquid phase
Figure 11: historic and forecasted price of cerium for the years 2009-2030 [380].
Figure 12: methane chemical looping reforming cycle for cerium dioxide oxygen carriers5
Figure 13: fixed and fluidized bed operating regimes [414]: fixed bed and non-entrainment fluidization (a); circulatin fluidized beds (b)6
Figure 14: experimental setup for chemical looping tests. TI=Temperature Indicator, FC= Flowmeter6 Figure 15: process model flowsheet in Aspen Adsorption™
Figure 16: gas composition profiles at reactor outlet over time for OCs exposed to 10% vol. CH4 flowrate at 1 NL/mir reaction temperature of 850 °C (a); reaction temperature of 950 °C (b)8
Figure 17: rates of PO step for TGA runs on cerium dioxide in 4% vol. CH <sub>4</sub> and air: $T_{PO}$ =900 °C, $T_{REG}$ =400 °C (a); $T_{PO}$ =90 °C, $T_{REG}$ =600 °C (b); $T_{PO}$ =950 °C, $T_{REG}$ =900 °C (c); $T_{PO}$ =1000 °C, $T_{REG}$ =900 °C (d)8
Figure 18: results of 60 min PO step under 10% vol. CH <sub>4</sub> at 1 NL/min at 900°C and 950 °C: cumulative reaction yields ove time and $H_2$ to CO ratio (a); reaction rates as function of carrier conversion (b)8
Figure 19: effect of feed composition on carrier regeneration: instantaneous rates of formation of CO and CO₂ durin regeneration step (a); comparison between total instantaneous rate of oxygen consumption and instantaneous rate o
oxygen consumed for CeO <sub>2</sub> regeneration only (b)8
Figure 20: results of redox cyclic tests at 950 °C in 10% vol. $CH_4$ (1 NL/min), with regeneration in 3% vol. $O_2$ (5 NL/min) partial oxidation time=30 min (a); partial oxidation time=20 min (b). C deposited represents the amount of carbo
formed by methane decomposition during partial oxidation step, C oxidized is the amount of carbon removed durin the following carrier regeneration step
Figure 21: results of redox cyclic tests at 950 °C in 10% vol. CH <sub>4</sub> (1 NL/min), with regeneration in 15% vol. CO <sub>2</sub> (1 NL/min
partial oxidation time=20 min. C deposited represents the amount of carbon formed by methane decomposition durin partial oxidation step, C oxidized is the amount of carbon removed during the following carrier regeneration step 8 Figure 22: results of redox cyclic tests at 950 °C in 1 NL/min $10\%$ vol. CH <sub>4</sub> on CeO <sub>2</sub> -Al <sub>2</sub> O <sub>3</sub> carrier, partial oxidation time=2
min: regeneration in 1 NL/min 3% vol. $O_2$ (a); regeneration in 1 NL/min 15% vol. $CO_2$ (b). C deposited represents th amount of carbon formed by methane decomposition during partial oxidation step, C oxidized is the amount of carbo
removed during the following carrier regeneration step. For cycle 6 regeneration was not recorded
Calliel altel reactivil at 200 C

Figure 24: SEM images of CeO $_2$ , chromite and CeO $_2$ -CuO oxygen carriers before and after activity screening cycles [453
CeO <sub>2</sub> before reaction (a); CeO <sub>2</sub> after reaction (b); Chromite before reaction (c); Chromite after reaction (d); CeO <sub>2</sub> -Cu
pefore rection (e); CeO <sub>2</sub> -CuO after rection (f). All images are at 10000× magnification9
Figure 25: SEM microscopy of CeO <sub>2</sub> and CeO <sub>2</sub> -Al <sub>2</sub> O <sub>3</sub> oxygen carriers before and after redox tests with 20 min parti
oxidation step [454]: CeO <sub>2</sub> before redox cycles (a, b); CeO <sub>2</sub> after reaction with O <sub>2</sub> regeneration (c, d); CeO <sub>2</sub> after reaction
cycles with $CO_2$ regeneration (e, f); $CeO_2$ -Al <sub>2</sub> O <sub>3</sub> before (g, h) and after cycles in both $O_2$ and $CO_2$ (i, j). Upper images an
at 10000× magnification, bottom images are at 40000× magnification9
Figure 26: comparison between experimental data, isothermal simulation and non-isothermal simulation of a redo
cycle for CeO <sub>2</sub> oxygen carrier for reduction in 10% vol. CH <sub>4</sub> (1 NL/min) and regeneration in 15% vol. CO <sub>2</sub> (1 NL/min) a
950 °C. The simulated gas outlet temperature for the non-isothermal simulation is also shown on secondary axis t
demonstrate that the simulated heating regime was able to maintain temperature sufficiently stable9
Figure 27: Major human health effects of exposure to some common VOCs [30]
Figure 28: VOCs emission sources and their contribution to total emission in a petroleum refinery in Shandong, Chir
[482]10
Figure 29: typical configuration for and adsorption-absorption combine VRU. AB=adsorber bed, F=feed valve, R=VO
recovery valve, P=purge valve, A=purified air valve10
Figure 30: scheme of adsorption columns used in simulation11
Figure 31: interpolated adsorption isotherms of butane and hexane at 298.15 K for the different activated carbo
adsorbents reported in literature
Figure 32: comparison of column internal adsorption profiles at different process time when multicomponer
adsorption is simulated with Extended Langmuir (EL) or Ideal Adsorbed Solution Theory (IAST)
Figure 33: results of 1 month of simulated continuous operation for the base column design: purified gas composition
(a); adsorbed VOC load in the column (b); internal adsorbed profile at the end of the 30 days (c)
Figure 34: effect of variation of column height on the normalized outlet concentration after 30 days of continuou
operation. Y-axis in log scale
Figure 35: effect of variation of column diameter on the normalized outlet concentration after 30 days of continuou
operation. Y-axis in log scale
Figure 36: effect of variation of column regeneration pressure on the normalized outlet concentration after 30 days of
continuous operation. Y-axis in log scale12
Figure 37: effect of variation of column purge feed on the normalized outlet concentration after 30 days of continuou
pperation. Y-axis in log scale

### **Table index**

Table 1: recap of hydrogen and syngas production technologies	38
Table 2: review of literature for CL reforming using pure CeO <sub>2</sub> ; Oxi=oxidant used for regeneration; n.a.=data not	
available, STP=standard temperature and pressure; TPR=temperature programmed reduction; TPO= temperature	
programmed oxidation	57
Table 3: reported composition of chromite sand	67
Table 4: kinetic constants, activation energies and enthalpy for the numerical model	73
Table 5: parameters of simulation and simulated cycle structure in isothermal and non-isothermal conditions. Refe	er to
Figure 15 for valve and stream names	76
Table 6: methane conversion and reaction selectivity at different degrees of OC conversion for CeO <sub>2</sub> , chromite and	t
CeO₂-CuO oxygen carriers. Results obtained for reaction at 950 °C	81
Table 7: inlet conditions for the adsorption process	. 113
Table 8: adsorption data for N2, O2 and hydrocarbon VOCs on activated carbon adsorbent	. 113
Table 9: adsorption data for N <sub>2</sub> , O <sub>2</sub> and hydrocarbon VOCs on zeolite adsorbent	. 117
Table 10: adsorption data for N₂, O₂ and hydrocarbon VOCs on silica adsorbent	. 120
Table 11: adsorption parameters and enthalpies for the simulation of cyclical PSA on activated carbon adsorbent	
chosen for process simulation	123
Table 12: adsorption column base design parameters. The mass transfer coefficients are obtained according to [57	/3].
Table 13: bed utilization percentage for each case study.	

#### Introduction

Over the past decades, anthropogenic activities have led to significant negative impacts on Earth's climate and environment. Ever increasing emissions of greenhouse gases, particularly carbon dioxide produced by fossil fuels combustion in industrial activities and vehicles have caused a significant rise of the average global temperature, leading to significant concern of the scientific community over the increasing rate and intensity of climate related disasters such as hurricanes [1], heat waves and prolonged drought [2], floods [3,4] and shortages of food and clean water availability in several regions of the world [5,6] causing significant damage to our planet ecosystem as well as to human society and economy, particularly in the less developed regions of the world [7,8]. The 2023 report of the Intergovernmental Panel on Climate Chage (IPCC) [9] evidences that in 2019 the average atmospheric concentration of carbon dioxide reached a maximum of 410 ppm, the highest value observed in the last 2 million years on the basis of available measurements and estimates from available data in fossil record, geological layers and Antarctic ice cores, with carbon dioxide equivalent emissions from human activities having increased more than 54% higher than those observed in 1990. Without the implementation of effective mitigation strategies to reduce emissions, their continuous increase will lead to unreversible and severe impacts on the ecosphere, as global average temperature will increase by more than 2°C. Figure 1 represents the plot of the atmospheric levels of carbon dioxide measured at the Mauna Loa Observatory, showing the evident increasing trend over the past decades.

#### Mauna Loa Observatory, Hawaii\* onthly Average Carbon Dioxide Concentration Data from Scripps CO<sub>2</sub> Program Last updated August 2024 420 1965 19 Maunakea data in blue 410 CO<sub>2</sub> Concentration (ppm) 400 390 380 370 360 350 340 330 320 SCRIPPS INSTITUTION OF 310 2020

Figure 1: monthly Average CO<sub>2</sub> atmospheric concentration measurements (part per million) taken at the Mauna Loa Observatory of the Scripps Institute of Oceanography, starting from year 1959 up to August 2024. Image taken from Scripps Institute of Oceanography website [10].

Year

Normative efforts for the reduction of carbon dioxide emissions have increased over the past years. Several countries, such as the European Union [11], the United States of America [12] and China [13] have set ambitious goals to achieve net zero carbon dioxide emissions within the end of the century. The Paris Agreement [14], which was subscribed by 195 countries all around the worlds legally binds its member countries to take measures to ensure that the maximum temperature increase will be limited to a maximum of 1.5° C by the end of the century. In particular, ever-increasing effort is being dedicated to the development of carbon capture, utilization and storage (CCUS) technologies [15,16], which, together with an increased utilization of renewable energy sources as alternative to fossil fuels, are of crucial importance in achieving the successful reduction of carbon dioxide emissions within the limits necessary to keep the warming within the boundaries of best-case scenarios. Capture technologies alone, though crucial, are not enough to meet this goal, and the development of new and more sustainable technologies as alternative to conventional industrial process is essential to meet the decarbonization requirements. The use of hydrogen as energy vector has long been considered an interesting and feasible alternative to the burning of fossil fuels for the energy industry [17] and the production of syngas mixture of hydrogen and carbon monoxide is also of crucial importance for the

chemical industry, as precursor to processes such as methanol synthesis and Fischer-Tropsch production of hydrocarbons [18,19]. Their current production processes however are based on the use of fossil fuels and are also associated to high environmental impact and greenhouse gas emissions. In order to achieve sustainability, the environmental impact and costs of its production need to be considerably reduced compared to current main production process of natural gas reforming, especially when considering the rapidly growing demand for both hydrogen and syngas use in the global market. Therefore, the first and main part of this thesis deals with the study and optimization of chemical looping reforming processes for hydrogen and syngas mixture production. First, a review of the state of the art of hydrogen and syngas production demand in the global market and their production processes will be presented, highlighting the main strengths and disadvantages of the production technologies currently commercially available or under research and their current technology readiness level (TRL). Then the chemical looping approach to reforming processes will be presented, with a discussion of the fundamentals of the process and particularly on the properties of the required oxygen carrier materials, with a focus on the use of cerium dioxide. Finally, the experimental activity performed using cerium dioxide oxygen carrier will be presented and its results and potential future developments will be discussed. A first approach to simulation of the process using the Aspen Adsorption<sup>TM</sup> software will also be presented.

Greenhouse gases are not the only concern when considering sustainability in energy and chemical production sectors. Releases of hazardous substances in the environment from production activities and accidental events constitute a risk to both chemical plant operators and the surrounding community and ecosystems [20–22]. Such releases not only can be immediately dangerous, but they can also cause relevant economic losses both due to the damage caused by their presence in the environment and also simply because valuable products are lost with very limited possibility of recovering them once they are dispersed. As such, the study of approaches to avoid these releases is of great importance both from an economic and safety point of view. Volatile Organic Compounds (VOCs) are a particularly concerning pollutant: the term is used to designate a vast list of organic compounds which are either gaseous or highly volatile in environmental conditions (atmospheric pressure, temperature of 293.15 K) [23], with the legislation of the United States of America also emphasizing their photochemical activity in the atmosphere [24]. VOCs are emitted from both natural sources and anthropogenic activities, with common emissions being associated with forest fires, agriculture, vehicle transportation and chemical industry [25], and are responsible of several serious effects both on environment and human health: the presence of photoreactive VOCs in the atmosphere leads to formation of ozone, aerosols, smog and other dangerous reactive species that contribute to

both pollution and climate change phenomena, and several VOCs are themselves directly dangerous to living organisms upon exposure due to their toxicity, causing respiratory problems, growth inhibition, irritation and inflammation of body tissues, and carcinogenicity [26,27]. It has been estimated that in the years 2000-2019, between 36.4 to 39.7% of the global population has come into risk of cancer due to exposure to harmful VOCs levels, with China reaching exposure levels as high as 84.3% of its total population. Exposure of the Chinese population to VOCs in the years 1980-2017 has been associated to increased risks of asthma, leukemia and low birth weight of children [28]. As shown in Figure 2, while emissions in Europe and the United States have decreased in the past years, the rest of the world has seen significant increase in VOCs releases, with the energy sector and the use of solvents being the main sources.

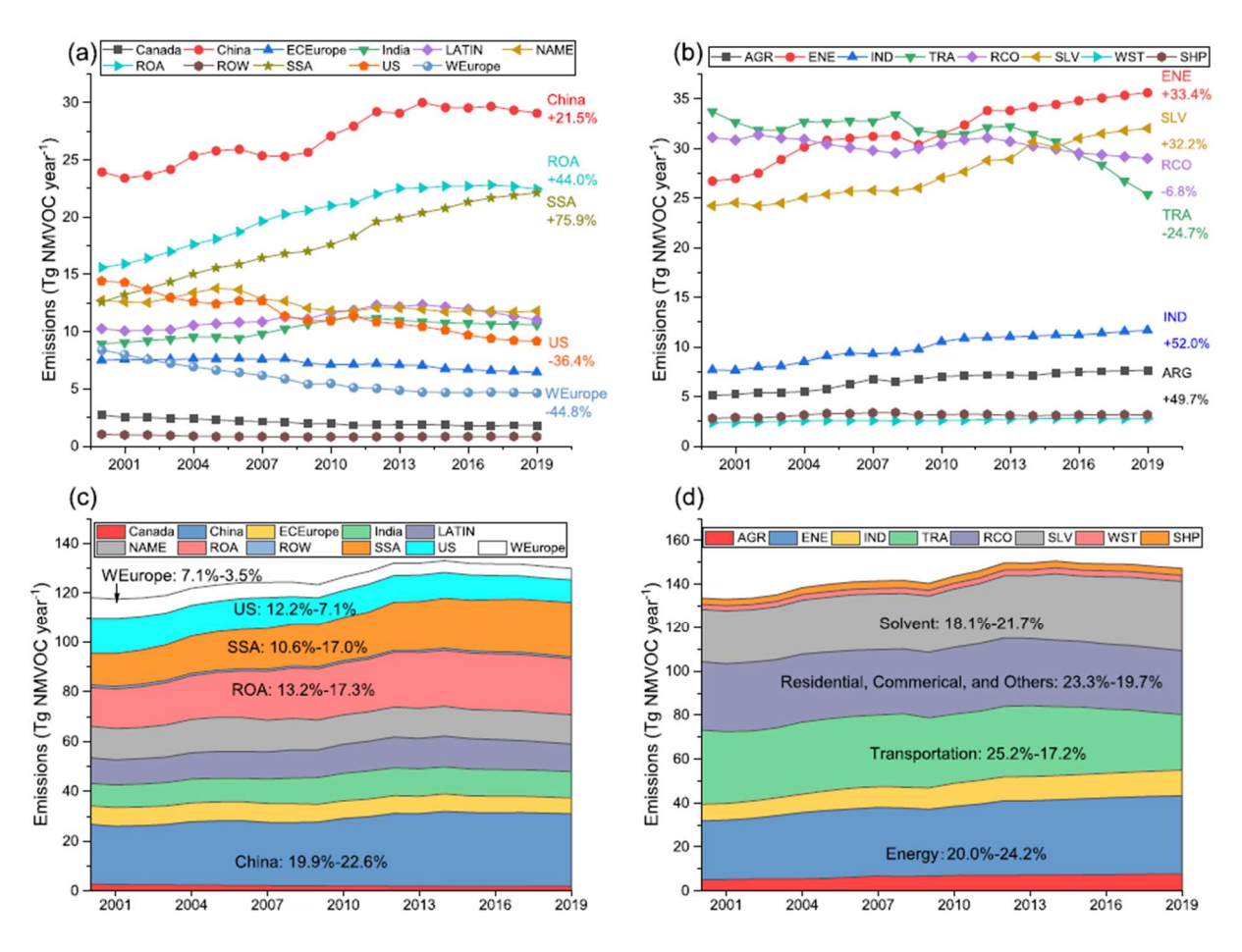


Figure 2: interannual variation of the annual total non-methane VOC (NMVOC) emissions during 2000–2019. (a, c) NMVOC emissions according to region; (b, d) emissions according to sector. Numbers in panels (a, b) represent the relative rate of change in NMVOC emissions during 2000–2019. Percentage values within panels (c, d) indicate the proportions of regional and sectoral emissions in the global annual total emissions for 2000–2019, respectively. ECEurope=Eastern and Central Europe), LATIN =Latin America, NAME=Northern Africa and the Middle East, ROA=Rest

of Asia, ROW=Rest of the World), SSA=Sub-Saharan Africa, WEurope=Western Europe, AGR=agriculture, ENE=energy production, IND=industry, TRA=transportation, RCO=residential, commercial, and other, SLV=solvent, WST=waste, SHP=international shipping [29].

Petroleum refineries are a major source of VOCs emissions, being the second most relevant source of anthropogenic VOCs after the transportation sector [30]. The operation of oil and fuel storage tanks and facilities, in particular, represents a significant point source of volatile organic compounds, which expose the surrounding environment to risks of toxicity both acute and chronic, as well as carcinogenic effects, potential risks of flammability of the light vapors and formation of ground level ozone [30,31]. VOCs from storage tanks can be released due to simple evaporation over time, but they can also be released in bursts during tank loading operations due to displacement of the tank vapors by the entering fuel [32]. Procedures and technologies to avoid these releases are therefore of great interest. Vapor recovery units (VRUs) utilizing various technologies, from cryogenic separation to membranes and adsorption, are nowadays commonly implemented in storage facilities to intercept these releases and reload the captured VOCs to the fuel tanks, thus avoiding these dangerous leakages [33,34]. Adsorption columns are a very common solution for the VRUs [35], however, the design and optimization of columns suitable for multicomponent adsorption is a rather difficult task, due to the complexity of the VOCs mixture that constitutes the vapors. For this reason, numerical tools that allow for the simulation of the column can provide most useful guidelines for optimizing column design and sizing. The second part of this elaborate will thus deal with the simulation of the operation of a multicomponent adsorption column for a VRU application, studying the effect of variation of different parameters on column operation using Aspen Adsorption<sup>TM</sup> software. This work was carried out in collaboration with the engineering firm Duemme Engineering of Bologna.

Nowadays, continuous processes represent the standard for several applications in the chemical and energy industry, especially for large scale applications. Compared to batch processes, continuous processes are generally easier to control and avoid the presence of non-productive dead times. However, sustainability is an ever-increasing concern for industrial production. In particular, the application of separation processes for the abatement of pollutants and carbon dioxide is bound to play a crucial role in the design of novel processes. Unfortunately, common separation processes possess several limitations, namely they are generally costly, particularly when treating diluted currents, and many are inherently discontinuous. As will be discussed more in detail in the following chapters, cyclical operation provides a pathway for process intensification both in reaction processes (chemical looping approach), allowing regeneration of the reaction catalysts and oxygen carriers and

obtaining inherent separation of product streams, and in separation processes, permitting continuous operation of inherently discontinuous processes such as adsorption. In both cases, optimization of cyclical operation and sizing of equipment are crucial to maximizing process efficiency. The present elaborate thus investigates these two cases of cyclical processes and shows the potential of applying numerical simulation to each case.

# Part 1: Chemical looping for syngas production: experimental and numerical study of the looping process using solid oxygen carriers for methane conversion with a focus on cerium oxide

#### 1.1-Hydrogen and syngas in the chemical and energy sector

#### 1.1.1-Hydrogen and syngas demand

Hydrogen is the lightest element in the periodic table, at an atomic number of 1. Molecular hydrogen formation was first scientifically observed by chemist and physicist Robert Boyle while experimenting with acids and iron around the year 1671. It was first recognized as an element by Henry Cavendish in 1766 [36] and it was then given its name by Antoine Lavoisier [37]. Hydrogen is a fundamental raw material in the chemical industry, where it finds its most relevant application in the synthesis of ammonia, which is an essential step toward production of fertilizer, and the production of methanol [38]. It is also widely used as a reducing agent for the steel industry [39] and for hydrotreating, cracking and desulfurization processes in refineries [40]. Finally, hydrogen finds some limited applications as fuel in aerospace and automotive industry. According to data from the International Energy Agency, in 2022 global hydrogen consumption reached 95 Mt, with China alone accounting for 30% of the total demand, followed by the United States of America [41]. About 41 Mt were used in refineries, while 53 Mt were consumed in the chemical and steel industry, 60% of them going into ammonia production, 30% into methanol synthesis and 10% into steel making. In 2023, the European Union consumed around 7.9 Mt of hydrogen [42], and total global demand surpassed 97 Mt [43], with an expected trend of continuous increase in the next decades following industrial growth. This increase in demand is unfortunately also intrinsically connected with an increase in pollution and greenhouse gases emissions: in fact, despite hydrogen being the most common element in the known Universe, constituting about 90% of its estimated number of atoms [44], on Earth's surface it is mostly found bound in compounds with other elements, forming molecules such as water and hydrocarbons, from which it needs to be extracted [45]. Nowadays, the hydrogen needed for industrial and energy applications is mostly obtained from non-renewable hydrocarbon fossil sources such as coal and natural gas, through steam reforming and gasification processes, with both production technologies being unfortunately characterized by significant carbon dioxide emissions [46]. The sole global utilization of hydrogen in petroleum refining in 2022 has been estimated to have caused more than 240 Mt of CO<sub>2</sub> emissions to the atmosphere [41]. Several other technologies are currently subject of research for hydrogen production, but none of them is as of now able to effectively outcompete steam reforming. In fact, these technologies still suffer from several downsides and have yet to achieve wide scale commercial application, with many still not having reached pilot scale development.

It should be noted that hydrogen is often not required alone, particularly in the chemical sector. Several crucial processes in the chemical industry use synthesis gas as raw material, that is to say a mixture of hydrogen and carbon monoxide (CO) in varying proportion, according to the process requirements. Syngas is the essential raw material for Fischer-Tropsch synthesis of higher hydrocarbons [47], methanol synthesis [48] and can be used as precursor for the production of several other compounds [49,50]. Indeed, the common hydrogen production processes from fossil fuels produce it as a syngas mixture of varying H<sub>2</sub> to CO ratio and are also the most common source of syngas for industrial applications. In 2023 the global syngas market demand was estimated at 230.05 million Nm<sup>3</sup>/h, with a predicted growth of 11.3% from 2024 to 2030 [51], and an increase of 10.8% in revenue [52]. Figure 3 shows an example of the prospected growth of the United States of America market alone during the aforementioned period, associated to a 12% increase in annual revenue. An increase in revenue of 5.9% has been predicted alone to be reached within 2030 compared to 2022 [53], with the European market growth alone being prospected to increase by more than 7% in the 2024-2029 period [54].

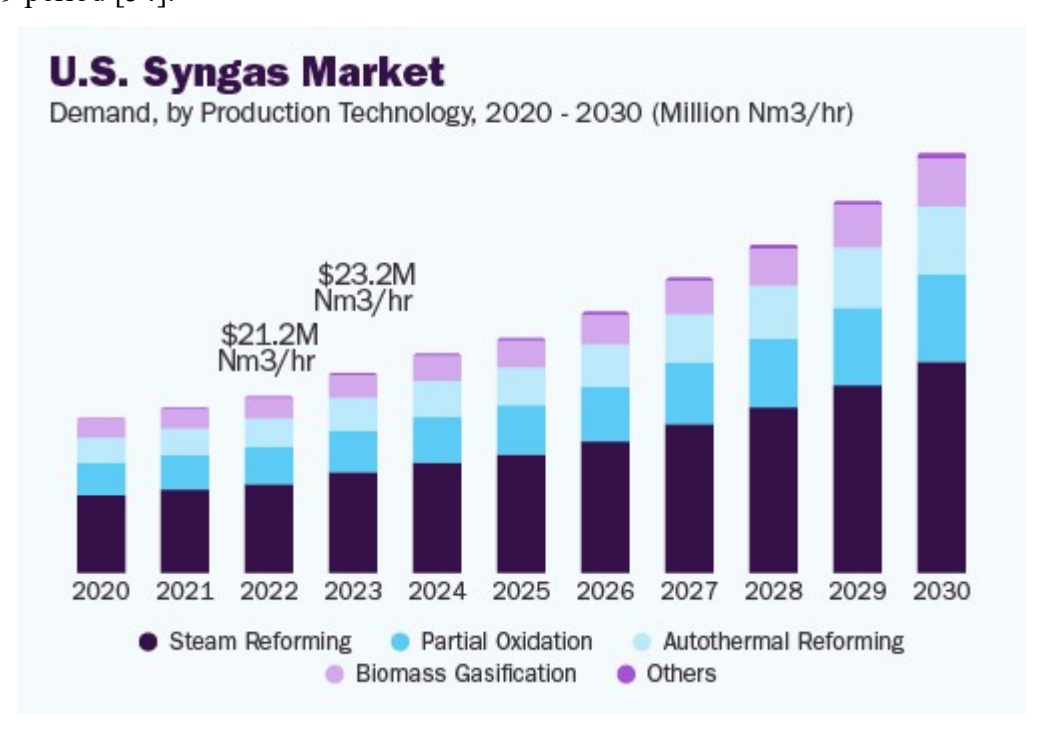


Figure 3: prospected growth of the syngas market in the U.S.A. by production technology in years 2020-2030 [51].

Given the industry's growing demand for both pure hydrogen and syngas, the development of more sustainable pathways for low carbon footprint production technologies is essential for the decarbonization of the chemical industry. Furthermore, international scientific and economic interest in the sustainable production of hydrogen has been also attracted by the potential that hydrogen has in contributing to the complete decarbonization of the energy sector, as well as other hard to abate industry sectors [55,56]. Hydrogen can provide a sustainable alternative to the combustion of fossil fuel with zero carbon dioxide emissions, and thus decrease greenhouse gases emissions in all fields of human activities: in particular, it can be used as a very efficient vector for energy storage and transport, being the chemical fuel with the highest mass specific energy density, with a Lower Heating Value-Higher Heating Value (LHV-HHV) window of 120-142 MJ/kg [55], much higher than gasoline and even methane. Power to hydrogen approaches can be used to store and transport energy obtained from renewable sources [57], overcoming the limits of traditional battery storage. Extensive implementation of hydrogen is seen as a necessary requirement for meeting the Sustainable Development Goals established by the United Nation Department of Economic and Social Affairs [58,59]. When considering also the increased industrial and normative trends towards favoring environmentally sustainable processes, the extensive use of hydrogen needed to achieve the prospected net zero emission scenarios could lead to a growth of global hydrogen demand up to as much as 8-folds by 2050 compared to 2020 [60]. Figure 4 displays the trends of hydrogen consumption estimated for the global market in the period 2019-2030, in the expected scenario of net zero emission policies implementation, clearly displaying the remarkable increase of consumption expected in such a scenario. Syngas can also be used as energy carrier in the power sector [61], particularly for biomass to energy conversions, though it is less efficient compared to the use of pure hydrogen. Therefore, in order to achieve the ambitious goal of net zero emissions, the development of sustainable hydrogen and syngas production is a mandatory requirement [62].

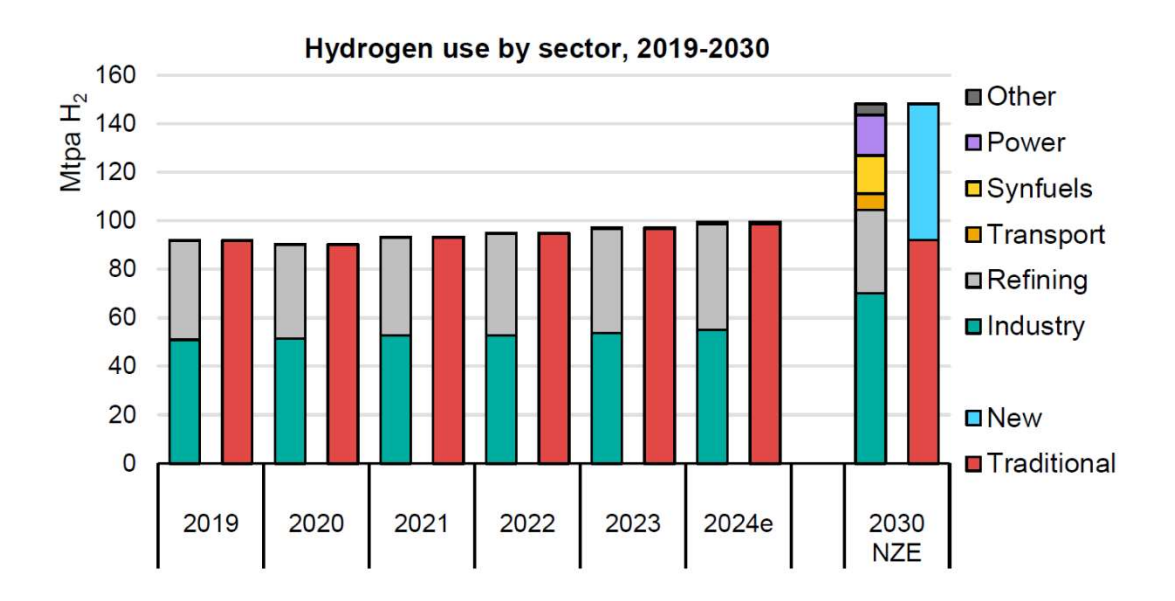


Figure 4: perspective of global hydrogen use: estimated growth by sector over the 2019-2030 period in the Net Zero Emissions by 2050 scenario (NZE). "Other" includes buildings and biofuels upgrading. 2024e = estimate for 2024. The estimated value for 2024 is a projection based on trends observed until June 2024 [43].

This section will therefore discuss in more detail the current state of the art of hydrogen and syngas production technologies, reporting their TRL, their main advantages and disadvantages. According to the method of production used, hydrogen has been commonly designated with different "colors" that symbolize its sustainability [63], although the choice of colors is not univocal, and these will also be introduced. A more in-depth examination of the chemical looping reforming approach will then be provided, with a review of the main literature available and the current state of the art of research. The next sections instead will deal with the further description of the experimental activity performed and the description of its goals and main results. Other crucial aspects for the development of hydrogen economy are the development of suitable transport and storage technologies and networks, but their discussion, while essential for the development of the field, is beyond the purpose of the current thesis, which is focused on hydrogen and syngas production, and will thus be omitted. For those interested, literature reviews on the state of the art of these two critical aspects can be found in the following references [64–67].

#### 1.1.2-Hydrogen and syngas production: the colors of hydrogen

#### 1.1.2.1-Hydrogen and syngas production from fossil sources

The use of fossil fuels has a long history in the development of human civilizations. Evidence exists for use of lignite coal combustion for fire and heat generation already in prehistoric times [68], while the first confirmed systematic use of coal for fuel has been dated to the Bronze Age in China [69]. With the advent of the First Industrial Revolution in the 1800s, coal became the main energy source for industries and cities, supplanting wood, charcoal and muscle power [70,71]. Coal was then supplanted by petroleum during the Second Industrial Revolution [72], with the latter remaining the main energy source up to our times. Furthermore, fossil fuels have long been the main source of production of several chemicals [73], and they are the main source of hydrogen production. Several different processes have been developed for hydrogen production from fossil fuel, which can be divided into two main families: reforming processes, applied to conversion of gaseous and liquid hydrocarbons, and gasification processes, applied to solid fuels. In the following, these processes will be discussed in detail.

#### Reforming of gaseous and liquid hydrocarbons: grey hydrogen

Liquid and gaseous hydrocarbons, particularly methane, are nowadays the principal source of hydrogen, obtained through reforming and oxidation reactions. Collectively, hydrogen produced from these processes is commonly referred as "grey hydrogen" [74], and is characterized by significant associated carbon dioxide emissions. The main reforming technologies can be essentially divided in steam reforming, dry reforming and partial oxidation, with the possibility of combing one or more of these processes in multi-reforming applications.

#### Steam reforming (SR)

Most of the world's hydrogen is produced through the SR process applied to methane, amounting to the 47% of the total produced hydrogen worldwide [75]. The reaction is as follows:

$$CH_{4(g)} + H_2O_{(g)} \rightleftarrows CO_{(g)} + 3H_{2(g)} \Delta H_0(298K) = +206 \frac{kJ}{mol}$$
 R1

The process was first introduced in 1930 in the USA [76] and has nowadays reached a high level of technological maturity, with a TRL of 9 [77]. The endothermic reaction of methane with water forms a syngas which is highly rich in hydrogen (H<sub>2</sub> to CO ratio of 3 or more). Figure 5 displays a typical scheme for a steam reforming process.

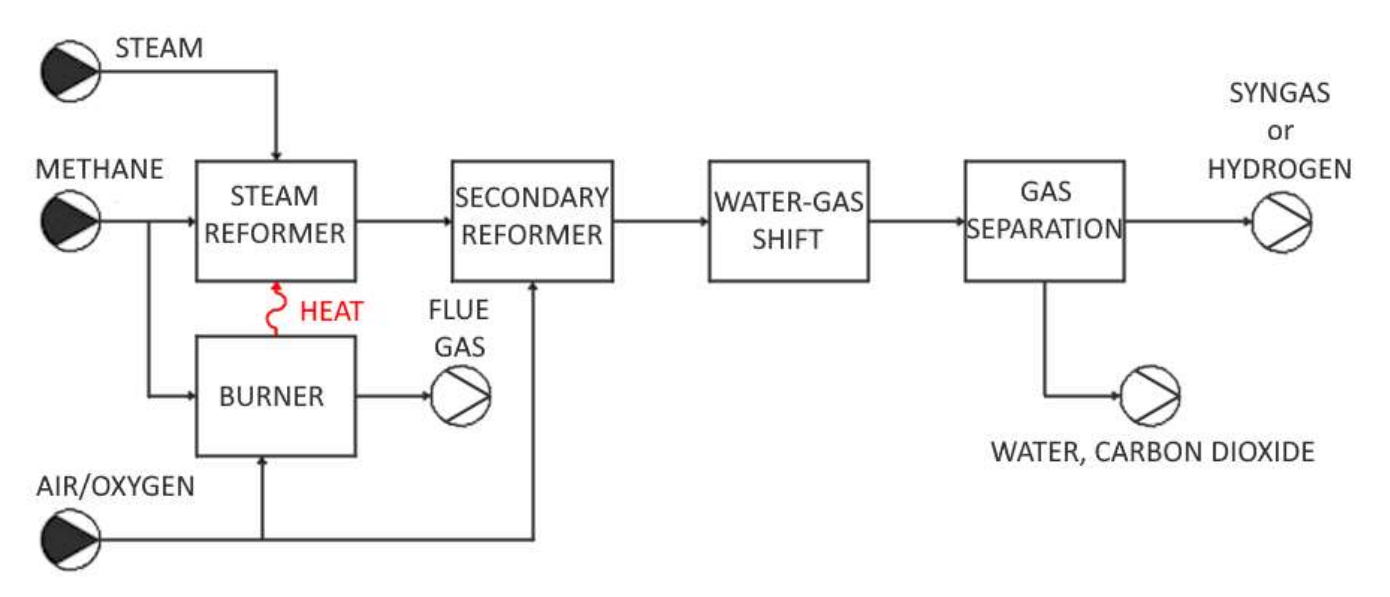


Figure 5: simplified scheme of a typical steam reforming process

The reaction is performed at high temperatures between 650 and 1000 °C and high pressure (5-40 bar) [78], comporting severe capital cost investment for the construction of the reforming plant. The common nickel-based catalysts used for the process also suffer severely from sintering and are subject to poisoning due to carbon deposition by methane cracking and to the presence of sulfur compounds [79–81]. In particular, excess amounts of superheated steam compared to reaction stoichiometry are required to avoid excessive carbon deposition, comporting significant costs and water consumption [82]. A secondary autothermal reformer can be placed after the primary steam reformer to further increase syngas production [83], then the water-gas shift (WGS) reaction [84] can be used to abate CO and further increase the hydrogen content of the produced syngas, the latter being used especially when the desired product is pure hydrogen. The high H<sub>2</sub> to CO ratio obtained by the process is beneficial for pure hydrogen recovery, but it can be a negative when the desired product is syngas destined to chemical synthesis, as the common methanol production and Fischer-Tropsch processes are favored by lower ratios closer to their reaction stoichiometry [47,85]. A great limit of SR is the high heat demand for the endothermic reforming reaction, which is usually met through the combustion of part of the fuel feed to provide reaction heat, causing the SR process to produce significant CO<sub>2</sub> emissions [86]. While methane is the most common alternative, liquid hydrocarbons can also undergo SR processes [87]. However, their use is limited by the low conversion and lack of optimized catalysts, coupled with high carbon deposition.

#### Partial oxidation (PO)

An alternative for syngas production from hydrocarbons is the PO reaction [88], which when considering methane as starting fuel can be written as:

$$CH_{4(g)} + \frac{1}{2}O_{2(g)} \rightleftharpoons CO_{(g)} + 2H_{2(g)} \Delta H_0(298K) = -36\frac{kJ}{mol}$$
 R2

Compared to steam reforming, the partial oxidation reaction produces a syngas poorer in hydrogen content (H<sub>2</sub>/CO=2), which is less useful for hydrogen production but is well suited for use in chemical synthesis [89]. Furthermore, the partial oxidation reaction is exothermic, thus not requiring the sacrifice of part of the feed to heat production, and the kinetics of reaction is much faster, allowing for smaller reactors and lower residence times. Partial oxidation can be carried out both as a pure thermal process, at temperatures of 1200-1500°C, or at lower temperature of 800-900°C if a catalyst is used [90]. The most relevant problem is presented by the need to control process selectivity as to avoid the occurrence of complete combustion of the hydrocarbon feed [91], which not only lowers the syngas yield of the process but is also cause of relevant safety concerns related to run-away of reactor temperature and the presence of potentially explosive hydrocarbon-oxygen mixtures [92,93]. Thermal PO has already seen implementation in commercial plants when applied to higher hydrocarbons [94], but it is hindered by the high temperature needed to steer selectivity, requiring tight temperature control and high capital costs. On the other hand, catalytic PO, while theoretically more favorable due to the lower temperature required, has yet to see any true industrial application due to the lack of a sufficiently selective and robust catalyst and it has so far been employed on projects only up to pilot scale [95]. Coke deposition is a common issue among the various proposed catalysts [96]. Lastly, the other relevant problem of partial oxidation is that it requires the use of pure oxygen as reactant, as the use of air would lead to dilution of reaction products by nitrogen, causing a dramatic increase in the cost of downstream separation processes. Partial oxidation reactors therefore require the implementation of high-cost air separation units (ASUs), which increase the overall capital and operative costs.

#### Dry reforming (DR)

DR is another possible pathway for syngas production from hydrocarbons that can address the problem of high carbon dioxide emissions in conventional SR [97]. Compared to steam reforming and partial oxidation, dry reforming is unique in that it offers a pathway for carbon dioxide utilization which could potentially allow the process to achieve net zero emissions, converting two greenhouse gases into useful chemical precursors. In the dry reforming reaction, methane is reacted with CO<sub>2</sub> rather than steam to produce a syngas with a H<sub>2</sub> to CO ratio close to 1:

$$CH_{4(g)} + CO_{2(g)} \rightleftharpoons 2CO_{(g)} + 2H_{2(g)} \Delta H_0(298K) = +247 \frac{kJ}{mol}$$
 R3

Due to the lower hydrogen concentration in the product compared to partial oxidation and steam reforming, dry reforming is ill suited for production of pure hydrogen, but the produced syngas is still of interest for chemical synthesis. The main drawbacks to the DR reaction are essentially three [98]: first, carbon dioxide is a highly stable molecules, thus the resulting reaction is even more endothermic than steam reforming; second, the selectivity of the reaction is badly affected by the simultaneous occurrence of WGS reaction, which reduces the H<sub>2</sub> to CO ratio of the produced syngas [99]; finally, all known catalysts are prone to fast deactivation following the clogging of active sites due to fast coke formation [100]. Catalyst sintering is also possible due to the high reaction temperature required (600-900°C [101]). Like SR and PO, DR can also be carried out on heavier hydrocarbon feedstocks than methane, but carbon deposition becomes an increasingly relevant issue with longer chains, and selectivity and conversion become overall lower [102].

#### Combined reforming and oxidation strategies

It is possible to combine SR, PO and DR to obtain optimized processes that achieve a balance between the advantages of the single processes while addressing their drawbacks.

Steam reforming and dry reforming can be combined in a dual reforming (2R) process [103], where both steam and carbon dioxide are simultaneously used as reforming gas. This process has already seen commercial application for the reforming of biogas, which naturally contains carbon dioxide in addition to methane [104]. In this case, the presence of steam reduces the problem of carbon deposition compared to pure DR process [105], as the water is able to react with the solid carbon oxidizing it into additional syngas, while the presence of carbon dioxide in addition to steam as the oxidant can lower the H<sub>2</sub> to CO ratio of the product syngas compared to SR alone [106]. Proper tuning of the CO<sub>2</sub> and steam ratio in the reactant feed can be used to optimize the H<sub>2</sub> to CO ratio of the product syngas. While this can improve the performance in terms of resistance of the catalyst to coke deposition, the 2R process remains highly endothermic and sintering of the catalyst remains a significant problem. Furthermore, carbon deposition is still more significant compared to SR alone and conversion of carbon dioxide remains a limiting factor on the overall reaction efficiency [104,107].

Another combined option allows to compensate for the high endothermicity of SR and DR by combining either process with PO to obtain what is called an autothermal reforming (AR) process [108]. Here, instead of combusting part of the feed to meet the heat requirement for the endothermic reforming reaction, oxygen is added directly to the feed to obtain both a partial combustion and a partial oxidation, which are used to provide the reaction heat required for a following DR or SR step

in the same reactor. The typical reactor of an AR process is thus divided in two zones: an oxidation zone near the inlet, where methane is reacted with oxygen starting the conversion to syngas and heat is produced, and a reforming zone further away, where the heat produced in the first zone and transported in the gas current is then used to perform the reforming reaction [109]. A dual catalyst reactor may also be used as an alternative to thermal partial oxidation [110], as the same catalyst is unlikely to be selective and efficient for both the oxidation and reforming reactions. Once started, the process is thus able to sustain itself without the need for further external heat introduction. The presence of oxygen and the lower reaction temperature compared to SR or DR on their own can also partly avoid the problem of carbon deposition, and the process can be tuned to a wide variety of feedstocks [111]. Despite this, AR still presents some significant drawbacks that limit its scope. Compared to 2R, here the produced H<sub>2</sub>/CO ratio is less tunable, as the autothermal requirement for the reaction imposes stricter limits on the feed composition in terms of useful O<sub>2</sub>/CH<sub>4</sub> and H<sub>2</sub>O/CH<sub>4</sub> (or CO<sub>2</sub>/CH<sub>4</sub>) ratios, especially when considering their effect on reaction temperature, heat recovery and coke formation [112,113]. Furthermore, the conventional reactor divided into two zones is subject to high temperature gradients [114,115], thus being potentially exposed to strong structural stresses and risks of catalyst degradation due to differential thermal dilatation [116,117]. Carbon deposition and catalyst sintering remain a source of concern and efficiency loss, especially in the reforming zone due to the high temperature that can be reached. Runaway of the temperature in the oxidation zone and loss of selectivity towards complete combustion is also still possible, and the potential explosivity of methane-oxygen mixtures poses a serious safety concern. Finally, AR shares the same essential drawback of PO, in that it requires pure oxygen for the reaction to avoid N<sub>2</sub> dilution of the products, thus needing the coupling of the process with an ASU, even though the requirement for pure oxygen is lower compared to PO on its own. Overall, AR has not seen large scale commercial application yet [118], but some industrial applications are nonetheless mature, for example its use as secondary reforming treatment after steam reforming [83], as shown in Figure 5, using either air, when the final use of the produced hydrogen is the production of ammonia, or oxygen, when used for production of pure hydrogen and syngas.

The last possible approach combines SR, DR and PO all together, in a so-called tri-reforming (3R) process [119]. Here, an autothermal process is obtained by covering the heat requirements of SR and DR through the PO reaction, the presence of oxygen and steam reduces the carbon deposition issues of DR, and the combined SR, PO and DR reactions lower the H<sub>2</sub> to CO ratio of the product syngas compared to SR, simplifying its use in chemical synthesis [120]. The obtained syngas H<sub>2</sub>/CO ratio is greatly tunable, and the process is a pathway for CO<sub>2</sub> abatement and valorization [121]. Despite these benefits, the 3R reaction presents also similar problems to 2R and is still not available at commercial

scale: thermal gradients in the reactor remain a concern affecting process safety and catalyst lifetime, with catalyst sintering and resistance to poisoning being the biggest issue [122]. Caution should also be put in the variation of feed composition: O<sub>2</sub> and water are both much more reactive compared to CO<sub>2</sub>, thus the presence of either of them in excess can lead to low or even negative carbon dioxide consumption, due to competition and presence of water gas shift reaction [123]. Finally, pure oxygen and ASU are usually still needed to avoid N<sub>2</sub> dilution of the products, despite some 3R processes being potentially able to use oxygen poor flue gas as feedstock [124], and the possibility of explosion due to improper gas mixing is still present.

#### Gasification (G) of coal: black and brown hydrogen

Before SR was developed, the first technology used in large scale hydrogen gas production was Coal Gasification (CG). Indeed, the first coal gasification plants were built in the 1800s, when their product, a mixture of H<sub>2</sub>, CO, CO<sub>2</sub> and CH<sub>4</sub>, was commonly known as "town gas", being used for public illumination and heating in industrialized cities before the advent of electricity [125]. Coal gasification for hydrogen production was largely supplanted by the advent of the cheaper SR technology, but some plants remain active even today, particularly in China [126], and it is still considered a mature technology. In this process, coal reacts with steam, carbon dioxide and/or low oxygen concentrations gas feeds in a complex reaction network coupling pyrolysis (R4), combustion, Boudouard reaction (R7), WGS (R9) and methanation reactions (R10) [127,128]:

$$Coal_{(s)} \rightarrow H_{2(g)} + Char_{(s)}(C) + Tar_{(l)}$$
 R4

$$C_{(s)} + O_{2(g)} \to CO_{2(g)} \Delta H_0(298K) = -393.51 \frac{kJ}{mol}$$
 R5

$$C_{(s)} + \frac{1}{2}O_{2(g)} \rightarrow CO_{(g)} \Delta H_0(298K) = -110.53 \frac{kJ}{mol}$$
 R6

$$C_{(s)} + CO_{2(g)} \rightarrow 2CO_{(g)} \Delta H_0(298K) = +172.50 \frac{kJ}{mol}$$
 R7

$$C_{(s)} + H_2 O_{(g)} \rightarrow C O_{(g)} + H_{2(g)} \Delta H_0(298K) = +131.30 \frac{kJ}{mol}$$
 R8

$$CO_{(g)} + H_2O_{(g)} \rightarrow CO_{2(g)} + H_{2(g)} \Delta H_0(298K) = -41.17 \frac{kJ}{mol}$$
 R9

$$C_{(s)} + 2H_{2(g)} \to CH_{4(g)} \Delta H_0(298K) = -74.60 \frac{kJ}{mol}$$
 R10

Coal gasification combines endothermic and exothermic reactions, but it is an overall endothermic process, requiring high temperature to minimize H<sub>2</sub>O and CO<sub>2</sub> fraction in the product syngas [129]. It is usually carried out either in fixed bed, fluidized bed or entrained bed reactors [130], all of which have seen some commercial application according to the characteristics of the available coke and the economic feasibility of each alternative. The process can be carried out without catalysts, but their use can increase the efficiency of coal conversion and hydrogen yield [131]. Recently, gasification

has seen an increased interest in the energy sector, particularly through the development of the Integrated Gasification Combined Cycle (IGCC) process [132], which has the potential of considerably reducing emission and increasing efficiency compared to traditional coal combustion plants for power generation [133]. The process, however, is still limited by its high costs and cannot compete with SR at large scale industrial application [108]. In general, coal gasification is impeded by the complexity of the process, its lower efficiency compared to SR and its high CO<sub>2</sub> emissions [134,135]. High costs and operational complexity derive from the need of expensive post treatment and cleaning of the produced gas to abate pollutants such as sulfur compounds, powders and tar, all of which being also a safety and economical concern due to risks of gasifier and purification equipment clogging and corrosion [136,137]. In addition, further difficulty in operation is introduced by the inherent inhomogeneity that coal may present in terms of shape, volatilization, tar formation, ash content and ash melting point, which limits the possibilities of using combined feedstocks from different sources on the same gasifier, as each design presents strong limitations in the characteristic of feedstock that it can treat. Finally, coal gasification is a very water-intensive process, requiring extensive wastewater treatment to avoid pollution of the discharge sites [138]. Alternatives to conventional coal gasification have been proposed in the form of plasma gasification [139], allowing efficient conversion of lower calorific value feedstocks thanks to relying in plasma torch instead of combustion-oxidation reactions to maintain temperature, and supercritical water coal gasification [140], but these solutions are thus far not suitable for large scale application. Figure 6 reports the schematics of typical commercial gasifiers.

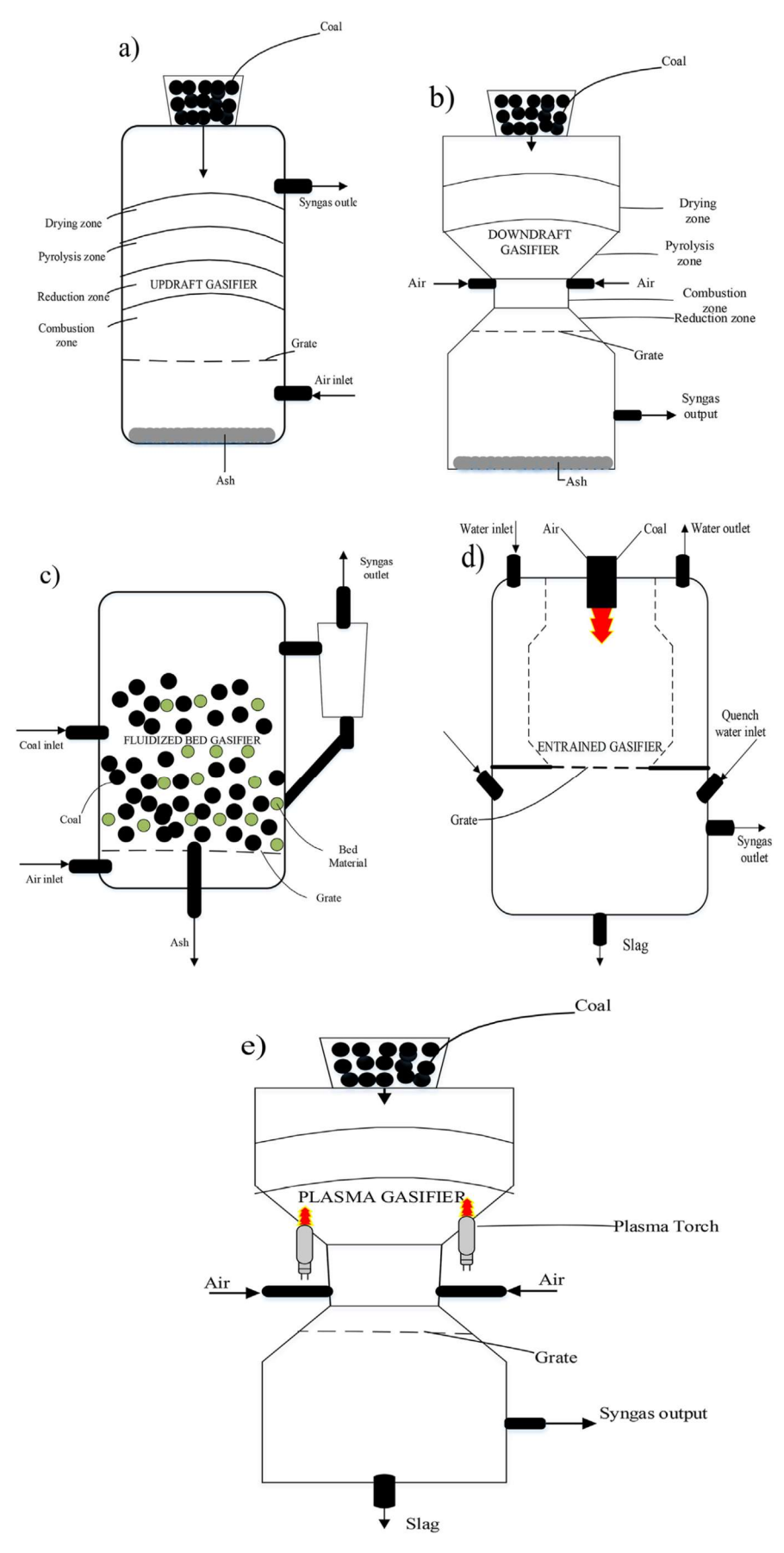


Figure 6: typologies of gasifier [137]: updraft gasifier (a); downdraft gasifier (b); fluidized bed gasifier (c); entrained gasifier (d); plasma gasifier (e).

A technology that has received significant research interest is the so-called underground coal gasification (UCG) [141]. In this kind of process, originally developed to allow for the utilization of hard to mine deep coal seams, the standard gasification reactions are carried out directly in-situ by injecting the gasifier agents (O<sub>2</sub>, H<sub>2</sub>O and CO<sub>2</sub>) in the coal seam and providing ignition, thus converting the surrounding carbon into syngas which is then extracted. Compared to the traditional gasification process, UCG has the advantage of possessing a potentially lower environmental impact, as the hazardous solid waste, ashes and liquid tars typically produced by gasification remain stored underground in the coal seam and the coal can be converted without the environmental issues and safety hazards of traditional mining technologies [142]. Furthermore, the emptied seam can potentially be further used as a CO<sub>2</sub> geological storage site. This process has already been used in several demonstration plants [143], and it is considered by some as a leading technology for clean coal utilization. However, concerns remain about the environmental impacts potentially caused by ground subsidence over the depleted coal seam, the possibility of groundwater contamination and the possibility of generating syngas leaks with high greenhouse potential, concerning toxicity and potential explosivity, which require good monitoring for a process that is intrinsically difficult to monitor due to the depth of the coal seams involved [144]. The product syngas composition is also difficult to control. UCG has so far reached a TRL of 6 [145], with pre-industrial applications already in function.

In general, hydrogen obtained from coal gasification is usually referred to as "black" or "brown" hydrogen according to the type of coal used, brown for lignite coal and black for bituminous coal [74].

#### Integration of CCUS technologies: blue hydrogen

As previously mentioned, all reforming and gasification technologies share the common problem of high carbon dioxide emissions as one of their bigger downsides, but on the other hand CG and SR are currently the only technologies that are mature and cheap enough to allow large scale hydrogen and syngas production in the short-term period [146]. Furthermore, sources for hydrogen production based on renewable energy sources are currently negatively affected by their uneven distribution and their temporal discontinuity [147]. As such, putting an immediate stop to the conventional production pathways would be unfeasible and economically disastrous. While global consumption of petroleum and coal is expected to decrease, the same cannot be said for natural gas, which, as a cleaner alternative, is expected to replace most other fossil fuels in chemical synthesis and power applications and remain a crucial part in the future energy mix and emission abatement effort [148,149].

Significant interest has been therefore dedicated to the decarbonization of conventional hydrogen production methods, with emphasis on the application of CCUS technologies [150] to both SR and coal gasification, producing what is commonly referred to as "blue hydrogen" [151]. While this potentially allows for a much cleaner production than its "grey", "brown" and "black" counterpart, and can be a feasible cost competitive strategy for short-term and mid-term hydrogen economy development, blue hydrogen cannot be really considered a sustainable alternative for hydrogen production, as it is still based on non-renewable fossil sources [152–155]; it should also be noted that there is also significant debate on the feasibility of blue hydrogen use for decarbonization, particularly on the tradeoff between the efficiency of abatement technologies, the higher associated costs and the real environmental impact of these processes when they are considered at a global level [95,156–158]. Implementation of CCUS to reforming and gasification has been estimated to be at TRL of 8 [159], ready for near-term commercialization.

#### Methane decomposition (MD): turquoise hydrogen

A promising approach to hydrogen production from methane is through the methane decomposition (MD) reaction, leading to the formation of solid carbon and gaseous hydrogen [160].

$$CH_{4(g)} \to C_{(s)} + 2H_{2(g)} \Delta H_0(298K) = 74.9 \frac{kJ}{mol}$$
 R11

This reaction, as mentioned before in the grey hydrogen production, is a common side reaction during SR, PO, AR, 2R, 3R and especially DR processes, where it represents a significant issue as it causes reactor clogging and catalyst poisoning, as well as worsening the overall heat exchange performance of the reactor and lowering the selectivity towards syngas production [161–163]. However, the reaction by itself has generated much interest in the research community due to its potential to be used to consistently and competitively produce near pure hydrogen starting from methane, with limited need for gas purification as the other product is easily separated solid carbon, and potential zero carbon dioxide emissions [164]. Compared to SR, the cracking reaction is much less endothermic, thus lowering the heat requirements for the process. Hydrogen produced through methane decomposition applied to fossil hydrocarbons has been recently dubbed as "turquoise" hydrogen [165]. However, like the previously discussed reforming technologies, turquoise hydrogen cannot really be considered a green alternative for hydrogen production, as most of the methane is obtained from fossil sources.

Thermal methane decomposition (TMD) and thermocatalytic methane decomposition (TCMD) Like PO process, methane decomposition can be implemented either as a pure thermal process or be facilitated at lower temperature through the introduction of a catalyst [166]. In addition to lowering

the temperature required for the process, the presence of a catalyst can offer the further benefit of providing a controllable microstructure for the produced carbon, for example forming nanorods and nanotubes, which then becomes a further value-added product of industrial interest [167]. No carbon dioxide or monoxide are directly formed by the reaction, so syngas is not directly obtainable, but it is possible to obtain carbon monoxide from regeneration of the catalyst by partial oxidation of the deposited carbon. The main limits of MD however are also to be found in the deposition of carbon, as it can easily lead to reactor clogging and to the deactivation of the catalyst, thus leading to a discontinuous production process due to the need to periodically remove the deposited carbon, with difficulty in ensuring its complete removal [98]. Currently, thermal and thermocatalytic processes for MD are at a TRL of 3 to 4 [168].

#### Plasma driven methane decomposition (PD-MD)

As an alternative to high temperature operation, plasma discharge can be used to activate the breakage of methane C-H bonds [169,170], sometimes also coupled with a catalyst [171]. Compared to thermal and thermocatalytic processes, the use of plasma for methane activation allows for an on/off operation of the process, avoiding long start up and shut down time and making it ideal for use in combination with intermittent renewable energy sources such as solar power and wind [172]. Thermal plasma processes (TPD-MD) have already been implemented on industrial scale for hydrogen and carbon black production, the technology being at a TRL of 8, though the original plant has since been decommissioned [168]. Thermal plasma can produce high quality carbon black and carbon nanomaterials together with high purity hydrogen, but the process is limited by the low energy efficiency [173]. Non-thermal plasma decomposition, either in pure plasma application (NTPD-MD) or in plasma-catalytic process (NTPDC-MD), has significant advantages compared to thermal processes, has it can be operated at much lower temperature and pressure and higher energy efficiency [174]. However, the technology is still in its early development phase, with TRL of 2-4 [168,175].

1.1.2.2-Hydrogen and syngas production from biomass and biogas: green hydrogen As mentioned before, all reforming and gasification technologies (SR, DR, PO, 2R, 3R, MD, and coal gasification) commonly produce hydrogen starting from fossil sources and cannot therefore be truly considered as clean pathways for hydrogen and syngas production. Applying CCUS can mitigate process emissions, but the problem of non-renewability of the feedstock cannot be addressed by traditional fuel sources. These production processes however still merit research interest, as they have the potential to be applied also to renewable feedstock, in particular biomass and biogas sources [176,177]. This is particularly interesting when considering that biomass waste materials from other

activities can be used as a potential feedstock for biomass conversion processes, providing an advantageous pathway for waste disposal and valorization as well as not competing for cultivated land availability with agriculture for food production [178,179]. The viability of these processes is, however, highly dependent on the availability of abundant and cheap biomass feedstocks, which can be subject to significant variability in both available quantity and composition, with substantial differences among geographical regions and time periods [180,181]. Finally, despite using a more environmentally friendly source for their feedstock, processes involving biofuels reforming can only be truly eco-friendly and zero carbon if they are also coupled with CCUS technologies and use of renewable sources for meeting the energy needs of the process: if these requirements are met, hydrogen from biomass can be designated as low carbon "green" hydrogen [182].

#### **Biogas reforming**

In the case of reforming technologies, substantial efforts have been dedicated to extending their application to biogas feedstocks. DR, 2R and 3R are of particular interest when dealing with biogas, which is already a mixture of mostly methane and carbon dioxide, commonly in even proportions. These technologies have the potential to be applied directly to biogas, without the need to first separate it into biomethane [104,183]. Other biomass originated chemicals have also been considered as reforming feedstocks for hydrogen production, such as methanol [184], ethanol [185] and glycerol [186]. However, difficulties in application of these technologies to biogas and other biomass derived feedstocks emerge when considering that these feedstocks commonly present much more impurities compared to natural gas, particularly sulfur compounds and siloxanes, that can easily lead to catalyst poisoning [187–190]. Furthermore, the problems related to the heat requirements of the process, the optimization of catalyst activity and product selectivity and the catalyst resistance to coking and sintering persist also for biogas feedstocks, as well as the additional costs for pure oxygen requirement of PO, 2R and 3R processes.

#### **Biomass gasification**

Just as reforming technologies can be adapted to use biogas and biofuels in place of fossil hydrocarbons, gasification and pyrolysis processes commonly applied to coal can be partially [191] or completely converted to use biomass feedstocks [192]. Several different biomass sources have been tested more or less successfully for hydrogen, syngas and energy production, ranging from agricultural waste to algal biomass, wastewater sludges, animal farms residues and urban wastes [193–198]. Compared to gasification of coal, the use of biomass feedstocks involves several complications due to their generally lower heating potential and their greater variability in

availability, composition and properties such as ash melting temperature and density [199,200], which can greatly affect gasification efficiency, syngas purity, yield and H<sub>2</sub>/CO ratio due to ash agglomeration, soot and tar formation and catalyst poisoning [201–203].

#### Hydrogen production from biofermentation (BF)

Both gasification and reforming technologies are typical thermochemical conversion pathways, generally requiring operation at high temperatures which negatively impact the cost of the process in terms of equipment cost, process safety, energy requirements and catalyst sintering. Recently, BF processes have been proposed as an alternative, less energy intensive hydrogen production pathway that can be carried out in milder conditions while also being able to convert waste materials [204,205]. Fermentation processes can be carried out in the presence of light (photo-fermentation, PF) or in its absence (dark fermentation, DF), with combined approaches also being possible [206]. PF uses anoxygenic photosynthetic bacteria and energy from visible light to convert substrates into hydrogen [207], while DF can use different strains of aerobic, anaerobic and facultative aerobic bacteria [208]. It should be observed that while PF can reach high level of substrate conversion, the requirement of light makes optimal reactor design difficult to achieve [209]; on the other hand, the hydrogen yield of DF is limited by volatile fatty acids accumulation formed by side reactions [210]. Combined DF and PF processes can be used to improve performances [211]. In general, at the current state of the art both technologies are limited by hydrogen yields much lower to other production methods, difficulty in obtaining useful bacterial strains and by the intrinsic complexity of operation of biochemical processes, where microbial growth and productivity can be negatively affected by several factors such as pH, temperature, oxygen level and presence of nutrients and toxic compounds in the substrate [212]. Also, while potentially useful for hydrogen production, syngas in general cannot be directly obtained from these processes, although biomass derived from these processes can then potentially be delivered to gasification or reforming facilities to be converted into syngas.

#### 1.1.2.3-Other hydrogen production sources

The above presented technologies applied to fossil sources and biomass allow for the production of hydrogen mainly in the form of syngas, with the exception of methane decomposition and biofermentation of biomass, which instead produce mostly only hydrogen. Other processes exist that instead focus more on the production of pure hydrogen and are therefore less useful for syngas production application. Here they will be briefly discussed for completeness of the review.

#### **Hydrogen production from water**

Water is the most common substance on Earth's surface [213], and is the main form in which hydrogen is available on our planet. Furthermore, the splitting of water into hydrogen and oxygen does not involve any intrinsic carbon dioxide formation.

$$H_2O_{(l)} \rightleftharpoons H_{2(g)} + \frac{1}{2}O_{2(g)} \Delta H_0(298K) = +285.83 \frac{kJ}{mol}$$
 R12

As such, water would be expected to be a primary source for hydrogen production, however only a limited amount of the world's hydrogen demand is produced using water as raw material. This is because water is a relatively stable molecule, and processes designed for its splitting into hydrogen and oxygen are generally very energy intensive [214]. Several different technologies have been proposed for water splitting, namely electrolysis, photocatalytic splitting and thermochemical cycles. Water electrolysis (WE) is the most common water splitting technology and is the only one that has seen industrial application, providing about 4% of the total hydrogen global production, mostly in small scale plants [215]. Different technologies have been developed while attempting to optimize the WE process, of which the main ones being alkaline water electrolysis (A-WE), anion exchange membrane water electrolysis (AEM-WE) electrolysis, proton exchange membrane water electrolysis (PEM-WE) electrolysis and solid oxide fuel cell water electrolysis (SOFC-WE). A-WE is the most technologically mature process, being commercially available since the early 1900s [216], followed by PEM-WE, also having some commercial application [217], SOFC-WE, currently near commercialization [218], and AEM-WE, currently the least mature technology and still in the research phase [219]. Figure 7 reports the schematics of these processes. Overall, the price of water splitting technology is still high compared to the cost of SMR, even though it is expected to decrease in the next years, and process efficiency and yield cannot yet compete at large scale [220]. SOFC could represent the option with the lowest environmental impact according to Life Cycle Analysis [221].

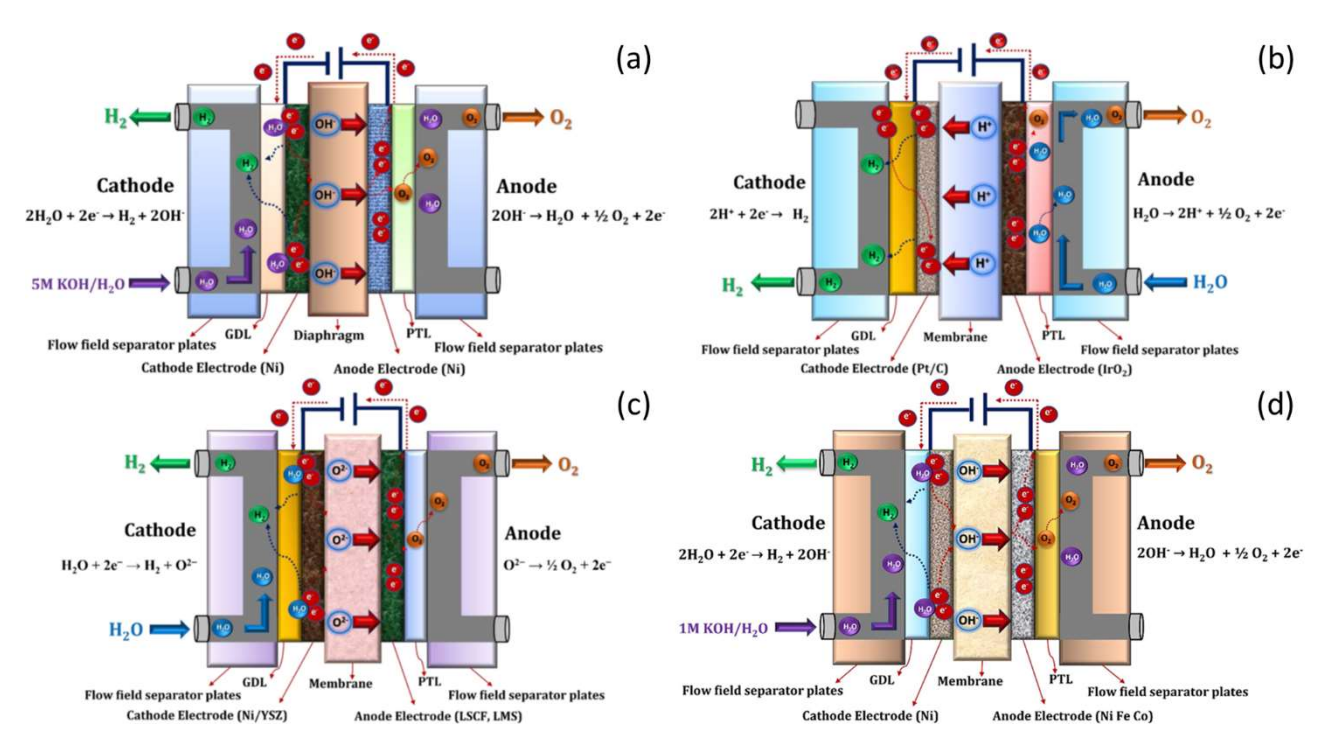


Figure 7: schemes of processes for water electrolysis [215]: A-WE (a); PEM-WE (b); SOFC-WE (c); AEM-WE (d). GDL=Gas Diffusion Layer, PTL= Proton Transfer Layer

Photocatalytic water decomposition (PC-WD) has recently drawn attention as a process for hydrogen production thanks to its potential high efficiency in solar energy to H<sub>2</sub> conversion, low cost, effective separation of H<sub>2</sub> and O<sub>2</sub> products and flexibility in reactor scale [222], however great challenges remain in finding more active, stable and kinetically favorable catalysts and designing efficient reactors needed for industrial application [223–225]. To this day, the process is still restricted to lab scale testing. A potential alternative would be the development of artificial systems capable of replicating natural photosynthesis processes that can be used for hydrogen production [226,227], but this approach is also still far from being a mature technology.

Biocatalytic water decomposition (BC-WD) by oxygenic photosynthetic organisms such as algae, plants and cyanobacteria has also been proposed as a pathway for hydrogen production [228]. Photosynthesis is perhaps the most important biological process for life on Earth, acting as the base for most of our world's ecosystems since it first developed [229]. BC-WD can be obtained either through a direct or an indirect process [230], but both processes require light. Non-oxygenic photosynthesis can also produce hydrogen [231], but it is not able to use water as electron donor, thus requiring less available and more costly sources such as organic acids which make it less suitable for large scale application [232]. Currently, BC-WD processes have been restricted to lab scale, with the main problems being the low production rates and the low yields due to inhibition of hydrogen production by the cogeneration of oxygen [233]. Nonetheless, improvements in these processes could

potentially be obtained by coupling oxygenic photosynthesis, non-oxygenic photosynthesis and fermentative processes [234].

Direct water thermolysis (DWT), where heat by itself is used to directly split the water molecule into hydrogen and oxygen, has attracted some interest in the past, but the technology is plagued by the need to work at very high temperatures (exceeding 2000 K) to have sufficient conversion and appreciable splitting kinetics, which complicates severely the separation of the hydrogen product from oxygen while also being extremely taxing on reactor design due to limited heat tolerance of materials and catalysts [235,236]. It also leads to low energy efficiency and high risks of reactor explosion and fires [237,238]. Combination of the process with high temperature electrolysis may improve efficiency but it is still far from industrial viability [239].

As such, in recent years the interest in DWT has been mostly supplanted by the study of thermochemical redox cycles water splitting (TRC-WS) using a solid carrier material [108,240]. In these processes, water splitting is mediated by the redox reaction of a solid phase, acting not simply as a catalyst, but as a true solid reactant. In the simplest variant, the solid phase is a metal oxide which is cyclically reduced and re-oxidized to act as an oxygen carrier (OC) in a two-step cycle [241]. Several different materials have been studied as oxygen carriers for two-step TRC-WS processes, ranging from cerium dioxide to perovskites and iron oxides [242–244]. Other more complex cycles have also been proposed, consisting of up to four cycle steps involving oxide-hydroxide, oxide-sulfate, metal-halide or oxide-halide pairings [245,246]. Compared to direct water thermolysis, this approach generally involves much lower temperatures and does not form a hydrogen-oxygen mixture as the two gases are produced in separate steps [245]. Overall, the technology readiness level is higher for multistep cycles as compared to the two-step ones, because multistep cycles usually can be carried out at lower temperature compared to two-step cycles, which require temperature above 1500 K for all known oxygen carriers [247], but the global TRL remains low to medium both when considering solar and nuclear energy as heat sources for these applications [248,249].

Overall, hydrogen production from water qualifies is designated as "green" hydrogen only if renewable energy is utilized for the process, with CCUS also included in the production process [250]. Nuclear power can also be used to provide the energy required with low carbon emissions, thus producing so called "magenta" or "pink" hydrogen if the nuclear produced energy is used to sustain electrolysis or "red" hydrogen if the nuclear generated heat is used to sustain thermochemical water splitting [251,252]. If the energy for the splitting is provided completely or in part from conventional fossil sources through the conventional energy grid, water splitting technologies cannot be considered really as zero carbon processes and the hydrogen produced is referred to as "yellow" hydrogen [63,251]. This imposes a limit on the use of these technologies for "green" hydrogen production, as

the distribution of many renewable sources is intrinsically uneven, and nuclear energy cannot be considered renewable.

#### Hydrogen production from hydrogen sulfide

Hydrogen sulfide (H<sub>2</sub>S) is a highly toxic, corrosive compound which is gaseous at room temperature, and can be found both in nature and as a result of human activities, being commonly present in sewage and industrial waste, particularly of crude oil refineries, and in natural gas and biogas streams [253,254]. In addition to its environmental risks, H<sub>2</sub>S presence in process streams poses a threat both to pipelines, equipment and engines due to its corrosivity [255] and to catalysts due to sulfur poisoning [256], therefore, its abatement is of high relevance for many processes. The traditional pathway for its abatement in natural gas and petroleum refineries is the thermochemical Claus process, first developed in 1883, which converts it to solid sulfur and water [257]. A potentially advantageous alternative process is using hydrogen sulfide as raw material for hydrogen production, thus coupling the abatement of a dangerous pollutant with production of a value-added product of much greater interest compared to sulfur only production from Claus process [258]. Approaches suggested for hydrogen production from H<sub>2</sub>S are split into two main pathways: reforming and decomposition.

As the name suggests, in H<sub>2</sub>S reforming (H<sub>2</sub>SR) H<sub>2</sub>S is used as reforming agent for methane instead of water or CO<sub>2</sub> [259], following the scheme:

$$2H_2S_{(g)} + CH_{4(g)} \rightarrow CS_{2(l)} + 4H_{2(g)} \Delta H_0(298K) + 232.38 \frac{kJ}{mol}$$
 R13

$$H_2S_{(g)} \rightarrow \frac{1}{2}S_{2(g)} + H_{2(g)} \Delta H_0(298K) + 79.87 \frac{kJ}{mol}$$
 R14

With the final reaction being methane decomposition (R11). This process is more endothermic compared to traditional SR, but it is advantageous in that it would remove the need for gas desulfurization, and the produced carbon disulfide is itself a value-added product which can be separated from the pure hydrogen product stream by condensation, while no greenhouse gases are produced by the reaction [260]. Autothermal operation may be achieved by combusting part of the product hydrogen, while still retaining good production [259], enhancing the energetic efficiency of the process. Carbon deposition remains the greatest concern in terms of catalyst deactivation and the main limitation in process development [261]. Costs of H<sub>2</sub>SR have been estimated to compare to SR with carbon capture implementation or to methane pyrolysis, with the process potentially even being able turn an ulterior profit thanks to the high value of the CS<sub>2</sub> byproduct [262]. However, the process remains rather water intensive. Overall, the technology readiness level of the process has been estimated at 6, not yet ready for industrial scale up, with research still mainly focused on finding

optimal catalysts and operative conditions to avoid carbon formation and maximize yield and efficiency [263,264]. The process also utilizes methane, which, unless obtained from biomass, remains a non-renewable fossil source.

Analogously to the methane decomposition and water splitting reactions, the H<sub>2</sub>S splitting reaction R14 can be used by itself for hydrogen production, and exactly like the aforementioned reactions, this is also an endothermic process. Several approaches have been proposed for this reaction, from conventional thermolysis to electro and photolysis [258].

Thermochemical H<sub>2</sub>S decomposition (TC-H<sub>2</sub>SD) has long been subject of interest for hydrogen production [265]. The main issue of the process is that both the purely thermal and the thermocatalytic approaches are intrinsically limited by strong thermodynamic restrictions to H<sub>2</sub>S conversion [266,267]. Most catalysts are unable to achieve conversions greater than 50%, with further great obstacles to catalytic activity being the occurrence of sulfur poisoning and sintering due to high temperature operation [268]. The need to separate great quantities of unreacted H<sub>2</sub>S from the product current also leads to further complications, as conventional treatments such as amine adsorption are costly and energy intensive, while alternative approaches such as membranes or supersonic separators have yet to achieve effective large-scale application [269].

Plasma-driven H<sub>2</sub>S decomposition (PD-H<sub>2</sub>SD), particularly non-thermal plasma coupled with catalyst, can achieve H<sub>2</sub>S splitting at lower operation temperature compared to thermal splitting [270], and they can bypass the equilibrium limitations [271]. Pilot scale production of hydrogen using PD-H<sub>2</sub>SD was tested with promising results by the Soviet Union, and the technology has an overall TRL of 6, comparable to H<sub>2</sub>SR [272]: with proper selection of plasma source and catalysts, conversions higher than 90% can be achieved at near room temperature and atmospheric pressure, however challenges remain in the operation of large-scale stable plasma reactor. The removal of sulfur in particular remains an issue for the continuous operation of the reactor [273].

Electrocatalytic H<sub>2</sub>S decomposition (EC-H<sub>2</sub>SD) can operate at lower temperature compared to thermal dissociation [274], and is advantageous in terms of ease of control and potential cost-effectiveness [275,276]. The splitting of hydrogen sulfide is much less energy intensive and has the further advantage of not forming a potentially explosive hydrogen-oxygen gas mixture, producing instead sulfur as an easier to separate solid product [277]. Both direct and indirect EC-H<sub>2</sub>SD processes have been studied [278]. The direct electrolysis process is the easiest and least energy intensive to operate [279], but it is hampered by the accumulation of elemental sulfur on the anode, which leads to electrode passivation and poisoning, greatly reducing further catalytic activity and reactant conversion [277,280]. Indirect electrolysis avoids the problem of sulfur passivation, thanks to its use of an intermediate adsorbent for H<sub>2</sub>S dissociation [281], but the process is generally more complex

and more energy intensive to operate compared to the direct route. It can also suffer from the degradation of the intermediate adsorbent. Overall, the TRL of electrocatalytic processes has been estimated as being between 4 and 5, with only bench scale tests being available so far [272].

Photochemical H<sub>2</sub>S decomposition (PC-H<sub>2</sub>SD) is an interesting process, as it would allow low temperature hydrogen production from a highly abundant and renewable energy source [282]. The process has been studied both in gas phase and in aqueous phase [283], but it is less mature compared to other technologies: the gas phase process suffers from bad energy efficiency, while the aqueous process is more complex, and it can suffer from corrosion and formation of byproducts. The aqueous process is the most studied and promising approach, but the lack of optimized catalysts and recovery strategies for sulfide species remains a problem for the overall process implementation [284]. Current catalysts are not yet able to maximize light utilization, suffer from photocorrosion phenomena and the mechanisms of reaction are not yet completely clear, which is an obstacle to optimized process and catalyst design [285]. Due to these downsides, the process is currently unable to be scaled up for competitive hydrogen production [286]. An alternative to pure photocatalytic processes has been proposed in the form of photo-electric processes, able to produce not only hydrogen and sulfur but also generating electricity in photoelectrochemical cells [283], which can work either in direct or indirect configuration, the latter using chains of redox couples to favor recovery of elemental sulfur [284,287]; however, stability and costs are limiting factors for the implementation of this technology. Overall, the current TRL of PC-H<sub>2</sub>SD has been estimated at 3 [272], being the least developed process.

Contrary to other technologies, no color has been conventionally associated with hydrogen derived from hydrogen sulfide yet.

#### Naturally available hydrogen: white hydrogen

While hydrogen on Earth is mostly found in other compounds rather than in its elemental form, under particular circumstances, it is indeed possible to find natural elemental hydrogen reservoirs and production sites, even at rather high concentrations [288]: this hydrogen is commonly referred to as "white" or "gold" hydrogen and it can be found as free gas, as an inclusion in rock formations, dissolved in underground aquifers or dispersed in sea and freshwater sediment. For example, hydrogen has been observed as adsorbed gas, as point defects in the crystal reticle of mantle minerals and also as trace water in the upper mantle, particularly in olivine minerals and near subduction zones [289]. Natural hydrogen can be of both biotic and abiotic origin, but biotic hydrogen is mainly formed by deep sea and underground microbial communities and it is likely to be produced and consumed in a tightly coupled cycle that for the most part does not reach the surface [290], so abiotic sources are

the most relevant for surface emissions [291]. Some of this abiotic hydrogen may be the result of release of gases originally trapped in the Earth's core and mantle during Earth's formation [292,293], while other can be produced by processes such as the serpentinization reaction, which occurs water comes into contact with magma containing iron containing minerals [294], the mechanoradical reaction of silicate minerals exposed to the strong mechanical stresses caused by earthquakes [295], the decomposition of hydrogen sulfide in volcanic gases [296] or the splitting of water due to the nearby decay of radioactive minerals [297]. Among these processes, serpentinization is commonly considered to be the main source of abiotic natural hydrogen [298], which is particularly relevant and has led to an enthusiastic industrial interest in its study and search, as it could effectively be a cheap, environmentally friendly and completely renewable source of hydrogen, since its extraction could be economically much less expensive than reforming and electrolysis processes, with minimal carbon emissions. Significant surface emissions of natural hydrogen likely to be produced by this process have been observed in the proximity of known seismic fault lines, such as the "eternal flames" of the Chimaera region in Turkey [299], and natural traps of large amounts of subsurface hydrogen have been discovered, the most famous being the Bourakebougou wells in Mali [300,301], where a pilot plant for extraction and utilization of the nearly 98% pure hydrogen stream for power generation has been successfully installed. Other relevant ground hydrogen emissions sites have been identified in several countries such as Spain [302], Canada [303], Saudi Arabia [304], China [305], Australia [306], Brazil [307], Albania [308], Russia [309] and the United States of America [310]. Despite the great hype and potential surrounding this new field, great uncertainties still remain on the real feasibility of natural hydrogen [311]: while past know-how in extraction technologies from the oil industry can be transported to extraction technologies for hydrogen, experience in proper identification of potential hydrogen wells and geological traps is still lacking, since the industry is still in its early stages and hydrogen itself being hard to detect [312,313]. Furthermore, there is still no certainty on the true amount of natural hydrogen that is available at feasible concentrations and depth for safe extraction [298,311].

Another alternative that has been considered is the production of hydrogen by artificially inducing serpentinization through pumping of carbon dioxide rich water into hot subsurface iron rich rock formations, coupling hydrogen production with carbon dioxide storage by mineralization [314], but knowledge on proper identification of production sites, operating conditions and hydrogen recovery technologies is still missing. Overall, the TRL for natural hydrogen utilization has been estimated as 6, with only the plant in Mali being active for consistent hydrogen production, but lacking estimation of the total reservoir [315].

# 1.1.2.4-Final remarks on hydrogen and syngas production technologies

Table 1 recaps the current state of the art of hydrogen and syngas production technologies. While methane decomposition, water splitting, H<sub>2</sub>S splitting and reforming and natural hydrogen are all promising sustainable pathways for environmentally sustainable production of pure hydrogen, they are less interesting when the desired product is syngas. Production of syngas therefore remains limited to fossil fuels and biomass as precursors, with the conventional technologies of reforming and gasification remaining the more viable options for its large-scale implementation. As such, improvements are required in order to increase the sustainability of conventional reforming processes and overcoming their traditional limitations.

Table 1: recap of hydrogen and syngas production technologies

Process	Raw material	Product	H <sub>2</sub> color	Advantages	Disadvantages	TRL
	CH <sub>4</sub>			Mature technology	Energy intensive	
	Liquid			High hydrogen	Catalyst deactivation	9 (for CH <sub>4</sub> )
	hydrocarbons			yield	(coke, sintering)	8 (for CH <sub>4</sub> with
	Biogas	C		High H <sub>2</sub> /CO ratio	High CO <sub>2</sub> emissions	CCUS)
SR	Biomass	Syngas		suitable for H <sub>2</sub>	Water intensive	6 (for glycerol
	derivates	(H <sub>2</sub> /CO≥3)		production	High H <sub>2</sub> /CO ratio is	and other
	(i.e.,				less suitable for	biomass
	glycerol)				chemical synthesis	derivatives)
	H <sub>2</sub> O					
				Exothermic reaction	Explosion risk	9 (thermal
			Grey (fossil	Fast kinetics	Pure O <sub>2</sub> required	process for
	CH		hydrocarbons,	Ideal H <sub>2</sub> /CO ratio	Catalyst deactivation	higher
	CH <sub>4</sub>		no CCUS)	for methanol	(coke, sintering)	hydrocarbons)
PO	Liquid	Syngas	Blue (fossil	synthesis	CO <sub>2</sub> emissions	3-6
PO	hydrocarbons Biogas	(H <sub>2</sub> /CO≈2)	hydrocarbons,		Selectivity difficult	(thermocatalytic
	O <sub>2</sub>		with CCUS)		to control	process for
	02		Green			methane)
			(biogas, with			
			CCUS)			
	CH <sub>4</sub>			Utilization of CO <sub>2</sub>	Energy intensive	
	Liquid			Direct application to	Catalyst deactivation	
DR	hydrocarbons	Syngas		biogas	(coke, sintering)	3-4
DK	Biogas	(H <sub>2</sub> /CO≈1)		Ideal H <sub>2</sub> /CO ratio	Interference of water	
	CO <sub>2</sub>			for Fischer-Tropsch	gas shift reaction	
	CO <sub>2</sub>			synthesis		
	CH <sub>4</sub>		1	Tunable H <sub>2</sub> /CO	Energy intensive	
2R	Liquid	Syngas		ratio	Catalyst deactivation	3-4
ZK	hydrocarbons	(3≥H <sub>2</sub> /CO≥1)		Reduced coke	(coke, sintering)	3-4
	Biogas			deposition		

	CO <sub>2</sub>			Directly applicable		
	H <sub>2</sub> O			to biogas		
				Reduced coke	Catalyst deactivation	
				deposition	(coke, sintering)	
	CH <sub>4</sub>			Autothermal	CO <sub>2</sub> emissions	
	Liquid			process	Reactor thermal	
	hydrocarbons	Syngas			stresses due to	9
ASR	Biogas	(3≥H <sub>2</sub> /CO≥2)			subdivision in	8 (with CCUS)
	$O_2$				exothermic and	
	H <sub>2</sub> O				endothermic reaction	
					zones	
					Pure O <sub>2</sub> required	
				Reduced coke	Catalyst deactivation	
				deposition	(coke, sintering)	
	CH <sub>4</sub>			Autothermal	Reactor thermal	
	Liquid			process	stresses due to	
ADR	hydrocarbons	Syngas		•	subdivision in	3-4
	Biogas	(2≥H <sub>2</sub> /CO≥1)			exothermic and	
	CO <sub>2</sub>				endothermic reaction	
	$O_2$				zones	
					Pure O <sub>2</sub> required	
	GTT			Tunable H <sub>2</sub> /CO	Catalyst deactivation	
	CH <sub>4</sub>			ratio	(coke, sintering)	
	Liquid			Reduced coke	CO <sub>2</sub> emissions	
	hydrocarbons	Syngas		deposition	Pure O <sub>2</sub> required	
3R	Biogas	(3≥H <sub>2</sub> /CO≥1)		Autothermal		3-4
	CO <sub>2</sub>			process		
	H <sub>2</sub> O			Directly applicable		
	O <sub>2</sub>			to biogas		
				No catalyst	High temperature	
TMD	CH <sub>4</sub>			Pure H <sub>2</sub> production	Coke deposition	3-4
TNID	CH4			Value added coke		3-4
				production		
				Lower operation	Catalyst deactivation	
				temperature	(coke deposition,	
			Turquoise	compared to	sintering)	
TC-MD	CH <sub>4</sub>	Hydrogen	(fossil CH <sub>4</sub> )	thermal process		3-4
		Carbon	Green	Pure H <sub>2</sub> production		
			(biomethane)	Value added coke		
				production		
				Pure H <sub>2</sub> production	Low energy	
TPD-MD	CH <sub>4</sub>			Value added coke	efficiency	8
				production		
NTPD-MD	CH <sub>4</sub>			Pure H <sub>2</sub> production	Reactor design not	2-3
					optimized	

production	
Energy efficient	
Low temperature	
operation	
Pure H <sub>2</sub> production Lack of efficient	
Value added coke catalyst	
NTPDC- production	
MD CH4 Energy efficient	2-3
Low temperature	
operation	
Only process to High cost	
Brown (lignite treat solid fuels Low energy	
coal, no Valorization of efficiency	
CCUS) waste materials Complex gas	
Black Mature technology purification	
(bituminous Water intensive	
G Coal Biogas (*) coal, no Inhomogeneity of	9
Biomass CCUS) feedstock	8 (with CCUS)
Blue (coal, complicates	
with CCUS) operation	
Green Sensitivity to sulfur	
(biomass, and metallic	
with CCUS) impurities presence	
Gasification in situ Environmental	
avoids the release of impacts potentially	
solid and liquid caused by ground	
Brown (lignite   waste   subsidence	
coal, no Coal can be Groundwater	
H <sub>2</sub> CCUS) converted without contamination	
CH <sub>4</sub> Black the need to mine it, Risk of syngas leaks	
UCG Coal CO (bituminous hard to mine (greenhouse	6
CO <sub>2</sub> coal, no resources can be potential, toxicity	
H <sub>2</sub> O CCUS) used and explosivity)	
Blue (coal, Can be coupled with Hard to monitor	
with CCUS) CO <sub>2</sub> geological Syngas composition	
storage hard to control	
Coal is non-	
renewable	
Mild operating Low yields	
conditions Difficult reactor	
BF Biomass H <sub>2</sub> Green Low CO <sub>2</sub> emissions design (for PF)	3
Limited toxic waste Inhibitions due to	
Can use waste volatile fatty acids	
biomass as source formation (for DF)	

					Difficult selection of bacterial strains Difficult optimization of	
					process conditions	
A-WE	H <sub>2</sub> O	H <sub>2</sub> O <sub>2</sub>		Low capital cost High stability Mature technology Longer lifetime No precious catalyst	Low current density Corrosivity of electrolyte Gas permeation and formation of explosive mixtures Slow Stop/go and load cycling Sensitivity to impurities in the water	9
PEM-WE	H <sub>2</sub> O	H <sub>2</sub> O <sub>2</sub>	Green (renewable energy) Yellow (conventional energy grid)	High-voltage efficiency Capability to operate under high pressure High current density High purity of hydrogen Quick response/start time	High cost of noble material membrane Low durability Acidic medium Precious catalyst	9
AEM-WE	H <sub>2</sub> O	H <sub>2</sub> O <sub>2</sub>	Magenta/Pink (nuclear energy)	Low Ohmic resistance Good gas separation High current density Use of affordable and abundant materials High performance and adaptability to different loads High gas purity Significantly lower material costs Flexibility in terms of loads driven and places of use	Limited efficiency (80%) High alkaline degradation Stability and durability issues	6
SOFC-WE	H <sub>2</sub> O	H <sub>2</sub>		Fast kinetics	Limited durability	7-8

		O <sub>2</sub>		High efficiency	Bulky system design	
				Low minimum load	Limited production	
				Low-cost catalysts	capacity	
				High efficiency	High capital	
				Low operating costs	investment	
				Dual-Reversibility	Only small-scale	
				(Electrolyzer/Fuel	availability	
				Cell)	High operating	
					temperature	
				Direct use of	Low catalyst activity	
				renewable energy	Slow kinetics	
PC-WS	H <sub>2</sub> O	H <sub>2</sub>	Green	with high efficiency	Most catalysts use	1-3
		$O_2$		Low cost	only UV-light	
				Size flexibility		
				No carbon dioxide	Low rates	
				emission	Low yields	
BC-WD	H <sub>2</sub> O	H <sub>2</sub>	Green	Mild reaction	Light requirement	1-3
				conditions	complicates reactor	
					design	
				Theoretically the	Very high	
				easiest design for	temperature	
		11		water splitting	operation	
DWT	H <sub>2</sub> O	H <sub>2</sub>			Risk of explosion	1-3
		O <sub>2</sub>			due to H <sub>2</sub> -O <sub>2</sub> mixture	
					Low energy	
					efficiency	
			Green	Lower operation	High operation	
			(renewable	temperature	temperature and poor	
			energy)	compared to DWT	energy efficiency	
			Red (nuclear	H <sub>2</sub> -O <sub>2</sub> mixture is	(two-steps cycles)	
			energy)	avoided	Complexity of	2-4 (two-step
TRC-WS	11.0	H <sub>2</sub>			operation (multi step	cycles)
TRC-WS	H <sub>2</sub> O	$O_2$			cycles)	3-7 (multi-step
					Degradation of	cycles)
					carrier materials	
					Need for solar	
					concentrator if solar	
					energy is used	
				Desulfurization of	Catalyst stability	
				gas no longer	Corrosion	
	CH	ш		required		
$H_2SR$	CH <sub>4</sub> H <sub>2</sub> S	H <sub>2</sub> CS <sub>2</sub>	/	Abatement of toxic		6
	1125	CS <sub>2</sub>		H <sub>2</sub> S		
				Production of value		
				added CS <sub>2</sub>		

			No CO <sub>2</sub> formation		
			Easy to operate	Low conversion	
			Lower temperature	Sulphur poisoning	
			than water splitting	Product separation	
TC-H <sub>2</sub> SD	H <sub>2</sub> S	H <sub>2</sub>	Abatement of toxic	Corrosion	4-5
		S	H <sub>2</sub> S		
			No methane		
			required		
			Abatement of toxic	Sulphur passivation	
			H <sub>2</sub> S	of anode in direct	
			No methane	splitting	
			required	Complex operation,	
EG H GD	II C	H <sub>2</sub>	Ease of control	intermediate reactant	4.5
EC-H <sub>2</sub> SD	H <sub>2</sub> S	S	Cost-effectiveness	degradation and	4-5
			Less energy	corrosivity in indirect	
			intensive than WS	splitting	
			No hydrogen-		
			oxygen gas mixture		
			Abatement of toxic	Complex reactor	
			H <sub>2</sub> S	design	
			No methane	Complex sulfur	
			required	removal	
		H <sub>2</sub>	Can bypass		
PD-H <sub>2</sub> SD	H <sub>2</sub> S	S S	thermodynamic		6
		5	equilibrium		
			limitations on		
			conversion		
			Low temperature		
			operation		
			Direct use of	Poor energy	
			renewable energy	efficiency (gas phase	
			Abatement of toxic	process)	
			H <sub>2</sub> S	Complex operation,	
			No methane	corrosion (aqueous	
		$H_2$	required	phase process)	
PC-H <sub>2</sub> SD	H <sub>2</sub> S	S	No hydrogen-	Lack of active	3
			oxygen gas mixture	catalyst	
				Current catalysts	
				only use UV light	
				Photocorrosion of	
				catalyst	
				Sulphur recovery	

				Possibly renewable	Uncertain total	
				High cost-	availability and	
				competitiveness	renewability	
N. d. 111		11	WI : /C 11	Extraction	Lack of reliable	
Natural H <sub>2</sub>	-	H <sub>2</sub>	White/Gold	technologies can be	methods for locating	6
				readily adapted	hydrogen wells	
				from the oil and gas	Environmental	
				sector	impacts of extraction	

<sup>(\*)</sup> Mixture of H<sub>2</sub>, CH<sub>4</sub>, CO, CO<sub>2</sub>, H<sub>2</sub>O

# 1.2-Overcoming the limits of conventional syngas production by reforming processes: the chemical looping approach

# 1.2.1-Chemical looping conversion of methane

Among the proposed technologies for improving conventional reforming processes for hydrogen and syngas production, the chemical looping (CL) approach, which is schematized in Figure 8, appears as particularly promising pathway; the approach is quite similar to TRC-WS processes discussed in Section 1.1.2.3, and is in fact derived by them, particularly the two step processes: methane is oxidized through reaction with an OC, generally a metal oxide, which is reduced in order to release the oxygen required for reaction. The process thus produces a mixture of hydrogen, water, carbon monoxide and carbon dioxide, with selectivity depending on process conditions and OC properties.

$$MeO_x + \delta CH_4 \rightarrow MeO_{x-\delta} + \delta CO + 2\delta H_2$$
 R15

$$MeO_x + \delta CO \rightarrow MeO_{x-\delta} + \delta CO_2$$
 R16

$$MeO_x + \delta H_2 \rightarrow MeO_{x-\delta} + \delta H_2 O$$
 R17

The reduced carrier is then regenerated by reaction with an oxidizer. The CL approach can be applied to all the conventional reforming processes: if oxygen is used as an oxidant (R18), chemical looping partial oxidation (CLPO) or combustion (CLC) are obtained according to degree of hydrocarbon oxidation reached; if water is the oxidant, a chemical looping steam reforming (CLSR) process is obtained and its reduction produces extra hydrogen (reverse of reaction R17); on the other hand, if CO<sub>2</sub> is used, the resulting process is chemical looping dry reforming (CLDR) and a stream of CO will instead be formed (R19).

$$MeO_{x-\delta} + \frac{\delta}{2}O_2 \rightarrow MeO_x$$
 R18

$$MeO_{x-\delta} + \delta CO_2 \rightarrow MeO_x + \delta CO$$
 R19

In the case of combustion/partial oxidation, the chemical looping approach thus allows to avoid mixing oxygen directly with methane, avoiding formation of potentially explosive streams, and allows for the use of air instead of pure oxygen, as the separation of reforming and regeneration steps prevents the reforming products from being diluted by the regeneration gases, facilitating carbon capture on the flue gas of CLC and purification of products in CLPO. In the case of CLSR and CLDR, the extra currents of hydrogen and carbon monoxide produced during carrier regeneration can either be mixed with the syngas previously produced to correct its H<sub>2</sub> to CO ratio or be used on their own as chemical or energy production feedstocks.

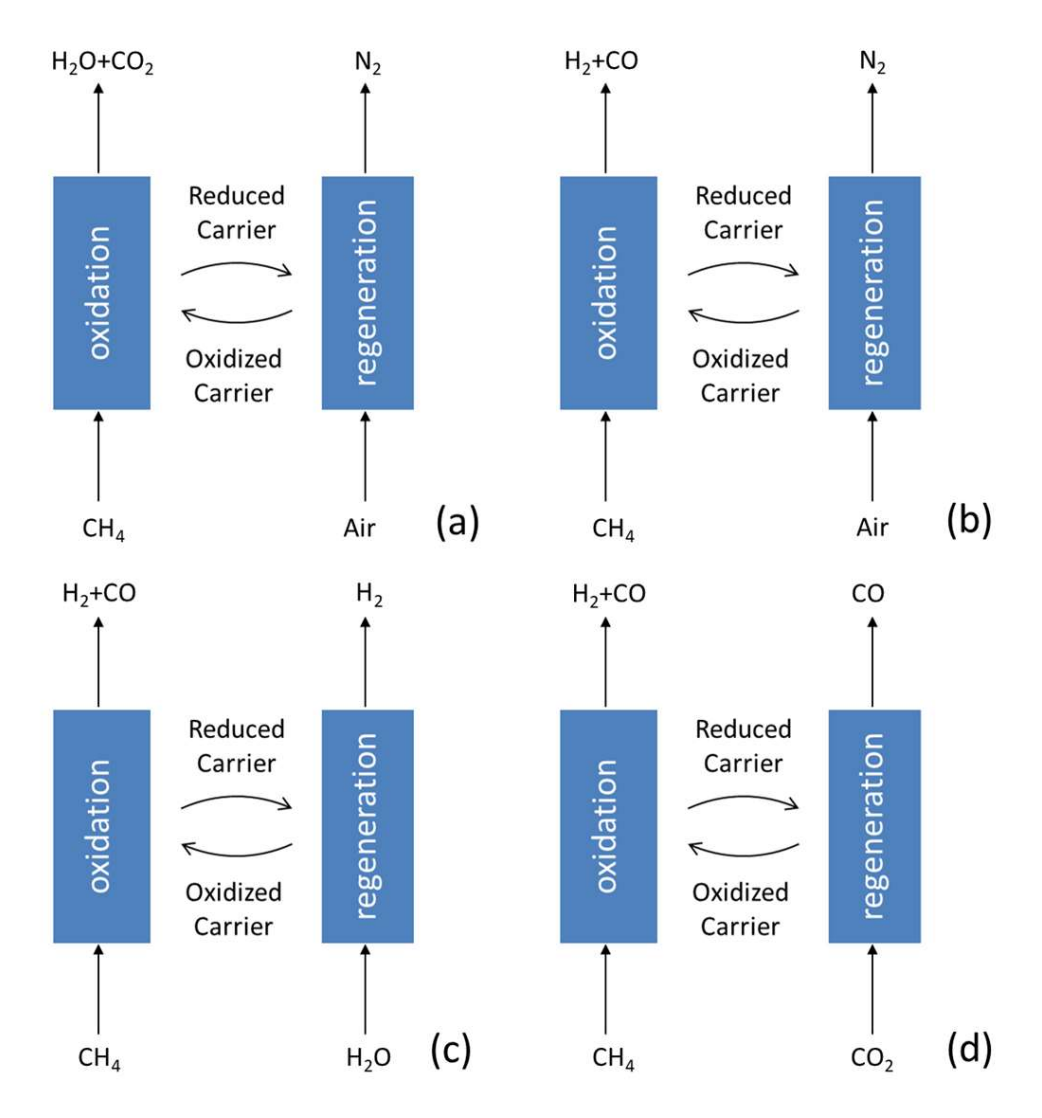


Figure 8: chemical looping processes for methane conversion: combustion (a); partial oxidation (b); steam reforming (c); dry reforming (d).

Compared to the purely thermal decomposition of the carrier used in TRC-WS, the CL approach is usually favored by the lower temperature required for the reduction of the carrier in presence of a reducing agent such as methane, which makes the use of two step processes much more feasible while also adding the opportunity to produce value added syngas to production of hydrogen by water. Furthermore, when considering reforming processes, the CL approach has another essential advantage compared to conventional designs, that is during the regeneration of the solid carrier, the oxidant can also remove any coke that was formed during the methane oxidation step through either its partial or complete combustion in the case of CLPO and CLC, through reverse Boudouard reaction in the case of CLDR, or through water reduction in the case of CLSR, thus avoiding the prevalent poisoning problem that badly affects catalyst activity in conventional SR and especially DR processes.

$$C_{(s)} + \frac{1}{2}O_{2(g)} \to CO_{(g)} \Delta H_0(298 K) = -110.53 \frac{kJ}{mol}$$
 R20

$$C_{(s)} + O_{2(g)} \rightarrow CO_{2(g)} \Delta H_0(298 K) = -393.52 \frac{\text{kJ}}{\text{mol}}$$
 R21

$$C_{(s)} + CO_{2(g)} \rightarrow 2CO_{(g)} \Delta H_0(298 K) = +173 \frac{\text{kJ}}{\text{mol}}$$
 R22

$$C_{(s)} + H_2 O_{(g)} \to C O_{(g)} + H_{2(g)} \Delta H_0(298 K) = +131.3 \frac{\text{kJ}}{\text{mol}}$$
 R23

Thanks to these advantages, chemical looping conversion of methane nowadays has been the subject of considerable research interests. Chemical looping combustion has been the subject of extended research since it first rose to interest in 1987 [316], currently standing at a TRL of 6, with a number of pilot scale plants for the combustion of natural gas, solid and liquid fuels [317,318]. Chemical looping approach to gasification (CLG) of coal and biomass has also attracted interest [319,320]. Most importantly, the chemical looping reforming of natural gas and biomethane for hydrogen and syngas production has also been the subject of increasing research efforts, with some first attempts at small scale pilot scale reactors showing promising results in terms of hydrogen yield and coke resistance [321-323]. Techno-economics analysis of the CL reforming processes has shown that while the prospected costs of hydrogen production at the current state of the art of the technology is higher than for steam reforming, they can be compensated by the CL process achieving better energetic performance and lower environmental impact, allowing the processes to compete especially in the presence of incentives such as carbon tax on greenhouse gas emissions [324,325]. In the following sections, two of the main aspects that are crucial to the development of chemical looping processes will be extensively discussed, namely the selection of oxygen carrier selection and reactor configuration.

# 1.2.2-Selection of oxygen carrier

The selection of a proper OC is perhaps the most important aspect to ensure selectivity of the reaction towards either syngas production or complete combustion and the overall efficiency of the process. The ideal properties for an oxygen carrier to be used in chemical looping processes can be summarized as follows [326,327]:

- High selectivity towards the desired reaction (syngas production/total combustion).
- High fuel conversion.
- High oxygen exchange capacity, defined as the maximum quantity of oxygen that can be reversibly exchanged during the redox cycle per mole or mass (kg or g) of material.
- Favorable reaction thermodynamics, allowing for low temperature and possibly isothermal operation.

- Fast reaction kinetics and complete regeneration upon exposure to air, water or carbon dioxide current.
- Mechanical, thermal and chemical stability even after repeated redox cycles (no sintering, no mechanical rupture due to drag or thermal stresses, no grain rupture due to phase changes or chemical reaction, no irreversible formation of inert species). Mechanical stability is especially important in fluidized bed applications.
- Coke resistance.
- Low cost (high availability, easy synthesis, no rare elements such as noble metals);
- Environmental friendliness and handling safety (no toxicity, no flammability).

Several different materials have been screened for use as OCs for both combustion and reforming applications, with several comprehensive reviews available in literature for both reforming and combustion processes [316,328,329]. The main typologies of oxides are briefly described in the following, with a greater emphasis on cerium oxide OC, which is the main subject of study of the experimental activity that will be presented in Chapter 3 of the first part of this elaborate.

# Copper oxides

Copper oxides have been subject of interest for looping processes, but they are mostly selective towards complete combustion rather than reforming, as they can undergo thermal reduction and release oxygen in gaseous form at a much lower temperature compared to other carriers [330]. This is advantageous for methane conversion, but their regeneration under isothermal operation of the cycle is difficult, thus potentially requiring temperature swing operation. They are also limited by their generally low melting point leading to fast sintering and deactivation, though adequate supports may improve their stability. Overall, purely Cu based carriers are best suited for CLC rather than reforming.

#### Ni oxides

NiO reduction to metallic Ni is mostly selective towards complete oxidation of methane rather than formation of syngas. Nickel catalysts are abundantly used in conventional steam reforming process thanks to the good activation of C-H bond leading to dissociative chemical adsorption of methane on nickel surfaces [331]; this interaction also helps in the case of oxygen carriers, as the weakening of the C-H bond allows for easier methane conversion, however it also leads to methane cracking reaction and coke deposition, causing fast deactivation of the carrier [316], with high costs, poisoning sensitivity and toxicity of the material also being obstacles to its implementation as oxygen carriers.

#### Iron oxides

Iron oxides have been extensively studied for both CLC and CLR. While the reduction from the completely oxidized state of Fe<sub>2</sub>O<sub>3</sub> to Fe<sub>3</sub>O<sub>4</sub> in presence of methane mostly results in complete combustion, the subsequent reduction of Fe<sub>3</sub>O<sub>4</sub> to FeO is mostly selective towards syngas production [332]. Subsequent complete reduction of FeO to metallic Fe is also selective towards syngas formation, though once the reduction extent is increased methane decomposition becomes instead favored [333]. Iron oxides are promising in terms of environmental compatibility and low costs [316], but are generally hindered by slow reaction kinetics and low methane conversion, as well as the fact that regeneration of the oxygen carrier is thermodynamically limited to formation of Fe<sub>3</sub>O<sub>4</sub> rather than Fe<sub>2</sub>O<sub>3</sub> when using water or carbon dioxide stream for carrier regeneration [334], thus rendering them unable to completely utilize their oxygen capacity unless regenerated in air or oxygen atmosphere. Doping the oxide with transition metals such as Cu, Co, and Y has been shown to increase oxygen mobility of the oxide at lower reaction temperature and form oxygen vacancies that promote syngas production, at the cost of more complex synthesis and increased carrier price [335].

#### Perovskites

Perovskites are a broad family of mixed oxides with basic formula ABO<sub>3</sub> [336], where A is the primary alkaline, alkaline-earth or rare earth cation coordinated by 12 other atoms, B is a secondary transition metal cation occupying face or body center sites in the crystal reticle. They are considered some of the most promising oxygen carriers for loping processes, and in particular both CLC and CLR, thanks to their customizability by apt substitution of B cations in the structure allowing to modify chemical, thermal and mechanical stability, as well as control the selectivity and conversion of the reaction through regulation of the release rate of lattice oxygen [337]; lanthanum-iron perovskites in particular appear as the best option for reforming processes. Selectivity towards complete or partial oxidation is determined by the availability of surface oxygen species [332], and it can be further tuned by partial substitution of A and B sites with other cations [338], introducing defects in the reticle. Care should be taken in the selection of A and B cations, in the cations used for their substitution and their ratio, as in some cases improper substitution may lead to structural instability, which leads to incomplete regeneration of the carrier and its decomposition into less active mixed oxide species [339], as well as poor selectivity and oxygen exchange capacity. Overall, the main limitations of perovskite are the upscaling of their complex preparation [340,341] (which requires fine tuning of substituent cations and may require the use of expensive and potentially toxic metal ions such as Ni as substituents [342]), limitations on oxygen exchange capacity when not modified with oxygen rich oxides [343], their limited surface area [344] and slow reaction kinetics [345]. Some progress has been made in the synthesis of perovskite from waste materials [346], but further investigation is still needed to obtain useful carriers for methane reforming.

#### Hexaaluminates

Hexaaluminates, hexagonal aluminate compounds with general formula AB<sub>x</sub>Al<sub>12-x</sub>O<sub>19</sub> (where A is a large metal cation, while B is a transition or noble metal substituting Al sites), have recently received notable interest for the development of catalysts [347], thanks to their high thermal stability, sintering resistance and the possibility of their structure to include significant defects while remaining stable, which provides reliable active centers for adsorption and catalysis. While stoichiometric hexaaluminates show limited activity, substitution of Al with different B metal cations greatly enhances their catalytic properties [348]. Like in the case of cation substituted perovskite, the addition of dopants in the B position offers the possibility of tuning oxygen transfer when using hexaaluminates as oxygen carriers [349]. Iron and nickel-substituted Ba, La and Ce hexaaluminates in particular have demonstrated good activity for syngas production [350–352]. However, hexaaluminates are negatively affected by their complex synthesis process, generally low surface area and lower catalytic activity compared to other traditional materials such as perovskites [353].

#### Cerium dioxide

Cerium dioxide (CeO<sub>2</sub>), also known as ceria, has been consistently studied for its role as catalysts and oxygen carriers [354], being characterized by its highly stable fluorite face centered cubic structure, shown in Figure 9, which is be maintained even at high temperature and also when ceria is reduced to greatly non-stoichiometric oxygen content ( $\delta$  up to 0.5), according to the reaction:

$$CeO_{2(s)} \rightarrow CeO_{2-\delta(s)} + \frac{\delta}{2}O_{2(g)} \Delta H_0(298 K) = +368.34 \frac{\text{kJ}}{\text{mol}} (complete \ reduction \ to \ Ce_2O_3)$$
 R24

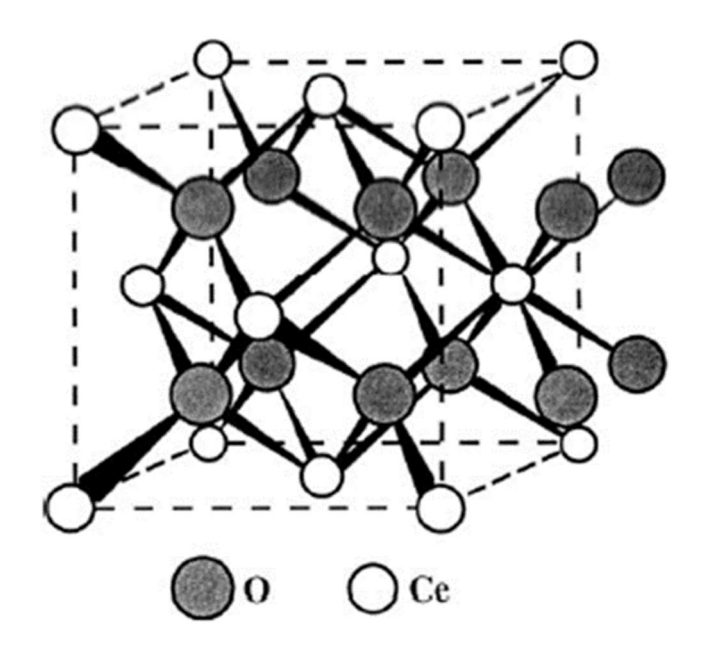


Figure 9: the fluorite structure of cerium dioxide [354].

The great stability of the fluorite structure over a continuous range of reduced forms and the excellent lattice oxygen mobility granted by it are the key to cerium oxide catalytic and oxygen storing capabilities [355,356], with ceria based catalysts having been so far used in several fields: in particular, CeO<sub>2</sub>-ZrO<sub>2</sub> solid solutions are the most common option for the Three way catalyst process used for emission abatement in automotive transport, reducing nitrogen oxides to nitrogen while oxidizing CO and unburned hydrocarbons into CO<sub>2</sub>. Ceria is also commonly used to facilitate soot combustion in diesel engines. CeO<sub>2</sub>-based catalysts have been investigated for use in innovative technologies such as fuel cells for power generation [355] and oxidative/non-oxidative coupling of methane for C<sub>2</sub> hydrocarbon synthesis [357,358], as well as for other more conventional applications such as the water-gas shift reaction [359,360], sulfur abatement from gaseous flows and hydrocarbon dehydrogenation [361], wastewater treatments [362], biomass conversion [363], methane combustion [364] and conventional PO [365–367], SR [368,369] and DR [369,370] processes for methane and higher hydrocarbons. Most recently, ceria-based nanomaterials have also found use in biomedical applications thanks to their antioxidant and anti-microbial activity [371,372].

Cerium dioxide is therefore a well-known material. Figure 10 reports the phase diagram for cerium oxides as reported by Okamoto [373], evidencing the existence of the non-stoichiometric species in between CeO<sub>2</sub> and reduced Ce<sub>2</sub>O<sub>3</sub> and the homogeneity of their solid solution. The oxygen non-stoichiometry manifests in the form of defects in the crystal lattice, particularly ionized oxygen vacancies, which are present as single vacancies at low reduction extent or as dimers and trimers with coupled with reduced Ce<sup>3+</sup> cations for higher reduction [374]. In Kroger-Vink notation, we have:

$$2Ce_{Ce}^{X} + O_{O}^{X} \longleftrightarrow 2Ce_{Ce}' + V_{O}^{\bullet \bullet} + \frac{1}{2}O_{2(g)}$$
 R25

Where  $Ce_{Ce}^X$  and  $O_O^X$  are, respectively, the Ce<sup>4+</sup> cation and the O<sup>2-</sup> anion of the oxidized CeO<sub>2</sub> lattice, while  $Ce_{Ce}^{\prime}$  and  $V_O^{\bullet\bullet}$  are the reduced Ce<sup>3+</sup> cation (electronic defect) and the positively charged oxygen vacancy, respectively. The presence of surface oxygen vacancies and the diffusion of oxygen ions in the crystal reticle play a crucial role in the reactivity of ceria as they affect adsorption of molecules and rate of oxygen transfer [375,376]. As observed in Figure 10, cerium dioxide is also characterized by a high melting point ( $\approx$ 2200°C), which makes it resistant to sintering.

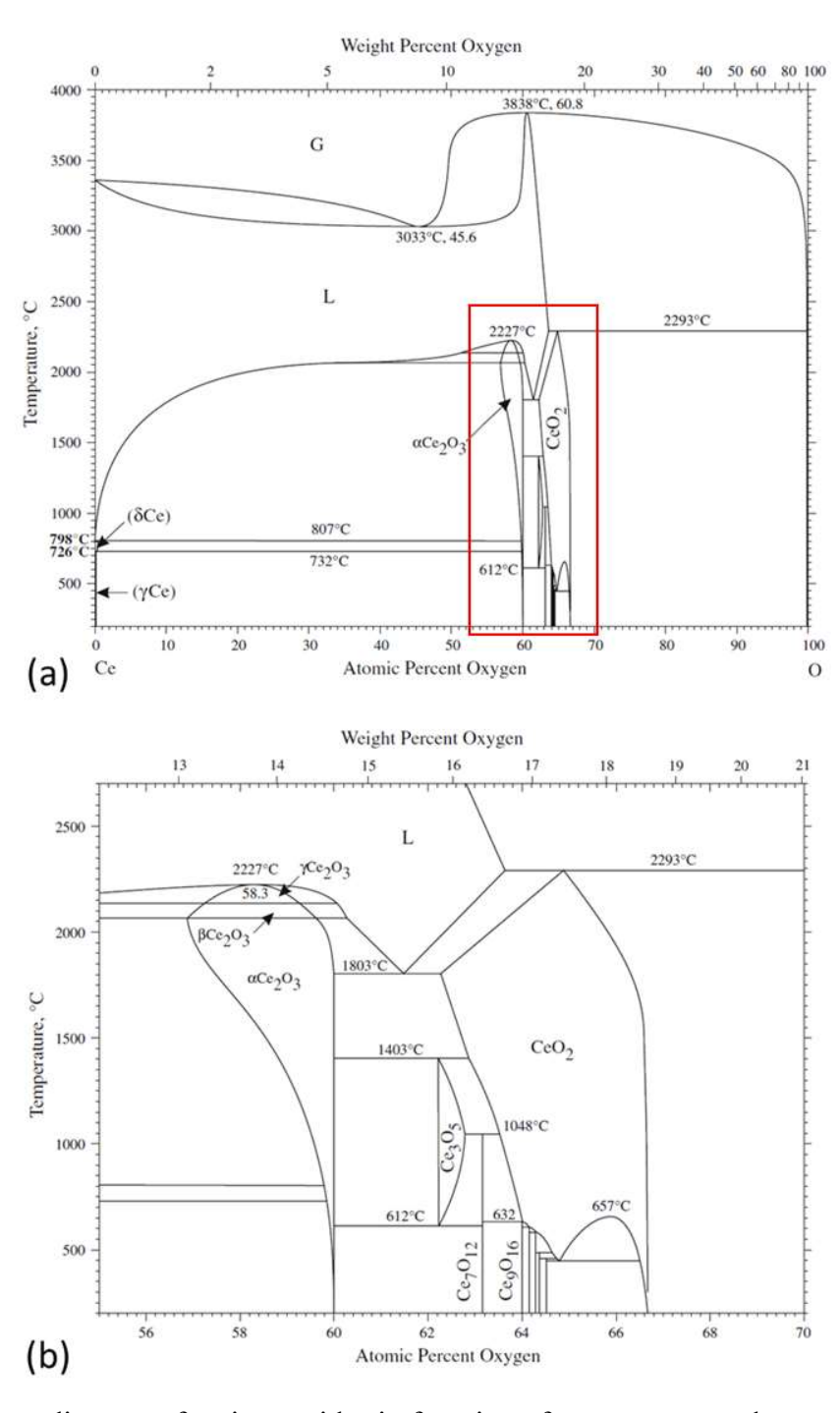


Figure 10: phase diagram of cerium oxides in function of temperature and oxygen content [373]: complete diagram (a); detail of the area in the red rectangle, atomic O content 55 to 70% (b). G=gas phase, L=liquid phase.

Fast redox kinetics, good lattice oxygen diffusion and oxygen storage capacity and thermochemical stability make cerium dioxide an ideal material for looping processes. Cerium is also the most common of the rare-earth elements, with an availability that is comparable to copper, nickel and zinc [377] and it is the easiest to extract from rare-earths rich bastnasite and monazite mixed minerals,

being commonly recovered by solvent extraction [378]. Its abundance and comparatively easy recovery maintain its price limited compared to not only other rare earths, but also to other conventional metals used for catalytic applications. As seen in Figure 11, except for the 2011 spike caused when China, one of the principal rare-earth exporters, implemented more stringent export policy and significantly reduced the export quotas following disputes with Japan [379], the price of cerium is expected to remain stable at least up to 2030 [380], remaining comparable if not lower than the forecasted prices for nickel (\$22,500-\$23,500) and copper (\$15,800) for the same time period [381,382].

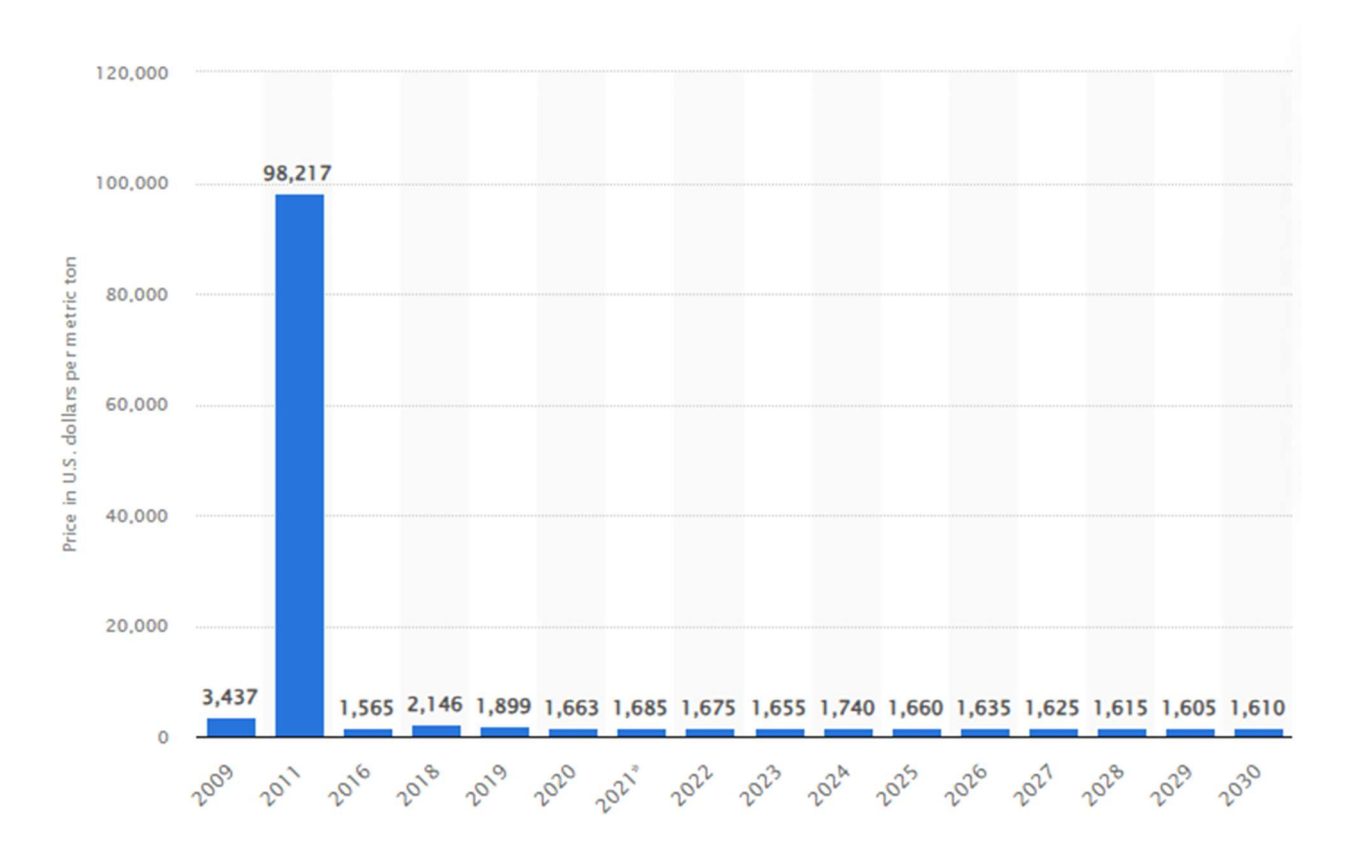


Figure 11: historic and forecasted price of cerium for the years 2009-2030 [380].

In conventional reforming, cerium dioxide has been consistently tested as support for active metal species such as Ni, particularly for the DR process, as the release of its mobile lattice oxygen species allows for the oxidation of coke deposited on its surface, thus preventing catalyst deactivation [369] and marking cerium oxides as coke resistant materials.

Cerium oxides were first considered as materials for the two-steps thermochemical looping water splitting, their reduced form being able to be quickly and completely oxidized by water, splitting it even at low temperature [383].

$$CeO_{2-\delta(s)} + \delta H_2O_{(g)} \rightarrow CeO_{2(s)} + \delta H_{2(g)} \quad \Delta H_0(298 \text{ K}) - 126.51 \frac{\text{kJ}}{\text{mol}} \text{ (regeneration } Ce_2O_3 \text{ to } CeO_2)$$
 R26

Reduced cerium oxides have also been observed to be able to similarly split carbon dioxide [384], therefore providing an interesting opportunity for carbon dioxide utilization.

$$CeO_{2-\delta(s)} + \delta CO_{2(g)} \rightarrow CeO_{2(s)} + \delta CO_{(g)} \Delta H_{298K}^0 = -85.4 \frac{kJ}{mol} (regeneration Ce_2O_3 to CeO_2)$$
 R27

Unfortunately, to achieve pure thermal reduction of cerium dioxide, temperature above 2000 K is needed to achieve complete cerium dioxide reduction to Ce<sub>2</sub>O<sub>3</sub>, which greatly limits the feasibility of a purely thermal cycle using undoped cerium oxides as OC, particularly if the reaction heat has to be provided through renewable sources such as solar energy, for which energy efficiency is still low [385]. Lower reduction extents can be reached at lower temperature and still be used of effective splitting, but this comes at cost of lower kinetics and incomplete utilization of the oxygen exchange capacity of the material. However, thermodynamic simulations and experimental results have shown that the presence of methane in chemical looping reforming allows to significantly lower the temperature required for complete CeO<sub>2</sub> reduction compared to the pure thermal case [386,387], with visible methane conversion and syngas production at temperature as low as 800°C, which are suitable for isothermal operation of the redox cycle.

$$CeO_2 + \delta CH_4 \rightarrow \delta CO + 2\delta H_2 + CeO_{2-\delta} \Delta H_{298K}^0 = 332.3 \frac{kJ}{mol}$$
(complete reduction to  $Ce_2O_3$ )

Figure 12 synthetizes the looping cycle for a cerium dioxide oxygen carrier. Reaction 5 and 6 of regeneration step correspond to CLSR, reactions 7 and 8 correspond to CLDR, reactions 9,10 and 11 correspond to CLPO.

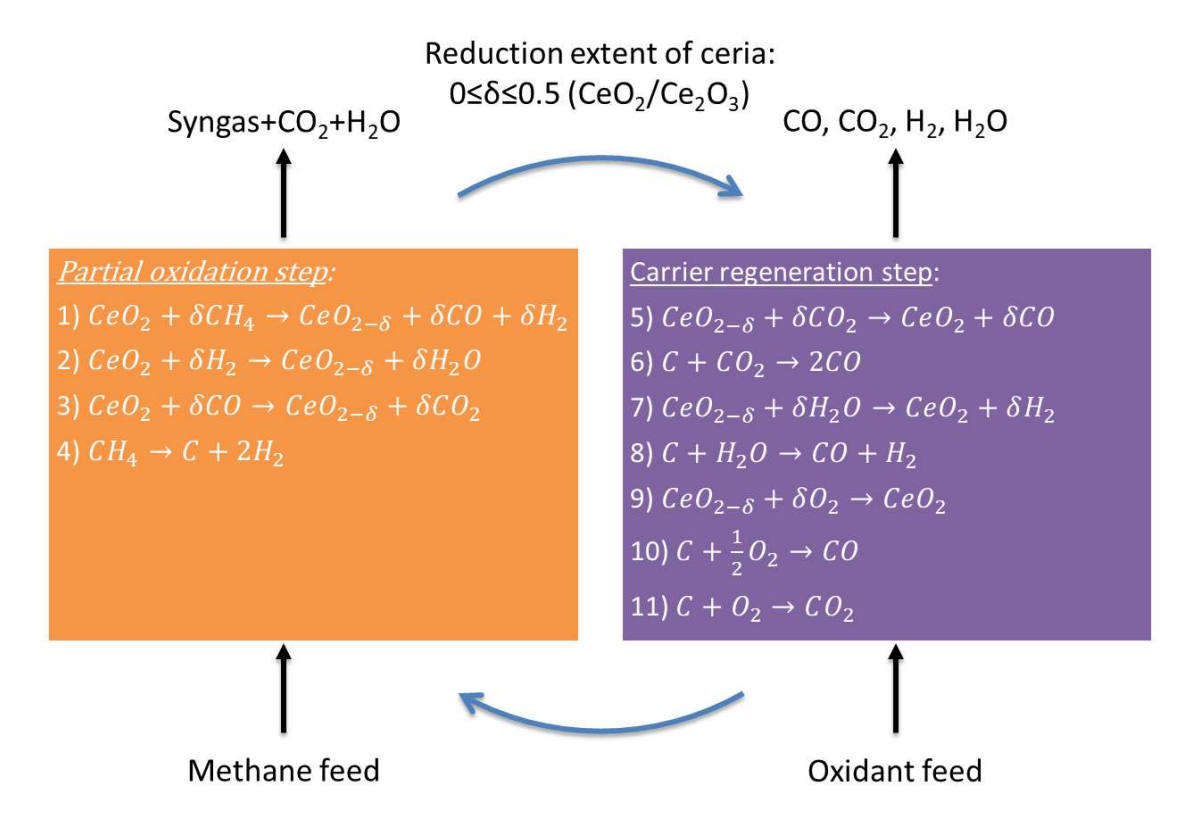


Figure 12: methane chemical looping reforming cycle for cerium dioxide oxygen carriers.

The use of ceria for methane chemical looping reforming was first studied in the works by Otsuka et al. [386,388], where it was observed that the oxidation of methane is highly selective to production of syngas, with very limited formation of CO<sub>2</sub> and water at the start of reaction. The initial complete combustion was attributed to the presence of highly available surface oxygen, which is then quickly depleted leaving place to the diffusion-limited transfer of bulk oxygen species. Interestingly the H<sub>2</sub>/CO ratio of the produced syngas remained stable to 2 for most of the reaction time, even when the carrier was mixed with Pt, despite Pt commonly catalyzing the combustion reaction. Pt addition significantly enhanced the kinetics of methane oxidation, while addition of Pd gave rise to significant carbon deposition; on the other hand, addition of alkaline metals showed no effect on conversion. When the carrier was regenerated in CO<sub>2</sub>, only 82% of the oxygen capacity could be recovered, and the following reduction showed lessened carbon dioxide and water formation, likely demonstrating that the weaker oxidizing strength of CO<sub>2</sub> did not allow for the recovery of the surface oxygen. Stable operation cycles were observed for a range of temperature 873-1073 K.

Ceria was thus found to be a promising material for the chemical looping conversion of methane to syngas and subsequently received great attention from the scientific community. For example, a recent comparison between chemical looping steam reforming on cerium oxide oxygen carrier and iron oxide carrier displayed cerium oxide superior performance as oxygen carrier, demonstrating

higher stable syngas yields, faster kinetics and enhanced regeneration for the ceria carrier [334]. Table 2 reports a brief review of pure cerium dioxide oxygen carrier testing in literature.

Table 2: review of literature for CL reforming using pure CeO<sub>2</sub>; Oxi=oxidant used for regeneration; n.a.=data not available, STP=standard temperature and pressure; TPR=temperature programmed reduction; TPO= temperature programmed oxidation.

Source	Method	m <sub>CeO2</sub>	D <sub>p</sub>	Preparation	T <sub>PO</sub>	CH <sub>4</sub>	$Q_{PO}$	Tregen	Oxi	%Oxi	Qregen
		(g)	(µm)		(°C)	(%)	(L/min)	(°C)			(L/min)
[389]	TPR/TPO	0.30	n.a.	Cerium nitrate precipitated with NH4OH and calcined at 1000°C	900	5	0.06	920	O <sub>2</sub>	10	0.06
[390]	TPR Tubular reactor	1.00	<106 (coat)	Cerium nitrate hexahydrate, coating precipitated over ZrO <sub>2</sub> support (10% CeO <sub>2</sub> /ZrO <sub>2</sub> ), then grounded, sieved and calcined at 899.85°C	799.85 to 899.85	10	30 (*)	799.85	H <sub>2</sub> O	27	37 (*)
[391]	Quartz tubular reactor	1.80	20 to 40 (mesh)	Cerium nitrate hexahydrate, precipitation, then grounded and calcined. Calcined at 800°C	850	16.67	0.06 (**)	700	H <sub>2</sub> O	n.a.	H <sub>2</sub> O 0.18 (***)
[392]	TPR/TPO	0.20	40 to 75	Cerium nitrate hexahydrate precipitated with NH4OH, with and without CTAB and H2O2 addition, calcined at 500°C or 900°C	900	1	0.03	800	O <sub>2</sub>	1	0.03
[393]	TPR/TPO	0.02	40 to 75	Cerium nitrate hexahydrate hydrothermal preparation with polyethylen glycol (PEG) and hexamethylenetetr amine (HMTA), calcined at 500°C  Cerium nitrate hexahydrate microwave assisted hydrothermal preparation with	900	1	0.03	800	O <sub>2</sub>	1	0.03

				PEG and HMTA,							
				calcined at 500°C							
[394]	Solar	0.30	40	Commercial	1000	40	0.50	1000	CO <sub>2</sub>	40	0.50
	reactor		to	cerium dioxide							
			75	powder as							
				purchased,							
				calcined at							
				1000°C							
				Cerium nitrate							
				hexahydrate:							
				-hydrothermal							
				templating with							
				glucose, calcined							
				at 1000°C							
				-self-assembled							
				with surfactant							
				Pluronic P123 and							
				calcined at 1000°C							
[205]	Tubular	0.15	0.005	Cerium acetate	899.85	8	0.25	899.85	CO <sub>2</sub>	4	0.25
[395]	reactor, IR	0.13	to	hydrate, flame	899.83	0	0.23	899.83	CO2	4	0.23
	heating		0.063	made preparation							
	neuting		0.003	made preparation							
				Cerium nitrate,							
				synthesis of							
				flower like							
				nanoparticles,							
				calcined at							
				599.85°C in N <sub>2</sub> ,							
				399.85°C in air							
				Cerium nitrate							
				hexahydrate							
				Sol-gel Pechini's							
				method, calcined							
				at 399.85°C							
				Commercial							
				cerium dioxide							
				powder, powder							
[396]	Solar	0.1	40	as purchased  Commercial	1100	mov	1	n o	n o	n o	n o
[066]	moving	to	40	cerium dioxide	to	max 10%	to	n.a.	n.a.	n.a.	n.a.
	particle			powder, powder	1350	10/0	4				
	reactor	$0.6\frac{g}{s}$		as acquired	1550		(**)				
[397]	Tubular	0.250	Nanoparticle	Cerium nitrate	899.85	10	0.25	899.85	CO <sub>2</sub>	CO <sub>2</sub>	0.25
[	reactor, IR	(±0.005)	1	hexahydrate,					H <sub>2</sub> O	4%	
	heating			precipitation and						Water	
				formation of						(****)	
				nanoparticles.							
				Calcined at							
				899.85°C							
L	<u> </u>	1	<u> </u>	<u> </u>	<u> </u>		<u> </u>	L	·		

[398]	Solar	300	500	Commercial	790	10	12	790	CO <sub>2</sub>	75.02	4.00
	reactor,	to	То	cerium dioxide	to	to		to			
	fixed bed	350	1400	powder calcined at	1170	25		1170			
				1200°C then							
				ground and sieved							
[399]	Solar	17.02	n.a.	Commercial	900	8.33	2.3	900	H <sub>2</sub> O	H <sub>2</sub> O	Ar
[]	reactor,	to		cerium dioxide	to	to	to	to	CO <sub>2</sub>	200	2
	fixed bed	27.98		powder:	1050	16.67	2.6	1050		(*****)	to
				- porous foam			(**)			$CO_2$	2.2
				formation with			( )			0.2	(**)
				solid carbon						(**)	
				particles, (pore							
				former) and							
				organic							
				polyurethane							
				template. First							
				calcination at							
				1000°C, second							
				calcination at							
				1400°C							
				-porous foam formation with							
				solid carbon							
				particles, (pore							
				former) and							
				organic							
				polyurethane							
				template. calcined							
				at 1000°C							
				-powder as							
				acquired mixed							
				with Al <sub>2</sub> O <sub>3</sub> (size							
				1.2 mm),							
				calcination at							
				1000°C only for							
				Al <sub>2</sub> O <sub>3</sub> . Mass ratio							
				$Al_2O_3/CeO_2 = 2.2$							
				-powder as							
				acquired							
[400]	Solar	17.01		Commanical	050	50	0.4	1000	II.O	55	II.O
[400]	tubular	17.01	n.a.	Commercial cerium dioxide	950	30	0.4 (**)	1000	H <sub>2</sub> O	55	H <sub>2</sub> O 200
		to			to		(**)				(****)
	reactor, fixed bed	18.37		powder:	1050						
	nxed bed			-powder as							Ar
				purchased							0.2
				-porous foam							(**)
F4013	0.1	10.25	D	formation	050	0.5	0.4	050	11.0		
[401]	Solar	18.37	Porous monolith	Polymer	950	0.5	0.4	950	H <sub>2</sub> O	55	Ar
	monolithic		mononth	templating	to		(**)	to			0.2
	reactor				1050			1050			(**)
											H <sub>2</sub> O
											200
F4023		0.25	22		000	20	0.12	1100	00	50	(*****)
[402]	Alumina	0.25	32	Commercial	900	20	0.12	1100	$CO_2$	50	0.120
	tubular			cerium dioxide	to	to	(**)				(**)
	reactor			powder, sample	1100	50					
			]	crushed and							

				sieved to desired							
				granulometry							
F4027	T 1 1		NI CI	0 : :. :	000	0	0.25	000	CO	CO	0.25
[403]	Tubular	n.a.	Nanoparticle	Cerium nitrate	900	8	0.25	900	CO <sub>2</sub>	CO <sub>2</sub>	0.25
	reactor, IR			hexahydrate,					H <sub>2</sub> O	4%	
	heating			precipitation and						Water	
				formation of						(*****)	
				nanoparticles.							
				Calcined at 900°C							
[404]	TPR/TPO	5	200	Commercial	940	4	28.8	940	O <sub>2</sub>	21	28.8
	Fluidized		to	cerium dioxide		to	(******)				(******)
	bed reactor		400	powder, and		8					
				commercial							
				cerium dioxide							
				powder mixed							
				with 30% wt.							
				Al <sub>2</sub> O <sub>3</sub> ; samples							
				pressed and							
				crushed, calcined							
	2			at 900 or 1200°C							

(\*) cm<sup>3</sup>/min (STP); (\*\*) NL/min; (\*\*\*) g/min; (\*\*\*\*) bubbled in 30 mL/min Ar and diluted with 220 mL/min Ar; (\*\*\*\*\*) mg/min; (\*\*\*\*\*\*) bubbled at 95°C; (\*\*\*\*\*\*) fluidization velocity in cm/s

While addition of noble metals such as Pt or Ru may enhance methane conversion at lower reaction temperature [386,405], their high costs and limited availability pose a significant limit to their use in commercial oxygen carriers. Transition metals are therefore often chosen as cheaper alternatives. Mixture of ceria with iron oxides [406,407], cobalt [408,409] and nickel [410,411] have all been tested for methane reforming reactions. While the addition of iron oxides has been shown to lower the selectivity of reaction towards dry reforming and negatively affects process kinetics, Co and Ni addition have both showed enhanced conversion of methane and syngas production, with Ni catalysts being more active and leading to higher methane conversion, but also higher coke deposition [412]. On the other hand, the addition of metals to the carrier and the use of more complex preparation methodologies all contribute to increase the cost of the material, can be negatively affected by sintering, and, in nickel case, it provides an additional source of concern for safety and environmental sustainability due to the toxicity of nickel [413], particularly when considering the disposal of spent oxygen carrier. Thus, the use of pure cerium dioxide, possibly associated with adequate supports, still merits interest. Pure cerium dioxide lower activity compared to metal loaded carriers may be compensated by optimization of reaction conditions such as process temperature, carrier structure and selection of adequate process times for the reforming and regeneration steps, as well as control of the methane and oxidant flowrates and the maximum carrier reduction extent reached. For example, Warren et al. determined that methane conversion and syngas yield significantly increase at higher operating temperature, typical of endothermic reactions, but that methane residence time also significantly affecting reaction selectivity, with long residence times leading to increased incidence

of total combustion on reaction products [398]. Excessively high methane flowrates on the other hand can cause carbon deposition to prevail, due to kinetic limitations in oxygen transport [399,402]. Previous literature suggests a very small reduction extent is required to avoid deposition of carbon, but this leads to poor utilization of the total oxygen capacity. Investigation of optimization of process conditions is thus a primary aspect of the development of the chemical looping process.

# 1.2.3-Looping configuration: fixed vs fluidized bed

The chemical looping approach, both for combustion and reforming, can be performed either in fixed bed or fluidized bed configuration, with both approaches having their strengths and drawbacks. Figure 13 illustrates the differences between these operating regimes.

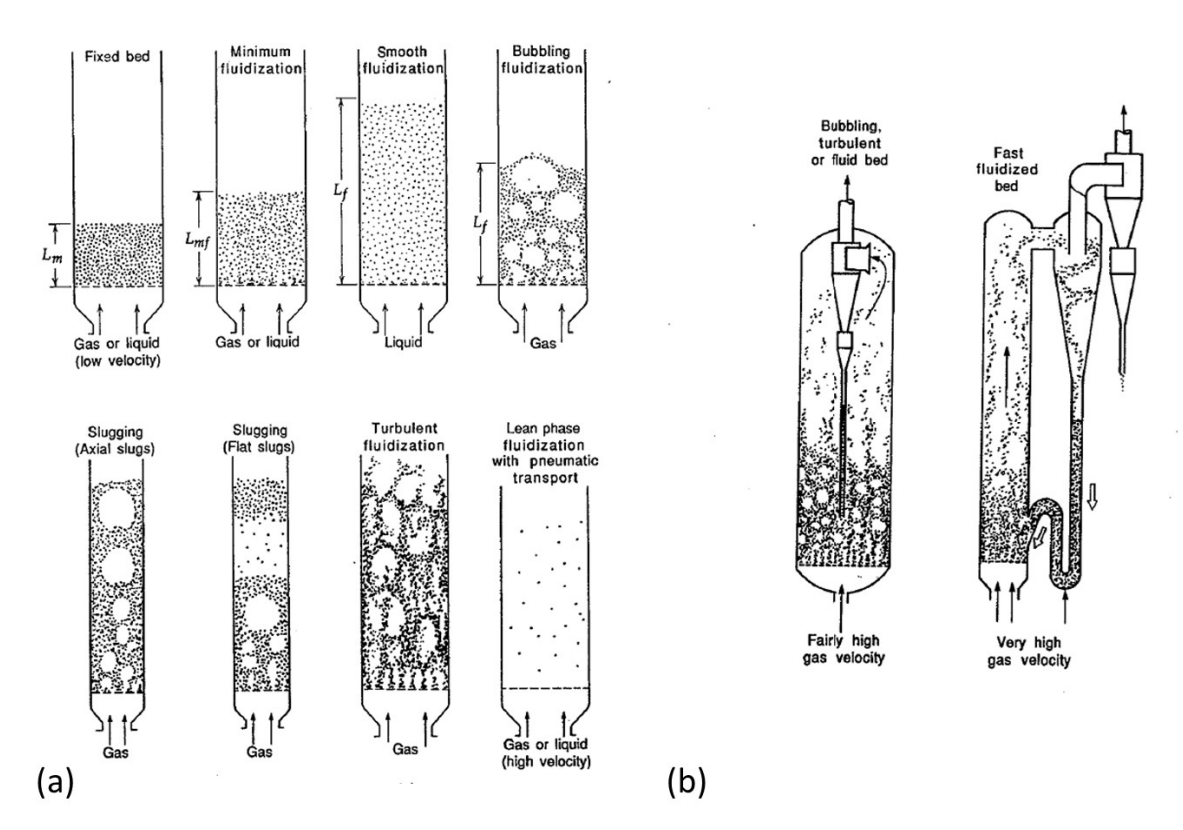


Figure 13: fixed and fluidized bed operating regimes [414]: fixed bed and non-entrainment fluidization (a); circulating fluidized beds (b).

#### 1.2.3.1-Fixed bed

Fixed bed operation, sometimes referred to as gas-switch process [415], is the simplest from a conceptual point of view, and the easier to scale up, particularly in the case of pressurized systems [416]. It is achieved simply by alternating the methane feed and the regeneration feed to the reactor, and continuous operation can be achieved by having multiple reactors working in parallel with alternated reaction steps: when one reactor is in regeneration, another is oxidizing methane and then

they switch operation. The great advantage of this configuration is that it does not require any extra energy or complex design for solid movement and can allow very good thermal integration between the endothermic partial oxidation and the generally exothermic carrier regeneration step [417]. The heat accumulated in the solid carrier during regeneration is used to fuel the following partial oxidation step. Also, in a fixed bed, the carrier undergoes very limited drag forces, therefore the risk of carrier degradation due to attrition, causing particle grinding into dust, is very limited under normal operating conditions [418]. Finally, the fixed bed configuration also does not require the addition of equipment for gas-solid separation such as cyclones. On the other hand, operating with a gas switching process requires the use of an expensive high temperature valve apparatus for fast switching of gas currents is needed [419], which is particularly difficult to operate reliably. Furthermore, in the fixed bed approach the contact between the reactive gas phase and the solid carrier is intrinsically limited: contact can only happen on the solid surface area, which is limited by geometry and porosity, and the gas can form preferential pathways and not come into contact at all with most of the carrier before exiting the reactor. Heat transfer to and from the reactor are also limited by the convective transport in the solid and undesired temperature gradients can be easily formed [417,420], particularly in the presence of highly endothermic and exothermic reactions. Sintering and surface area reduction of particles is also favored, as they are strongly in contact with each other for the whole length of the high temperature process. Finally, as continuous operation requires alternated switch of the reactor between partial oxidation and carrier regeneration step, cross contamination in the product gases is also possible, with residual products of the previous step being still present in reactor outlet at the start of the new step [416], and even in the case were introduction of a purge gas current flowed into the reactors between each step is used to prevent this contamination, residual purge would still cause initial product gas dilution at the start of the following step.

#### 1.2.3.2-Fluidized bed

Fluidized beds have long been introduced in the field of combustion since its first appearance in the 1970s [421]. According to the gas feed velocity, fluidized beds can be operated under different regimes [422], from the simple bubbling bed fluidization, in which the gas keeps the solids suspended by opposing their weight and forms bubbles, but does not transport the solid outside the reactor, to the more complex circulating beds, where the solid is completely entrained by the gas flow, to be then intercepted at reactor outlet and returned to the reactor (see Figure 13b).

Generally, fluidized beds are able to provide a more intimate contact between gas and solid phases [423], allowing for improved heat and mass transfer and avoiding formation of preferential pathways and dead zones where contact between phases is absent. The constant movement of the solid particles

also helps to prevent their aggregation. On the other hand, in a fluidized bed the problem of drag resistance of the OC becomes a crucial matter [424], as the constant movement of the particles can lead easily to their grinding and subsequent loss as the powder is entrained away by the gas; OC for fluidized bed applications therefore need much higher mechanical resistance than those destined to fixed bed utilization. The gas-switch approach discussed for fixed beds has also been applied to CLR in fluidized beds with promising results [425,426], but the same observations on the need of high temperature valves and potential gas mixing during step changes still hold true. Another alternative is the coupling of two circulating fluidized bed reactors, with the solid being continuously transferred from one reactor to the other, with one reactor carrying out the reforming reaction and the other regenerating the carrier. This approach was one of the first proposed and the most studied for chemical looping, as it allows for the physical separation of the partial oxidation and regeneration reactions, reducing the possibility of product gases mixing between the two phases and also allowing the two reactions to hypothetically operate at different temperatures in a completely continuous process which does not require alternating flowrates. However, the complex circulation system for the solids is difficult to operate and scale up [427]: the two reactor beds need to be pressurized separately, and any pressure imbalance that may occur between the two can lead to insufficient solid circulation if not complete clogging of the solid transport [428]. The possibility of having gas leaks in the circulation system is also still present, and the movement of solids is energy intensive. Finally, it is difficult to optimize the heat insulation of the transfer system to achieve thermal integration of the process, which can lead to lower overall energetic efficiency.

# 1.2.4-Final remarks on chemical looping reforming

The CL approach offers great opportunities for achieving more sustainable and cost-effective reforming technologies. Multiple technoeconomic analysis of the process with various oxygen carrier have consistently shown CL capacity of obtaining hydrogen and syngas production at costs competitive with conventional SR, at higher energetic efficiency and lower carbon footprint [429–433], and its ability to realize technically feasible dry reforming for CO<sub>2</sub> utilization [434,435]. Among the various tested OC, cerium dioxide, perovskite and hexaaluminates appear as the most promising choices for the production of hydrogen and syngas, with ceria providing advantages in terms of simplified synthesis. While the traditional circulating fluidized bed approach for chemical looping processes difficulties in scale up, these complications may be successfully overcome by operation in fixed or fluidized bed gas-switch configuration. A crucial aspect of development of CL processes is the optimization of reaction conditions, with reaction selectivity depending strongly on process temperature and OC reduction extent. Information on optimized reaction conditions is still

lacking in literature. Novel development of non-toxic OC and OC based on widely available natural materials and wastes would be beneficial to the development of sustainable processes. Finally, despite cerium dioxide being considered one of the most promising materials for syngas CL production, most of the literature presents data obtained only on limited quantities of OC. As such, the experimental activity that will be discussed in this thesis proposes investigating more in depth the activity of cerium dioxide for CLPO and CLDR processes. Natural chromite minerals, CuO-CeO<sub>2</sub> and CeO<sub>2</sub>-Al<sub>2</sub>O<sub>3</sub> mixtures are also investigated for reforming activity. Furthermore, development of process simulation for CL processes can provide useful data for optimization of reaction conditions, but so far, simulation efforts for these processes, and particularly for cerium dioxide oxygen carriers, have been limited in literature.

# 1.3-Experimental evaluation of chemical looping partial oxidation and dry reforming fixed bed reactor with focus on cerium dioxide oxygen carrier in and modelling activity

# 1.3.1-Scope of the activity

Cerium dioxide is considered one of the most promising OC for CL reforming processes of methane, particularly CLDR. Obtaining a clear understanding of optimal reaction conditions for CL process using ceria oxygen carrier is essential to be able to develop industrially viable processes. It has been shown in previous literature that both reaction temperature and carrier reduction extent are essential parameters in the control of reaction selectivity, but studies detailing optimal cerium dioxide conversion have been limited. Studies have focused on a temperature range for reaction between 700 and 1300°C and mainly on steam reforming rather than CLDR (see Table 2 of Section 1.2.2), testing limited quantities of cerium dioxide. Further testing of cerium dioxide using greater mass of OC and development of simulations for the chemical looping process are essential for the optimization of CL operation. The use of supports and mixed oxides has also shown success in increasing syngas yield and carrier activity. The addition of metal species and mixed oxides might improve cerium activity. Nickel has been observed to improve cerium dioxide activity in methane splitting, increasing methane conversion and hydrogen production but also increasing the influence of coke deposition on the reaction. Furthermore, the cost and toxicity of nickel would suggest the need to find alternatives to increase methane activation. On the other hand, copper oxide has been commonly tested as a catalyst for complete combustion, but it is not clear whether it would be possible for mixed copper oxide and ceria to be used also for reforming applications. For example, Wang et al. [436] demonstrated the synthesis of CuO-CeO<sub>2</sub>-ZrO<sub>2</sub> mixture selective for methane reforming. Addition of alumina has also been shown to increase ceria activity [404], with 30% wt. alumina-ceria mixture appearing to offer increased reaction yields compared to pure ceria, but stability of this mixed carrier has not been clearly tested. Thus, stability, activity and selectivity of cerium dioxide-CuO mixture and CeO<sub>2</sub>-Al<sub>2</sub>O<sub>3</sub> mixture have been investigated.

Iron oxides have also shown activity for CLR, and the utilization of naturally available materials as OCs could lead to a remarkable reduction in production costs. Chromite is a natural mixture of mostly chromium and iron oxide, as well as other species such as magnesium, alumina and silica [437], commonly used as industrial source of Cr [438] and as foundry sand in metallurgy [439], thanks to its high refractory properties. As a catalyst, chromite and metal-chromite have been found useful for CO oxidation [439], hydrogenation reactions [440,441] and hydrocarbon combustion [442,443] and

have been observed in nature to contribute to abiotic methane formation [444]. While laterite ores obtained from chromite mine wastes have been observed to be active as oxygen carriers [445,446], the activity of the parent mineral has not been tested in literature thus far. Given the significant presence of iron oxides species in low grade chromite sand, it might be expected that these materials would be able to provide methane conversion in chemical looping operation.

Therefore, in the present thesis the optimization of chemical looping methane reforming using various oxygen carriers is investigated. Namely, the following points are addressed:

- The activity of cerium dioxide based carriers has been assessed. Pure cerium dioxide, coppercerium oxides mixture and cerium-alumina mixture are tested for methane conversion, syngas yields, selectivity and coke deposition.
- Activity of natural chromite ore as oxygen carrier is assessed.
- Optimal reaction times for the chemical looping process are investigated in bench scale reactor tests. The trade-off between methane conversion, OC conversion, reaction yield and selectivity is analyzed in function of reaction conditions.
- Regenerability of the carrier in both oxygen and carbon dioxide is investigated.
- A first attempt at modelling the reaction process using kinetic data available in literature is performed.

Following up on these activities, future developments will further address process optimization. Other novel carriers will need to be addressed, as well as further optimization of cerium dioxide based carriers to obtain nickel free active materials for the methane reforming reaction, and detailed kinetic data will be obtained to develop complete numerical models for process optimization.

### 1.3.2-Materials and methods

# 1.3.2.1-Material preparation

Redox tests have been performed on four different types of OCs, being natural chromite sand (Cromitec 400, hereafter defined Chro), commercial CeO<sub>2</sub> (PI-KEM, Tamworth, UK, purity 99.9%), CeO<sub>2</sub>-Al<sub>2</sub>O<sub>3</sub> mixture (30% wt. in Al<sub>2</sub>O<sub>3</sub>, KMS96, Martinswerk GmbH, Bergheim, Germany) and CeO<sub>2</sub>/CuO (50% mol in CuO, Merck, Darmstadt, Germany) granules. Chromite sand was tested without previous aggregation, as it already displayed high granule dimensions, while the other samples were prepared from fine powders by uniaxially pressing the powder into pellets and then crushing and sieving them to the desired granulometry. Its composition as reported from the producer is reported in Table 3.

CeO<sub>2</sub> samples were prepared by pressing them at either 90 or 250 MPa. The CeO<sub>2</sub>-Al<sub>2</sub>O<sub>3</sub> sample was prepared by pressing at 250 MPa carefully mechanically mixed CeO<sub>2</sub> and Al<sub>2</sub>O<sub>3</sub> powder, while the

CeO<sub>2</sub>-CuO sample was obtained by mixing the two oxides in a 50% mol ratio and then pressing them at 90 MPa. All CeO<sub>2</sub> based samples were crushed and sieved to a granulometry of 0.595 to 0.841 mm. The obtained granules were then calcined in air at 900 °C for 1 h (heating rate of 3 °C/min starting from room temperature). The obtained samples were characterized by X-ray powder diffractometry (XRD) in a Bruker D8 Advance (Bruker–Karlsruhe, Karlsruhe, Germany, D) diffractometer.

Table 3: reported composition of chromite sand.

Species	% wt.
Cr <sub>2</sub> O <sub>3</sub>	47
FeO	26
Al <sub>2</sub> O <sub>3</sub>	15
MgO	10
SiO <sub>2</sub>	1

#### 1.3.2.2-Thermogravimetric Analysis (TGA)

CeO<sub>2</sub> redox behavior was first investigated on a STA 449 C Jupiter thermogravimetric balance (NETZSCH, Selb, Germany). CeO<sub>2</sub> reduction was performed in 4% vol. CH<sub>4</sub> in Ar, at a flow rate of 180 mL/min, while an air flow rate of 100 mL/min was used to regenerate the carrier. Around ~80 mg of CeO<sub>2</sub> were studied in each test. Samples were preheated in pure Ar flowrate before reaction, with a ramp of 30 °C/min. Carrier reduction step length of 40 min and carrier regeneration of 15 min were repeated over each sample. For the first set of tests, variable reduction temperatures within the range of 900–1000 °C were investigated, while keeping the oxidation temperature constant at 900 °C; then, variable oxidation temperatures within a range of 400–900 °C were investigated, keeping reduction temperature at 900 °C. Elaboration of TGA curves was produced through NETZSCH Proteus software (Version 6.1.0), with the results obtained as mass variations in the functions of time and temperature. These tests offered the opportunity to pre-screen cerium dioxide activity before proceeding with the looping tests in the tubular reactor. The other samples were not tested in TGA due to unavailability of the instrument after the tests on pure cerium dioxide were completed, for those materials the screening of reaction temperature was performed directly into the tubular reactor.

# 1.3.2.3-Chemical Looping Tests

Figure 14 displays the experimental apparatus used to perform the chemical looping reaction tests. Three flowmeters (Bronkhorst) provided the required flowrate of reactant gases, alternating each reaction step with a purge in pure N<sub>2</sub>. This gas switch operation with nitrogen purge ensured that no gas from the partial oxidation of methane remained in the reactor during OC regeneration and vice versa.

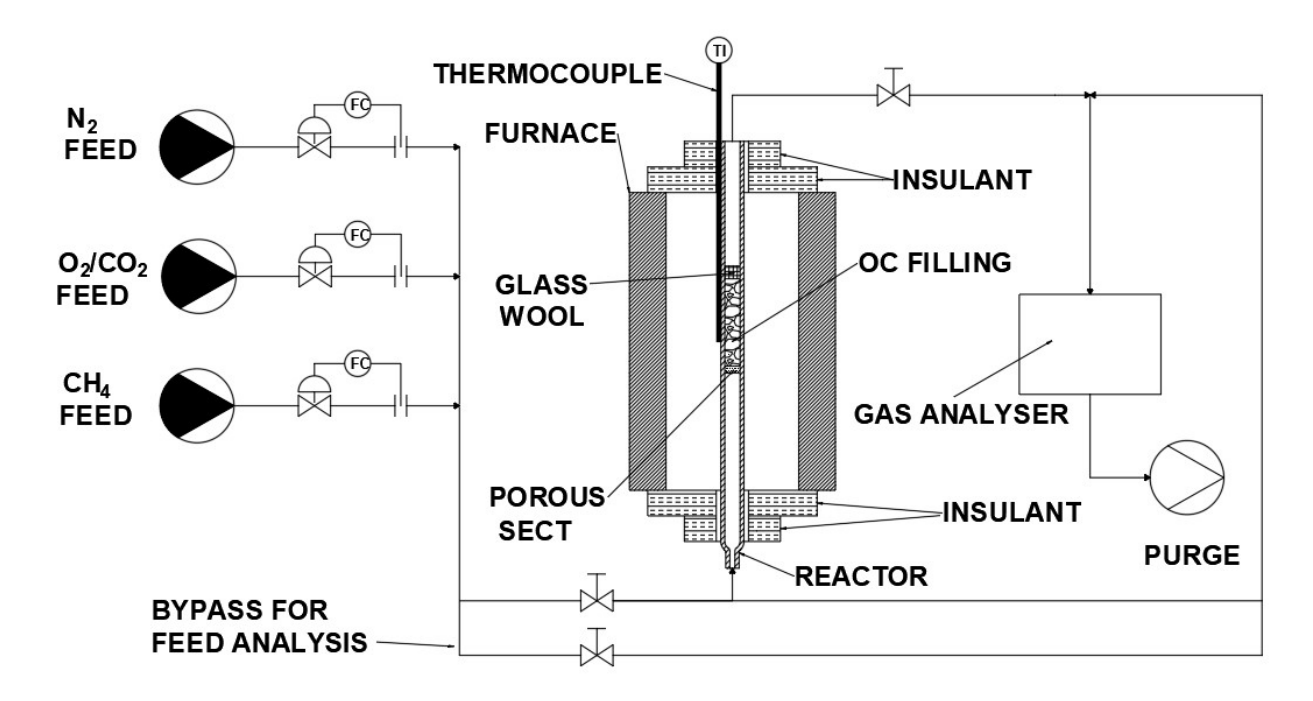


Figure 14: experimental setup for chemical looping tests. TI=Temperature Indicator, FC= Flowmeter.

The composition of the outgoing gases was measured continuously through an online syngas analyzer (GEIT 3100 P+ Syngas) with a thermal conductivity detector, an infrared detector, and an electrochemical oxygen sensor. Initially, an AISI-316 stainless steel reactor (internal diameter ID=10 mm) in fixed bed configuration was considered for the reaction, but after enough cycles it showed significant oxidation and degradation of the reactor walls, so it was substituted with a quartz reactor with the same internal diameter and a porous sect for gas distribution, as pictured in the figure. To provide the required reaction heat for the endothermic reforming reactions, the reactor was enclosed within a tubular electric furnace and thermal insulation was ensured by placement of layers of quartz wool. A cap of quartz wool was also used to avoid entrainment of the carrier outside the reactor. A K-type thermocouple was inserted from the top on the external wall of the reactor to monitor the wall temperature near the bed. Initially, the thermocouple was tested to be placed directly at the center of the reactor, but exposure of the thermocouple to reactive environment risked it to incur into damage,

so it was moved to the reactor wall. The catalyst was placed in the reactor at a height ensuring that it was at the center of the furnace. In a typical experiment, a 7 cm height OC carrier layer was placed in the reactor, which for  $CeO_2$  consisted of about ~15 g of material. Blank test runs, for which the OC bed was replaced with an analogous volume of inert quartzite filling, were performed in methane, CO,  $CO_2$  and  $H_2$  feed (diluted in nitrogen) to assess the inertness of the reactor walls and to determine the delay time in the gas analyzer response to changes in concentrations, which were then used to correct the results during data elaboration.

Reduction steps were carried out in a flowrate of 1 NL/min of CH<sub>4</sub> at 10, 15 and 20 %vol. in N<sub>2</sub>. On the other hand, regeneration was carried out either in O<sub>2</sub> at 1, 3 or 5 NL/min) with different O<sub>2</sub> contents (3, 5, and 21 vol.% in N<sub>2</sub>) or in 1 NL/min flowrate of CO<sub>2</sub> at 15%vol. in N<sub>2</sub>. Reaction temperatures between 800 and 950°C were tested for the various oxygen carriers. Finally, the surface of the carriers before and after the redox cycles was examined under scanning electron microscopy (SEM, Field Emission GUN-FEG MIRA 3 XMU and Zeiss SIGMA, Carl Zeiss Microscopy GmbH, Jena, Germany, D) to inspect structural changes linked to the reaction cycles.

#### 1.3.2.4-Numerical elaboration of data

The estimated oxygen availability of each carrier was estimated according to their expected maximum reduction, evaluated through thermodynamic simulation. For cerium dioxide in the presence of methane, the maximum expected reduction is to Ce<sub>2</sub>O<sub>3</sub>, Fe<sub>2</sub>O<sub>3</sub> content in chromite is expected to be reduced to FeO and CuO is reduced to metallic copper. Al<sub>2</sub>O<sub>3</sub> and Cr species are instead expected to remain inert. This results in the following formula for oxygen capacities of the oxides:

$$q_{O_2}^{CeO_2} = \frac{1}{4} \cdot \frac{m_{CeO_2}}{M_{CeO_2}} \tag{1}$$

$$q_{O_2}^{Chromite} = \frac{1}{4} \cdot \frac{m_{Chromite} \cdot \omega_{FeO}}{M_{FeO}}$$
 (2)

$$q_{O_2}^{CuO} = \frac{1}{4} \cdot \frac{m_{CuO}}{M_{CuO}} \tag{3}$$

Thermogravimetric data for cerium dioxide redox cycles was elaborated to obtain the reaction rates at different temperatures. The instantaneous reaction rates of partial oxidation and carrier regeneration between time  $t_1$  and  $t_2$  were calculated from the time required to achieve the maximum carrier conversion:

$$Rate_{PO} = \frac{|(\omega_{PO}^2 - \omega_{PO}^1)|}{(t_{PO}^2 - t_{PO}^1)} \tag{4}$$

$$Rate_{REG} = \frac{|(\omega_{REG}^2 - \omega_{REG}^1)|}{(t_{REG}^2 - t_{REG}^1)}$$
(5)

where  $\omega^1$  and  $\omega^2$  are the initial and final weight of the sample, expressed as weight percentage on the total sample weight. The oxygen non-stoichiometry of ceria was calculated considering that the loss in mass corresponded to the release of an equal mass of oxygen by the oxide, with complete reduction to Ce<sub>2</sub>O<sub>3</sub> leading to a weight loss of 4.65%.

For looping tests in the tubular reactor, methane conversion and reaction yields were obtained from elaboration of the concentration profiles measure at reactor outlet, solving the mass balances according to the feed composition. The moles of reactant consumed and product generated in the reaction step  $(n_{gen})$  were calculated from the inlet and outlet gas concentration assuming ideal behavior of the gas stream and considering nitrogen as inert for the purpose of the mass balance solution.

$$\dot{n}_{out} = \dot{n}_{in} \cdot \frac{y_{in}^{N_2}}{y_{out}^{N_2}} \tag{6}$$

$$n_{gen}^{i}(t) = \int_{t_0}^{t} (\dot{n}_{in} \cdot y_{in}^{i} - \dot{n}_{out} \cdot y_{out}^{i}) dt$$

$$(7)$$

Where  $\dot{n}$  represents the flowrate and y is the molar fraction. Subscript in and out denote the inlet and outlet streams, respectively, while superscript i denotes the reactant/product species (CH<sub>4</sub>, CO, CO<sub>2</sub>, H<sub>2</sub>). H<sub>2</sub>O could not be directly detected by the gas analyzer, so its total produced amount was obtained from the total hydrogen balance.

$$n_{gen}^{H_2O} = 4 \cdot n_{gen}^{CH_4} - 2 \cdot n_{gen}^{H_2} \tag{8}$$

Carbon mass balance instead was used to determine the amount of coke deposited during the partial oxidation step  $(n_{gen,PO}^{C})$  and the one removed during regeneration of the carrier  $(n_{gen,REG}^{C})$ , with the amount of caron accumulated in the cycle  $(n_{acc}^{C})$  being calculated as their difference:

$$n_{gen,PO}^{C} = n_{gen,PO}^{CH_4} - n_{gen,PO}^{CO} - n_{gen,PO}^{CO_2}$$
(9)

$$n_{gen,REG}^{\mathcal{C}} = n_{gen,REG}^{\mathcal{C}O} + n_{gen,REG}^{\mathcal{C}O_2} \tag{10}$$

$$n_{acc}^{\mathcal{C}} = n_{gen,PO}^{\mathcal{C}} - n_{gen,REG}^{\mathcal{C}} \tag{11}$$

From the amount of deposited coke during partial oxidation, the amount of hydrogen produced by methane cracking instead of methane partial oxidation  $(n_C^{H_2})$  was estimated as:

$$n_C^{H_2} = 2 \cdot n_{gen,PO}^C \tag{12}$$

Instantaneous rates of formation/consumption of each species were determined as the derivative over time of the amount produced, approximated by the difference quotient:

$$\frac{dn_{gen}^i}{dt} \cong \frac{\left(n_{gen}^i(t+\Delta t) - n_{gen}^i(t)\right)}{\Delta t} \tag{13}$$

The average reduction extent of the bed ( $\delta$ , bed oxygen non-stoichiometry) and the oxygen carrier conversion during partial oxidation ( $\chi_{OC}^{PO}$ ) can be calculated as:

$$\delta = \frac{\left(n_{gen,PO}^{CO} + 2 \cdot n_{gen,PO}^{CO_2} + n_{gen,PO}^{H_2O}\right)}{n_{OC}} \tag{14}$$

$$\chi_{OC}^{PO} = \frac{\delta}{\delta_{max}} \cdot 100 \tag{15}$$

Where  $\delta_{\text{max}}$  is the maximum reduction extent that the carrier can thermodynamically reach in the reaction conditions. On the other hand, for the conversion of the oxygen carrier during the regeneration step ( $\chi_{OC}^{REG}$ ) we consider the amount of moles of oxidant consumed, subtracting the contribution of coke oxidation, compared to the moles of oxygen released during the previous partial oxidation step to assess the percentage of oxygen reintegrated into the carrier:

$$\chi_{OC}^{REG} = \frac{n_{gen,REG}^{OX} - n_{gen,REG}^{CO} - n_{gen,REG}^{CO_2}}{n_{gen,PO}^{CO_2} + 2 \cdot n_{gen,PO}^{CO_2} + n_{gen,PO}^{H_{2O}}} \cdot 100$$
(16)

Finally, methane conversion, oxidant conversion and reaction selectivity are calculated as:

$$\chi_{CH_4}^{PO} = \frac{n_{gen,PO}^{CH_4}}{n_{in,PO}^{CH_4}} \cdot 100 \tag{17}$$

$$\chi_{OX}^{REG} = \frac{n_{gen,PO}^{OX}}{n_{in,REG}^{OX}} \cdot 100 \tag{18}$$

$$\eta_i = \frac{\int_{t_0}^t n_{gen}^{i} dt}{\int_{t_0}^t n_{in}^{CH_4} dt} \cdot 100 \tag{19}$$

Where n<sub>in</sub> denotes the total moles of reactant fed to the reactor during the respective reaction steps.

# 1.3.2.5-Mathematical model and simulation of the chemical looping process

Numerical simulations offer great opportunity to optimize processes without the need of performing repeated expensive and time-consuming experiments. Several numerical studies are available for numerical modeling of methane combustion and reforming in chemical looping configuration, but no modeling studies have considered pure cerium dioxide as oxygen carrier yet. Information on the reforming mechanism of cerium dioxide in literature is still lacking. The most complete reaction mechanism has been proposed by Zhenlong Zhao [447]. In Kroger-Vink notation, the proposed model reports the following reactions as the kinetically relevant steps for methane reforming on ceria surface:

$$CH_4(g) + 6Ce_{Ce}^{\chi} + 5O_0^{\chi} \rightarrow 6Ce_{Ce}' + 4OH_0^{\bullet} + V_0^{\bullet \bullet} + CO(g)$$
 R29

$$20H_0^{\bullet} + 2Ce_{Ce}' \rightleftarrows 20_0^x + 2Ce_{Ce}^x + H_2(g)$$
 R30

$$CH_4(g) + V_0^{\bullet \bullet} + 4Ce'_{Ce} \rightarrow C_0^{"} + 4Ce^{x}_{Ce} + 2H_2(g)$$
 R31

$$C_0'' + 6Ce_{Ce}^x + O_0^x \to 2V_0^{\bullet \bullet} + 6Ce_{Ce}' + CO(g)$$
 R32

$$H_2O(g) + V_0^{\bullet \bullet} + O_0^x \rightleftarrows 20H_0^{\bullet}$$
 R33

$$CO_2(g) + V_0^{\bullet \bullet} + O_0^{\alpha} \rightleftarrows (CO_3)_0^{\bullet \bullet}$$
 R34

$$(CO_3)_0^{\bullet \bullet} + 2Ce_{Ce}' \rightleftharpoons 2Ce_{Ce}^{\chi} + 2O_0^{\chi} + CO(g)$$
 R35

$$V_0^{\bullet\bullet}(b) - O_0^x(b) - 2Ce_{Ce}^x(b) + 2Ce_{Ce}'(b) \rightleftharpoons V_0^{\bullet\bullet}(s) - O_0^x(s) - 2Ce_{Ce}^x(s) + 2Ce_{Ce}'(s)$$
 R36

Methane can be activated on cerium surface according to two different mechanisms: R29 is prevalent on oxidized ceria surface, whereas R31 reaction occurs on partially reduced surface. Both reactions are considered irreversible. Reaction R30 leads to the production of hydrogen from surface hydroxyls species and occurs both during partial oxidation step, forming hydrogen from the hydroxyls formed by methane splitting, and during regeneration of the OC in water. Reaction R32 denotes the consumption of deposited coke on ceria surface with formation of carbon monoxide. Reaction R33 and R34 are the adsorption of water and CO<sub>2</sub> on reduced ceria surface, which represent the first step of carrier regeneration in presence of those oxidants, and reaction R35 represents the dissociation of carbonate species adsorbed on ceria surface to form CO. Reverse reactions of R33, R34 and R35 are the ones involved in the complete combustion of CH<sub>4</sub> on ceria surface, forming CO<sub>2</sub> and H<sub>2</sub>O. Reaction R36 represents the diffusive transfer of defects, namely oxygen vacancies, from the bulk (b) to the surface (s) of the oxide and vice versa. Reaction kinetics are presented according to the law of mass action and Arrhenius type equations, in function of the normalized surface concentrations of intermediates:

$$r_{29} = k_{29}^{0} \cdot e^{\frac{-E_{a}^{29}}{RT}} \cdot P_{CH_{4}} \cdot [Ce_{Ce}^{x}]_{s}^{4} \cdot [O_{O}^{x}]_{s}^{4}$$
(20)

$$r_{30} = k_{30,f}^{0} \cdot e^{\frac{-E_{a}^{30,f}}{RT}} \cdot [OH_{o}^{\bullet}]_{s}^{2} \cdot [Ce_{ce}']_{s}^{2} - k_{30,b}^{0} \cdot e^{\frac{-E_{a}^{30,b}}{RT}} \cdot P_{H_{2}} \cdot [O_{o}^{x}]_{s}^{2} \cdot [Ce_{ce}^{x}]_{s}^{2}$$
(21)

$$r_{31} = k_{31}^{0} \cdot e^{\frac{-E_{a}^{31}}{RT}} \cdot P_{CH_{4}} \cdot [V_{O}^{\bullet \bullet}]_{s} \cdot [O_{O}^{x}]_{s}$$
(22)

$$r_{32} = k_{32}^{0} \cdot e^{\frac{-E_{a}^{32}}{RT}} \cdot [C_{O}'']_{s} \cdot [O_{O}^{x}]_{s} \cdot [Ce_{Ce}^{x}]_{s}^{6}$$
(23)

$$r_{33} = k_{33,f}^{0} \cdot e^{\frac{-E_{a}^{33,f}}{RT}} \cdot P_{H_{2}O} \cdot [V_{O}^{\bullet \bullet}]_{s} \cdot [O_{O}^{x}]_{s} - k_{33,b}^{0} \cdot e^{\frac{-E_{a}^{33,b}}{RT}} \cdot [OH_{O}^{\bullet}]_{s}^{2}$$
(24)

$$r_{34} = k_{34,f}^{0} \cdot e^{\frac{-E_{a}^{34,f}}{RT}} \cdot P_{CO_{2}} \cdot [V_{O}^{\bullet \bullet}]_{s} \cdot [O_{O}^{x}]_{s} - k_{34,b}^{0} \cdot e^{\frac{-E_{a}^{34,b}}{RT}} \cdot [(CO_{3})_{O}^{\bullet \bullet}]_{s}$$

$$(25)$$

$$r_{35} = k_{35,f}^{0} \cdot e^{\frac{-E_{a}^{35,f}}{RT}} \cdot [(CO_{3})_{O}^{\bullet \bullet}]_{s} \cdot [Ce_{Ce}']_{s}^{2} - k_{35,b}^{0} \cdot e^{\frac{-E_{a}^{35,b}}{RT}} \cdot P_{CO} \cdot [O_{O}^{x}]_{s}^{2} \cdot [Ce_{Ce}^{x}]_{s}^{2}$$
(26)

For reaction R36, instead of presenting reaction kinetics the model assumes that the reaction is constantly at equilibrium, thus oxygen transfer in the ceria reticle is considered non limiting to process kinetics:

$$\frac{[v_o^{\bullet}]_{s^*}[ce_{Ce}^x]_s^2}{[o_O^x]_{s^*}[ce_{Ce}^x]_s^2} \cdot \frac{[o_O^x]_{b^*}[ce_{Ce}^x]_b^2}{[v_o^{\bullet}]_{b^*}[ce_{Ce}^x]_b^2} = exp\left(\frac{-\Delta H - T}{RT}\right)$$
(27)

With  $\Delta H$ =-107.6 kJ/mol and  $\Delta S$ =-54 J/(mol·K). To close the system of equations, the author considered the balances of charge, cerium sites and oxygen sites for both the surface and the bulk of cerium dioxide:

$$[Ce'_{Ce}]_S + [Ce^{\chi}_{Ce}]_S = 1 \tag{28}$$

$$[V_O^{\bullet\bullet}]_s + [O_O^x]_s + [OH_O^{\bullet}]_s + [C_O'']_s + [(CO_3)_O^{\bullet\bullet}]_s = 2$$
(29)

$$2[V_0^{\bullet\bullet}]_s + 2[OH_0^{\bullet}]_s + 2[(CO_3)_0^{\bullet\bullet}]_s = [Ce_{Ce}']_s + 2[C_0'']_s$$
(30)

$$[Ce'_{Ce}]_b + [Ce^x_{Ce}]_b = 1 (31)$$

$$[V_O^*]_b + [O_O^x]_b = 2 \tag{32}$$

$$2[V_O^{\bullet\bullet}]_b = [Ce'_{Ce}]_b \tag{33}$$

The differential equations of the model thus become:

$$d\frac{(\rho_{Ce}V_{part}[V_O^{\bullet *}]_b)}{dt} = S_{part} \cdot \rho_{Ce,s} \cdot (r_{29} - r_{31} + 2 \cdot r_{32} - r_{33} - r_{34})$$
(34)

$$\rho_{Ce,s} \frac{d[OH_O^{\bullet}]_s}{dt} = \rho_{Ce,s} \cdot (r_{29} - r_{30} + r_{33})$$
(35)

$$\rho_{Ce,s} \frac{d[c_0'']_s}{dt} = \rho_{Ce,s} \cdot (r_{31} - r_{32}) \tag{36}$$

$$\rho_{Ce,s} \frac{d[(CO_3)_0^{\bullet}]_s}{dt} = \rho_{Ce,s} \cdot (r_{34} - r_{35})$$
(37)

Where  $V_{part}$  is the particle volume,  $S_{part}$  is the particle surface area,  $\rho_{Ce}$  is the bulk density of cerium dioxide in mol/m<sup>3</sup> and  $\rho_{Ce,s}$  is the surface density in mol/m<sup>2</sup>. The author fitted the model on experimental data to obtain the kinetic constants and activation energies for all reactions, which are summarized in Table 4.

While this represents the most detailed model for the redox of cerium dioxide in presence of methane, no attempts of implementing it for process simulation were found in the literature. Furthermore, Zhao does not provide any value for the reaction enthalpies, which are necessary for non-isothermal modeling of the process. Enthalpy data availability in literature is rather spotty for the elementary steps presented. Table 4 also reports the available thermodynamic data for the reactions.

Table 4: kinetic constants, activation energies and enthalpy for the numerical model.

		k <sub>0</sub> (s <sup>-1</sup> )	E <sub>a</sub> (kJ/kmol)	ΔH <sub>R</sub> (MJ/kmol)	Source for ΔH <sub>R</sub>	
R29		790	104000	-117.152	[448]	
R30	f	1.5·10 <sup>14</sup>	190000	+92	[447]	
	b	44000	97000	-92		
R31		3500000	150000	+137.97	[449]	
R32		2.1·10 <sup>12</sup>	156000	271.1	[450]	

R33	f	130	7000	-203	
	b	8.2·10 <sup>14</sup>	210000	+203	
R34	f	130	12000	-239	[447]
	b	9.4·10 <sup>14</sup>	251100	+239	
R35	f	1.4·10 <sup>13</sup>	209000	+160	
	b	98	49000	-160	

Aspen Adsorption<sup>TM</sup> is a commercial software for the dynamic simulation of cyclic adsorption and reaction processes provided by Aspentech [451]. It provides access to an extensive library of properties for several chemicals and to extensive tools for simulation of mass and heat transfer in commercial fixed-bed reactors. The previously discussed kinetic model for methane reforming on CeO<sub>2</sub> was thus implemented in Aspen Adsorption<sup>TM</sup> to obtain a complete tool for the simulation of the reforming process. Figure 15 reports the scheme of the simulation.

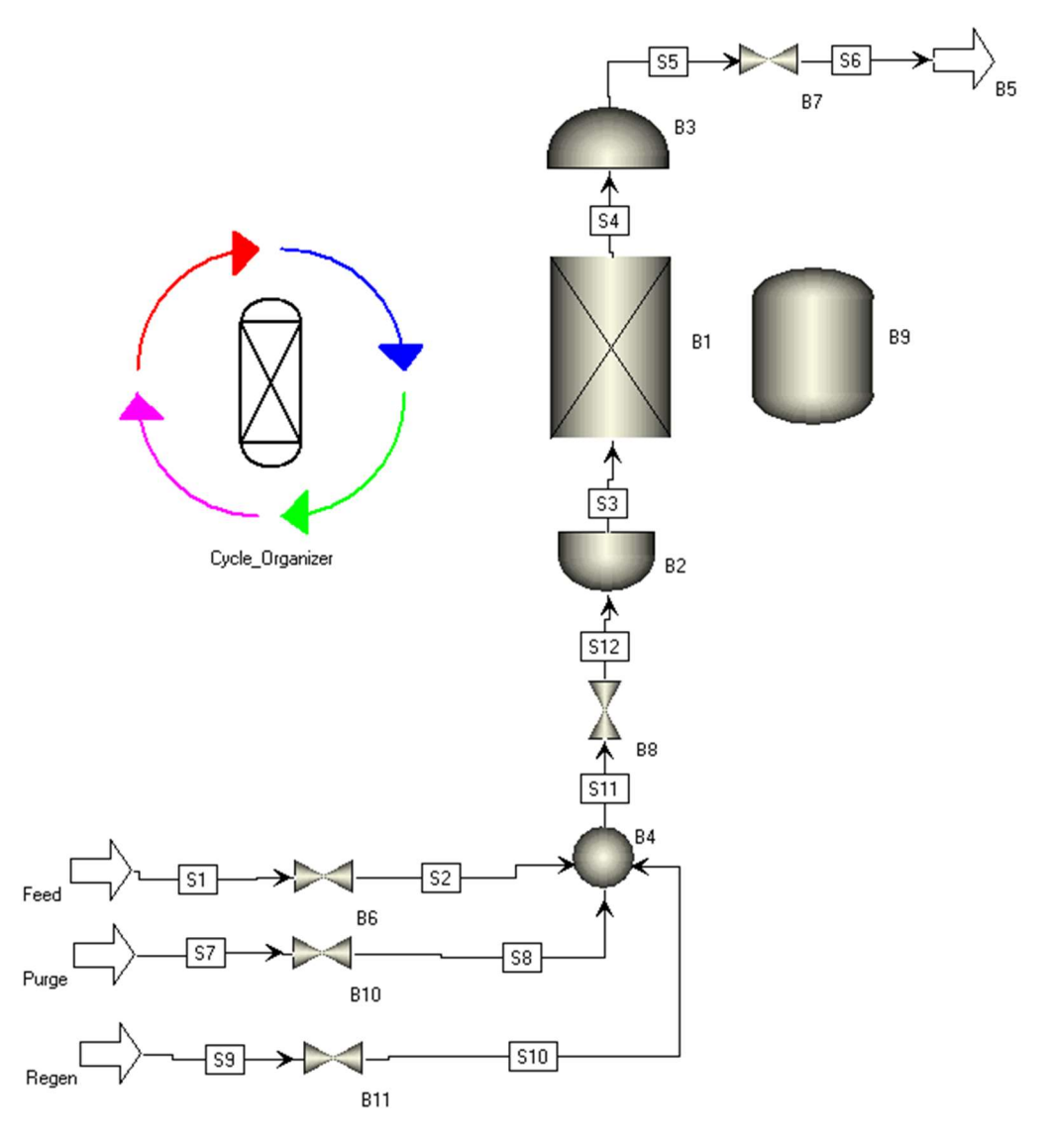


Figure 15: process model flowsheet in Aspen Adsorption<sup>TM</sup>.

The detailed discussion of mass, energy and momentum balance in Aspen Adsorption<sup>TM</sup> software is reported in the Appendix. The assumption made for model implementation are the following:

- The reactor operates in plug flow regime, with no axial dispersion or radial properties gradients. The reactor was subdivided into 10 calculation nodes.
- The Ergun equation was used for estimating the gas pressure drop through the fixed bed.
- A linear driving force with constant mass transfer coefficient of 10<sup>-3</sup> s<sup>-1</sup> was used for mass transfer.
- Physical adsorption of gases on the bed was considered negligible, with Henry's law model being selected with a low adsorption coefficient (10<sup>-20</sup>). Adsorption heat of components was set at zero.
- The bed starts operation while filled with nitrogen.

- The diameter of simulated particle is the average diameter of the experimental particles, which as mentioned before are in the range of 0.595 to 0.841 mm, as Aspen Adsorption<sup>TM</sup> does not allow the simulation of particles with non-homogeneous diameter, and the particles were assumed spherical.
- Conductive heat transport is considered negligible, heat is only exchanged through convection.

While block B1 simulated the interaction between gases and ceria surface, in block B9 the bulk of cerium dioxide was simulated, connected to block B1 results by the equilibrium equation R36. Both isothermal and adiabatic simulations were performed.

Both isothermal and non-isothermal reaction simulations were carried out. Since Aspen Adsorption<sup>TM</sup> does not allow to simulate radiative heat exchange, the flux of external heat of the electric furnace used in the experimental tests was instead simulated considering the reactor to be surrounded by a jacket heat exchanger, whose parameters were tuned to ensure that the simulated temperature remained within the limits observed in experimental tests. External heat transfer coefficient was also tuned to provide a reactor temperature profile similar to the one observed experimentally. A 5 mm thickness was assumed for reactor walls, with an external temperature of 25 °C. Table 5 reports the parameters of the simulated bed. The stream compositions, flowrates and the length of the partial oxidation, purge and regeneration steps were chosen to match the flowrate of the experimental conditions (1 nL/min). The simulation implemented the loop operation as an eight-step cycle in which the inlet flowrates were cyclically switched. While the actual process consists of four steps, namely partial oxidation, regeneration and the in-between two purges, for the purpose of numerical simulation an additional four steps were implemented simulating a gradual switch from one step to the other, with a partial opening of valves. This was done to improve model stability and avoid numerical errors due to sudden switch in boundary conditions between steps, and the length of such steps was kept low (3 s) to minimize their effect on the overall simulation. Not reported in the table are the values of the simulated valves constants, but it should be noted that their value was simply used to ensure that the column remained at atmospheric pressure during the whole run and ensure numerical stability of the simulation.

Table 5: parameters of simulation and simulated cycle structure in isothermal and non-isothermal conditions. Refer to Figure 15 for valve and stream names.

Parameter	Isothermal	Non-isothermal
H <sub>b</sub> , bed height, m	0.07	0.07
D <sub>b</sub> , bed diameter, m	0.0127	0.0127

W/ had swall this leading and	0.005	0.005			
W <sub>b</sub> , bed wall thickness, m	0.005				
$\varepsilon_i$ , inter-particle void fraction	0.5207	0.5207			
$\varepsilon_{\rm p}$ , intra-particle void fraction	0.5	0.5			
r <sub>p</sub> , particle radius (m)	7.05×10 <sup>-4</sup>	$7.05 \times 10^{-4}$			
Φ, particle sphericity	1	1			
ρ <sub>s</sub> , solid density, kg/m <sup>3</sup>	7220	7220			
Mass transfer model	Linear driving force	Linear driving force			
MTC, mass transfer coefficient, s <sup>-1</sup>	10-3	10-3			
Adsorption model	Henry's law	Henry's law			
IP <sub>Lang</sub> (all gases), adsorption	10 <sup>-20</sup>	10-20			
coefficient	10				
C <sub>ps</sub> , solid heat capacity, MJ/(kg×K)	-	10-3			
Hw, wall-air heat transfer		10-5			
coefficient, MW/(m <sup>2</sup> ×K)	-	10 °			
T <sub>env</sub> , External temperature, °C	-	25			
a <sub>H<sub>x</sub></sub> , Specific surface area of heat		5			
exchanger, m <sup>-1</sup>	-	3			
U <sub>Hx</sub> , heat transfer coefficient in heat		10			
exchanger, MW/(m <sup>2</sup> ×K)	-				
Mass flowrate of heating medium,		6000			
kg/s	-	6000			
Heat capacity of heat exchanger		0.0			
fluid, MJ//(kg×K)	-	0.8			
T <sub>Hx</sub> , Inlet temperature of heat		950			
exchanger fluid, °C	-				
	Inlet conditions				
Chran	Composition	Flowrate			
Stream	(%mol)	(kmol/s)			
Partial oxidation inlet flowrate (S1)	10% mol. CH <sub>4</sub> in N <sub>2</sub>	7.43×10 <sup>-7</sup>			
Purge flowrate (S7)	100% N <sub>2</sub>	7.43×10 <sup>-7</sup>			
Regeneration flowrate (S9)	15% mol. CO <sub>2</sub> in N <sub>2</sub>	7.43×10 <sup>-7</sup>			
Cycle structure					
Step Duration	Descr	ription			

(s)			
	Step for initialization of the column at the start of each		
0	cycle, valve B6 open at constant flowrate, valves B10 and		
	B11 closed		
900	Partial oxidation step, valve B6 open at constant flowrate,		
900	valve B10 and B11 closed		
2	Switch to purge, valves B6 and B10 partially open, valve		
3	B11 closed		
400	Purge, valve B10 open at constant flowrate, valves B6 and		
400	B11 closed		
2	Switch to regeneration, valve B10 and B11 partially open,		
3	valve B6 closed		
600	Regeneration, valve B11 open at constant flowrate, valves		
000	B6 and B10 closed		
2	Switch to purge, valves B10 and B11 partially open, valve		
3	B6 closed		
400	Purge, valve B10 open at constant flowrate, valves B6 and		
400	B11 closed		
2	Switch to partial oxidation, valves B6 and B10 partially		
3	open, valve B11 closed		

### 1.3.3-Results and discussion

# 1.3.3.1-Comparison of oxygen carrier activity

Rapid test runs for the oxygen carriers were performed using the tubular reactor setup to screen the activity of the different carriers for reaction with methane. Cerium dioxide, chromite and CeO<sub>2</sub>-CuO OCs were tested at 850 and 950°C in 5%, 10% and 20% CH<sub>4</sub> flowrate (1 NL/min) to compare their behavior. For example, Figure 16 reports the composition profiles obtained for a 10% vol. CH<sub>4</sub> feed at the two reaction temperatures. It is immediate to notice the difference between the three OCs. At 850 °C (Figure 16a), cerium dioxide (continuous line) does not produce significant methane conversion, and only a small amount of hydrogen is produced, which is likely attributed to methane thermal decomposition rather than any activity of the carrier, as no significant CO or CO<sub>2</sub> production is present. Meanwhile, at the same temperature, chromite (dotted line) demonstrates limited activity to methane complete oxidation, shown by the lower methane outlet concentration coupled with an

increase in CO<sub>2</sub> concentration. CO<sub>2</sub> production remains stable for about 1 min, then methane conversion decreases and only H<sub>2</sub> production due to thermal degradation is seen. On the other hand, the CeO<sub>2</sub>-CuO carrier is the most active, showing complete conversion of methane for the whole time, with complete selectivity towards total methane combustion to CO<sub>2</sub>. At 950 °C (Figure 16b) CeO<sub>2</sub> shows greatly increased conversion compared to the lower temperature and except for an initial spike in CO<sub>2</sub> formation, the reaction is selective towards syngas formation at almost constant composition. Chromite also becomes more active at higher temperature but shows a much different behavior. Production of carbon dioxide on chromite lasts longer and is then replaced by a significant spike in carbon monoxide and hydrogen production. Here the gap between hydrogen and CO production appears wider compared to CeO<sub>2</sub>, likely suggesting an increased occurrence of methane decomposition on chromite. The CeO<sub>2</sub>-CuO carrier does not demonstrate noticeable difference in behavior compared to the lower reaction temperature, being once again completely selective towards total combustion and achieving complete methane conversion.

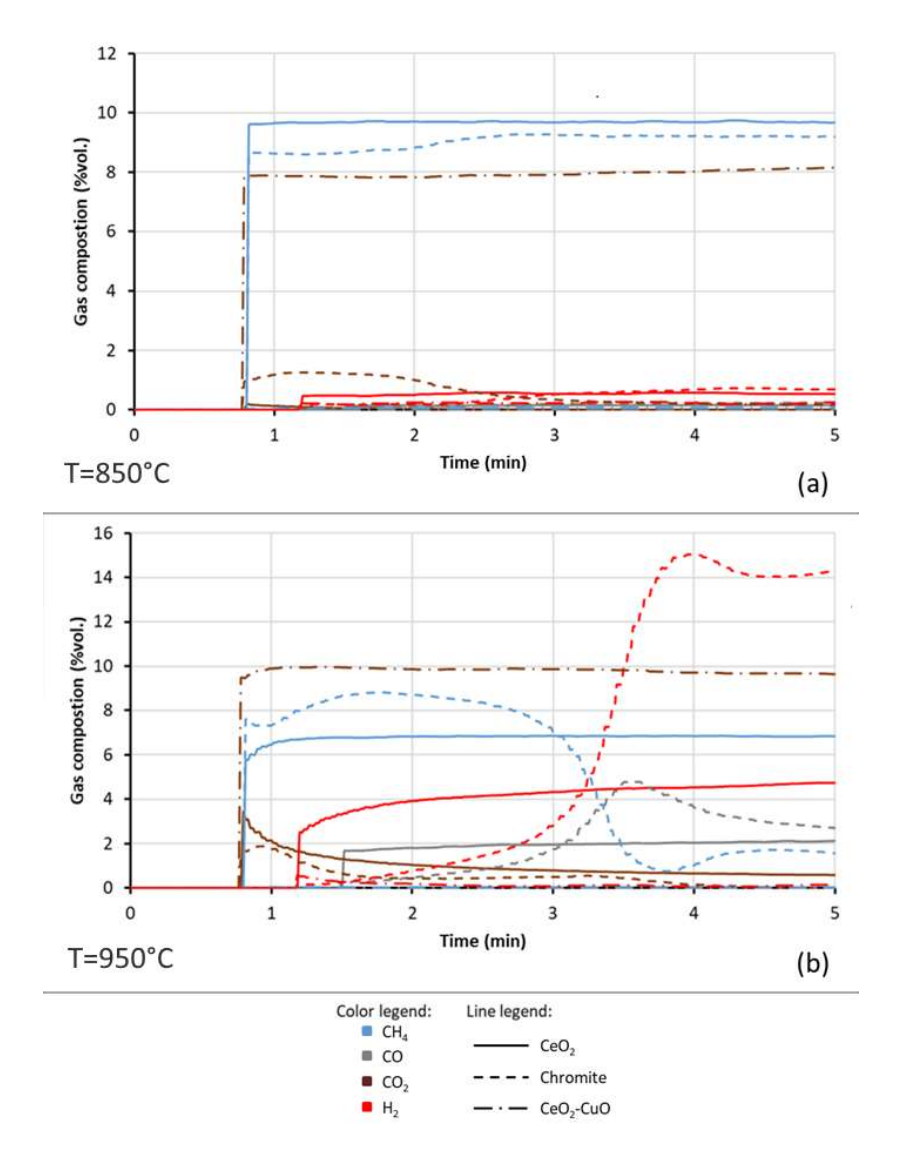


Figure 16: gas composition profiles at reactor outlet over time for OCs exposed to 10% vol. CH<sub>4</sub> flowrate at 1 NL/min: reaction temperature of 850 °C (a); reaction temperature of 950 °C (b).

Table 6 reports the methane conversion and reaction selectivity obtained on each OC in function of its reduction extent (10 or 20%) and the concentration of methane in the inlet feed (5, 10 or 20% vol.), at temperature of 950°C. Again, we can see that for cerium dioxide, at low OC conversion selectivity can favor complete oxidation rather than syngas production, especially when methane concentration in the feed is lower. At higher methane concentration, partial oxidation gains advantage, but so does coke formation, therefore careful balance of carrier reduction extent is needed to ensure selective syngas production. Chromite does not provide a good performance as an oxygen carrier for reforming, displaying generally worse methane conversion compared to cerium dioxide and also being mostly selective to complete methane combustion rather than syngas formation. Furthermore, it also is affected by severe coke deposition and its performance at the investigated temperature appears unstable, as seen by the significant errors affecting the results of repeated experiments. After

extraction of the sample from the reactor, it was observed that the chromite sand had suffered severe sintering during the reaction process, having formed macroscopic aggregates. The CeO<sub>2</sub>-CuO OC on the other hand displayed the highest methane conversion and was selective towards complete oxidation in all feed conditions and for all carrier reduction extents. As expected from reaction thermodynamics and previous literature, it was also the only one observed to release gaseous oxygen during the reaction. For higher methane concentration, significant coke formation was also observed. This may be due to the fact that reduced copper can catalyze methane splitting, which cannot be removed once available oxygen becomes insufficient. The release of oxygen from the carrier at reaction temperature also makes it difficult to completely regenerate the carrier in isothermal conditions, and repeated cycles show unstable performance (see the significant error on selectivity).

Table 6: methane conversion and reaction selectivity at different degrees of OC conversion for CeO<sub>2</sub>, chromite and CeO<sub>2</sub>-CuO oxygen carriers. Results obtained for reaction at 950 °C.

	y <sub>CH4</sub> ->	0.05		0.10		0.20	
Carrier	χος (%) ->	10	20	10	20	10	20
CeO <sub>2</sub>	$\chi_{\mathrm{CH_4}}(\%)$	29.7±0.4	(-)	22.04±0.05	20.99±0.08	16.0±1.0	(-)
	$\eta_{\mathrm{CO}_2}(\%)$	73.2±0.8	(-)	58.0±2.0	41.2±0.5	45.1±0.2	(-)
	ηςο (%)	35.0±2.0	(-)	42.00±2.0	$59.9 \pm 0.7$	49.0±1.0	(-)
	$\eta_{C}\left(\% ight)$	0±3.0	(-)	0.0±4.0	0±1	6.0±2.0	(-)
Chromite	$\chi_{\mathrm{CH_4}}(\%)$	14.0±6.0	14.50±0.01	12.0±4.0	27.0±18	(-)	(-)
	$\eta_{\mathrm{CO}_2}\left(\% ight)$	81.0±25.0	71.9±0.1	63.0±5.0	44.0±10.0	(-)	(-)
	η <sub>CO</sub> (%)	17.0±2	37.8±0.1	14.0±5.0	36.0±10.0	(-)	(-)
	$\eta_{C}\left(\% ight)$	2.0±33.0	0.0±0.2	23.0±15.0	20.0±37.0	(-)	(-)
CeO <sub>2</sub> -CuO	$\chi_{\mathrm{CH_4}}(\%)$	72.72±0.01	72.72±0.01	73.82±0.05	73.86±0.01	74.03±0.03	74.04±0.01
	$\eta_{\mathrm{CO}_2}\left(\% ight)$	100.0±4.0	100.0±4.0	100.0±0.6	100±0.1	74.0±18.0	75.0±18.0
	η <sub>CO</sub> (%)	0.0±0.1	0.0±0.1	0.0±0.1	$0.0\pm0.1$	0.0±0.1	0.0±0.1
	η <sub>C</sub> (%)	0.0±4.0	0.0±4.0	$0.0 \pm 0.6$	0.0±0.1	26.0±18.0	25.0±18.0

# 1.3.3.2-TGA investigation of cerium dioxide

Cerium dioxide demonstrates interesting activity for methane reforming. Its behavior was thus tested in more detail using TGA analysis, performing runs of 4 consecutive redox cycles in different conditions. In the first run, partial oxidation step was carried out at 900 °C, with regeneration step at 400 °C; the second run again involved a partial oxidation step at 900 °C, but a regeneration temperature of 650°C; in the third run, partial oxidation temperature of 950 °C and regeneration temperature of 900 °C were selected; finally, the last run used a partial oxidation temperature of 1000

°C and a regeneration temperature of 900 °C. Together, the runs enabled to assess the effect of regeneration and partial oxidation temperature on the cyclical performance of CeO2. Results of TGA tests are reported in Figure 17. While cerium dioxide was previously shown to be inactive at 850 °C (Figure 16a), TGA tests confirm that cerium dioxide becomes active for methane reforming at T≥900 °C, as predicted by thermodynamic simulation [387]. It is immediately apparent that the maximum reaction rates and also the maximum reduction extent are increased with increasing reaction temperature. This is particularly significant when considering the difference between PO step at 900 °C (Figure 17a and b) and 950 °C (Figure 17c), where reaction rates appear to be doubled at higher temperature. The increase in reaction rate is less noticeable when increasing reaction temperature further to 1000°C (Figure 17d). Changing regeneration temperature on the other hand had no effect on carrier performance, as the regeneration of the carrier proved to be complete and fast at all observed temperatures. It should be noted that when conducting the PO reaction at 1000 °C, a noticeable weight increase of the sample was observed at the end of reduction even before the regeneration of the carrier was started. This can be likely attributed to the high temperature causing significant coke deposition. Therefore, 950 °C appears to be the optimal temperature for the reforming process, as a good compromise between fast kinetics, optimal utilization of the carrier's oxygen capacity and avoidance of coke deposition. Further tests were performed in the reactor setup to confirm these results and investigate the optimization of reaction time.

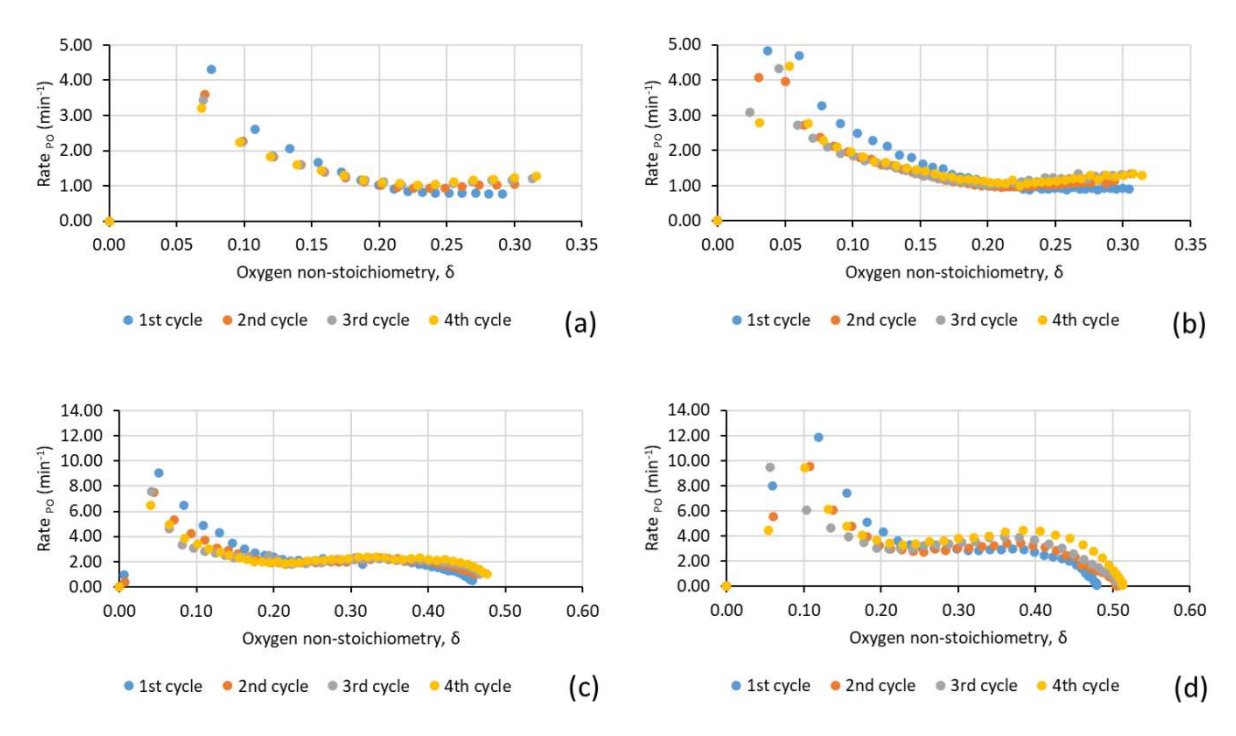


Figure 17: rates of PO step for TGA runs on cerium dioxide in 4% vol. CH<sub>4</sub> and air:  $T_{PO}$ =900 °C,  $T_{REG}$ =400 °C (a);  $T_{PO}$ =900 °C,  $T_{REG}$ =600 °C (b);  $T_{PO}$ =950 °C,  $T_{REG}$ =900 °C (c);  $T_{PO}$ =1000 °C,  $T_{REG}$ =900 °C (d).

# 1.3.3.3-Optimization of reaction time for reforming on CeO<sub>2</sub>

To confirm TGA results, CeO<sub>2</sub> oxygen carrier was tested under a 60 min reduction in the reactor bed, at both 900 and 950 °C under 10% vol. CH<sub>4</sub>. The temperature of 1000 °C was not investigated as TGA tests indicated increased carbon deposition without significant increase in oxygen carrier conversion. Results of this screening are reported in Figure 18 in the form of cumulative reaction yields. As previously observed in the initial screening (Table 6), cerium dioxide demonstrates high selectivity for syngas formation, with only a very limited amount of CO<sub>2</sub> being produced (less than 0.1 mmol/g<sub>CeO<sub>2</sub></sub>) at both temperatures. Carbon dioxide production reaches its maximum yield within less than 5 minutes of reaction and then is replaced by selective oxidation. Presumably, water is also produced at the start of reaction together with CO<sub>2</sub>, since hydrogen breakthrough from the reactor is also delayed. Carbon dioxide yield increases at higher temperature, likely as a result of the increased oxygen mobility, with water production also presumably following suit. This limited initial contribution of complete combustion however does not significantly affect syngas quality, since reaction rapidly becomes selective towards partial oxidation only. Partial oxidation yields are also slightly increased at higher temperatures, as can be seen observing the CO and H<sub>2</sub> yields at 60 min for the two temperatures. At 900°C, the maximum yields of reaction are 5.0±1.0, 2.0±0.2 and

0.04±0.01 mmol/g<sub>CeO2</sub> for H<sub>2</sub>, CO and CO<sub>2</sub>, respectively, while at 950 °C the maximum yields observed are 6.0±0.3, 2.05±0.06 and 0.084±0.007 mmol/g<sub>CeO2</sub>. The yields of CO and CO<sub>2</sub> reach a plateau before the end of the reaction, after which their production ceases, suggesting that lattice oxygen of ceria was exhausted within the 60 min of reaction; on the other hand, production of hydrogen keeps increasing up to the end of the run. This can most likely be attributed to carbon deposition, and as expected it is particularly evident at higher temperature. Looking at H<sub>2</sub> to CO ratio, after 60 min of reaction a value of 2.5 is observed at 900 °C, while a value of 2.9 is observed at 950 °C. Figure 18b reports the observed production yields for each gas species as function of the carrier conversion. For production of hydrogen, both the total rate of production and the corrected rate accounting only for the contribution of partial oxidation are shown, their difference being the rate of hydrogen formation due to methane decomposition. Looking at the profiles, it can be seen that at both temperatures, methane decomposition becomes particularly relevant once cerium dioxide conversion reaches ~40%, which also corresponds to the peak in the rate of total hydrogen production. Past this point, the rate of partial oxidation decays at both temperatures, as can also be seen by the decrease in production rate of CO. Once the carrier approaches 80% conversion, the rate of partial oxidation rapidly falls to zero and only methane decomposition is left, with hydrogen production rate stabilizing at a non-zero value. The results of TGA analysis for the effect of temperature on kinetics are here confirmed, with rates at 950 °C being consistently almost double the rates at 900 °C. Operation at higher temperature allows to reach significantly higher yields in lower process time: at 900 °C, reaction was completed within 40 min, while at 950 °C completion of the reaction required about 30 min. Peak production rates were achieved after 20 min of reaction at lower temperature, while at 10 min at 950 °C. These much faster rates of reaction and the increased carrier conversion and yields suggest that 950°C is the ideal temperature to carry out the reforming reaction. However, optimal reaction time needs to be properly determined to avoid the occurrence of excessive carbon deposition. It was seen that CO production at 950 °C remained significant up to 20 min of reaction, at a carrier conversion ~70%. At this point, a syngas ratio of ~2.3 is obtained, suggesting a still limited carbon deposition, and the reaction reaches ~78% of its maximum yield in CO and ~62% of its maximum H<sub>2</sub> yield. After this point, the rate of partial oxidation rapidly decays, with carbon deposition becoming increasingly relevant and the H<sub>2</sub> to CO ratio rapidly increasing. Therefore, operation past this point appears unattractive in terms of syngas quality and coke avoidance, and 20 minutes of reaction and 70% carrier conversion appear to be the optimal point to stop the partial oxidation reaction and start carrier regeneration, allowing to obtain a significant fraction of the maximum reaction yield while still maintaining good selectivity in reaction products. To test these conclusions, repeated redox cyclic tests were performed. Before performing the repeated tests, different

regeneration conditions were tested to ensure that carbon removal and restoration of lattice oxygen could be properly carried out between each partial oxidation step. TGA tests previously showed that kinetics of carrier regeneration are not limited by temperature. However, the effect of oxidant concentration in the regeneration feed and of feed flowrate needs to be assessed to ensure cyclical stable performance.

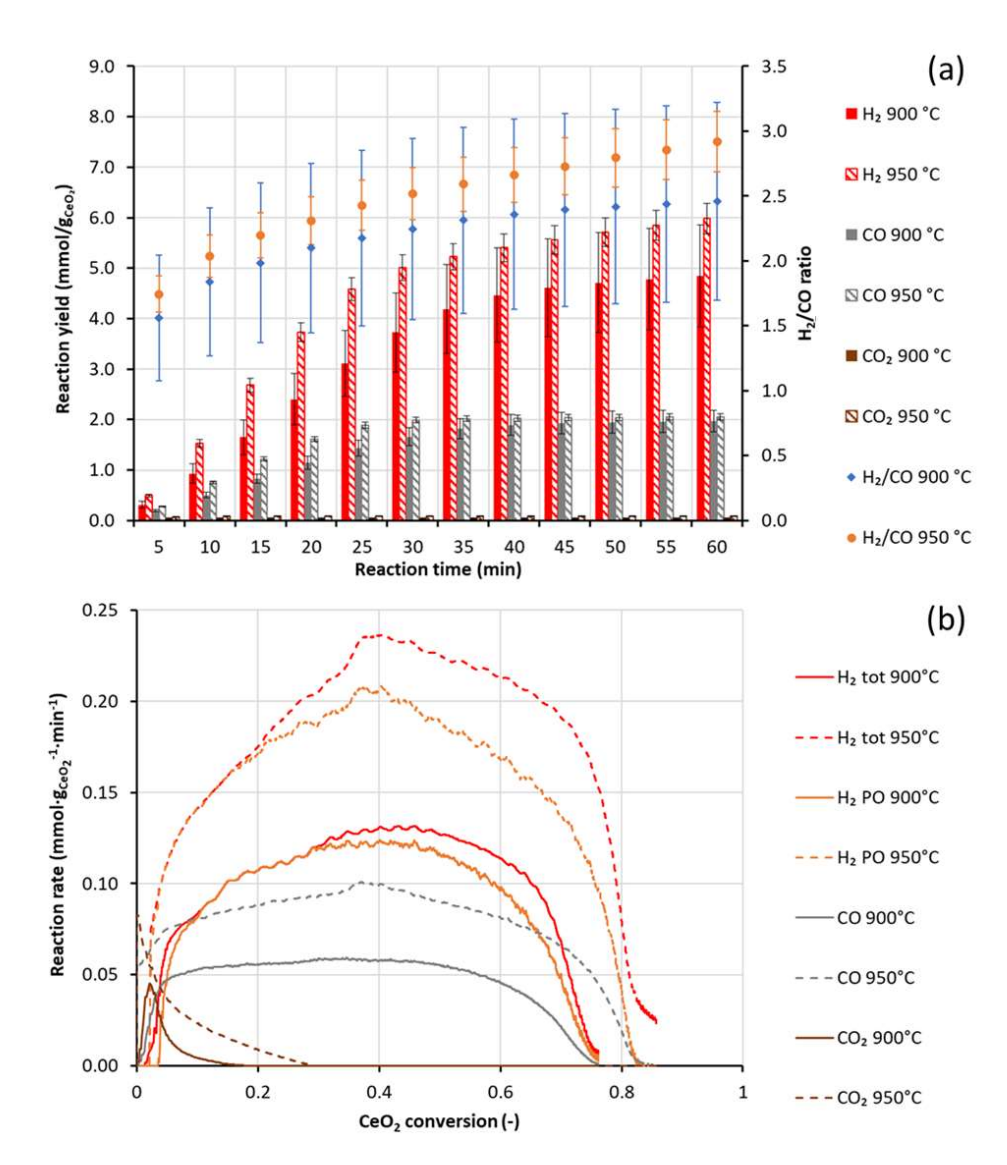


Figure 18: results of 60 min PO step under 10% vol. CH<sub>4</sub> at 1 NL/min at 900°C and 950 °C: cumulative reaction yields over time and H<sub>2</sub> to CO ratio (a); reaction rates as function of carrier conversion (b).

Figure 19 reports the results for carrier regeneration after the partial oxidation steps of Figure 18. It can be immediately seen that regeneration follows the same pattern in all conditions: at first, CO is produced as a result of the O<sub>2</sub> feed, suggesting that indeed coke was deposited during the previous partial oxidation step. At this point, coke is converted to CO as its oxidation is actively competing with carrier regeneration, as seen by comparing the curves of total oxygen consumption and

consumption of oxygen for CeO<sub>2</sub> regeneration of Figure 19b being closer to each other at this point. Once cerium oxide regeneration advances, its competition with coke removal recedes and the remaining coke is combusted to CO<sub>2</sub>. Even though higher flowrate and oxygen concentration increase regeneration rate, it can be seen that for all tested conditions regeneration is rather fast, especially compared to partial oxidation: regeneration of the carrier is in all conditions mostly completed already within 6 min of reaction. The regeneration condition for cyclic tests therefore was not determined on the basis of reaction rate, as it is not limiting on the process, but rather on safety concerns: regenerating in high oxygen concentration and low regeneration flowrate was observed to lead to a dramatic increase in bed temperature, overshooting 1100 °C. Therefore, to avoid risks to experimental apparatus and operator safety, a flowrate of 5 NL/min at 3% vol. O<sub>2</sub> concentration was chosen as the regeneration condition for cyclic tests, as the low oxygen concentration and high flowrate limited reactor overheating while still accomplishing efficient regeneration.

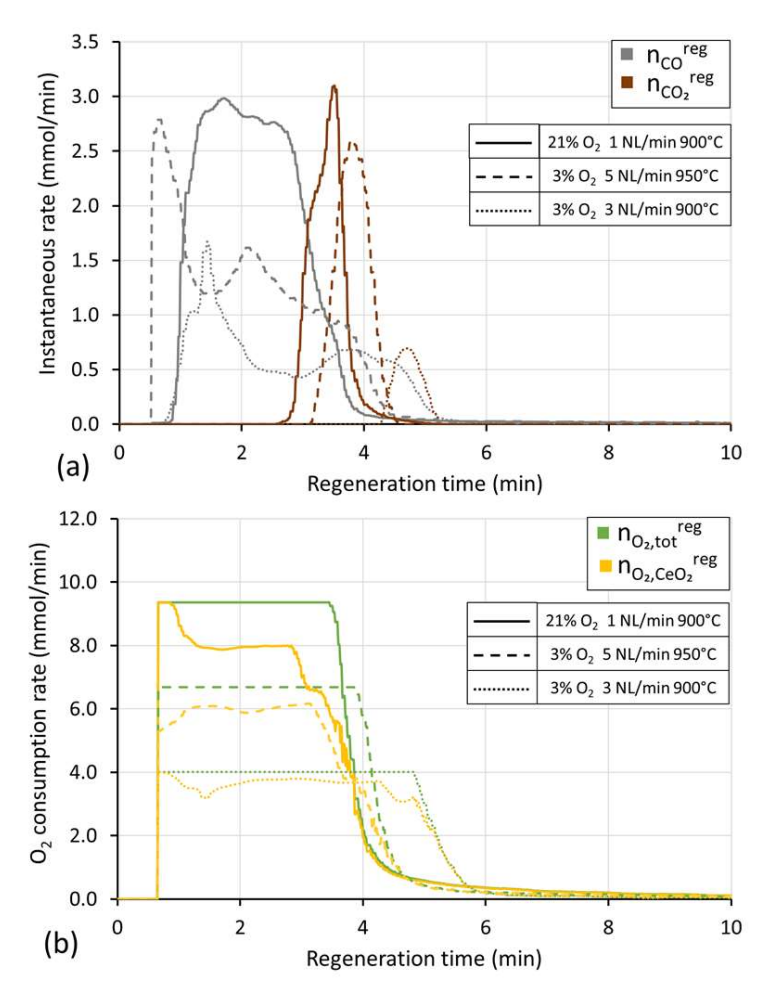


Figure 19: effect of feed composition on carrier regeneration: instantaneous rates of formation of CO and CO<sub>2</sub> during regeneration step (a); comparison between total instantaneous rate of oxygen consumption and instantaneous rate of oxygen consumed for CeO<sub>2</sub> regeneration only (b).

Results of cyclic tests at 950 °C are reported in Figure 20. Two sets of cycles were investigated, the first having a partial oxidation step of 30 min, which as discussed previously corresponds to completion of the reaction at the selected temperature, and 20 min, which instead coincides with decline in the CO production rate. In between each partial oxidation, regeneration step length was based upon disappearance of CO and CO<sub>2</sub> among the product and breakthrough of the oxygen concentration profile. This generally amounted to a regeneration step length of about 6 min.

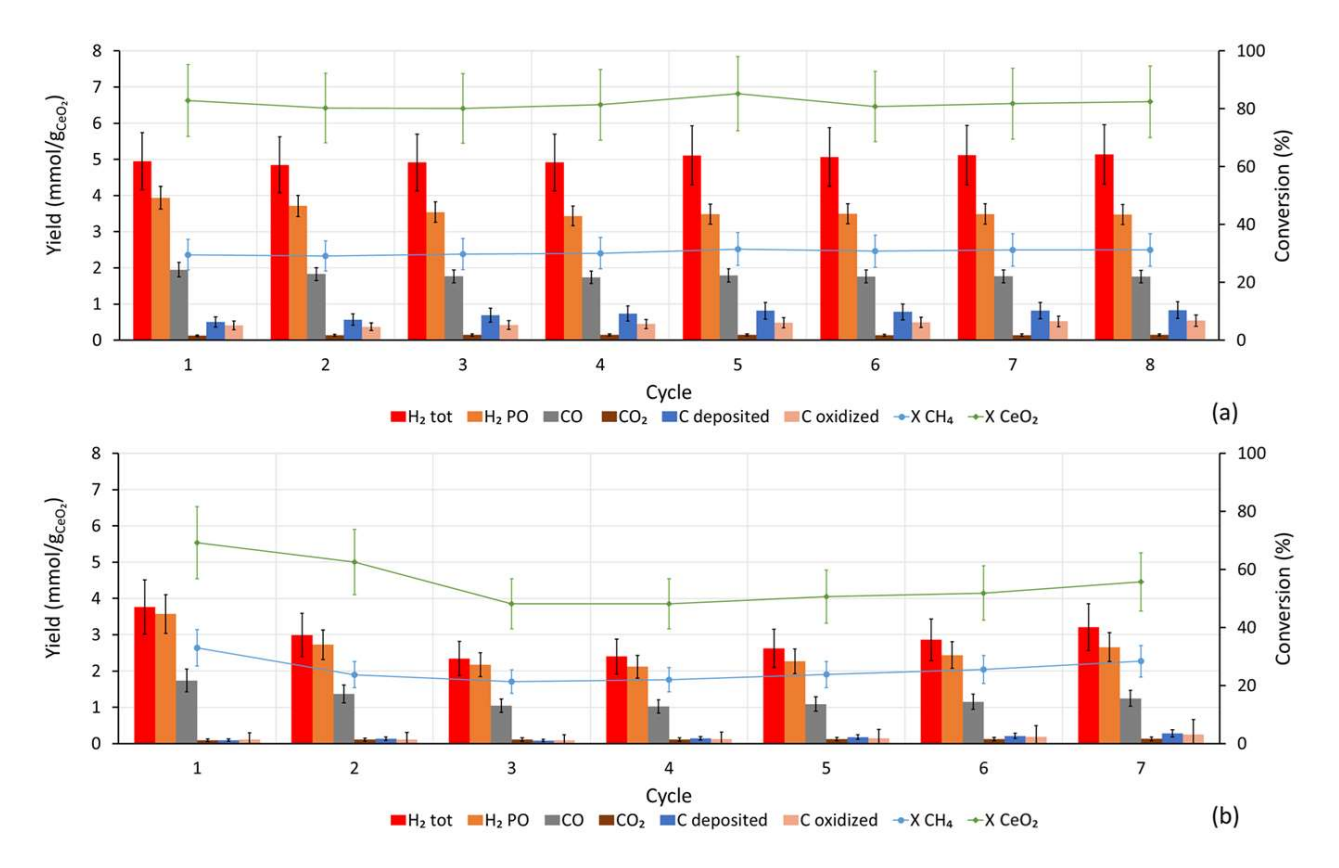


Figure 20: results of redox cyclic tests at 950 °C in 10% vol. CH<sub>4</sub> (1 NL/min), with regeneration in 3% vol. O<sub>2</sub> (5 NL/min): partial oxidation time=30 min (a); partial oxidation time=20 min (b). C deposited represents the amount of carbon formed by methane decomposition during partial oxidation step, C oxidized is the amount of carbon removed during the following carrier regeneration step.

Syngas production is stable over 8 cycles for both conditions, however, the difference in the relevance of carbon formation is immediately visible. In Figure 20a, the longer partial oxidation step leads to an average carbon formation of  $0.7\pm0.2$  mmol/ $g_{CeO_2}$  for each partial oxidation step, and the following regeneration step does not appear to be able to remove it completely, possibly due to formation of more refractory carbon species after accumulation. Indeed, the sample extracted from the reactor upon the end of the test did display the presence of small coke particles upon visual inspection, appearing visibly blackened. This leads to a syngas with an average  $H_2/CO=2.8\pm0.1$ , with an average  $H_2$  total yield of  $5.0\pm0.1$  mmol/ $g_{CeO_2}$  and an average CO yield of  $1.79\pm0.07$  mmol/ $g_{CeO_2}$ . In comparison, the shorter reaction step of Figure 20b leads to almost negligible carbon formation, with

an average of 0.16±0.06 mmol/g<sub>CeO2</sub> per step, which are completely removed during the following regeneration. Average yields of H<sub>2</sub> and CO amounted to 2.9±0.5 and 1.2±0.2 mmol/g<sub>CeO<sub>2</sub></sub>, respectively, that is to say they were ~58% and ~69% of the yields for the longer reaction step, respectively. Carbon deposition is instead decreased by ~78%. Methane conversion was not significantly affected by the shorter reaction time, with an average of 30.3±0.9% for the longer cycles and 25±4% for the shorter ones. The benefit to selectivity is therefore immediately apparent. However, the obtained yield of CO is lower than the 78% of total yield expected from observations on Figure 18. It can also be observed that the yields of reaction over cycles indeed present some instability, particularly during the cycles with shorter partial oxidation. This could possibly be attributed to thermal instability of the reactor system. As mentioned before while discussing regeneration conditions, the low O<sub>2</sub> concentration and high flowrate used for the regeneration step were selected to avoid excessive temperature peaks during the experiment. Regeneration of ceria in oxygen however is highly exothermic and even in these milder conditions lead to temperature spikes during each regeneration step, while during the endothermic partial oxidation step, temperature minima were observed. As such, particularly for the shorter cycles it was difficult to maintain reaction temperature stable, as the reactor did not have time to properly equilibrate itself between reaction steps. Furthermore, the sharp temperature spikes may lead to partial sintering of ceria, despite its thermal stability, with the loss in surface area resulting in hampered oxygen exchange and greater methane decomposition. The use of a milder oxidant can avoid this problem. Carbon dioxide has been shown to be able to oxidize cerium dioxide, and its use for reforming is particularly interesting in the framework of CCSU technologies, as discussed previously in Section 1.1.2 when talking about reforming. Therefore, a further set of cyclic tests using carbon dioxide for carrier regeneration was performed, using a CO<sub>2</sub> flowrate of 1 NL/min at 15% vol. CO<sub>2</sub> concentration. This value was chosen because it matches the typical concentration of CO<sub>2</sub> in industrial flue gasses, thus the intent was to evaluate the case of CLDR being used directly for carbon capture. The results are presented in Figure 21. For the first cycle, a partial oxidation step of 30 minutes was carried out, while all following cycles used a partial oxidation step of 20 minutes. Here also it is evident how the longer partial oxidation step is not particularly beneficial, as it mostly increases only the occurrence of carbon deposition without particularly benefitting reaction yield, ceria and methane conversion.

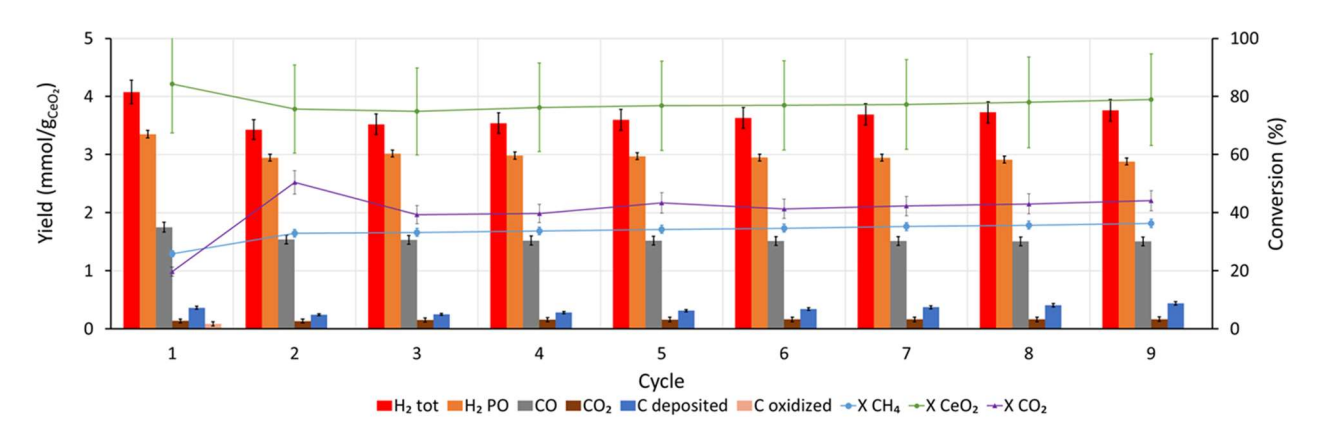


Figure 21: results of redox cyclic tests at 950 °C in 10% vol. CH<sub>4</sub> (1 NL/min), with regeneration in 15% vol. CO<sub>2</sub> (1 NL/min), partial oxidation time=20 min. C deposited represents the amount of carbon formed by methane decomposition during partial oxidation step, C oxidized is the amount of carbon removed during the following carrier regeneration step.

For the cycles with 20 min partial oxidation step (2 to 9), it can be immediately seen that the observed performance is much more stable than what observed for regeneration in oxygen, and no temperature spikes were observed during regeneration step, and the reaction yields are not compromised by the milder oxidant. On the contrary, the observed yields are higher than those of Figure 20b, with average yields of CO, CO<sub>2</sub>, and total H<sub>2</sub> equal to 1.52±0.01, 0.16±0.01, and 3.6±0.1 mmol/g<sub>CeO<sub>2</sub></sub>, respectively, demonstrating the beneficial effect of the more constant reaction temperature. Approximately 76% of the maximum syngas yield of the tests with 30 min partial oxidation is achieved, much closer to the 78% expected from Figure 18. Stable methane conversion of  $34.5 \pm 1.2\%$  and ceria conversion of  $76.8 \pm 1.3\%$  are obtained with selectivity to partial oxidation at an average value  $0.76 \pm 0.03$  based on CO formation, which is higher than what is observed for samples regenerated in oxygen. However, regeneration in carbon dioxide is less efficient for removal: an average of  $0.33 \pm 0.07$  mmol/g<sub>CeO2</sub>, are formed in each partial oxidation step, and do not appear to be removed during the following regeneration step, despite CO<sub>2</sub> being otherwise effective in restoring the oxygen capacity of ceria. Furthermore, regeneration of ceria in CO<sub>2</sub> was significantly slower compared to oxygen, requiring an oxidation time of 15 min compared to the 5 needed in oxygen. Despite the apparently ineffective coke removal, it is observed the performance of cerium dioxide remains remarkably stable for cycles with carbon dioxide in the tested conditions. Cerium dioxide appears to be highly resistant to carbon formation, so the unstable activity of the cycles with regeneration in oxygen likely is not caused by coking. As mentioned before, sintering may be the cause for the loss in activity. Cerium dioxide has a high melting temperature and is generally resistant to major sintering, but it nonetheless may occur, especially in the form of grain growth. To reduce sintering, more refractory supports can be used in mixture with cerium dioxide to help prevent particle aggregation. Alumina is one such refractory

material, commonly used as support for catalysts due to its high thermal stability, mechanical resistance and low cost [452]. In previous work, a mixture of Al<sub>2</sub>O<sub>3</sub> and CeO<sub>2</sub> at 30% wt. Al<sub>2</sub>O<sub>3</sub> showed improved performance for methane reforming [404]. Such a sample is here tested again to better assess its performance. Results of these tests are shown in Figure 22.

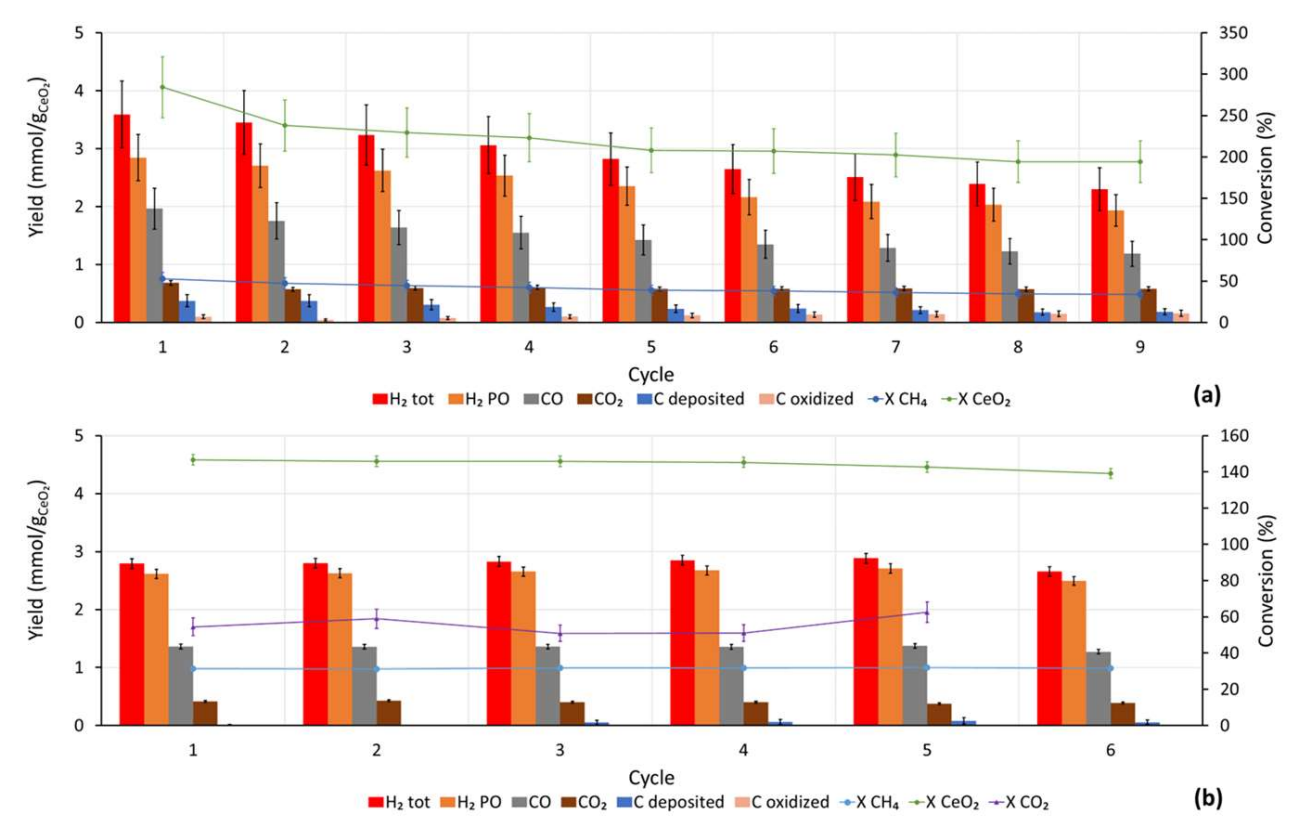


Figure 22: results of redox cyclic tests at 950 °C in 1 NL/min 10% vol. CH<sub>4</sub> on CeO<sub>2</sub>-Al<sub>2</sub>O<sub>3</sub> carrier, partial oxidation time=20 min: regeneration in 1 NL/min 3% vol. O<sub>2</sub> (a); regeneration in 1 NL/min 15% vol. CO<sub>2</sub> (b). C deposited represents the amount of carbon formed by methane decomposition during partial oxidation step, C oxidized is the amount of carbon removed during the following carrier regeneration step. For cycle 6 regeneration was not recorded.

Figure 22a reports the results for cycles performed with regeneration in oxygen, while cycles in Figure 22b are carried out with regeneration in 15% vol. CO<sub>2</sub>. Again, instabilities in performance are observed when regenerating in oxygen likely due to the thermal excursion caused by the exothermic regeneration step. Average yields observed in this condition are of 2.9±0.5, 1.5±0.3 and 0.59±0.03 mmol/g<sub>CeO2</sub> for H<sub>2</sub>, CO and CO<sub>2</sub>, respectively, with average H<sub>2</sub>/CO of 1.95±0.05. Carbon formation amounts to an average of 0.27±0.07 mmol/g<sub>CeO2</sub> per partial oxidation step, which do not appear to be completely oxidized during regeneration. When regenerating in CO<sub>2</sub> instead, average yields amount to 2.80±0.01, 1.35±0.04 and 0.40±0.02 mmol/g<sub>CeO2</sub> for H<sub>2</sub>, CO and CO<sub>2</sub>, respectively, and average

H<sub>2</sub>/CO=2.08±0.02. Carbon formation here appears higher, at an average of 0.7±0.4 mmol/g<sub>CeO2</sub>, but performance of the oxygen carrier is nonetheless stable for the investigated cycles. It is interesting to observe that here the yields of CO almost match the yields of CO observed for pure CeO<sub>2</sub> oxygen carrier at 20 min partial oxidation time in either O<sub>2</sub> (1.2±0.2 mmol/g<sub>CeO2</sub>) or CO (1.52±0.01 mmol/g<sub>CeO2</sub>) atmosphere and display an improved H<sub>2</sub>/CO ratio much closer to the stoichiometric 2, despite the lower amount of CeO<sub>2</sub> present in the mixed oxide oxygen carrier. This may demonstrate that the mixed oxide displays improved oxygen mobility, and can be further deduced from the fact that in these cases, the mixed OC appears to reach a reduction extent higher than what would be expected by pure ceria (see CeO<sub>2</sub> conversion plotted in Figure 22). Conversion of methane is also generally higher on the mixed oxide carrier, averaging at 41±6% when regenerating in oxygen and 31.6±0.3% when regenerating in CO<sub>2</sub>. CO<sub>2</sub> conversion also appears enhanced, at an average of 56±6%. To obtain further insight into the oxygen carrier behavior, XRD and SEM analysis were performed on samples as prepared and after reaction.

## 1.3.3.4-XRD and SEM analysis of the tested oxygen carriers

XRD analysis of the prescreened CeO<sub>2</sub>, chromite and CeO<sub>2</sub>-CuO oxygen carriers is shown in Figure 23. Samples of the pristine oxygen carriers as well as of the carriers after reaction cycles at 950 °C were investigated to assess eventual changes in their phase structure.

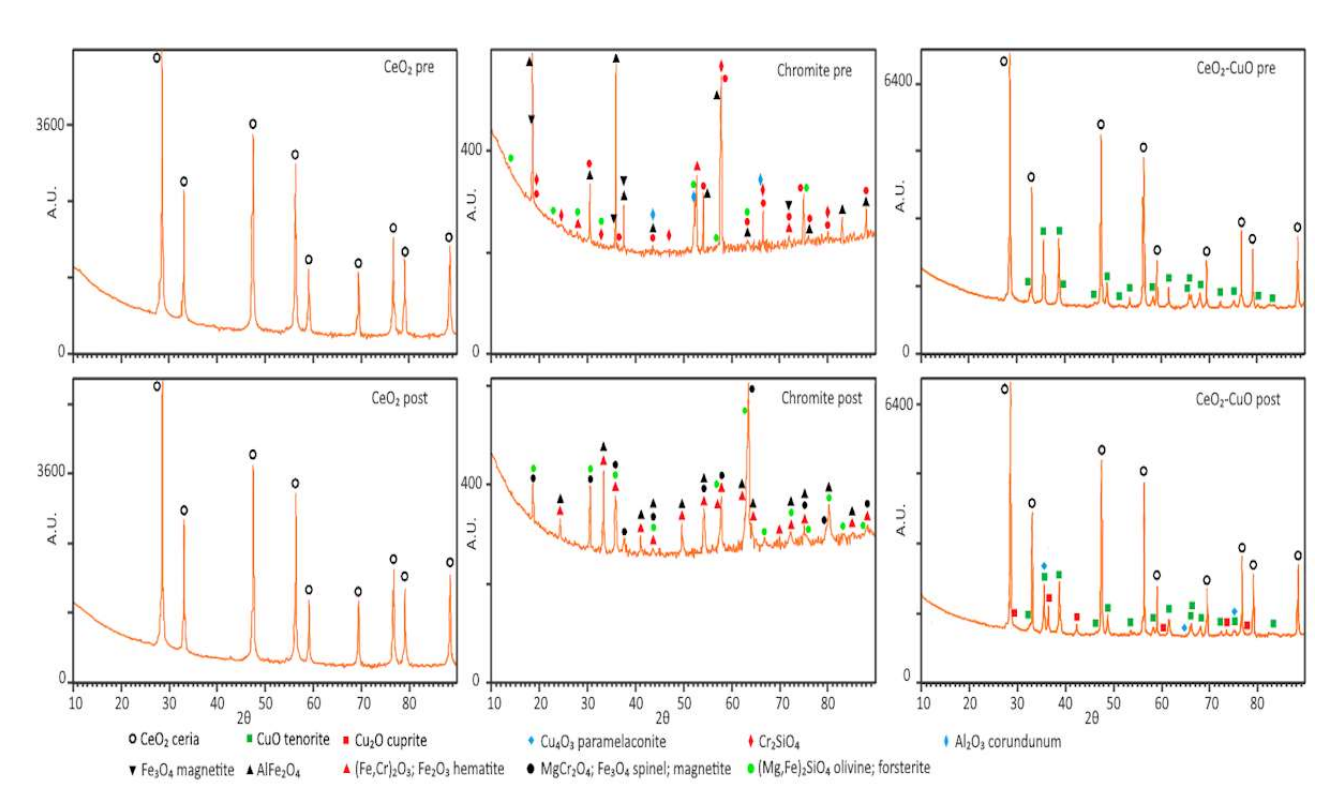


Figure 23: XRD analysis of CeO<sub>2</sub>, chromite and CeO<sub>2</sub>-CuO oxygen carriers. Pre=pristine oxygen carrier; Post=oxygen carrier after reaction at 950°C.

It is immediately evident that the carriers differed significantly in behavior among each other. The pure CeO<sub>2</sub> carrier was unchanged before and after reaction in terms of phases, presenting only a pure CeO<sub>2</sub> phase which is maintained after the redox cycles are complete, and also in terms of cell parameters, showing completely coherent spacing and intensity of reflections before and after treatment. None of the thermodynamically possible reduced forms of cerium oxides (i.e. Ce<sub>2</sub>O<sub>3</sub>, Ce<sub>3</sub>O<sub>5</sub>, etc.) appear in the spectrum of the carrier after redox cycles. This suggests that regeneration of the carrier was indeed complete, and that cerium dioxide is resistant to multiple redox cycles at the tested temperature (950 °C).

On the other hand, the chromite carrier appears severely altered after the redox cycles. In particular, appearance of a Fe<sub>2</sub>O<sub>3</sub> phase is clearly evident in the sample after reaction, effectively confirming that the iron content of chromite can be effectively oxidized and used to exchange oxygen during redox cycles with methane. However, several other structures appear also after reaction, with iron and chromium oxides forming spinel species. Furthermore, the disappearance of some chromium species (Cr<sub>2</sub>SiO<sub>4</sub>) in the spectra after reaction might also suggest that a segregation of iron phases on grain surface has occurred. A higher baseline is observed for the spectra of chromite compared to the other carriers, which can be attributed to the lower crystallinity of this natural material compared to the other carriers. The baseline and intensity of the peaks are also altered after reaction suggesting

that the material modified its crystallinity during reaction. Indeed, severe sintering was observed to occur for this oxygen carrier, as observed in Section 1.3.3.1. Therefore, in the tested conditions, chromite structure is not stable, and the material cannot be effectively regenerated, as the formation of spinel phases sequesters active iron species from participating in the redox reaction.

Finally, the CeO<sub>2</sub>-CuO shows some differences before and after reaction. Before reaction, the only phases present are the two pure oxides, with no visible impurities. After the reaction cycles however, the carrier shows evidence of incomplete regeneration, with reduced copper oxide species being present (Cu<sub>2</sub>O, Cu<sub>4</sub>O<sub>3</sub>). The incomplete regeneration of copper oxide can be attributed to the high release of gaseous oxygen from the oxide at high temperature, which makes regenerating the carrier more difficult compared to cerium oxide, which instead appears here to also be completely regenerated. A certain difference in crystallite size can also be appreciated before and after reaction, pointing to the occurrence of grain growth.

Oxygen carrier samples were further investigated under SEM to observe the structure of their surface before and after reaction, shown in Figure 24. Again, it is immediately noticeable how the surface of CeO<sub>2</sub> appears unchanged after reaction, again confirming its stability. On the other hand, both the CeO<sub>2</sub>-CuO and especially the chromite oxygen carriers demonstrate evidence of sintering on their surface, with chromite oxide in particular displaying a greatly altered surface structure.

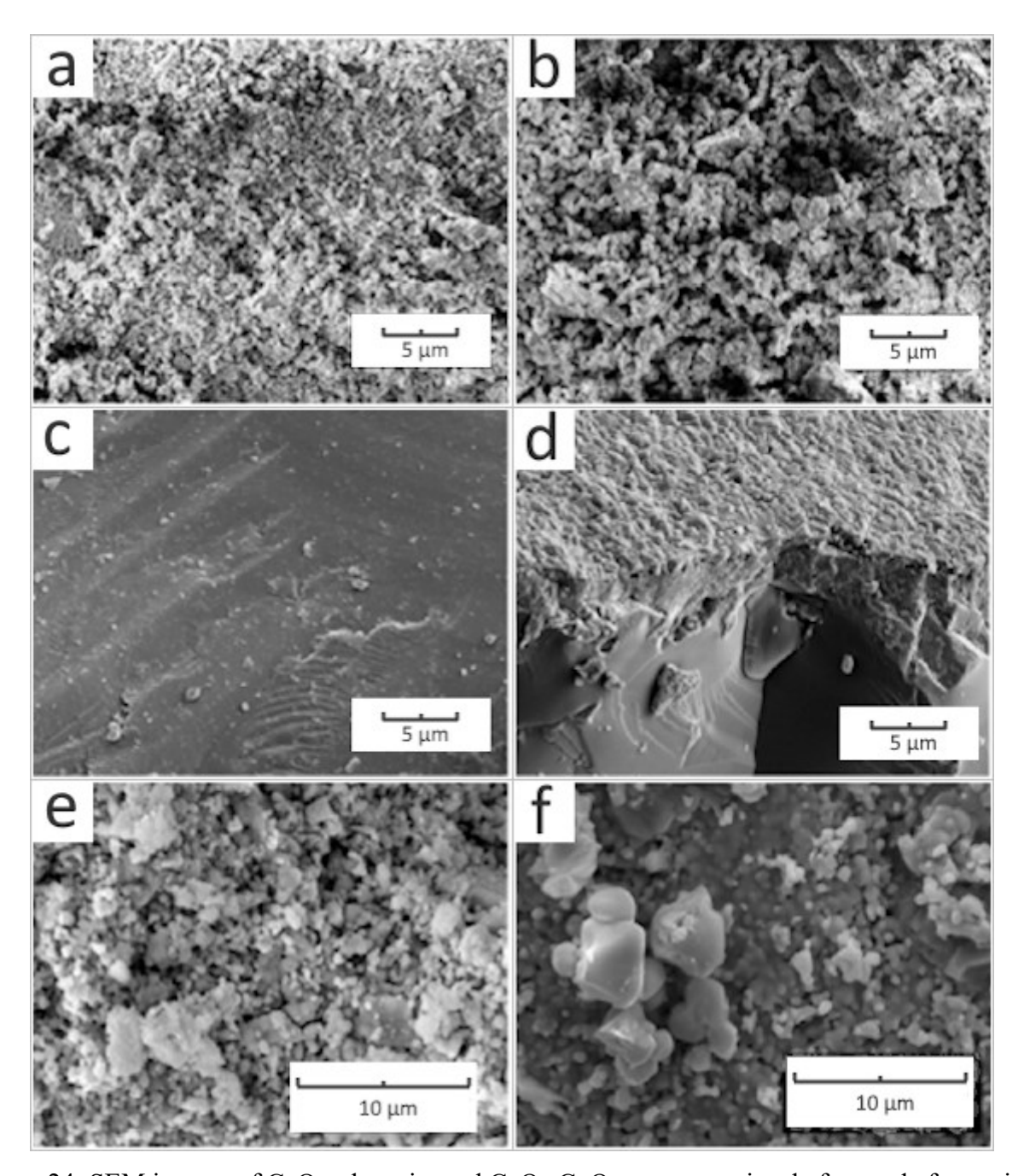


Figure 24: SEM images of CeO<sub>2</sub>, chromite and CeO<sub>2</sub>-CuO oxygen carriers before and after activity screening cycles [453]. CeO<sub>2</sub> before reaction (a); CeO<sub>2</sub> after reaction (b); Chromite before reaction (c); Chromite after reaction (d); CeO<sub>2</sub>-CuO before rection (e); CeO<sub>2</sub>-CuO after rection (f). All images are at 10000× magnification.

A further SEM examination was performed on the cerium dioxide and CeO<sub>2</sub>-Al<sub>2</sub>O<sub>3</sub> oxygen carriers before and after the long reaction tests with regeneration in oxygen or carbon dioxide. These are shown in Figure 25. For these longer reaction cycles, pure cerium dioxide shows evidence of grain growth both when regenerated in oxygen (Figure 25c and d) and CO<sub>2</sub> (Figure 25e and f), although aggregation is much more noticeable in the sample regenerated in oxygen. Samples after reaction

cycles indeed display apparently larger surface particles with smoother surface compared to the pristine oxygen carrier. This aggregation is likely the cause of the increasing carbon deposition occurring on ceria regenerated in oxygen, seen in Figure 20, as the loss in surface area may lead to impeded oxygen release(Figure 25g and h) not only displays smaller surface grains, but also decreased sintering after reaction (Figure 25i and j) thus possibly explaining its more stable performance seen in Figure 22.

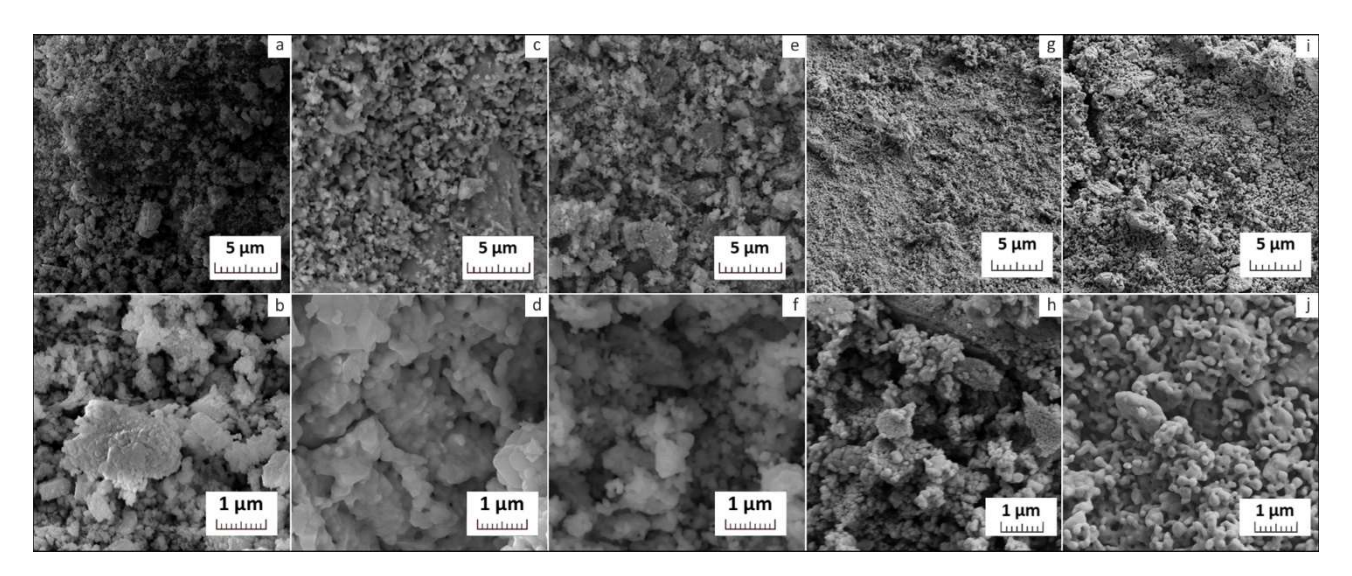


Figure 25: SEM microscopy of CeO<sub>2</sub> and CeO<sub>2</sub>-Al<sub>2</sub>O<sub>3</sub> oxygen carriers before and after redox tests with 20 min partial oxidation step [454]: CeO<sub>2</sub> before redox cycles (a, b); CeO<sub>2</sub> after reaction with O<sub>2</sub> regeneration (c, d); CeO<sub>2</sub> after reaction cycles with CO<sub>2</sub> regeneration (e, f); CeO<sub>2</sub>-Al<sub>2</sub>O<sub>3</sub> before (g, h) and after cycles in both O<sub>2</sub> and CO<sub>2</sub> (i, j). Upper images are at 10000× magnification, bottom images are at 40000× magnification.

### 1.3.3.5-Results of numerical simulation

Numerical simulation in Aspen Adsorption<sup>TM</sup>, using kinetics by Zhao 2016 [447], was performed to attempt to replicate experimental results for the pure CeO<sub>2</sub> sample regenerated in CO<sub>2</sub>, in a first attempt at performing a complete process simulation. The experimental and simulated results for gas profile at reactor outlet are compared in Figure 26.

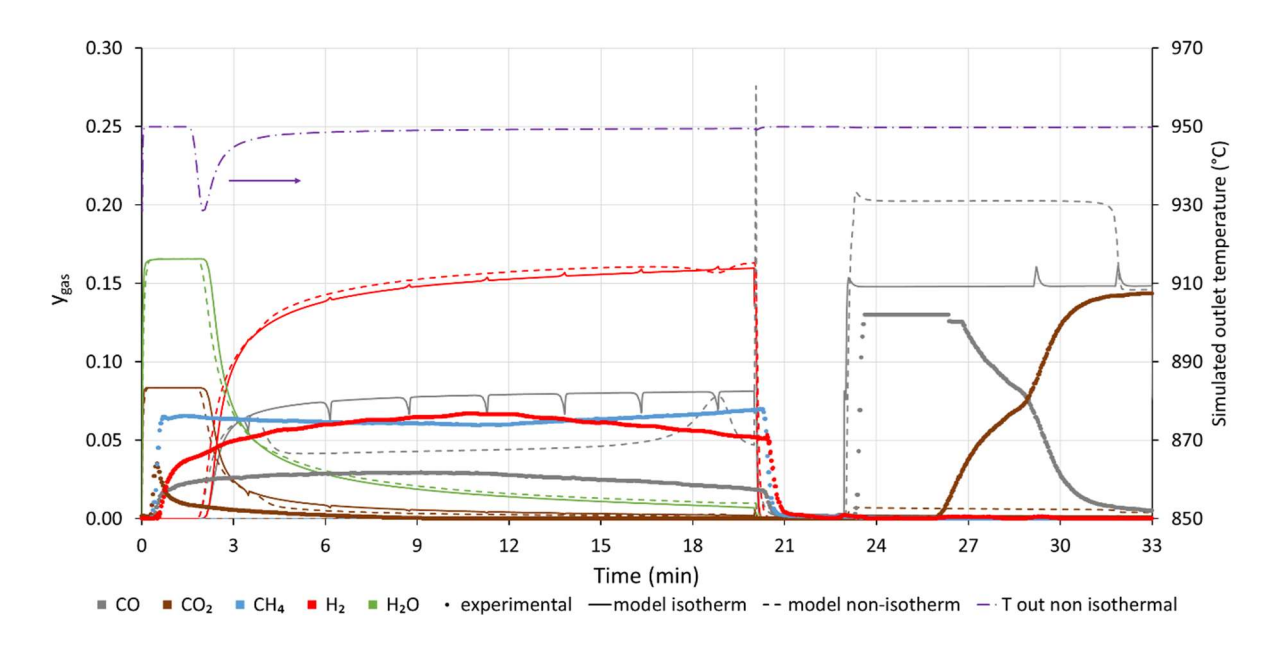


Figure 26: comparison between experimental data, isothermal simulation and non-isothermal simulation of a redox cycle for CeO<sub>2</sub> oxygen carrier for reduction in 10% vol. CH<sub>4</sub> (1 NL/min) and regeneration in 15% vol. CO<sub>2</sub> (1 NL/min) at 950 °C. The simulated gas outlet temperature for the non-isothermal simulation is also shown on secondary axis to demonstrate that the simulated heating regime was able to maintain temperature sufficiently stable.

It can be observed that while the simulated profiles qualitatively show the same behavior of the experimental data, with initial complete oxidation followed by selective syngas generation, quantitatively the prediction provided by the literature model is not accurate. It can be seen that using the kinetic rates as reported in literature, complete methane conversion is obtained both for isothermal and non-isothermal simulation, thus the estimated production of all gases is much greater than the experimental results suggest. Regeneration of the oxygen carrier is also characterized by a great overestimation of carbon dioxide conversion. It is currently unclear whether the divergence of simulated results from experimental values can be attributed to the kinetic model or if improved modelling of mass transfer in the column may improve the results. However, it should be observed that the current kinetic model was unable to simulate the complete reduction of cerium dioxide. Attempt at simulating a partial oxidation step of 30 min, which experimentally was shown to lead to complete carrier reduction, lead to premature crashing of the numerical solver. A possible issue is that the kinetic model as proposed by Zhao [447] was only tested for a more limited reduction extent of the carrier, and was thus unable to properly account for the decrease in kinetics of partial oxidation as oxygen lattice is depleted. The qualitative match between the model and the experimental results suggests that the current proposed mechanism could be able to correctly represent the chemical looping reforming of methane on cerium dioxide oxygen carrier, but more accurate fine tuning at

higher carrier reduction extent is needed to produce accurate simulations. More accurate data for reaction enthalpy of non-stoichiometric cerium dioxide with methane is also needed to complete the reaction mechanism investigation and correctly simulate the process.

### 1.3.4-Conclusion and future perspectives

The chemical looping approach offers the opportunity of developing more sustainable reforming processes and is particularly interesting for the purpose of dry reforming with coupled carbon capture and utilization. Development of cheap and efficient oxygen carriers is the key to developing competitive chemical looping reforming processes. Different oxygen carriers were here tested for the purpose of producing syngas with stable H<sub>2</sub> to CO ratio close to 2. Chromite is a natural mineral rich in iron and chromium, with waste for its mining industry having already been investigated for its use as oxygen carrier. In the present thesis, chromite itself was for the first time assessed as an oxygen carrier for methane reforming. The chromite oxygen carrier did not perform well for production of syngas, demonstrating low yields and selectivity, favoring instead complete combustion and carbon formation. Visual investigation, XRD and SEM analysis of the carrier after being exposed to chemical looping cycles in methane show evident occurrence of sintering and alteration of surface morphology and composition, explaining the carrier unstable performance under reforming conditions. Cerium dioxide instead was confirmed as a stable oxygen carrier selective for syngas production. Kinetic investigation showed that the cerium dioxide carrier developed in this study provides low performance at temperature below 900 °C. On the other hand, when going from 900 °C to 950 °C, the reaction rates of methane oxidation are almost doubled, with carbon deposition becoming relevant only upon 40% carrier conversion for a methane feed at 10% vol. CH<sub>4</sub>. A temperature of 950 °C appears as the best compromise between fast redox reaction kinetics and low coke deposition, thus greater emphasis was put on the need of optimizing utilization of the oxygen carrier while compromising between selectivity and yield through proper selection of the partial oxidation step duration. At 20 min of partial oxidation time and temperature of 950 °C, the obtained average yields for pure cerium dioxide are 2.9±0.5 and 1.2±0.2 mmol/g<sub>CeO2</sub> for H<sub>2</sub> and CO, respectively, when regenerating the sample using 3% vol. oxygen atmosphere. In these conditions, an average of 0.16±0.06 mmol/g<sub>CeO2</sub> moles of carbon are formed in each partial oxidation step and the average conversions of methane and ceria are of 25±4% and 55±7%, respectively. The obtained partial oxidation yield in these conditions reaches as high as 69% of the yield obtained for longer cycles with 30 min partial oxidation step while demonstrating a decrease of 78% in the amount of coke deposited. Regeneration in oxygen allows for complete coke removal upon optimization of reaction time. When regenerated in 15% vol. CO<sub>2</sub>, pure cerium dioxide instead displayed average yields of CO, and H<sub>2</sub>

equal to 1.52 $\pm$ 0.01 and 3.6 $\pm$ 0.1 mmol/g<sub>CeO2</sub>, respectively, with stable methane conversion of 34.5  $\pm$ 1.2%, ceria conversion of 76.8  $\pm$  1.3% and an average yield for coke formation of 0.33  $\pm$  0.07 mmol/g<sub>CeO2</sub> in each partial oxidation step. The less exothermic regeneration reaction leads to lower catalyst sintering, as supported by SEM analysis, and thus more stable performance. In these conditions, the oxygen carrier was able to reach 76% of the partial oxidation yield achieved for the oxygen carrier exposed to the longer partial oxidation cycles with regeneration in oxygen, which is well correlated with the observed 76.8% conversion of cerium dioxide. Removal of coke is worse when compared to regeneration steps carried out in oxygen, however this does not seem to alter the performance of the oxygen carrier for at least the 8 cycles tested in the present work. Further tests with greater number of reaction cycles are needed to better assess the continued performance of the oxygen carrier in these conditions. Overall, cerium dioxide shows good selectivity to syngas formation and stable performance over repeated cycles, however efforts are needed to improve methane activation on its surface and increase conversion. Addition of 50% mol CuO to the carrier negatively affected the reforming reaction, completely switching selectivity towards complete combustion due to the release of gaseous oxygen from copper oxide. On the other hand, working with a 30% wt. mixture of Al<sub>2</sub>O<sub>3</sub> in CeO<sub>2</sub> appeared to benefit the utilization of carrier lattice oxygen, stabilizing syngas production and lowering coke deposition while apparently allowing for deeper carrier reduction and increasing methane conversion. Average yields for the CeO<sub>2</sub>-Al<sub>2</sub>O<sub>3</sub> carrier are of 2.9±0.5 and 1.5±0.3 mmol/g<sub>CeO2</sub> for H<sub>2</sub> and CO, respectively, with average carbon formation of 0.27±0.07 mmol/g<sub>CeO2</sub> per partial oxidation step and 41±6% average methane conversion when regenerating the carrier in 3% vol. oxygen. When regenerating in CO<sub>2</sub> instead, average yields amount to 2.80±0.01 and 1.35±0.04 mmol/g<sub>CeO2</sub> for H<sub>2</sub> and CO, with average coke formation of 0.7±0.4 mmol/g<sub>CeO2</sub> per partial oxidation step and 31.6±0.3% average methane conversion. The maximum instantaneous methane conversion observed in cerium dioxide carriers approaches 70% at the start of reduction step, coinciding with the onset of complete oxidation, but conversion then quickly decreases for all OCs stabilizing around 30%, before decreasing again up to 10% once cerium dioxide approaches 40% reduction. Future development of cerium dioxide oxygen carriers will require to obtain carriers with stable and greater surface area and improved methane activation without utilizing toxic and expensive nickel coating. Nanostructured cerium dioxide materials therefore appear as a good option for chemical looping reforming. The improved methane activation on CeO<sub>2</sub>-Al<sub>2</sub>O<sub>3</sub> mixture points to the possibility of obtaining better performing carriers utilizing cheap material supports.

Finally, an attempt at numerical simulation of the process was carried out using available literature data for kinetics and mechanism of methane-cerium dioxide reaction. Numerical simulation results

qualitatively match experimental observation, however fine tuning of the model, particularly on deeper reduced cerium dioxide, and further data on the thermodynamics of the elemental reaction steps of non-stoichiometric ceria are required to obtain accurate quantitative prediction of process yields. Furthermore, the current kinetic model does not consider other common surface species that can be formed from reaction of cerium oxide surface with methane, water and hydrogen, such as surface hydrides, which have already been observed to form on ceria surface and might play an important role in the mechanism of water splitting and hydrogen formation [455–457]. The complete kinetic model could then be used to provide useful data on the optimization of reaction conditions for the reforming process.

# Part 2: Numerical simulation of a multicomponent adsorption column for a Vapor Recovery Unit for capture of fuel storage tank VOCs vapors using Aspen Adsorption<sup>TM</sup> software.

# 2.1- Incidence and harmful effects of exposure to VOCs in refineries

As mentioned in the introduction, VOCs are among the most relevant pollutants produced by human activities. VOCs exposure is a serious concern both for human health and for the safety of the environment. For example. Abundant literature exists on the negative effects of VOCs on human health; positive correlations have been found between exposure to VOCs and incidence of atopic dermatitis in children [458], respiratory problems [459,460], lung cancer [461], breast cancer [462], neurological disturbs [463] and several other pathologies [26,464–466]. Figure 27 reports the documented health effects for some common VOCs. In addition to their direct toxicity, several VOCs can also lead to ground level ozone formation, itself a dangerous secondary pollutant [467].

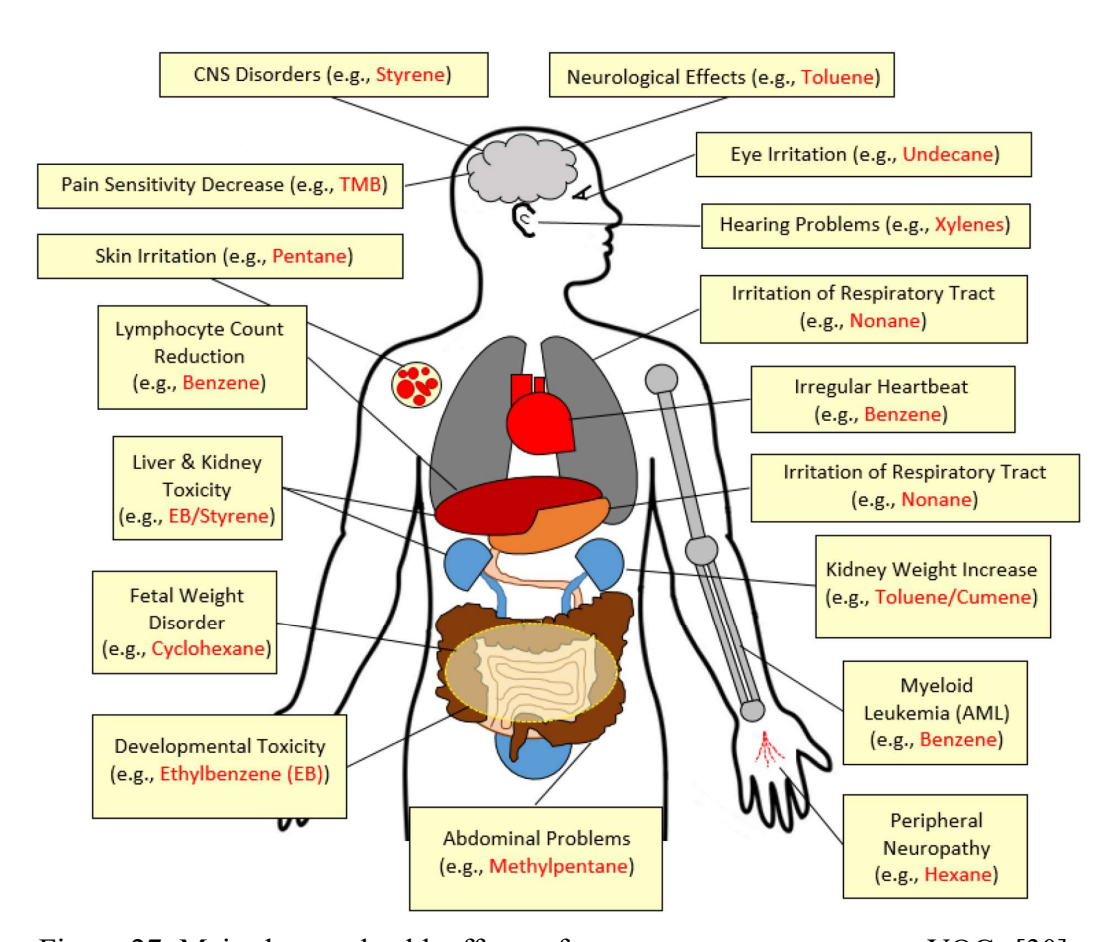


Figure 27: Major human health effects of exposure to some common VOCs [30].

The petrochemical industry is one of the principal sources of anthropogenic VOCs emissions. Potentially concerning levels of VOCs concentrations have been observed in the air near refineries around petroleum treatment plants around the world [468–471]. Population living near refineries have shown increased incidence of pathologies such as leukemia [472], respiratory inflammation and lung cancer [473]. Indeed, despite some contrasting studies [474], the presence of refineries has been generally correlated with increased risk of several types of cancer in the surrounding area [475–477], and literature consistently reports particularly increased risk for refinery workers that face daily exposure to potentially dangerous levels of VOCs [478–480]. In addition to their health and environmental threat, emissions of VOCs are also a relevant economic loss, as potentially valuable refinery products are dispersed in the environment. For example, even considering a rate of evaporation of crude oil limited to 1%, as much as 488267 \$/day of product can be lost [481]. Therefore, abatement of VOCs emissions, coupled with recovery of the abated products, plays an essential role in optimization of refinery processes. VOCs can be emitted along the whole chain of refinery processes. Figure 28 shows an example of emission source distribution in a refinery.

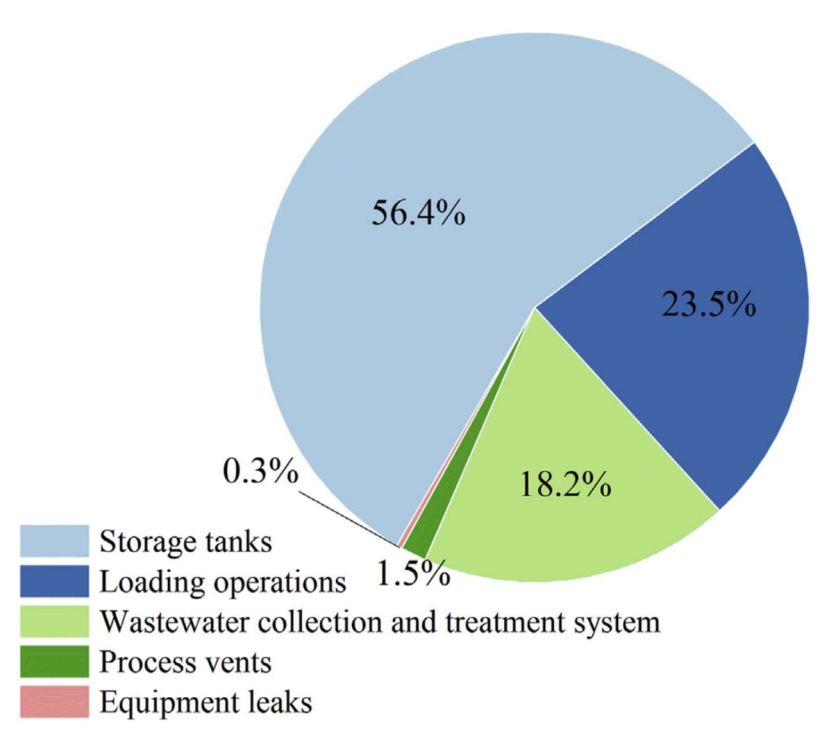


Figure 28: VOCs emission sources and their contribution to total emission in a petroleum refinery in Shandong, China [482].

It is immediately evident how storage tanks and their loading operations are associated alone with 79.9% of the total refinery emissions, constituting therefore the main source of VOCs releases. In

general, storage tanks have been reported as a consistent point source of VOCs emissions in literature, amounting to 20-40% of total emissions of refineries [483,484]. As such, strategies to control tank emissions are crucial to reducing risks and increasing revenues. Emission from storage tanks, in the absence of critical equipment failure, can be mainly of two types: evaporation losses [485], which cause gradual release distributed over time, and working losses [486], more intense point losses which are caused by the rapid displacement of tank vapors and flash evaporation of liquid during loading and unloading operations. Significant efforted has been attributed in literature to the analysis and simulation of VOCs emissions from storage tanks. Literature analysis points at light alkanes as the main VOCs that are emitted, but significant traces of alkenes and aromatics can also be present [482,486]. Composition of VOCs emitted can greatly vary according to the nature of their parent liquid fuel [487], and can even be subjected to seasonality, as the different environmental conditions affect the evaporation rate of the various compounds [488]. Different models have also been proposed to simulate their emission rate [489-491]. In general, the complexity and variability of composition of crude oil hydrocarbon mixtures makes the treatment of their associated VOCs emissions a complicated issue. In the following section, the main technologies for VOCs abatement will be briefly presented, with a focus on the use of adsorption as the most common option.

# 2.2-Vapor recovery units

Given the hazards and economic losses associated with VOCs releases from storage tanks, several solutions have been proposed to mitigate losses. Optimization of design of tanks, their sealing and their careful maintenance can noticeably reduce emissions [492,493], and noticeable effort has been put on monitoring systems for quick detection of losses [494,495]. However, these measures alone cannot effectively mitigate the problem, especially when considering losses during loading operation or triggering safety pressure valves. In the past such emissions would typically be flared as a measure of VOCs abatement, which is not an ideal solution as it can lead to imperfect abatement with formation of secondary pollutants, while at the same time destroying what could be valuable products [496,497]. As such, nowadays it is commonly required that refineries utilize vapor recovery units (VRUs) [498], that is to say installations with the purpose of capturing the fugitive VOCs emission and reinserting them in the storage tank, to avoid losses. Different technologies have been proposed for VOCs recovery [499]; the following sections will offer a brief overview on the available alternatives.

### 2.2.1-Condensation/cryogenic separation

Condensation is perhaps the conceptually simplest approach to VOCs abatement. Here, fugitive streams are intercepted, compressed and then cooled to liquefy the VOCs and then recycle them to the storage tanks. Since VOCs are by definition characterized by their high volatility and thus low boiling points, a cryogenic cycle is used to obtain temperature low enough for their efficient condensation [500]. Dunn et al. [501] first proposed an approach for optimal selection of condensation method focused on three essential questions:

- Which refrigerants ought to be used for cooling/condensation?
- What is the optimal load to be removed by each refrigerant?
- What is the sequence of waste stream/refrigerant matches and how should the system be configured?

Liquid nitrogen is a common refrigerant for VOCs recovery application, commonly organized in a three-step refrigeration cascade [502], but some thermodynamic studies suggest that use of mixed refrigerants might allow for enhanced performance [503]. Condensers are essentially of two types [504]: surface condensers such as the typical pipe-and-shell design exchange heat through an intermediate solid surface without direct physical contact between the gas stream and the refrigerant, while contact condensers exchange heat by direct two. While the latter allow for much faster heat exchange, they are less used as the refrigerant cannot be efficiently recycled and is mostly lost in the process. A common problem of condensation is its sensitivity to the presence of humidity in the gas

current, which can freeze and cause damage to equipment, as well as hinder recovery efficiency by reducing heat exchange [505]. In general, cryogenic condensation is best suited to work on rather concentrated currents (>5000 ppm) and can guarantee recoveries greater than 99% when properly optimized, however the outlet concentration is strictly dependent on the refrigeration temperature reached, with temperatures as low as -160 °C may be needed to meet these requirements [506,507], with considerable costs and energy expense for the refrigeration cycle. The lower boiling point light hydrocarbons such as ethane and propane in particular are very difficult to remove, especially considering the stricter environmental laws on emission limits of the late years. Additionally, possible polymerization of VOCs and explosion risks due to the crossing of upper flammability concentration thresholds during VOCs condensation are other problems associated to condensation separation [508].

### 2.2.2-Membrane separation

Membranes have been often proposed as a solution for VOCs abatement. They are operationally simple to implement, and can offer good selectivity, scalability and high recovery at a low energy intensity [508,509]. For example, Choi et al. evaluated that hollow fiber membrane modules could provide a useful solution for VOCs emission abatement in oil tankers [510]. Zhao et al. demonstrated improved permeability and selectivity for toluene and cyclohexane separation from N<sub>2</sub> in octyl-modified polyhydromethylsiloxane membranes [511]. Shirke et al. proposed SiO<sub>2</sub> based hollow fiber composite membranes for recovery of toluene from toluene/N<sub>2</sub> mixtures [512]. Several other types of membranes, ranging from polymeric to composite and liquid membranes, have been tested for VOC separation, however, despite promising results, membrane have not yet seen wide scale application in vapor recovery, with the main obstacles being provided by the usually high costs and difficulty of membrane fabrication coupled with their still limited efficiency and durability under industrial operation conditions [513,514].

# 2.2.3-Absorption

Liquid absorption of VOCs in tower scrubbers has already been effectively employed for VOCs abatement, saving as much as 606800 \$/year of product loss [33,515]. Fixed bed column contactors are the most common choice for gas-liquid absorption processes, due to their ability to offer enhanced surface area for gas-liquid mass transfer [516]. The absorption process can be either purely physical, with the separation depending only on the vapor pressure and on the solubility of the gaseous species in the selected solvent, or reactive, with the presence of active chemical reaction between solvent species and gas acting to enhance the capture [517,518]. In general, while physical absorbents may

be less effective than chemical absorption in terms of level of emission abatement reached, they are easier to regenerate and allow for more effective non-destructive recovery of products. While several different liquids have been proposed for VOCs abatement in different industry fields, from ionic liquids to deep eutectic solvents [519–521], when considering the purpose of vapor recovery for storage tanks the most cost-effective solution is to simply use part of the tank liquid content to scrub the produced vapors, physically absorbing the VOCs, and then reintroducing the VOCs containing liquid stream directly to the tank, thus avoiding the costs of solvent regeneration by stripping normally involved in absorption processes [522]. With this optimized approach, up to 95% recovery of VOCs can be achieved [522]. However, liquid absorption alone is often insufficient to meet the required levels of abatement and recovery required by environmental regulation and cost effectiveness goals [523].

### 2.2.4-Adsorption

Adsorption technology involves the capture of VOCs on the surface of solid material adsorbents and has seen much development for the purpose of VOCs abatement and vapor recovery [524], thanks to its high removal efficiency, cost effectiveness and low energy consumption [525]. Dwidedi et al. compared adsorption to cryogenic concentration and found it much more effective in dealing with low concentration emissions [526]. As in the case of liquid absorption, both purely physical adsorption and chemical adsorption may be employed, based on the strength of the bonds formed between the adsorbent and the adsorbed compounds [527], although in the case of VOCs emission abatement chemisorption is mostly associated with destructive abatement rather than product recovery [528]. Several different adsorbent materials have been studied for the purpose of VOCs abatement and recovery, each with its own advantages and disadvantages [529]. Activated carbons are a common choice for these applications, thanks to their relatively low cost, high surface area and good capture efficiency [530,531]. Effective activated carbons can be produced from renewable sources such as biomass, providing opportunities for waste valorization [532,533]. A downside of the use of activated carbon is their flammability, which requires the installation of fire monitoring and extinction inside the adsorption columns, and gradual loss of adsorption capacity requiring periodic high temperature regeneration [530]. Zeolites [534] and metal-organic frameworks (MOFs) [535] are the other common choices for adsorbent materials, with zeolites offering good thermal stability and MOFs providing great tunability of adsorption selectivity, however they are hindered by the complexity of their synthesis and high costs of production [525]. Finally, silica gels have also been evaluated for VOCs abatement applications [536]. Adsorption can be performed in different configurations:

- Pressure swing adsorption (PSA) [537]: in this configuration, adsorption is performed at high pressure, then the adsorbent is regenerated by lowering the pressure. A variant of this process is the Vacuum swing adsorption (VSA) [538], in which adsorption is carried out around atmospheric pressure and the adsorbent is regenerated under vacuum.
- Temperature swing adsorption (TSA) [539]: here, adsorption, which is a typically exothermic process, is carried out at low temperature, then the adsorbent is regenerated by heating.
- Combined temperature-pressure swing approaches [540,541].

So far, PSA operation has found the significant application for VOC recovery [542], thanks to the shorter operation cycles, lower risk for flammability and lack of requirements for heat exchange equipment and utilities, but is negatively affected by the more complex operation, limited bed size allowed and high degree of vacuum that may be required for effective adsorbent regeneration. Nonetheless, PSA has already successfully been applied to VOCs recovery from hydrocarbon storage tanks [543,544].

# 2.2.5-Combined approaches

Each of the above-mentioned technologies displays its own advantages and criticalities. Much attention has thus been dedicated in literature to the study of combined separation processes that strive to combine them in order to cover for their respective weaknesses and improve the overall performance of the separation process. Gupta et al. suggested through a modeling study that condensation could be used as an effective pretreatment to adsorption, lowering the complications related to excessive temperature increase in adsorption column due to release of adsorption heat and improving VOCs abatement [545]. For such a combination, Liang et al. recently estimated a promising 99.2% abatement efficiency, with a payback time of 2.3 years [546]. Membrane based separation has been also evaluated to be used in combination with condensation, proving particularly efficient for the separation of lower boiling point substances [547]. Pervaporation membranes have also been proposed as a more energy efficient alternative to stripping for solvent regeneration in liquid adsorption processes [548]. Membranes could also be used as effective pre or post treatment for adsorption processes [549]. Nowadays, the most common solution for vapor recovery is the combination of adsorption and absorption processes [35,498], shown in Figure 29 in its simplest form. The gaseous mixture to abate is first fed to one of two cyclically operating adsorption beds, from which purified air is obtained, while the other bed undergoes regeneration (either temperature or pressure swing and with or without the use of purge gas) the gaseous stream from the regenerating bed is sent to the adsorber, where liquid feed from the tank is used to reabsorb remaining VOCs content to be sent back to the tank. The gaseous stream exiting the absorber is recycled in the feed to the adsorption beds. Periodically the two adsorption beds switch between adsorption and regeneration phase, ensuring that outlet gas purity is maintained stable during the operation. This approach has seen different patents deposited along the years [550–552] and has seen successful commercial application, such as in the SORBATHENE<sup>TM</sup> process proposed by DOW [553].

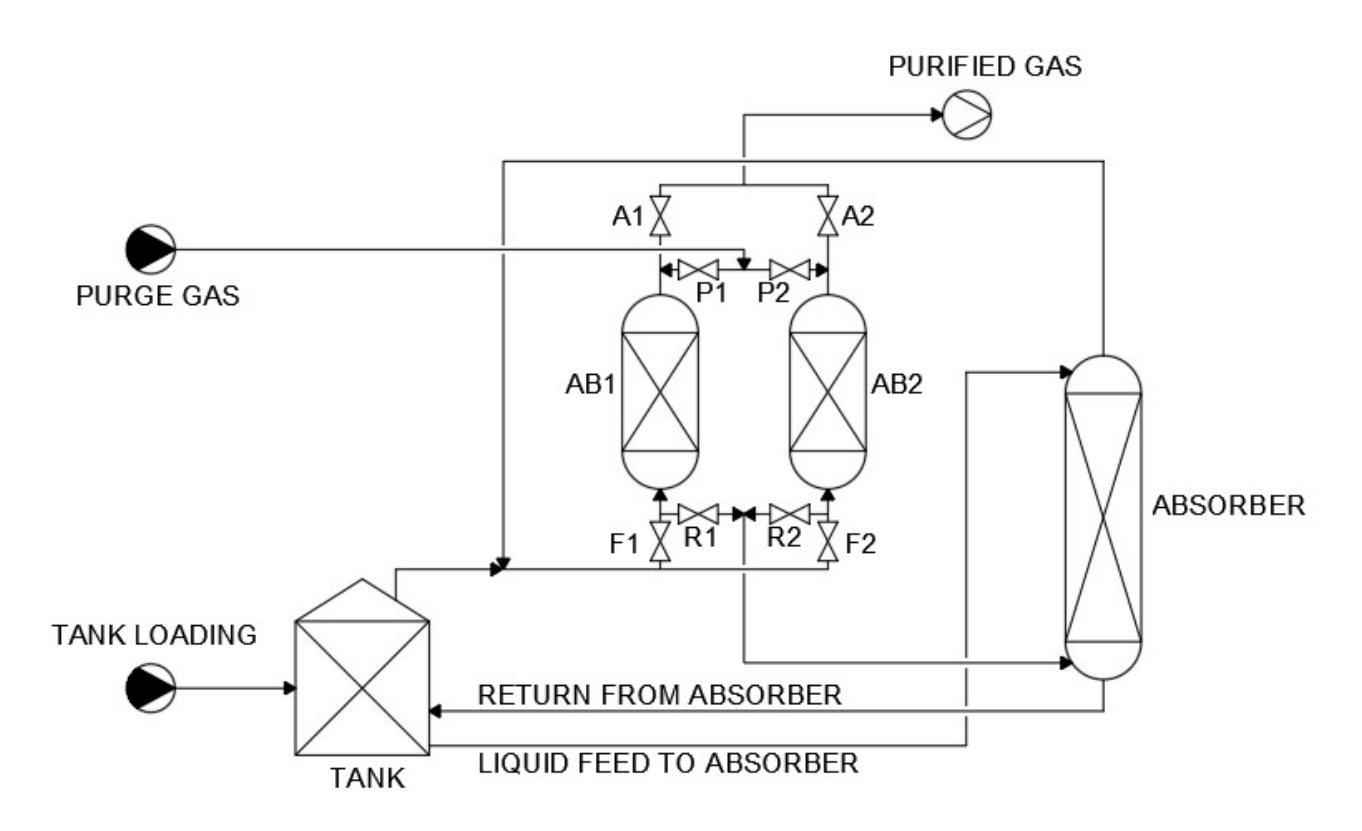


Figure 29: typical configuration for and adsorption-absorption combine VRU. AB=adsorber bed, F=feed valve, R=VOC recovery valve, P=purge valve, A=purified air valve.

# 2.2.6-Final remarks on Vapor Recovery Units and separation technology

VOCs emissions are a growing concern in all industrial processes, with refineries being the most critical source of emissions. Considering the international goals imposed on the reduction of environmental impact of human activities and the significant danger to human health caused by exposure to dangerous levels of VOCs around the world, it is evident that the development of effective abatement technologies is of crucial importance. Membranes offer interesting opportunities for selective separation of VOCs; however, they are still mostly unable to provide sufficiently stable performance for industrial scale separation over prolonged operation times. Liquid absorption was one of the first developed techniques for VOCs recovery, but nowadays it is generally unable to meet abatement requirements when used on its own, and the use of external solvents is impractical in VOC recovery from storage tanks. Cryogenic separation is technologically mature, but it faces limitations

in the high energy requirements of the refrigeration cycle and in the difficulty of condensing the lighter VOCs and operating on less concentrated components. Adsorption can achieve effective abatement of components even in the ppm concentration range, but it is limited by slow heat exchange in the case of TSA and by complexity of vacuum swing operation.

The combination of separation technologies therefore appears as the best approach to obtain optimized performances. Among the available alternatives, the coupled PSA-absorption process appears today as the most promising and developed solution. However, criticalities remain in the design and optimization of such a process. Particularly, adsorption of multicomponent mixtures is a complex phenomenon, with competitive effects between mixture components deeply affecting the performance of columns. As of now, while standardized approaches exist for the design of single component adsorption column [554], no such criterium can be readily applied to multicomponent separation. As such, the following section will deal on the modeling of a multicomponent adsorption bed meant for application in an adsorption-absorption VRU, using the commercial Aspen Adsorption<sup>TM</sup> software, with the purpose of obtaining useful guidelines for process optimization.

## 2.3-Numerical simulation of multicomponent adsorption of VOCs on activated carbon solvent for the treatment of oil storage tank emissions

#### 2.3.1-Scope of the activity

As mentioned in Section 2.2, the design of multicomponent adsorption processes is a complex task. To start with, in order to properly dimension the adsorption column, it is necessary to have data on the adsorption capacity of the selected adsorbent material in a range of variable operating conditions; in particular, the adsorption isotherms for the various gas species on the selected adsorbent need to be known in the operational range of pression and temperature. While experimental data is available for adsorption of some hydrocarbon mixtures on different adsorbents [555–557], it is impossible to test every possible adsorbent-gas mixture pairing. Since obtaining experimental data for each design case would be prohibitively expensive and time consuming, the use of reliable numerical models is essential for the development of such processes [558], allowing to properly assess the influence of process parameters on performance and offer optimized designs. The simulation of adsorption processes for gas separation has received significant interest in literature. For example, already in 1968 Chen et al. proposed the use of computer simulation for studying the scale up of adsorption columns [559], evidencing the fundamental advantages of this approach. Chung et al. described a simplified methodology for assessing PSA performance based on the assumption of batch operation in the adsorption and desorption steps [560]. Nilchan and Pantelides studied the optimization of periodic adsorption process and developed constraints and boundary conditions allowing to account for cyclical operation and interaction between multiple beds [561]. Da Silva et al. also produced a general package for modeling cyclical adsorption-desorption processes [562], addressing both adsorption and mass transport mechanisms, and used it to evaluate separation of propylene/propane and paraffines mixtures using TSA and VSA processes. Argawal et al. studied the optimization of a PSA process for hydrogen purification using a simplified Reduced Order Model [563]. Most recently, hydrogen purification [564] and carbon capture [565] have been two of the most significant applications for adsorption simulation and optimization. VOCs adsorption has also received considerable interest [566-569], however, the use of simulations for the recovery of VOCs from hydrocarbon storage tanks has been scarcely reported in literature [570,571].

Thus, in the present work the commercial software Aspen Adsorption<sup>TM</sup> [451] is used to model a multicomponent adsorption column to be used in a VRU and evaluate the effects of process parameters on its operation, with the purpose of obtaining guidelines for the optimization of its design. Optimization of column size and operating pressure is performed taking into account the competitive

effect of multicomponent adsorption. To support model development, an extensive literature review of available adsorption datasets for activated carbon, zeolites and silica adsorbents has also been performed, representing to the author's knowledge one of the few extensive compilations of adsorption data for these adsorbents. Based on the current work, gaps in available adsorption data are evidenced, and future research may be oriented to gather the missing information and enhance modeling activities for adsorption processes. Furthermore, experimental data should be gathered to provide extensive validation for the model.

#### 2.3.2-Material and methods

#### 2.3.2.1-Literature review of adsorption data for VOCs

In order to obtain an accurate simulation of the adsorption process, it is essential to have reliable data on the adsorption capacity of the desired adsorbents for the desired compounds to abate. Therefore, the first step of this work consisted on an in-depth literature search to construct a database of adsorption data for VOCs on different adsorbents, namely on zeolite, activated carbons and silica gel. Since the dependence of adsorption capacity on temperature in general plays a crucial role in adsorption processes, the collected data was restricted to papers reporting isotherms at least two different temperatures for each substance, also allowing for the evaluation of adsorption heat. The Langmuir 3 isotherm option of Aspen Adsorption<sup>TM</sup> was chosen to represent sorbent capacity, being a simple model capable of accurately displaying the dependence of adsorption capacity on both temperature and pressure.

$$q_{ads,k} = \frac{\left( (IP1_k - IP2_k \cdot T) \cdot IP3_i \cdot exp\left(\frac{IP4_k}{T}\right) \cdot P_k \right)}{\left( 1 + IP3_k \cdot exp\left(\frac{IP4_k}{T}\right) \cdot P_k \right)} \tag{38}$$

Where IP1, IP2, IP3 and IP4 are the adsorption parameters of species k. Each set of experimental data was thus refitted to this equation to obtain the adsorption parameters, independently of the original isotherm used in literature. The fitting was performed using the Linear Least Squares approach, implemented both through the internal Solver function of Microsoft Excel<sup>TM</sup> and through aptly written Matlab<sup>TM</sup> scripts. In addition to hydrocarbons VOCs, adsorption data for both nitrogen and oxygen was also collected and fitted to the Langmuir 3 isotherm, as to also consider their presence in the complete model. Adsorption heat was determined taking into account the Clausius-Clapeyron relationship [572] and the Langmuir 3 isotherm:

$$\Delta H_{ads,k} = -RT^2 \left( \frac{\partial ln(P_k)}{\partial T} \right)_q = -RT^2 * \left( \frac{-IP1_k * IP4_k * (IP2_k * T + q_{ads,k}) - IP2_k * T^2}{T^2 * (-IP1_k + IP2_k * T + q_{ads,k})} \right)$$
(39)

To simplify the model, the temperature-averaged adsorption heat calculated at zero load was used as constant adsorption heat in the simulation of the adsorption process. The average was carried out for

each available dataset, according to their reported temperature range. The collected literature data was also employed to determine the adsorbent to simulate in Aspen Adsorption<sup>TM</sup>, with selection falling onto the adsorbent with the greatest availability of reliable adsorption data.

#### 2.3.2.2-Mathematical model and simulation of the adsorption process

The numerical model for adsorption was implemented according to the options available in the Aspen Adsorption<sup>TM</sup> software [451]. The software models adsorption by solving continuity, energy and momentum balance equations for all the phases and compounds involved. Detailed discussion of the equations used by the model is reported in the Appendix. Briefly, the assumptions made when modeling PSA operation are as follows:

- The column operates in a one-dimensional plug flow regime, therefore radial and axial dispersion terms in mass balance were excluded. The bed has been divided into 10 calculation nodes, as a compromise between calculation speed and detail of bed profile.
- The column is considered adiabatic, having no heat exchange with the external environment.
- Conductive heat transfer and adsorbed species contribution to heat exchange are considered negligible, with heat transfer in the column depending mainly on convection.
- No reactions occur, with adsorption being purely physical.
- Ergun equation is used for estimating the gas pressure drop through the fixed bed. For the purpose of simulation, the bed has been divided into 10 calculation nodes, as a compromise between calculation speed and detail of bed profile.
- The physical and chemical properties of the gas phase were obtained from the internal library
  of the software and the Peng-Robinson equation was chosen as equation of state for the gas
  phase.
- The mass transfer coefficients for the linear driving force model are calculated under the
  hypothesis of pore diffusion being the limiting resistance to mass transfer, using the functional
  groups based model of Fuller et al. [573] to calculate the diffusion coefficients and linear
  driving force mass transfer coefficient for each gaseous species.
- The heat of adsorption of each species was considered constant and independent of adsorbed load and temperature. The values obtained for zero load from equation 39 are used in the simulation.

Figure 30 shows the scheme of the process used in the simulation. The bottom and top voids of the bed were modeled according to the bed dimension to simulate the bottom and top of the column, while the gas voids blocks named Feed\_void, Recovery\_void, Purge\_void and Product\_void were simply inserted to ease the solving process by numerically decoupling the feed regulating valves

(V\_feed, V\_purge, V\_product, V\_recovery) from the valves controlling cyclic operation (V11, V12, V13, V14), as recommended by the software instructions.

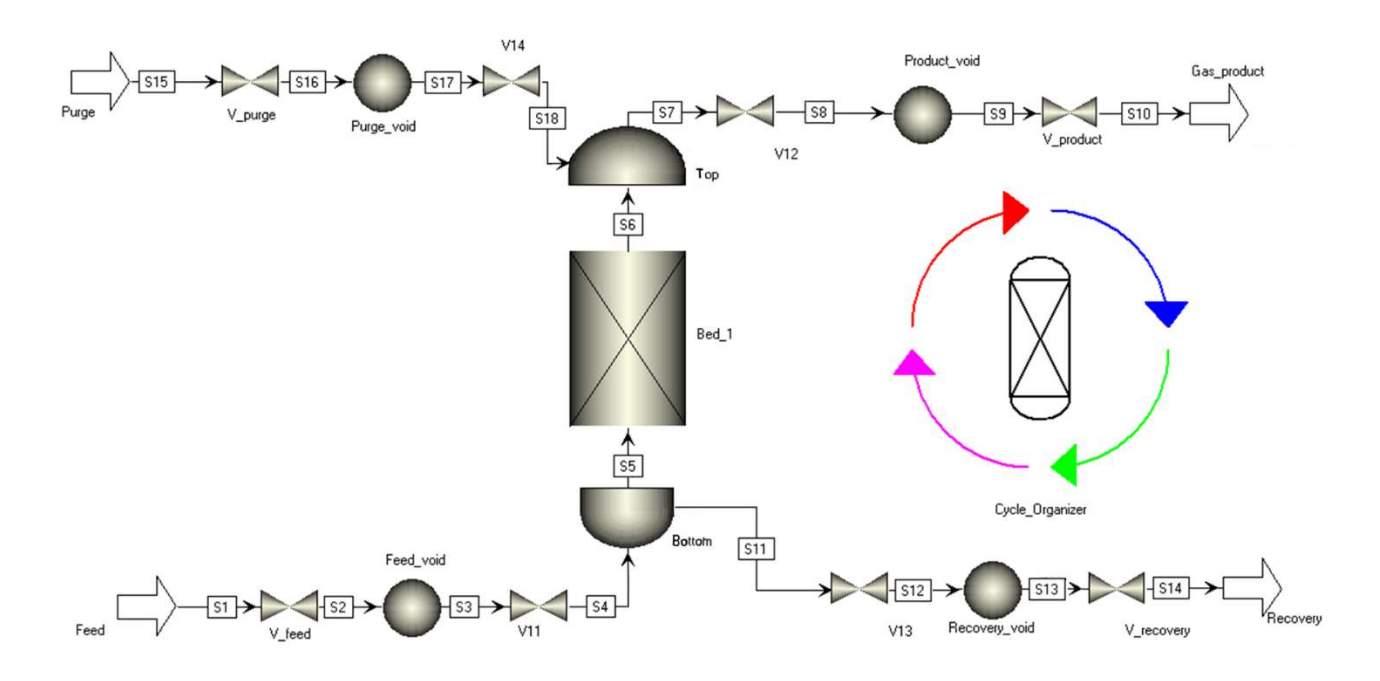


Figure 30: scheme of adsorption columns used in simulation.

When considering the adsorption of a mixture of compounds, the pure component isotherms are no longer valid to estimate the real behavior of the column. To deal with mixtures, Aspen Adsorption<sup>TM</sup> offers two main strategies, the extended Langmuir (EL) model, which computes mixture isotherms starting from the isotherms for the pure component, and the ideal adsorbed solution theory (IAST), which models the adsorption considering the adsorbed species as an ideal solution and calculates their equilibrium according to their fugacity. Both of these approaches were tested and their results compared to assess their performance. The equation for EL model applied to Langmuir 3 isotherm for species k is as follows:

$$q_{ads,k} = \frac{\left( (IP1_k - IP2_k \cdot T) \cdot IP3_i \cdot exp\left(\frac{IP4_k}{T}\right) \cdot P_k \right)}{\left( 1 + \sum_i IP3_i \cdot exp\left(\frac{IP4_i}{T}\right) \cdot P_i \right)} \tag{40}$$

On the other hand, IAST works by equating the chemical potential between gas ( $\mu_{gas}$ ) and adsorbed phase ( $\mu_{ads}$ ) and calculating the species spreading pressure ( $\Pi$ ) as function of the selected isotherm:

$$\mu_{ads,k} = \mu_k^0(T) + RT \ln \left( P_k^0(\Pi) \right) + RT \ln \left( \gamma_k x_k \right) = \mu_k^0(T) + RT \ln(y_k P) = \mu_{gas,k}$$
 (41)

$$\frac{A\Pi_k^0}{RT} = \int_0^{P_k^0} \frac{f_{eq}(T, P, IP)}{P} dP \tag{42}$$

Where  $f_{eq}(T,P,IP)$  is the pure component adsorption isotherm equation, with IP as the isotherm parameters vector. For a more complete description you may refer to the internal software manual f Aspen Adsorption<sup>TM</sup>.

The base design parameters for the bed dimensions were determined on the basis of adsorption of pure components, with a safety factor applied to account for the competition between the compounds. The inlet feed flowrate of the stream to be purified in the simulation runs is based on data for a real case scenario of storage tank loading in a refinery railway loading terminal (the data used is similar but does not exactly replicate the actual case scenario data due to non-disclosure agreement with the data provider, this thesis's author and Duemme Engineering company), while the feed composition is based on the composition of gasoline vapors reported by Kalay et al. [34]. The complete inlet conditions are presented in Table 7.

Table 7: inlet conditions for the adsorption process.

Inlet composition (molar fraction)				
N <sub>2</sub>	0.474			
O <sub>2</sub>	0.126			
Propane	0.015			
2-Methylpropene	0.08			
Butane	0.1			
Pentane	0.14			
Hexane	0.06			
Benzene	0.005			
Inlet conditions				
Flowrate (m³/h)	849			
Т (К)	313.15			
P (bar)	1.1			

#### 2.3.5-Results and discussion

#### 2.3.5.1-Results of literature search of adsorption data

In general, the Langmuir 3 isotherm provided a good fit for most of the available data, confirming it as a good choice for representing adsorption. The complete literature review of data collected for activated carbon adsorbent is reported in Table 8, Table 9 reports data for zeolite adsorbents and Table 10 reports data for silica adsorbent.

Table 8: adsorption data for N<sub>2</sub>, O<sub>2</sub> and hydrocarbon VOCs on activated carbon adsorbent.

Adso	rbent Substances	P range (bar)	T range (K)	Source
------	------------------	---------------	-------------	--------

CENTAUR activated carbon  BPL Activated carbon  F30_470 Activated carbon  WS42 Activated carbon  CMS1 Activated carbon	O <sub>2</sub> , N <sub>2</sub> , CH <sub>4</sub>	0-38	283-323	[574]
Kuraray activated carbon Kuraray carbon molecular sieve	O <sub>2</sub> , N <sub>2</sub>	0-10	293-323	[575]
Norit RB 2 Activated carbon  Chemviron AP 4-60 Activated carbon	N <sub>2</sub> , CH <sub>4</sub> , ethane, propane	0-80 (N <sub>2</sub> , CH <sub>4</sub> ) 0-20 (ethane) 0-7 (propane) 0-60 (N <sub>2</sub> , CH <sub>4</sub> ) 0-30 (ethane) 0-7 (propane)	300-400	[576]
Saran highly activated carbon		0-60 (N <sub>2</sub> ) 0-40 (CH <sub>4</sub> ) 0-20 (ethane) 0-8 (propane)		
BPL activated carbon (Calgon Carbon)  F-600 activated carbon (Calgon Carbon)  OLC activated carbon (Calgon Carbon)  NZ activated carbon (Activated Carbon NZ LTD)  Activated Carbon Cloth (Spectracorp)  M-30 activated carbon (Spectracorp)	O <sub>2</sub> , N <sub>2</sub>	0-6	283.15-363.15	[577]
Steam-activated carbon RX 1.5 Extra (Cabot Corporation)	Ethane, propane, butane	0-0.01	193.15-293.15	[578]
Activated carbon grade RV950G (R.V. Corporation)	CH4, ethane, propane, 2- methylpropane, pentane, hexane	0-90 (CH <sub>4</sub> ) 0-30 (ethane) 0-5 (propane) 0-2 (2methylpropane)	293-358	[579]

		0-0.4 (pentane)		
		0-0.1 (hexane)		
BPL F-3 activated				
carbon (Cargon	Butane	0-0.35	298.15-328.15	[580]
Carbon Corp.)				
Activated carbon Type	Ethane, butane,	0-1 (ethane)		
976 (Ajax chemical	pentane	0-0.6 (butane)	283.15-423.15	[581]
company)	pentane	0-0.2 (pentane)		
	Propane, butane,		303.15-325.15 (propane, butane)	
Ajax activated carbon	hexane	0-0.1	313.15-333.15 (hexane)	[582]
	nexane			
G-BAC Kontisorbon				
Activated carbon	Benzene	0-0.6	323.15-423.15	[583]
(Kurea Chem. Ind.	2 sinceric	0 0.0	325112 125112	[600]
Co.)				
Coal-based extruded		0-80 (CH <sub>4</sub> )		
activated carbon	CH <sub>4</sub> , ethane,	0-40 (ethane)	284-325	[584]
(Sutcliffe Speakman	propane, butane	0-14 (propane)	25.525	[00.]
Carbons Ltd.)		0-4 (butane)		
Cylindrical activated				
carbon grains	Butane	0-0.9	268.15-358.15	[585]
produced by an		• • • • • • • • • • • • • • • • • • • •		[200]
extrusion process.				
Vulcan 3G activated	Propane, propene	0-1	273-313	[586]
carbon	1 /1 1			. ,
BPL SS no.2	CH <sub>4</sub> , propane,	0-1 (CH <sub>4</sub> , hexane)	250-350 (CH <sub>4</sub> , propane, butane,	
(Pittsburgh	butane, pentane,	0-0.25 (propane)	pentane)	[587]
Chemical Company)	hexane	0-0.2 (butane)	273-298 (hexane)	
		0-0.05 (pentane)		
Ajax Activated carbon	Butane	0-1.2	283.15-423.15	[588]
Activated carbon	CO <sub>2</sub> , CH <sub>4</sub> ,	0-1 (CO <sub>2</sub> , CH <sub>4</sub> , ethane)		
Fiber KF-1500	ethane, propene,	0-0.7 (propene)	273.15-323.15	[589]
(Toyobo Co., Ltd.)	2-methylbutane	0-0.45 (2-methylbutane)		
Activated carbon				
produced from	Benzene	0-0.000014	293-323	[590]
Elaeagnus				
angustifolia seeds				
Coal derived activated				
carbon (China	Hexane	0-0.6	288.15-318.15	[591]
Activated Carbon				
Industries Co.)				
Coconut-shell granular				
activated carbon m-	Benzene	0-0.09	303-328	[592]
GAC (Liyang Tianlun				
Environmental				

Materials Ltd.)				
Activated Carbon (Singapore Refining Co. Ltd.)	CH <sub>4</sub> , ethane,	0-6 (CH <sub>4</sub> , ethane) 0-1.4 (propane)	299.15-338.15	[593]
F30/470 Activated crbon (Chemviron Carbon).	2-methylpropane, butane, 1-butene	0-2 (2-methylpropane, 1-butene) 0-2.5 (butane)	278-303	[594]
F30/470 Activated crbon (Chemviron Carbon).	2-methylpropene, 1,3-butadiene	0-2.5 (2-methylpropene) 0-3 (1,3-butadiene)	278-303	[595]
F30/470 Activated crbon (Chemviron Carbon).	Propane, propene, propadiene	0-8 (propane) 0-9 (propene) 0-4 (propadiene)	278-303	[596]
BPL activated carbon (Calgon Carbon Corp.)	CH <sub>4</sub> , ethane, butane, hexane	0-6 (CH <sub>4</sub> , ethane) 0-2.5 (butane) 0-1 (hexane)	273.15-348.15 (CH <sub>4</sub> , ethane) 298.15-348.15 (butane) 298.15-423.15 (hexane)	[597]
Microporous activated	CH <sub>4</sub> , propane,	0-18 (CH <sub>4</sub> , propane)	373.15-423.15 (CH <sub>4</sub> , pentane)	[598]
carbon (Ecosorb)  Activated carbon fiber cloth	pentane Benzene	0-14 (pentane) 0-0.12	303.15-423.15 (propane) 293.15-323.15	[599]
Activated Carbon Cloth from Tencel® (lyocell-based fabric) precursor, synthesis at 864°C	Hexane, benzene,	0-0.2 (hexane) 0-0.012 (benzene) 0-0.025 (toluene)	273-298	[600]
Activated Carbon Cloth from Tencel® (lyocell-based fabric) precursor, synthesis at 963°C	toluene	0-0.2 (hexane) 0-0.012 (benzene) 0-0.02 (toluene)	273-298	_ [000]
BPL granular carbon (Calgon Carbon Corp.)	Ethane, propane, hexane	0-1 (ethane) 0-1.2 (propane) 0-0.8 (hexane)	273-323 (ethane, propane) 298-398 (hexane)	[601]
Maxsorb III activated carbon (Kansai Coke and Chemicals Co.	Butane	0-3	298.15-328.15	[602]
BPL activated carbon (Calgon Carbon Corp.)	Pentane	0-0.06	273.15-448.15	[603]
SLG-2PS activated carbon (Dong Yang Company)	Hexane	0-0.12	298.15-318.15	[604]

Ajax-activated carbon type 976 (Ajax Company)	Benzene, toluene	0-0.12 (benzene) 0-0.035 (toluene)	303-423 (benzene) 303-363 (toluene)	[605]
NucharWV-A 1100 activated carbon (MeadWestvaco)	Pentane, hexane, heptane	0-0.6 (pentane) 0-0.18 (hexane) 0-0.035 (heptane)	293-323	[606]
Sorbonorit B4 activated carbon (Norit)	Benzene, toluene	0-0.07 (benzene) 0-0.02 (toluene)	303.15-343.15	[607]
Activated carbon fiber (Toyobo type KF- 1500)	Benzene, toluene	0-0.09 (benzene) 0-0.035 (toluene)	298.15-348.15	[608]
Activated carbon (Kureha Chemical Industry)	Butane, 2- methylpropane	0-1.1 (butane) 0-1.2 (2-methylbutane)	298-393	[609]
Steam-activated carbon RX 1.5 Extra (Cabot Corp.)	Ethene, propene	0-0.0125	193.15-293.15	[610]
Activated carbon (Tangshan United Carbon Technology)	Toluene	0-0.35	298-318	[611]

Table 9: adsorption data for  $N_2,\,O_2$  and hydrocarbon VOCs on zeolite adsorbent.

Adsorbent	Substances	P range (bar)	T range (K)	Source
Zeolite 13X APG  MOLSIV  (Honeywell UOP)	Ethane, ethene, propane, propene	0-0.0125	193.15-293.15	[610]
Zeolite 13X		0-2.5	298-338	
Ca exchanged zeolite 13X	CH <sub>4</sub>	0-2	313-338	[612]
Mg exchanged zeolite 13X		0-2.5	298-338	
		0-0.045 (propane)	297.15-333.15 (propane)	1
Zeolite NaX	D	0-0.03 (cyclohexane)	433.15-493.15 (cyclohexane)	
	Propane,	0-0.016 (benzene)	493.15-533.15 (benzene)	[612]
	cyclohexane,	0-0.12 (propane)	292.15-323.15 (propane)	[613]
Zeolite NaY	benzene	0-0.02 (cyclohexane)	393.15-433.15 (cyclohexane)	
		0-0.025 (benzene)	473.15-523.15 (benzene)	
Zeolite 13X	Propane, propene, 2-methylpropane	0-1.6	333-393	[614]
Zeolite 5A	Butane, heptane	0-1 (butane)	553-653	[615]
Zeome 3A	Butane, neptane	0-0.7 (heptane)	333-033	[615]
Zeolite 5A	Hexane, octane,	0-0.04 (hexane)	593.15-638.15	[616]
Zeonte 3A	decane, dodecane,	0-0.02 (octane)	373.13-030.13	

	tridecane,	0-0.025 (decane)		
	hexadecane	0-0.015 (dodecane)		
	1101111110	0-0.0015 (tridecane)		
		0-0.0002 (hexadecane)		
	N. CH. 4	0-18 (N <sub>2</sub> , ethene)		
Zeolite 5A	N <sub>2</sub> , CH <sub>4</sub> , ethane,	0-16 (CH <sub>4</sub> )	293.15-313.15	[617]
-	ethene	0-14 (ethane)		
Zeolite 13X	N <sub>2</sub> , CH <sub>4</sub>	0-10	293-323	[618]
		0-0.5 (ethane)	272.15.245 ( .1 )	
	Ethane, propane,	0-0.13 (propane)	273.15-345 (ethane)	
Zeolite 5A	butane, pentane,	0-0.4 (butane)	323-348 (propane)	[619]
	hexane	0-0.6 (pentane)	323-498 (butane)	
		0-0.18 (hexane)	373-573 (pentane, hexane)	
7. 17. 5.	D	0-0.1 (pentane)	400.550	F ( 2 0 1
Zeolite 5A	Pentane, hexane	0-0.06 (hexane)	423-573	[620]
	Dantana astana	0-0.11 (pentane)	523.15-674.15 (pentane)	
Zeolite 5A (Linde)	Pentane, octane,	0-0.016 (octane)	522.15-668.15 (octane)	[621]
	decane	0-0.002 (decane)	523.15-596.15 (decane)	
Zeolite 13X	CH4	0-100	273.134-298.15	[622]
Zeolite 5A	Hexane	0-0.17	657.15-863.15	[623]
Zeolite 5A				
(Zeochem)				
Zeolite 5A (HKC				
Corp.)				
Zeolite 5A (UOP				
Co.)				
Zeolite 5A (W.R.				
Grace)				
Zeolite 5A (Tosoh)	N. CH	0.20	202 522	[(24]
Zeolite 13X	N <sub>2</sub> , CH <sub>4</sub>	0-30	293-523	[624]
(Zeochem)				
Zeolite 13X (HKC				
Corp.)				
Zeolite 13X (UOP				
Co.)				
Zeolite 13X (Linde)				
Zeolite 13X				
(CECA)				
Zeolite 5A crystals	D	0.1	222 422	[(25]
Zeolite 5A pellets	Propane, propene	0-1	323-423	[625]
Partially	Benzene, toluene,	0-0.07 (benzene)	400 500 (1	
dealuminated	ethylbenzene, orto-	0-0.029 (toluene)	423-503 (benzene, toluene)	[(2/3
	i		443-523 (ethylbenzene, orto-	[626]
faujasite type DAY	xylene, meta-	0-0.016 (ethylbenzene)	xylene, meta-xylene, para-xylene)	

zeolite (DEGUSSA		0.015 (meta-xylene)		
AG)		0-0.019 (para-xylene)		
Zeolite 13X				
(CECA)	Propane, propene	0-1.1	303-473	[627]
Zeolite 4A		¥		[ [ [ ]
			195 (CH <sub>4</sub> )	
	CH4, ethane,		273-323 (ethane)	
	propane, butane,	0-0.037 (CH <sub>4</sub> )	303-323 (propane)	
		0-0.02 (ethane, propane, butane,	303-323 (propane)	
	pentane,	pentane)	` ′	
G'1' 1' 1	cyclopentane,	0-0.4 (cyclopentane)	273-450 (pentane)	
Silicalite-1	hexane,	0-0.016 (hexane)	273-443 (cyclopentane)	
	cyclohexane,	0-0.10 (benzene, cyclohexane)	336-448 (hexane)	
	benzene, toluene,	0-0.013 (toluene, ethylbenzene)	323-373 (cyclohexane)	[628]
	ethylbenzene, para-	0-0.031 (para-xylene)	273-435 (benzene)	
	xylene	4 3	323-435 (toluene, ethylbenzene)	
			323-373 (para-xylene)	
	Cyclopentane,	0-0.43 (cyclopentane)	303-373 (cyclopentane,	1
AlPO <sub>4</sub> -5	cyclohexane,	0-0.11 (cyclohexane, benzene)	cyclohexane)	
AIPO4-3	benzene, para-	, <del>-</del>	273-373 (benzene)	
	xylene	0-0.013 (paraxylene)	303-373 (para.xylene)	
DETER 11:	2,2 dimethylbutane,			
BETA zeolite	2,3-dimethylbutane,			
(SÜD-CHEMIE	3-methylpentane,	0-0.3	423-523	[629]
AG)	hexane			
Zeolite 13X	Ethane, ethene	0-6	303-343	[630]
Zeolite 5A	n-heptane	0-0.06	409-491	[631]
	_	0-4 (propane)	423-473 (propane)	
Zeolite 4A (CECA)	Propane, propene	0-5 (propene)	373-473 (propene)	[632]
Zeolite 13X	Propane, propene	0-5	283-363	[633]
Zeolite 13X	CH <sub>4</sub> , N <sub>2</sub>	0-10	273-343	[634]
200110 1311	C114, 1 12	0-18 (CH <sub>4</sub> )	273 313	[03.1]
Zeolite 5A (Linde)		0-3 (propane)		
	CH <sub>4</sub> , propane		275-350	[635]
Zeolite 13X (Linde)		0-14 (CH <sub>4</sub> )		
		0-3 (propane)	222.240.6	
5A molecular sieve	Propane, propene,	0-0.13 (propane, propene)	323-348 (propane)	
(Davison C-521)	1-butene	0-0.26 (1-butene)	323-448 (propene)	
			348-448 (1-butene)	
5A molecular sieve	Propene, 1-butene	0-0.13 (propene)	323-398 (propene)	[636]
(Davison C-626)		0-0.26 (1-butene)	348 (1-butene)	_ [,
	Propane, propene,	0-0.13 (propane, propene)	323-348 (propane)	7
Zeolite 5A (Linde)	1-butene	0-0.13 (propane, propene)	323-448 (propene)	
	1-outelle	0-0.2 (1-butche)	348-448 (1-butene)	
Zeolite 5A (Rhône-	n-pentane	0-0.6	373-573	[637]
				103/1

5A effective pore- size calcium microtraps (Davison	Ethane, ethene, propane, propene, butane, 1-butene	0-0.21	298.15-348.15	[638]
Chemical Co.)	butane, 1-butene			

Table 10: adsorption data for  $N_2,\,O_2$  and hydrocarbon VOCs on silica adsorbent.

Adsorbent	Substances	P range (bar)	T range (K)	Source
Silica gel PA 400 (Davison Chemical Co.)	Butane, pentane, hexane	0-2.5 (butane) 0-0.8 (pentane) 0-0.25 (hexane)	283-303	[639]
Silica gel (Davison Chemical Co.)	Butane	0-0.045	303.15-33.15	[640]
Silica Gel (Singapore Refining Co. Ltd.)	CH <sub>4</sub> , ethane, propane	0-6 (CH <sub>4</sub> , ethane) 0-1 (propane)	299.15-338.15	[593]
KC silica gel (Kali- Chemie AG)	CH <sub>4</sub> , ethane, ethene, propane, propadiene, 2- methylpropane, butane	0-35 (CH <sub>4</sub> , ethene) 0-32 (ethane) 0-10 (propane) 0-4.5 (propadiene) 0-2.2 (2-methylpropane, butane)	278-303	[641]
Silica gel grade 9385	CH <sub>4</sub>	0-100	273.156-323.156	[642]
Silica gel	CH <sub>4</sub>	0-0.4	152.4-175.2	[643]
Silica gel (Davison Chemical Co.)	Ethene	0-1	273.15-499.15	[644]
Silica gel (Jiyida Silica Reagent Factory)	Toluene	0-0.35	298-318	[611]
Microporous SiO <sub>2</sub>	Benzene, toluene, para- xylene	0-0.24 (benzene) 0-0.19 (toluene) 0-0.16 (para-xylene)	523-473	[645]
Silica gel	Propane	0-0.077	298.15-363.15	[646]
Commercial grade silica gel (ZEOCHEM)	N <sub>2</sub>	0-1	293.15-313.15	[647]
Silica gel, high area- narrow pores (Grace Davison)  Silica gel, low area- wide pores (Grace Davison)	Propane, propene	0-1	303-343	[648]
Silica gel (Davison Chemical Co.)	Hexane, benzene	0-0.024	343.15-403.15	[649]
	L	<u>[</u>	1	

Nanoporous MCM-41				
Silica with different	Hexane	0-0.54	303-323	[650]
pore sizes				

Observing the available data, it is immediate to notice that there are remarkable differences in the adsorption capacities reported for the different kinds of activated carbon. Figure 31 for example shows the obtained interpolated isotherms for butane and hexane on the different carbon adsorbents reported in literature: while a most isotherms for both compounds are grouped close together, displaying somewhat similar capacities between different carbons, the gap between many of them is still quite noticeable and some appear to be complete outliers compared to the other isotherms, such as the case of the adsorption isotherm of Saha et al. 2008 for the adsorption of butane. For silica gel, availability of adsorption data was limited compared to the other adsorbents.

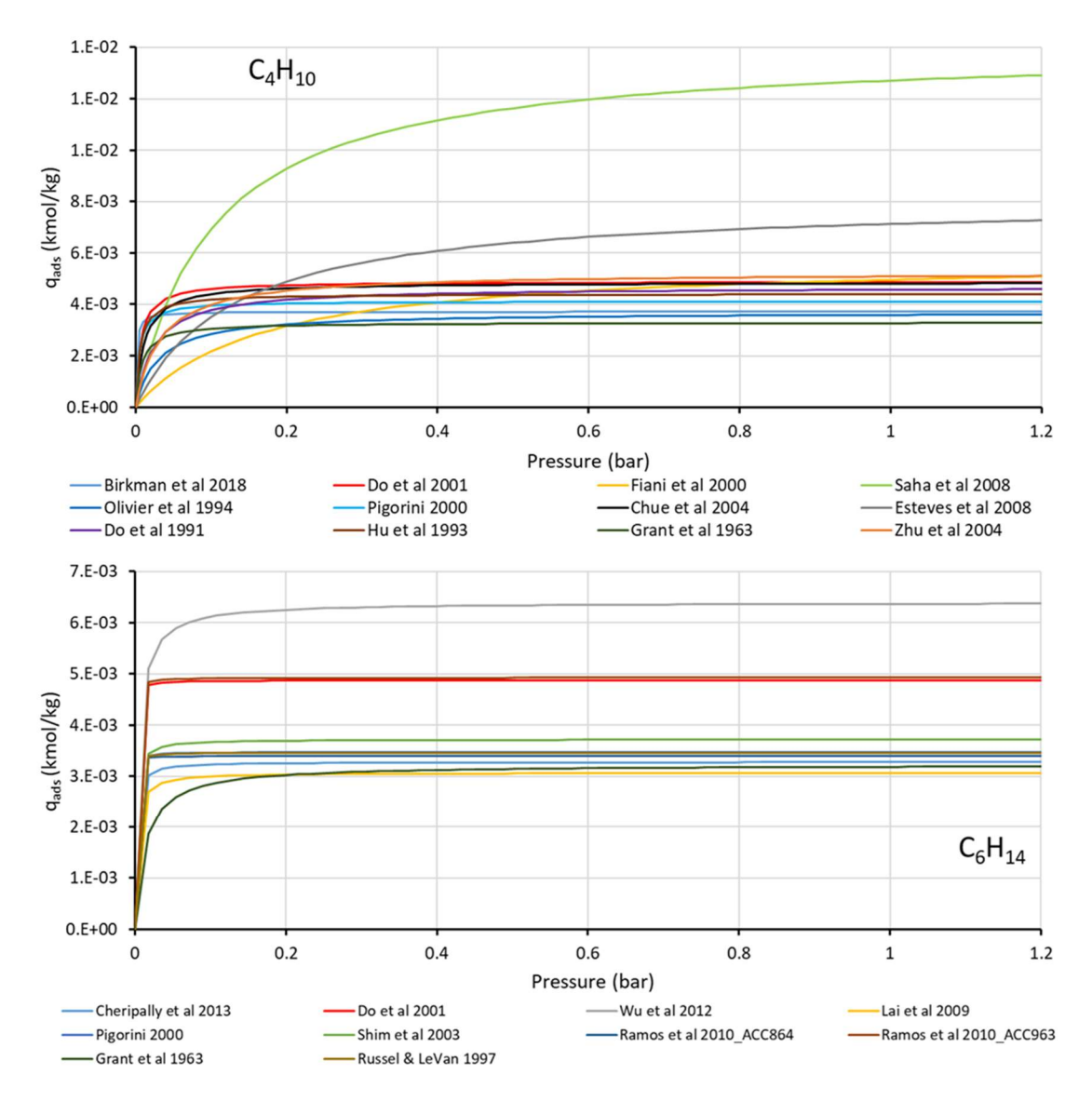


Figure 31: interpolated adsorption isotherms of butane and hexane at 298.15 K for the different activated carbon adsorbents reported in literature.

It should be noted, that the difference in isotherms between different kinds of zeolite appeared in general to be much more marked compared to the difference between different kinds of activated carbon. This is likely attributed to the much more ordered pore shapes and sizes of the crystalline zeolite structure contributing to a significantly greater difference in adsorption mechanism and capacity, compared to the amorphous nature of activated carbon. It is also essential to notice that no adsorbent was found for which a complete set of adsorption data existed for each VOC of interest for the purpose of this simulation on any of the reported adsorbents. Thus, for the purpose of the simulation, approximation was needed. Activated carbon was chosen as the adsorbent to simulate, both thanks to its common use in actual industrial applications and to the abundance of adsorption data available; the adsorption parameters were selected considering a fictional activated carbon

obtained by combining the adsorption data of similar activated carbons as to have a complete adsorption parameter set, which is reported in Table 11. Since adsorption data for 2-methylpropene was not available in literature, its adsorption was approximated with adsorption parameters for 2-methylpropane.

Table 11: adsorption parameters and enthalpies for the simulation of cyclical PSA on activated carbon adsorbent chosen for process simulation.

Substance	IP1	IP2	IP3	IP4	ΔH (MJ/kmol)	Source
$N_2$	0.0096591	2.09E-01	0.0073265	830.94	-12.36	[575]
O <sub>2</sub>	0.0136670	3.06E-01	0.0044757	873.25	-13.34	[575]
Propane	0.0105280	1.96E-01	0.1013600	1363.2	-14.98	[579]
2-Methylpropene (*)	0.0086259	1.54E-01	0.2172200	1420.0	-15.12	[579]
Butane	0.0099548	1.77E-01	0.2839500	1486.8	-15.63	[595]
Pentane	0.0068349	1.16E-01	0.5588300	2026.7	-19.82	[579]
Hexane	0.0067095	1.15E-01	0.6586300	2057.1	-20.12	[579]
Benzene	0.0084317	1.35E-01	0.0723410	3388.6	-30.80	[600]

<sup>(\*)</sup> parameters for 2-methylpropane are used due to lack of data in literature.

#### 2.3.5.2-Simulation of adsorption

From the adsorption data obtained from literature, a base design of the adsorption column was obtained considering the required mass for the total capture of all the VOCs present in the current. To limit column height requirements, the feed stream was divided equally between two identical columns working in parallel, each handling half of the total feed, for a total of four beds (two in adsorption and two in regeneration cyclically alternating). The initial setup of the column used in the simulation is thus reported in Table 12. The estimates for adsorbent sphericity (φ) and bed void fractions were obtained from the correlation of Kunii & Levenspiel [651]. The bed was assumed to start the adsorption saturated in air, with no hydrocarbon present. A countercurrent air purge was used to enhance bed regeneration, as previously suggested by Liu et al. [570] in their own simulations, where they evidenced how using carrier gas for column pressurization avoided early saturation of the adsorbent and noticeably improved adsorbent performance and lifetime. A four step Skarstrom cycle [652], consisting of pressurization, adsorption, depressurization and regeneration, was chosen for the column, as the simplest operation cycle possible for a PSA column. The adsorption step length was set at 20 minutes, according to guidelines provided by Huang et al. [653] indicating that adsorption step should last no longer than 30 min, and the regeneration step had the same length. Adsorbent specific heat capacity and gas phase heat conductivity constant were left at the default values of Aspen Adsorption<sup>TM</sup>, as realistic values for simulation. The emission limits to respect for each case scenario

were that the total outlet concentration of VOCs could not surpass  $10~g/Nm^3$  and that benzene outlet concentrations could not surpass  $0.001~10~g/Nm^3$ .

Table 12: adsorption column base design parameters. The mass transfer coefficients are obtained according to [573].

Colum base design parameters			
H <sub>b</sub> (m)	6.4		
D <sub>b</sub> (m)	2		
εί	0.42		
$\epsilon_{p}$	0.47		
$\rho_s$ (kg/m <sup>3</sup> )	1584.91		
r <sub>p</sub> (m)	0.003		
ф	0.74		
C <sub>ps</sub> (MJ/(kg×K))	1.00E-03		
Gas phase heat conductivity, kg (MW/(m×K))	1.60E-07		
a <sub>p</sub> (1/m)	580		
Process base design param	eters		
Adsorbent	Activated carbon		
Air purge flowrate (m³/h)	28.40		
Adsorption pressure (bar)	1.01		
Regeneration pressure (bar)	0.05		
Starting column temperature (K)	313.15		
Starting column atmosphere	Pure air (79% vol. N <sub>2</sub> , 21% vol. O <sub>2</sub> )		
Cyclic step time (s)			
Adsorption/regeneration step	1200		
Pressurization/depressurization step	90		
Emission limits for purified o	urrent		
Total VOCs concentration	≤10 g/Nm <sup>3</sup>		
Benzene concentration	≤0.001 g/Nm <sup>3</sup>		
Mass transfer coefficients for linear driving	ng force model (1/s)		
$N_2$	0.0750987		
O <sub>2</sub>	0.0707302		
Propane	0.0597866		
2-Methylpropene	0.0520837		
Butane	0.0520966		
Pentane	0.0468020		
Hexane	0.0427559		
Benzene	0.0449781		

Once the column initial design was selected, the first thing that was evaluated was the model to use for adsorption of mixture. Figure 32 shows the comparison of results between Extended Langmuir model and IAST simulation for a prolonged cyclical adsorption simulation. It can be immediately

seen that for the simulated mixture, the difference between the two models is negligible. The two models effectively predict the same results in terms of VOCs adsorbed load, gas outlet composition and internal column temperature. Therefore, for the following simulations, the Extended Langmuir model was chosen as the approach to mixture isotherm simulation, as it is the computationally less intensive approach.

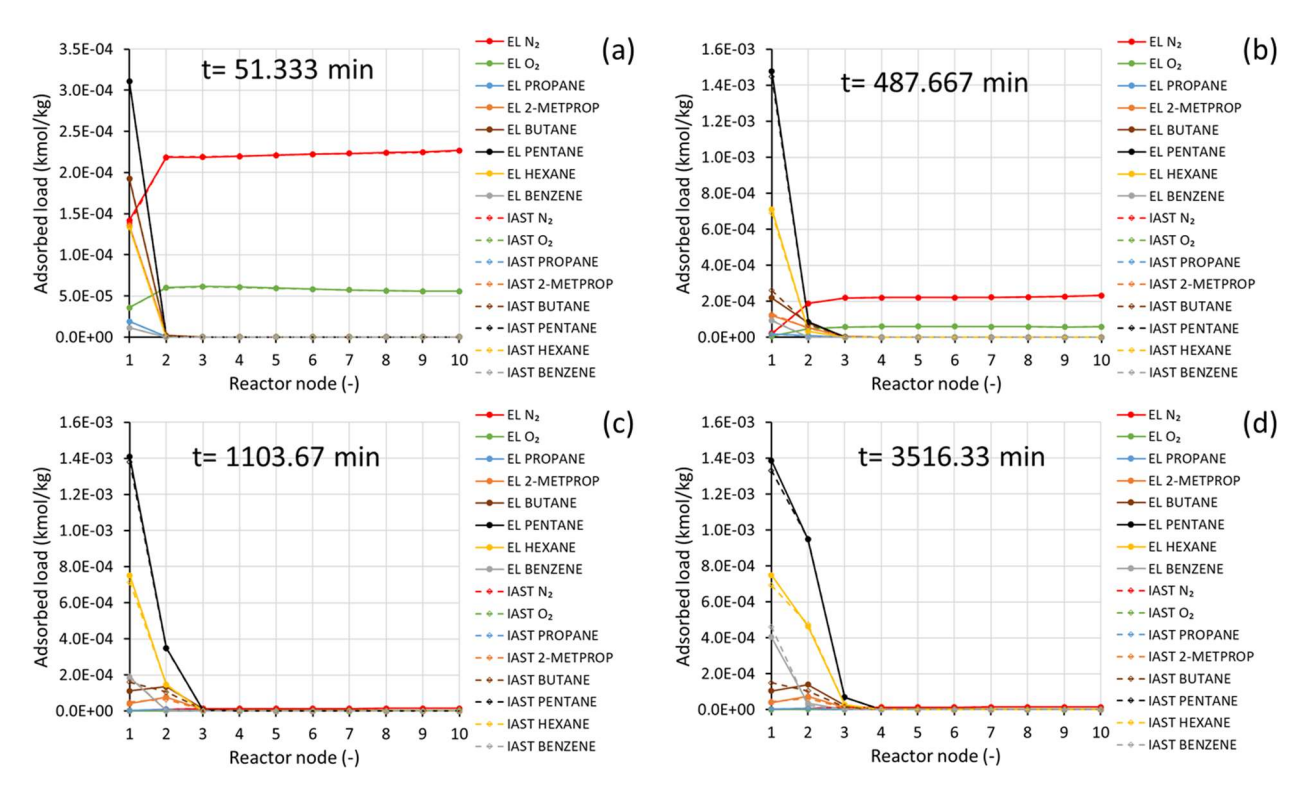


Figure 32: comparison of column internal adsorption profiles at different process time when multicomponent adsorption is simulated with Extended Langmuir (EL) or Ideal Adsorbed Solution Theory (IAST). Each node corresponds to 0.64 m of column height.

A 1-month (30 days) run was thus performed to assess the performance of the base column design, with Figure 33 displaying its results. The outlet gas concentration profile is presented in Figure 33a. It is immediately apparent that the column as designed is well able to meet the emission limits requirements within the 1 month of operation, greatly exceeding the required performance. The outlet concentration of all substances remains within the ppm range within the whole period, with near zero benzene emissions. However, it is apparent that the efficiency of the column is indeed decreasing over time, as shown by the increase in outlet concentration of all substances over time. As expected, the first substances to become noticeable at reactor outlet are the lighter hydrocarbons propane, 2-methylpropene and butane, who all appear within 5 days of operation. On the other hand, breakthroughs of pentane and hexane occurred only after 10 operation days, once they have gradually started to displace the lighter compounds in the adsorbed bed. Benzene breakthrough is not observed

in the current conditions, as expected from the low concentration of benzene in the inlet feed and the high adsorption capacity of the activated carbon. During adsorption, the column reached a maximum temperature of 70 °C during adsorption, and a minimum temperature of 33 °C during desorption. The maximum temperature was reached during the first adsorption step, when the column started with completely fresh adsorbent. The presence of these significant temperature peaks evidences the requirement of simulating the adsorption as a non-isothermal process, as such a relevant thermal excursion can greatly affect the adsorption capacity of the column. After initial cycles with significant temperature gradients, the thermal excursion decreased during the remaining process time, with the column reaching a thermal cyclical steady state by the end of the simulation period. The total adsorbed loads in the column are shown in Figure 33b. Looking at the figure, it can be seen that by the end of the simulation period the total adsorbed loads reached a good level of stability, thus evidencing how the column is likely to maintain its performance for extended process time. However, it should be noted that the base column appears overall to be oversized, with the internal profiles of adsorption showing that by the end of the month, only 40% of the total bed volume has actually participated to the adsorption, as seen in Figure 33c. While a certain level oversizing is usually accepted as a safety measure to account for possible inlet feed composition and flowrate changes, excessive oversizing of the column comports an unjustified increase in the cost of the adsorbent, the column and the vacuum equipment required for regeneration. Therefore, the following simulations were performed to evaluate the performance of columns when varying column height, diameter, purge flowrate and regeneration pressure compared to the base design. All the runs lasted for 1 month and only one parameter effect at a time was assessed, with the other parameters remaining constant. At the end of each simulation, the final outlet concentration, the adsorbed amounts and the internal adsorption profile of the bed were compared. The effects of the various parameters on the final outlet concentration of purified gas are reported in Figure 34-37. Outlet concentration is reported normalized to the inlet feed concentration, and the parameters are also presented in normalized form, with bed height, bed diameter and purge flowrate being normalized with respect to their value in the base design, while regeneration pressure is presented as the normalized pressure difference compared to the regeneration pressure of the base case design.

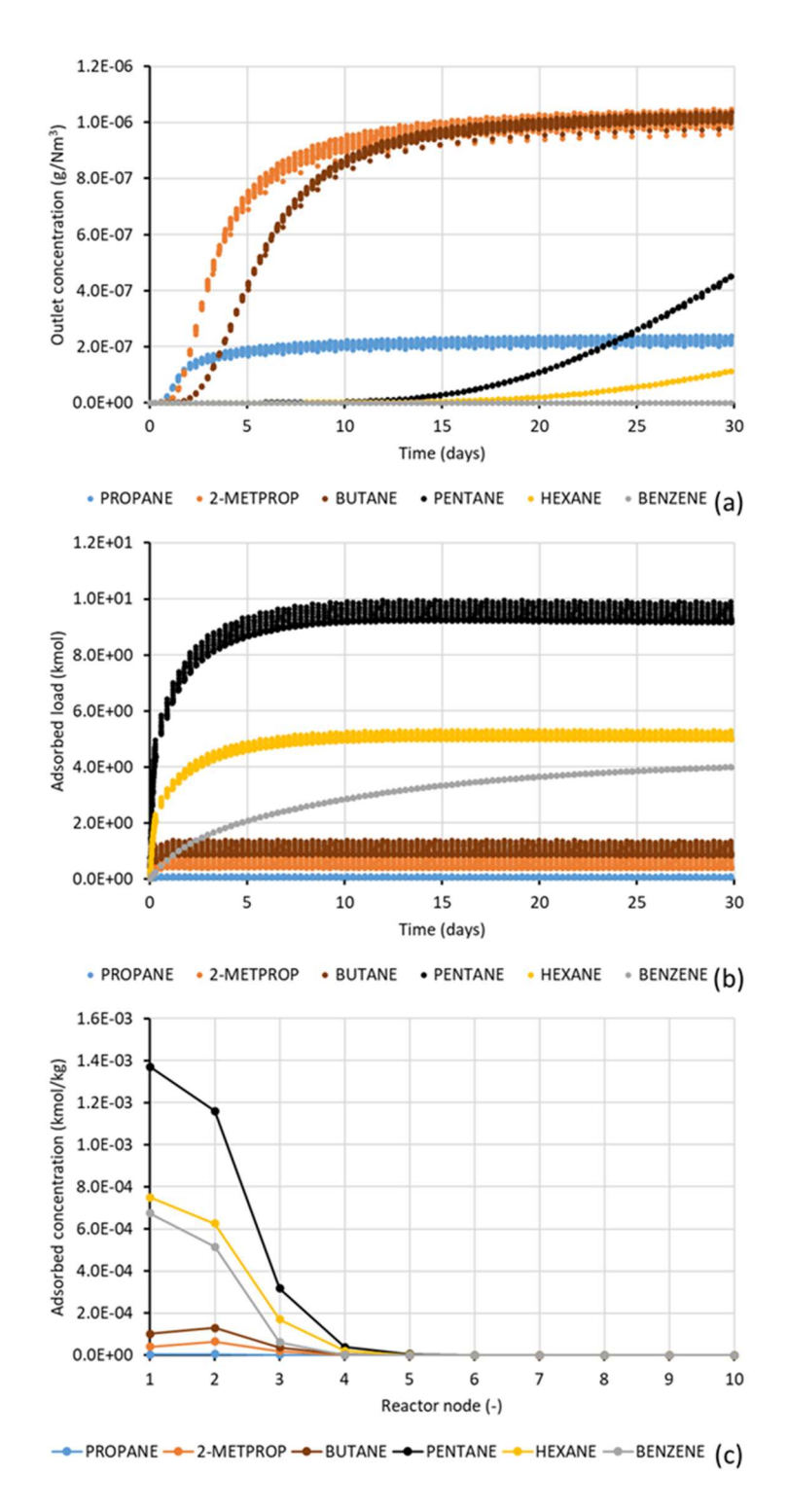


Figure 33: results of 1 month of simulated continuous operation for the base column design: purified gas composition (a); adsorbed VOC load in the column (b); internal adsorbed profile at the end of the 30 days (c). Each node corresponds to 0.64 m of column height.

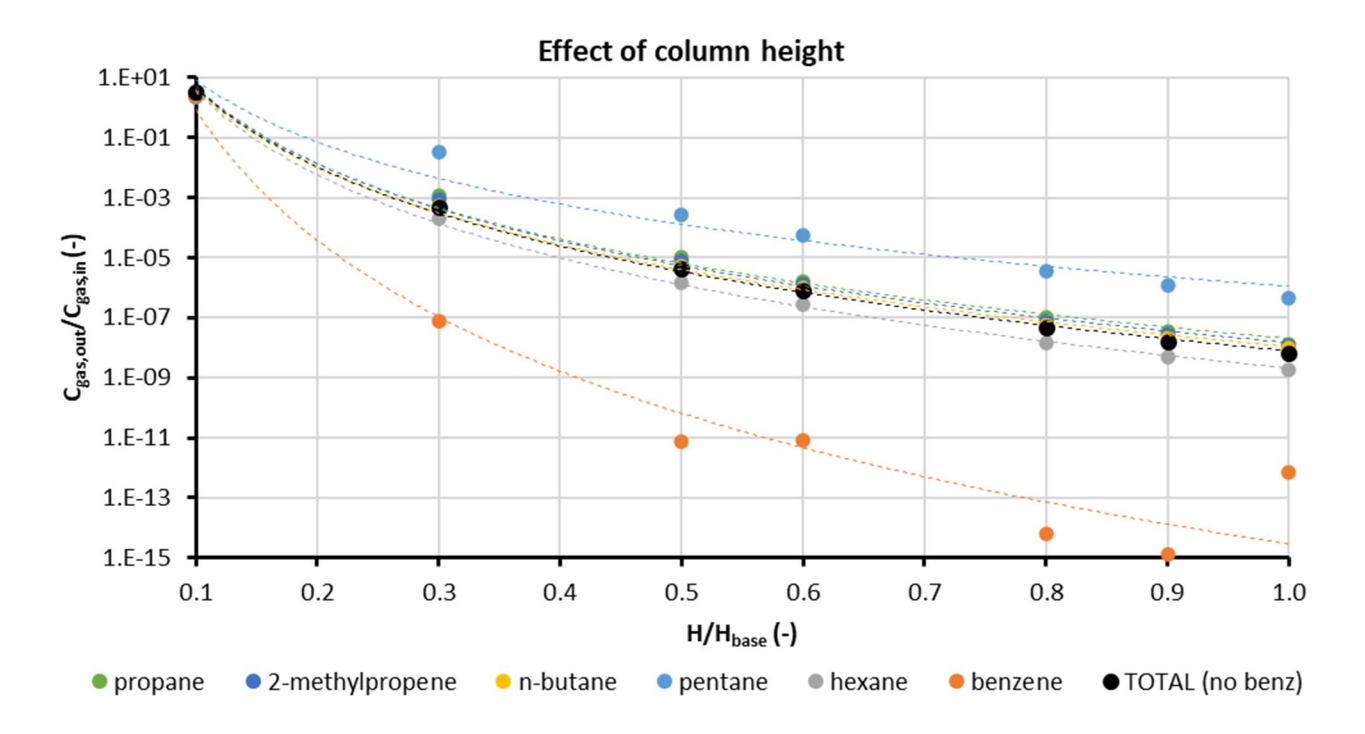


Figure 34: effect of variation of column height on the normalized outlet concentration after 30 days of continuous operation. Y-axis in log scale.

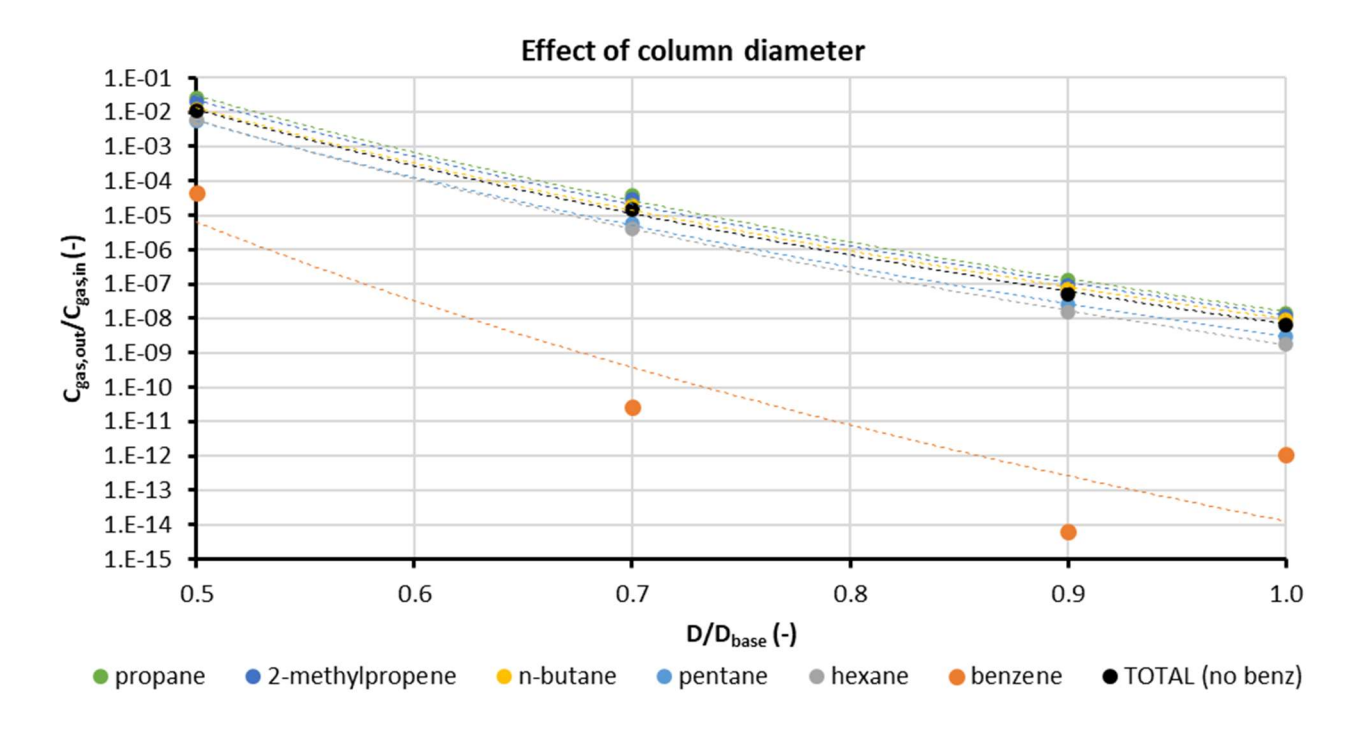


Figure 35: effect of variation of column diameter on the normalized outlet concentration after 30 days of continuous operation. Y-axis in log scale.

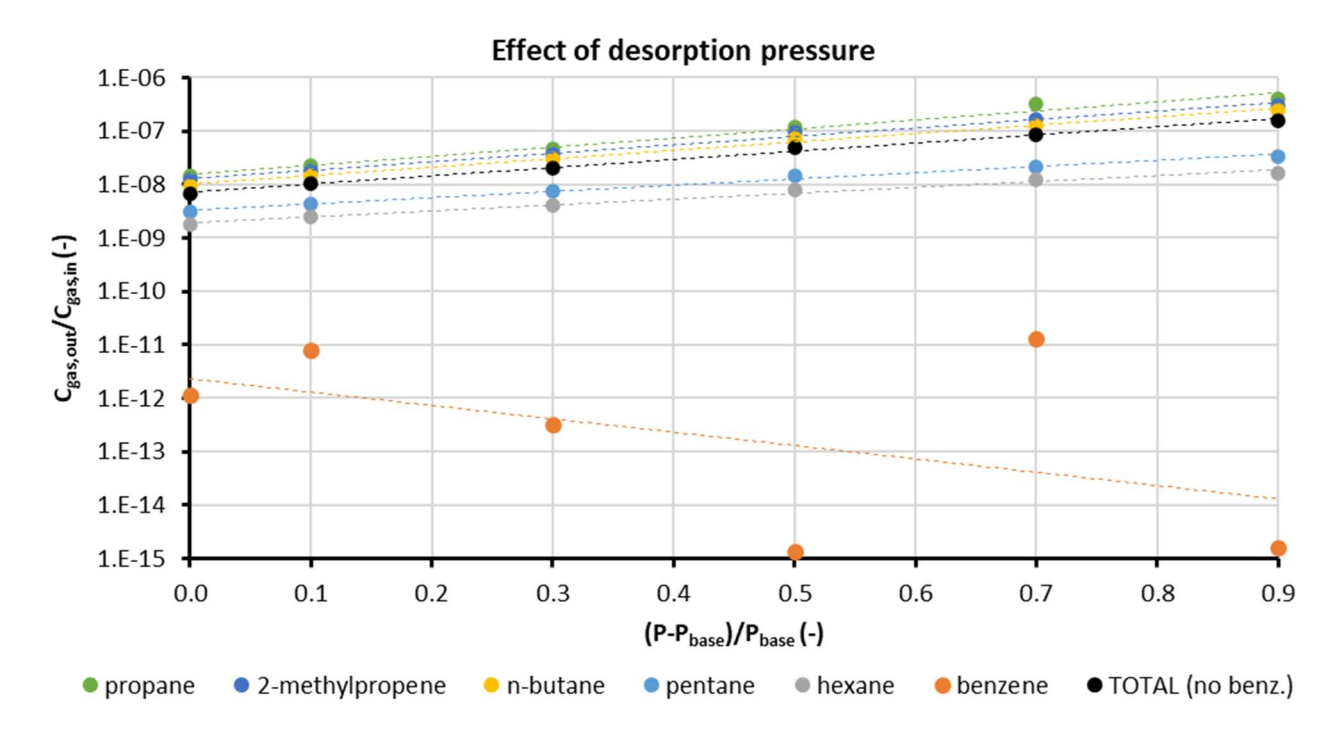


Figure 36: effect of variation of column regeneration pressure on the normalized outlet concentration after 30 days of continuous operation. Y-axis in log scale.

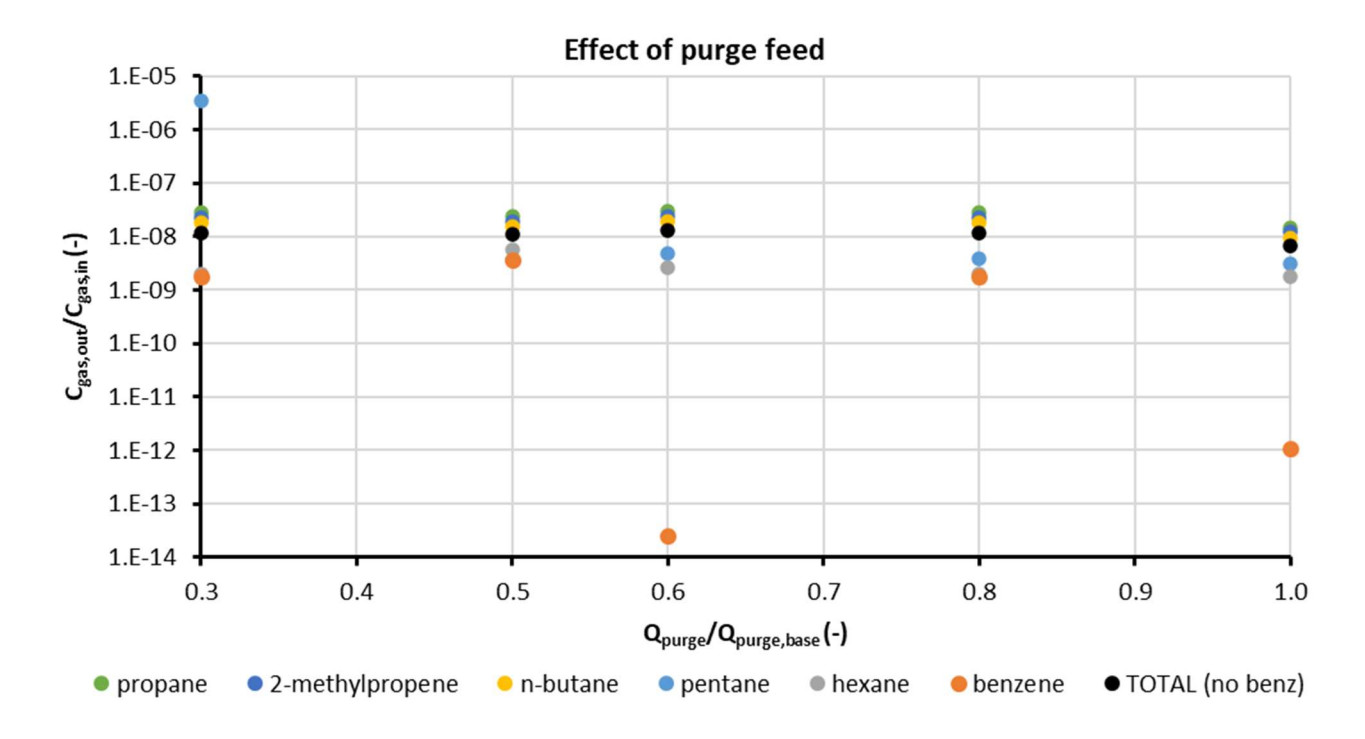


Figure 37: effect of variation of column purge feed on the normalized outlet concentration after 30 days of continuous operation. Y-axis in log scale.

Figure 34 shows the effect of reducing column height compared to the base design. As expected, a shorter column leads to a higher outlet concentration. Interestingly, the final outlet concentration of all substances showed a power law dependence of the kind y=A×x<sup>B</sup> with respect to the height of the column. Power law dependence is also seen in the case of diameter variation displayed in Figure 35. It should be noted that both decreasing column height and decreasing diameter have the effect of reducing the column volume, therefore the mass of the adsorbent involved, likely explaining the similar relationship. However, a percentage variation of column diameter has an overall greater impact on outlet concentration compared to similar percentage variation of bed height, likely as a combined effect of both the higher variation of volume associated with diameter variation compared to height variation and of the increase in gas velocity resulting from the reduction of diameter. A 50% decrease in diameter leads to a 5 orders of magnitude variation of the outlet concentration, while a 50% reduction in column height only leads to a difference in outlet concentration of 1 to 2 orders of magnitude. Figure 36 on the other hand shows an exponential relationship of the kind  $y=A\times\exp(B\times x)$ between the outlet concentration and the difference in regeneration pressure. While as expected increasing the regeneration pressure overall lowers the efficiency of capture, with higher concentrations seen at the end of the simulation, in the considered process conditions regeneration pressure appears to have a limited effect on the outlet conditions, with a 90% increase in regeneration pressure leading to only a 1 order of magnitude increase in outlet concentration, a much more limited effect compared to that of variation of column height and diameter. Finally, according to Figure 37, the effect of purge flowrate was the least relevant among the parameters evaluated, with a variation of less than 1 order of magnitude for the outlet concentration of most substances. It should be noted that in all the cases observed, benzene displayed slightly different behavior compared to the other VOCs. This may be due to its much lower concentration in the process feed, leading to greater uncertainty in the results for this compound as they could be more easily affected by numerical errors. Table 13 reports the bed utilization percentage for all case scenarios. It is apparent how purge flowrate does not appear to significantly affect column performance, while downsizing column height to 70% of the base design or diameter to 50% of the base case leads to complete bed utilization, which is undesired as an oversize-margin is necessary to account for possible feed variability. In conclusion, in the present case an optimized design could be obtained by reducing column height by 40%, while increasing regeneration pressure by 90% and reducing purge by 50%. From the available data, such a design would be able to provide effective VOCs abatement while lowering equipment and adsorbent cost.

Table 13: bed utilization percentage for each case study.

Bed utilization (%)			
40			
ariation			
40			
50			
60			
70			
100			
100			
variation			
50			
70			
100			
essure variation			
40			
40			
50			
50			
50			
Purge variation			
40			
40			
40			
40			

#### 2.3.6-Conclusion and future perspectives

Abatement of VOCs emission is a primary concern for the petrochemical sector, with several available solutions having been proposed. Adsorption technologies, especially when combined with a further absorption process, is nowadays one of the most relevant technologies for VOCs abatement thanks to its high capture efficiency and energy efficiency. However, simulation of multicomponent adsorption processes is a complex task, especially as the competition between adsorbed species does not allow to consider pure component adsorption data only for the design of column. Numerical

simulations can be used to study the optimization of the process without relying on hard to obtain experimental results. In the present work, an optimization of adsorption process for VOCs recovery from storage tanks was performed using Aspen Adsorption<sup>TM</sup> commercial software. The Extended Langmuir model and the Ideal Adsorbed Solution Theory were shown to provide similar results for hydrocarbon mixtures, and a detailed literature review was performed to collect adsorption parameters for use in the simulation. To the author's knowledge, the present thesis reports the most complete literature review for adsorption of hydrocarbons on silica, zeolite and activated carbon adsorbents. However, critical aspects appear from the data collected: namely, availability of adsorption data shows several gaps. While for some compounds several datasets are available on a number of adsorbents, many other compounds which could be of interest for abatement do not have any adsorption data available in the literature. For example, isotherm data for 2-methylpropane had to be used for 2-methylpropane in the current simulations, as no data was found in literature for the adsorption of the latter. Many literature datasets report only isotherms at a single temperature, which are of limited usefulness as the temperature variation occurring during adsorption processes can have a very significant effect on the performance of the process. Furthermore, significant differences exist between the various adsorption datasets reported in literature, showing different performances even between similar adsorbents. This great variability further complicates the utilization of numerical simulation of adsorption processes, as to obtain the most reliable results one should have adsorption data on the selected adsorbent at least at two different temperatures for each substance of interest to be able to correctly model multicomponent adsorption taking into account both temperature and species competition effects. In the present simulation, a representative activated carbon was obtained by comparing adsorption data for similar activated carbons adsorbents for which adsorption data was available for one or more of the VOCs present in the feed, however this is a limited approach and is only a first approximation of the complete behavior of a possible activated carbon adsorbent. On the other hand, performing adsorption experiments for each substance on every possible adsorbent would be prohibitively expensive and time consuming. The author proposes that a possible solution to this problem could be obtained with the development of reliable models such as quantitative structure activity relationship models (QSAR) capable of predicting adsorption capacities starting from relatively easier to measure physical and chemical adsorbent properties such as surface area, pore size distribution and surface charge, as well as adsorbed phase molecular structure. Furthermore, the use of artificial intelligence could be of significant help in this field, with the papers reviewed here as a possible basis for training and testing datasets construction. Another crucial aspect is that the column should be designed on the actual composition of the mixture to abate. The present work used a representative literature composition for gasoline vapors for reference, but in a real case of column

design should always use real experimental concentration data obtained for its particular case, as composition of storage tanks vapors can show great variability on the basis of the composition of the stored oil and the storage conditions. From the simulation of 1-month cyclical PSA column using Aspen Adsorption<sup>TM</sup>, the design of the multicomponent adsorption column can be efficiently optimized, and interesting design considerations are observed, namely the final concentration of VOCs at the end of the simulation showed a power law dependence on both column height and diameter, while an exponential dependence on regeneration pressure was obtained. Compared to other parameters, the purge flowrate does not appear to have a significant effect on process performance. Compared to the starting design obtained from pure component isotherms, column height could be downsized up to 40%, while regeneration pressure could be increased up to 90% and purge flowrate could be reduced by 70%, decreasing the overall cost while still meeting the desired abatement thresholds. Evident thermal effects are observed, especially at the start of operation on a fresh bed, showing the importance of considering adsorption as non-isothermal for the purpose of column design. Experimental evaluation of adsorption processes is a complex and time-consuming task, and numerical simulations may allow to cheaply and quickly investigate process optimization. However, experimental validation of model results is essential to ensure reliability of numerical predictions. As such, future work should be dedicated to enhance the availability of multicomponent adsorption data and experimentally validate the optimization guidelines hereby presented.

#### **General conclusions**

In the last centuries, the development of human activities has greatly impacted our planet's ecosystems. The ever-increasing growth of human population and our hunger for resources to fuel our economies has placed critical pressure on our planet's capacity to sustain our species and has brought severe consequences, already showing remarkable damage to the biosphere, with a frightening number of species being threatened or on the brink of extinction, widespread pollution and destruction of natural habitat. Global warming due to greenhouse gases emissions in particular is already showing its dramatic consequences, with extreme climate phenomena already on the rise. This puts our civilization in front of a critical choice. If we are not able to significantly mitigate our environmental impact over the next decade, particularly reducing greenhouse gases emissions, the increase in average global temperature will surpass the point of no return, with drastic consequences both for the environment and for our own survival. The development of hydrogen economy could allow us to achieve sustainable energy usage and help us to replace the use of fossil fuels, but considerable developments are still needed before this can be effectively achieved. With an everdecreasing time available to make relevant changes and contain the already ongoing ecological effects, it is crucial that further research efforts be devoted to the development of this field. Chemical looping technology can be used to achieve more sustainable syngas and hydrogen production through reforming and partial oxidation of methane; however, research is still needed to identify optimal oxygen carriers to use for the process. In particular, more effort should be devoted to the development of numerical models for the simulation of chemical looping processes, as such models are necessary to help in process optimization.

While innovative and more sustainable processes need to be quickly developed, on the other hand conventional processes are difficult to completely replace in a short time. Therefore, in the meantime it is necessary to ensure that the environmental impact of such processes is reduced to a minimum. Oil refineries in particular are the most predominant source of industrial VOCs emissions, which are a severe danger both to the environment and to human health. Therefore, effective and cost competitive abatement strategies need to be developed. Adsorption is an effective technology for the separation of gas phases; however, the separation of multicomponent gaseous mixtures is a complex phenomenon. The use of numerical models can help in optimizing abatement strategy, however, literature data on adsorption of pollutants presents several gaps that need to be addressed. In this thesis, a literature review of adsorption data for hydrocarbon VOCs has been presented for silica, zeolite and activated carbon adsorbents, providing a first database for future research. The use of this data for the design of an optimized adsorption column has also been examined, obtaining guidelines for the simulation of such processes.

As discussed in this thesis, the crucial point for the development of numerical simulations is the availability of reliable experimental data to validate the models. In both CLR and PSA simulation, the implementation of numerical simulations likely suffers from the low availability of experimental data: in the case of CLR reforming, more effort is needed in determining the reaction mechanism of methane on oxygen carriers in varying operation conditions. At present, the available literature model for cerium dioxide oxygen carrier kinetics has been found ineffective in predicting quantitatively the experimental results of the present activity. This can be likely attributed to the incomplete availability of data in terms of activation energies, reaction enthalpies and kinetic constants, with potential pathways such as hydride formation being left out of model considerations. Furthermore, the effect of dopant presence is not considered in current models. As shown by the experimental activity reported in this thesis, cerium dioxide is an active oxygen carrier for methane reforming, capable of very selectively oxidizing methane to syngas with minimal carbon formation and good regenerability even in the case of a chemical looping dry reforming process. However, on its own cerium dioxide offers limited methane conversion. Use of dopants and supports can enhance the performance of the carrier, but so far there is limited study on the effect of such dopants on reaction mechanism and especially reaction kinetics.

On the other hand, PSA simulations can provide an effective tool for process design, however the current databases of adsorption data are still severely incomplete. The time-consuming experiments and the great variability in adsorbent structures and possible adsorbed species make the process of gathering such data a daunting task. The development of predictive models based on functional groups approach or Artificial Intelligence may thus greatly help in obtaining accurate estimations for such complex processes. The adsorption data collection presented in this thesis may thus provide a useful starting point for future developments.

# Appendix: description of Aspen Adsorption models for CLR and PSA

Aspen Adsorption<sup>TM</sup> software provides a series of detailed options for the simulation of cyclical processes in dynamic conditions. As a numerical tool, the main function of Aspen AdsorptionTM is the numerical solution of mass, energy and momentum balances for each component in all phases, which is performed for each reaction block included in the simulation.

For both CLR and PSA simulations, a one-dimensional plug-flow regime is considered, therefore the axial and radial dispersion terms are neglected from mass balances. The mass balances solved by the software can thus be summed up in the following equations:

$$\frac{\partial(v_g c_k)}{\partial z} + \varepsilon_B \frac{\partial c_k}{\partial t} + J_k = 0 \tag{43}$$

$$\frac{\partial w_i}{\partial t} - R_{sol,i} = 0 \tag{44}$$

Where  $v_g$  is the gas speed in the bed,  $c_k$  is the gas phase concentration of species k,  $w_i$  is the concentration of solid species I,  $R_{sol,i}$  is the rate of formation of solid species i and  $\epsilon_B$  is the total bed voidage. The first term is the convective transport of gas in the axial direction, the second term is the accumulation of gas in the column, and  $J_k$  represents the flux of species k between gas and solid phase, which is given by the sum of adsorption, solid phase and gas phase reactions:

$$J_k = J_{ads.k} + J_{cat,reac,k} + J_{gas,reac,k}$$

$$\tag{45}$$

Where  $J_{ads,k}$  is the physical adsorption rate,  $J_{cat,reac,k}$  indicates the reaction rates on the solid surface of a catalyst and  $J_{gas,reac,k}$  is the reaction rate of homogeneous reactions in the gas phase. For both the CLR reforming model and the PSA model, no homogeneous reactions are considered to take place, therefore  $J_{gas,reac,k} = 0$  for both cases, leaving:

$$J_k = J_{ads.k} + J_{cat,reac,k} \tag{46}$$

In the case of CLR modeling  $J_{cat,reac,k}$  is calculated according to equations 20-26 and 34-37, while for the simulation of PSA, it is assumed that no reaction takes place ( $J_{cat,reac,k} = 0$ ). In both cases, physical adsorption is assumed to follow a Linear Driving Force model:

$$J_{ads,k} = MTC \cdot (w_i^* - w_i) \tag{47}$$

Where  $w_i^*$  is the interfacial concentration of species k and MTC is the mass transfer coefficient. The mass transfer coefficient is assumed to be constant for both CLR and PSA simulations, but the values considered are different, as described in the respective sections.

The solid species balance instead involves the formation/consumption of species in the solid phase, with the rate of formation for each component being calculated according to equations 20-26 and 34-

37 for the CLR model, while for the simulation of PSA, it is again assumed that no reaction takes place, therefore R<sub>sol,i</sub>=0 for every component.

As per the energy balances, conductive heat transfer is considered negligible for both CLR and PSA simulation, and the heat resistance of the reactor wall is also neglected. The energy balances thus become:

$$C_{vg}v_{g}\rho_{g}\frac{\partial T_{gas}}{\partial z} + \varepsilon_{B}C_{vg}\rho_{g}\frac{\partial T_{gas}}{\partial t} + P\frac{\partial v_{g}}{\partial z} + HTC \cdot a_{p} \cdot \left(T_{gas} - T_{solid}\right) + \frac{4H_{w}}{D_{b}}\left(T_{gas} - T_{ext}\right) + H_{r} + \rho_{cat}C_{p,cat}\frac{\partial T_{gas}}{\partial t} + a_{H_{x}}Q_{H_{x}} = 0$$

$$\tag{48}$$

$$\rho_{s}C_{ps}\frac{\partial T_{s}}{\partial t} + \rho_{s}\sum_{k}\left(\Delta H_{ads,k}\frac{\partial w_{k}}{\partial t}\right) + HTC \cdot \alpha_{p} \cdot \left(T_{gas} - T_{solid}\right) = 0 \tag{49}$$

With the first equation describing the gas phase and the second equation the solid phase. In these equations,  $\rho_g$  is the gas phase density,  $\rho_s$  is the density of the solid adsorbent,  $w_k$  is the adsorbed amount of species k,  $\epsilon_i$  is the interparticle voidage,  $J_k$  is the diffusion rate of species k between gas and adsorbent,  $C_{vg}$  is the isochoric specific heat of gas phase,  $C_{ps}$  is the specific heat of adsorbent,  $T_{gas}$  is gas temperature,  $T_{solid}$  is solid temperature,  $T_{ext}$  is the ambient temperature,  $P_{ext}$  is gas phase pressure,  $\Delta H_{ads,k}$  is the adsorption heat of species k, HTC is the convective heat transfer coefficient between gas and solid,  $H_w$  is the heat transfer coefficient to ambient,  $D_b$  is bed diameter,  $H_r$  is the enthalpy generation term,  $a_p$  is the specific area of the solid-gas interface,  $a_{H_x}$  is the area of the internal heat exchanger and  $Q_{H_x}$  is the heat flux to heat exchanger. For gas phase balance, the first term is the convective transfer along the axial direction, the second term is the accumulation of enthalpy in gas phase, the third term is the effect of gas compression, the fourth term is the heat transfer from gas to solid phase, the fifth term is heat exchange with the environment, the seventh term is the enthalpy accumulation in solid catalytic phase and the last term is heat exchange with internal/external heat exchanger equipment. The heat transfer coefficient between gas and solid phase (HTC) is estimated by the software as a function of the Reynolds and Prandtl numbers

$$Re = \frac{2r_p M_{gas} \rho_g v_g}{\mu} \tag{50}$$

$$Pr = \frac{\mu C_{pg}}{k_g M_{gas}} \tag{51}$$

$$j = \begin{cases} 1.660Re^{-0.51} & \text{if } Re < 190\\ 0.983Re^{-0.41} & \text{if } Re \ge 190 \end{cases}$$
 (52)

$$HTC = jC_{pg}v_g\rho_g \operatorname{Pr}^{-\frac{2}{3}}$$
 (53)

Where  $\mu$  is the gas viscosity,  $C_{pg}$  is the isobaric heat capacity of gas,  $k_g$  is gas phase heat conductivity and  $M_{gas}$  is the gas molecular weight.

The term for heat exchange with the environment is considered only in the case of non-isothermal CLR simulation, while it is neglected in all other cases.

For the CLR simulation, the enthalpy generation rate is obtained from the heterogeneous reaction heats ( $\Delta H_R$ ) and reaction rates obtained from equations 20-26:

$$H_r = \varepsilon_i \sum_{n=1}^{n_{reac,cat}} \Delta H_{R,n} r_n \tag{54}$$

In the case of PSA simulation, this term is assumed instead to be zero.

Finally, the heat exchange term for the internal heat exchanger is also assumed null for the case of PSA simulation, while for CLR simulation it is used to approximate the radiative heat exchange of heat provided by the electric furnace.

$$Q_{H_X} = U_{H_X} \left( T_{gas} - T_{H_X} \right) \tag{55}$$

Where  $U_{H_x}$  is the global heat transfer coefficient and  $T_{H_x}$  is the temperature of the heat exchanger fluid current. The heat exchanger parameters were selected to replicate the effect of electrical furnace in experimental tests, keeping reactor temperature above  $800^{\circ}$ C even during endothermic reaction. As per the solid phase energy balance, the first term represents enthalpy accumulation in the solid, the second term represents enthalpy generation from physical adsorption and the last term is heat transfer between solid and gas. The adsorption heats are assumed to be zero for CLR modeling, while their value has been obtained from literature adsorption data and equation 39 for PSA simulation.

Finally, the Ergun equation is used to model axial pressure drop in the columns.

$$\frac{\partial P}{\partial z} = -\left(\frac{1.5 \cdot 10^{-3} * (1 - \varepsilon_i)^2}{(2r_p \Phi)^2 \varepsilon_i^3} \mu v_g + 1.75 \cdot 10^{-5} M_{gas} \rho_g \frac{(1 - \varepsilon_i)}{2r_p \Phi \varepsilon_i^3} v_g^2\right)$$
 (56)

where  $\Phi$  is the particle sphericity, assumed to be 1 for both CLR and PSA simulation.

## Lists of mathematical symbols

Symbol	Symbol Explanation	
	Parameters	
A	Surface area	m <sup>2</sup>
$a_p$	Specific surface area of adsorbent	1/m
$a_{\mathrm{H_x}}$	Specific surface area of heat exchanger	m <sup>2</sup>
С	Gas phase concentration	kmol/m³
$C_{ m ps}$	Solid heat capacity (oxygen carrier for CLR, adsorbent for PSA)	MJ/(kg×K)
$C_{ m vg}$	Heat capacity of gas phase	MJ/(kg×K)
D <sub>b</sub>	Oxygen carrier/adsorbent bed diameter	m
E <sub>a</sub>	Activation energy of reaction n	MJ/kmol
$ m f_{eq}$	Isotherm equation	-
Нь	Height of solid bed (oxygen carrier or adsorbent)	m
$H_{ m w}$	Wall-ambient heat transfer coefficient	$MW/(m^2 \times K)$
НТС	Gas-solid heat transfer coefficient	$MW/(m^2 \times K)$
$k_n^0$	Kinetic constant of reaction n	1/s
$\mathrm{IP}_{\mathrm{Lang}}$	Adsorption parameter of Henry's isotherm for CLR simulation	-
IP1, IP2, IP3, IP4	Adsorption parameters of Extended Langmuir model for PSA simulation	-
M	Solid molar mass	g/mol
$ m M_{gas}$	Gas molar mass	g/mol
MTC	Gas-solid mass transfer coefficient	1/s
m	Carrier mass	QQ
ń	Flowrate	mol/s
n	Moles	mol
$J_k$	Mass transfer rate of species k from adsorbent to gas phase	$kmol/(m^3 \times s)$
$ m J_{ads,k}$	Flux of species k physically adsorbed from gas to solid phase	$\text{kmol/}(\text{m}^3 \times \text{s})$
J <sub>cat, reac, k</sub>	Flux of species k consumed by catalytic heterogeneous reactions between gas and solid phase	kmol/(m <sup>3</sup> ×s)

	T1 C ' 1 11	
Ţ	Flux of species k consumed by	1, = 1/(3 × =)
$ m J_{ m gas,  reac,  k}$	homogeneous reactions in gas	$\text{kmol/(m}^3 \times \text{s})$
	phase Coefficient for HTC	
j	calculation	-
$\mathbf{k}_{\mathbf{g}}$	Gas phase thermal conductivity	$MW/(m\times K)$
P	Pressure	bar
Pr	Prandtl number	Uai
$Q_{H_x}$	Heat exchanger flux	$J/(m^2 \times s)$
ŲH <sub>x</sub>	Available oxygen per mole of	3/(III ^S)
q	adsorbent	mol
$ m q_{ads}$	Adsorbed quantity	kmol/kg
Rate	Normalized rate of mass loss	-
R	Universal gas constant	J/(mol×K)
Re	Reynolds number	-
$r_n$	Rate of reaction n	1/s
$r_{ m p}$	Solid particle radius	m
C	Oxygen carrier particle surface	$m^2$
$S_{part}$	area	111
T	Temperature	K
t	Time	S
$U_{H_x}$	Heat transfer coefficient in	$MW/(m^2 \times K)$
	heat exchanger	
$V_{ m part}$	Solid particle volume	
$V_{g}$	Gas phase velocity	m/s
$W_k$	Solid phase concentration of	kmol/kg
	adsorbed species k	
$W_{\mathfrak{b}}$	Wall thickness	m
у	Gas phase molar fraction	-
ΔΗ	Enthalpy of CeO <sub>2</sub> surface-bulk equilibrium	kJ/kmol
$\Delta H_{ads}$	Enthalpy of adsorption	MJ/kmol
$\Delta H_R$	Enthalpy of reaction	MJ/kmol
	Entropy of CeO <sub>2</sub> surface-bulk	
$\Delta \mathrm{S}$	equilibrium	$J/(mol \times K)$
	Greek symbols	
γ	Activity coefficient	_
δ	Carrier reduction extent	
0	Maximum carrier reduction	
$\delta_{ ext{max}}$	extent	-
η	Oxygen carrier selectivity	-
$\epsilon_{\mathrm{B}}$	Total bed void fraction	-
εį	inter-particle void fraction	-
$\epsilon_{ m p}$	intra-particle void fraction	-
μ	Gas dynamic viscosity	$N \times s/m^2$
•	Chemical potential of adsorbed	
$\mu_{ m ads}$	phase	MJ/kmol

$\mu_{ m gas}$	Chemical potential of gas phase	MJ/kmol
	Standard chemical potential of	
$\mu_k^0$	species i	MJ/kmol
П	Spreading pressure	bar×m
$\rho_{\mathrm{s}}$	Solid phase mass bulk density	kg/m <sup>3</sup>
	Cerium oxide molar bulk	mol/m <sup>3</sup>
ρСе	density	
$ ho_{\mathrm{Ce,s}}$	Cerium oxide surface density	mol/m <sup>2</sup>
Φ	Particle sphericity	-
χ	Reagent conversion	-
ω	Mass fraction	-
	Subscripts	
acc	accumulated	-
ь	Backward reaction	-
С	Carbon	-
CH <sub>4</sub>	Methane	-
Chromite	Chromite	-
CeO <sub>2</sub>	Cerium dioxide	-
CuO	Copper oxide	-
CO	Carbon monoxide	-
$CO_2$	Carbon dioxide	-
f	Forward reaction	-
FeO	Iron oxide	-
gen	generated	-
gas	Gas phase	-
$H_2$	Hydrogen	-
H <sub>2</sub> O	Water	-
in	inlet	-
$O_2$	Oxygen	-
OC	Oxygen carrier	-
OX	Oxidant	-
out	outlet	-
PO	Partial oxidation	-
REG	Regeneration	-
solid	Solid phase	-
	Superscripts	
ь	Backward reaction	-
С	Carbon	-
Chromite	Chromite	-
CeO <sub>2</sub>	Cerium dioxide	-
CuO	Copper oxide	-
CH <sub>4</sub>	Methane	-
СО	Carbon monoxide	-
CO <sub>2</sub>	Carbon dioxide	-
f	Forward reaction	-
gen	generated	-
H <sub>2</sub>	Hydrogen	-
H <sub>2</sub> O	Water	-

$N_2$	Nitrogen	-
PO	Partial oxidation	-
REG	Regeneration	-

## List of acronyms

	Acronyms	
ADR	Autothermal dry reforming	
AEM-WE	Anion exchange membrane water electrolysis	
AR	Autothermal reforming	
ASU	Air separation unit	
ASR	Autothermal steam reforming	
A-WE	Alkaline water electrolysis	
BC-WD	Biocatalytic water decomposition	
BF	Biofermentation	
CCUS	Carbon capture utilization and storage	
CL	Chemical looping	
CLC	Chemical looping combustion	
CLDR	Chemical looping dry reforming	
CLG	Chemical looping gasification	
CLPO	Chemical looping partial oxidation	
CLSR	Chemical looping steam reforming	
DF	Dark fermentation	
DR	Dry reforming	
DWT	Direct water thermolysis	
EC-H <sub>2</sub> SD	Electrocatalytic H <sub>2</sub> S decomposition	
EL	Extended Langmuir	
G	Gasification	
HHV	Higher heating value	
$H_2SR$	H <sub>2</sub> S reforming	
IAST	Ideal adsorbed solution theory	
IGCC	Integrated gasification combined cycle	
IPCC	Intergovernmental Panel on Climate Change	
LHV	Lower heating value	
MD	Methane decomposition	
MOF	Metal-organic framework	
NMVOC	Non-methane volatile organic compound	
NTPD-MD	Non-thermal plasma driven methane decomposition	
NTPDC-MD	Non-thermal plasma driven catalytic methane decomposition	
OC	Oxygen carrier	
PC-WS	Photocatalytic water splitting	
PC-H <sub>2</sub> SD	Photocatalytic H <sub>2</sub> S decomposition	
PD-H <sub>2</sub> SD	Plasma-driven H <sub>2</sub> S decomposition	
PEM-WE	Proton exchange membrane water electrolysis	
PSA	Pressure swing adsorption	
PF	Photo-fermentation	
PO	Partial oxidation	
QSAR	Quantitative structure–activity relationship models	
SEM	Scanning electron microscopy	
SOFC-WE	Solid oxide fuel cell water electrolysis	
SR	Steam Reforming	
TC-H <sub>2</sub> SD	Thermochemical H <sub>2</sub> S decomposition	
TC-MD	Thermochemical methane decomposition	

TGA	Thermogravimetric analysis
TMD	Thermal methane decomposition
TPD-MD	Thermal plasma driven methane decomposition
TRC-WS	Thermochemical redox cycles water splitting
TRL	Technology readiness level
TSA	Temperature swing adsorption
UCG	Underground coal gasification
VOC	Volatile organic compound
VRU	Vapor recovery unit
VSA	Vacuum swing adsorption
WE	Water electrolysis
WGS	Water gas shift
XRD	X-ray powder diffractometry
2R	Dual reforming
3R	Tri reforming

## Acknowledgements

The author would like to thank Prof. Ferruccio Doghieri, the supervisor of this Ph.D. project. Thank you for mentoring me in these three years, for offering me the opportunity of participating to this process and for believing in my abilities to the end. I also thank Prof. Matteo Minelli, who also collaborated closely with us and helped me with my experiences in the lab, and Prof. Miccio Francesco, for his patient contributions and helpful insights on the preparation and publication of our papers. Thank you to the people of Duemme Engineering and especially to its owner Francesca Nappini, for offering me the opportunity to work together on real industrial design cases and helping me in the process of understanding the use of Aspen simulation software. I would also like to thank the University of Bologna and its staff for providing the means of carrying out these activities. In particular, thanks to Lorella Guadagnini and Micaela Pasquini. A special thanks goes to all my colleagues at DICAM, and especially to Alba Storione, who preceded me in the work on methane reforming, and to Virginia Signorini for her patience while helping me to understand how to deal with lab procedures. I know that we had a somewhat rough start, but I am glad that we managed to get along well in the end. Thank you all for not only being good colleagues, but also for helping me to grow as a person, and for being good company in and outside work. You are my friends, and I am glad to have met you. Finally, my biggest thank you goes to my family, for always being there for me no matter what we go through, and even in my grumpiest and lower moments. I could not hope to have better people in my life.

## References

- [1] G. Holland, C.L. Bruyère, Recent intense hurricane response to global climate change, Clim Dyn 42 (2014) 617–627. <a href="https://doi.org/10.1007/s00382-013-1713-0">https://doi.org/10.1007/s00382-013-1713-0</a>.
- [2] K.P. Tripathy, S. Mukherjee, A.K. Mishra, M.E. Mann, A.P. Williams, Climate change will accelerate the high-end risk of compound drought and heatwave events, Proceedings of the National Academy of Sciences 120 (2023). https://doi.org/10.1073/pnas.2219825120.
- [3] F.E.L. Otto, M. Zachariah, F. Saeed, A. Siddiqi, S. Kamil, H. Mushtaq, T. Arulalan, K. AchutaRao, S.T. Chaithra, C. Barnes, S. Philip, S. Kew, R. Vautard, G. Koren, I. Pinto, P. Wolski, M. Vahlberg, R. Singh, J. Arrighi, M. van Aalst, L. Thalheimer, E. Raju, S. Li, W. Yang, L.J. Harrington, B. Clarke, Climate change increased extreme monsoon rainfall, flooding highly vulnerable communities in Pakistan, Environmental Research: Climate 2 (2023) 025001. <a href="https://doi.org/10.1088/2752-5295/acbfd5">https://doi.org/10.1088/2752-5295/acbfd5</a>.
- [4] O. Tamm, E. Saaremäe, K. Rahkema, J. Jaagus, T. Tamm, The intensification of short-duration rainfall extremes due to climate change Need for a frequent update of intensity–duration–frequency curves, Clim Serv 30 (2023) 100349. <a href="https://doi.org/10.1016/j.cliser.2023.100349">https://doi.org/10.1016/j.cliser.2023.100349</a>.
- [5] I.J. Mirón, C. Linares, J. Díaz, The influence of climate change on food production and food safety, Environ Res 216 (2023) 114674. <a href="https://doi.org/10.1016/j.envres.2022.114674">https://doi.org/10.1016/j.envres.2022.114674</a>.
- [6] X.-Y. Zou, X.-Y. Peng, X.-X. Zhao, C.-P. Chang, The impact of extreme weather events on water quality: international evidence, Natural Hazards 115 (2023) 1–21. <a href="https://doi.org/10.1007/s11069-022-05548-9">https://doi.org/10.1007/s11069-022-05548-9</a>.
- [7] R. Newman, I. Noy, The global costs of extreme weather that are attributable to climate change, Nat Commun 14 (2023) 6103. https://doi.org/10.1038/s41467-023-41888-1.
- [8] A.L. Pigot, C. Merow, A. Wilson, C.H. Trisos, Abrupt expansion of climate change risks for species globally, Nat Ecol Evol 7 (2023) 1060–1071. https://doi.org/10.1038/s41559-023-02070-4.
- [9] K. Calvin, D. Dasgupta, G. Krinner, A. Mukherji, P.W. Thorne, C. Trisos, J. Romero, P. Aldunce, K. Barrett, G. Blanco, W.W.L. Cheung, S. Connors, F. Denton, A. Diongue-Niang, D. Dodman, M. Garschagen, O. Geden, B. Hayward, C. Jones, F. Jotzo, T. Krug, R. Lasco, Y.-Y. Lee, V. Masson-Delmotte, M. Meinshausen, K. Mintenbeck, A. Mokssit, F.E.L. Otto, M. Pathak, A. Pirani, E. Poloczanska, H.-O. Pörtner, A. Revi, D.C. Roberts, J. Roy, A.C. Ruane, J. Skea, P.R. Shukla, R. Slade, A. Slangen, Y. Sokona, A.A. Sörensson, M. Tignor, D. van Vuuren, Y.-M. Wei, H. Winkler, P. Zhai, Z. Zommers, J.-C. Hourcade, F.X. Johnson, S. Pachauri, N.P. Simpson, C. Singh, A. Thomas, E. Totin, A. Alegría, K. Armour, B. Bednar-Friedl, K. Blok, G. Cissé, F. Dentener, S. Eriksen, E. Fischer, G. Garner, C. Guivarch, M. Haasnoot, G. Hansen, M. Hauser, E. Hawkins, T. Hermans, R. Kopp, N. Leprince-Ringuet, J. Lewis, D. Ley, C. Ludden, L. Niamir, Z. Nicholls, S. Some, S. Szopa, B. Trewin, K.-I. van der Wijst, G. Winter, M. Witting, A. Birt, M. Ha, IPCC, 2023: Climate Change 2023: Synthesis Report. Contribution of Working Groups I, II and III to the Sixth Assessment Report of the Intergovernmental Panel on Climate Change [Core Writing Team, H. Lee and J. Romero (eds.)]. IPCC, Geneva, Switzerland., 2023. https://doi.org/10.59327/IPCC/AR6-9789291691647.
- [10] Scripps CO<sub>2</sub> program, Mauna Loa Record, Scripps Institution of Oceanography at UC San Diego (2024). <a href="https://scrippsco2.ucsd.edu/graphics\_gallery/mauna\_loa\_record/mauna\_loa\_record.html">https://scrippsco2.ucsd.edu/graphics\_gallery/mauna\_loa\_record.html</a> (accessed September 2, 2024).
- [11] European Union (EU), Long-term low greenhouse gas emission development strategy of the European Union and its Member States, European Union (EU), 2020. <a href="https://unfccc.int/documents/210328">https://unfccc.int/documents/210328</a> (accessed September 2, 2024).
- [12] United States of America, The Long-Term Strategy of the United States: Pathways to Net-Zero Greenhouse Gas Emissions by 2050, United States Department of State, United States Executive Office of the President, 2021. <a href="https://www.whitehouse.gov/wp-content/uploads/2021/10/us-long-term-strategy.pdf">https://www.whitehouse.gov/wp-content/uploads/2021/10/us-long-term-strategy.pdf</a> (accessed September 2, 2024).

- [13] People's Republic of China, China's Policies and Actions for Addressing Climate Change, China, 2022. <a href="https://english.mee.gov.cn/Resources/Reports/reports/202211/P020221110605466439270.pdf">https://english.mee.gov.cn/Resources/Reports/reports/202211/P020221110605466439270.pdf</a> (accessed October 10, 2024).
- [14] UNFCC, The Paris Agreement Publication, in: Paris Climate Change Conference November 2015-COP21, 2018. <a href="https://unfccc.int/sites/default/files/resource/parisagreement\_publication.pdf">https://unfccc.int/sites/default/files/resource/parisagreement\_publication.pdf</a> (accessed September 2, 2024).
- [15] M. Boscherini, F. Miccio, E. Papa, V. Medri, E. Landi, F. Doghieri, M. Minelli, The relevance of thermal effects during CO<sub>2</sub> adsorption and regeneration in a geopolymer-zeolite composite: Experimental and modelling insights, Chemical Engineering Journal 408 (2021). https://doi.org/10.1016/j.cej.2020.127315.
- [16] N. Bahman, M. Al-Khalifa, S. Al Baharna, Z. Abdulmohsen, E. Khan, Review of carbon capture and storage technologies in selected industries: potentials and challenges, Rev Environ Sci Biotechnol 22 (2023) 451–470. https://doi.org/10.1007/s11157-023-09649-0.
- [17] S. Griffiths, B.K. Sovacool, J. Kim, M. Bazilian, J.M. Uratani, Industrial decarbonization via hydrogen: A critical and systematic review of developments, socio-technical systems and policy options, Energy Res Soc Sci 80 (2021). https://doi.org/10.1016/j.erss.2021.102208.
- [18] F. Ausfelder, A. Bazzanella, Hydrogen in the Chemical Industry, in: Hydrogen Science and Engineering: Materials, Processes, Systems and Technology, Wiley, 2016: pp. 19–40. https://doi.org/10.1002/9783527674268.ch02.
- [19] P. Basu, Production of Synthetic Fuels and Chemicals from Biomass, in: Biomass Gasification, Pyrolysis and Torrefaction, Elsevier, 2018: pp. 415–443. <a href="https://doi.org/10.1016/B978-0-12-812992-0.00012-1">https://doi.org/10.1016/B978-0-12-812992-0.00012-1</a>.
- [20] S.S. Shetty, D. D, H. S, S. Sonkusare, P.B. Naik, S. Kumari N, H. Madhyastha, Environmental pollutants and their effects on human health, Heliyon 9 (2023) e19496. https://doi.org/10.1016/j.heliyon.2023.e19496.
- [21] A. Pozzer, S.C. Anenberg, S. Dey, A. Haines, J. Lelieveld, S. Chowdhury, Mortality Attributable to Ambient Air Pollution: A Review of Global Estimates, Geohealth 7 (2023). <a href="https://doi.org/10.1029/2022GH000711">https://doi.org/10.1029/2022GH000711</a>.
- [22] A.S. Kolawole, A.O. Iyiola, Environmental Pollution: Threats, Impact on Biodiversity, and Protection Strategies, in: 2023: pp. 377–409. https://doi.org/10.1007/978-981-19-6974-4 14.
- [23] European Union, IPPC Industrial Emissions Directive, Directive 2010/75/EU of the European Parliament and of the Council of 24 November 2010 on industrial emissions (integrated pollution prevention and control), European Parliament and Council of the European Union, 2010. <a href="http://data.europa.eu/eli/dir/2010/75/oj">http://data.europa.eu/eli/dir/2010/75/oj</a> (accessed November 20, 2024).
- [24] United States Environmental Protection Agency (EPA), Technical Overview of Volatile Organic Compounds, United States Environmental Protection Agency (EPA) (2024). <a href="https://www.epa.gov/indoor-air-quality-iaq/technical-overview-volatile-organic-compounds">https://www.epa.gov/indoor-air-quality-iaq/technical-overview-volatile-organic-compounds</a> (accessed November 20, 2024).
- [25] P. Pandey, R. Yadav, A Review on Volatile Organic Compounds (VOCs) as Environmental Pollutants: Fate and Distribution, International Journal of Plant and Environment 4 (2018) 14–26. <a href="https://doi.org/10.18811/ijpen.v4i02.2">https://doi.org/10.18811/ijpen.v4i02.2</a>.
- [26] V. Soni, P. Singh, V. Shree, V. Goel, Effects of VOCs on Human Health, in: N. Sharma, A.K. Agarwal, P. Eastwood, T. Gupta, A.P. Singh (Eds.), Energy, Environment, and Sustainability-Air Pollution and Control, 1st ed., Springer Singapore, Singapore, 2018: pp. 119–142. https://doi.org/10.1007/978-981-10-7185-0 8.
- [27] X. Zhou, X. Zhou, C. Wang, H. Zhou, Environmental and human health impacts of volatile organic compounds: A perspective review, Chemosphere 313 (2023). <a href="https://doi.org/10.1016/j.chemosphere.2022.137489">https://doi.org/10.1016/j.chemosphere.2022.137489</a>.
- [28] N. Liu, Z. Bu, W. Liu, H. Kan, Z. Zhao, F. Deng, C. Huang, B. Zhao, X. Zeng, Y. Sun, H. Qian, J. Mo, C. Sun, J. Guo, X. Zheng, L.B. Weschler, Y. Zhang, Health effects of exposure to indoor volatile

- organic compounds from 1980 to 2017: A systematic review and meta-analysis, Indoor Air 32 (2022). https://doi.org/10.1111/ina.13038.
- [29] Y. Xiong, K. Du, Y. Huang, One-third of global population at cancer risk due to elevated volatile organic compounds levels, NPJ Clim Atmos Sci 7 (2024). <a href="https://doi.org/10.1038/s41612-024-00598-1">https://doi.org/10.1038/s41612-024-00598-1</a>.
- [30] H. Rajabi, M. Hadi Mosleh, P. Mandal, A. Lea-Langton, M. Sedighi, Emissions of volatile organic compounds from crude oil processing Global emission inventory and environmental release, Science of The Total Environment 727 (2020) 138654. https://doi.org/10.1016/j.scitotenv.2020.138654.
- [31] M. Tamaddoni, R. Sotudeh-Gharebagh, S. Nario, M. Hajihosseinzadeh, N. Mostoufi, Experimental study of the VOC emitted from crude oil tankers, Process Safety and Environmental Protection 92 (2014) 929–937. https://doi.org/10.1016/j.psep.2013.10.005.
- [32] S. Saikomol, S. Thepanondh, W. Laowagul, Emission losses and dispersion of volatile organic compounds from tank farm of petroleum refinery complex, J Environ Health Sci Eng 17 (2019) 561–570. https://doi.org/10.1007/s40201-019-00370-1.
- [33] US EPA, GasSTAR, Lessons Learned from Natural Gas STAR Partners: Installing Vapor Recovery Units on Storage Tanks, Washington, DC, 2006. <a href="https://19january2017snapshot.epa.gov/sites/production/files/2016-06/documents/ll\_final\_vap.pdf">https://19january2017snapshot.epa.gov/sites/production/files/2016-06/documents/ll\_final\_vap.pdf</a> (accessed December 22, 2023).
- [34] E. Kalay, H. Sarıoğlu, İ. Özkul, Investigation of emission control efficiency with gasoline vapor recovery units, Advanced Engineering Science 2 (2022) 9–14. http://publish.mersin.edu.tr/index.php/ades.
- [35] W. Huang, Y. Wang, Y. Lin, C. Zhao, Gasoline vapor recovery based on integrated technology of absorption-adsorption, in: Applied Mechanics and Materials, 2013: pp. 1482–1485. https://doi.org/10.4028/www.scientific.net/AMM.295-298.1482.
- [36] National Center for Biotechnology Information, PubChem Element Summary for Atomic Number 1, Hydrogen., National Institutes of Health (NIH), Pubchem (2024). <a href="https://pubchem.ncbi.nlm.nih.gov/element/Hydrogen#section=History">https://pubchem.ncbi.nlm.nih.gov/element/Hydrogen#section=History</a> (accessed October 10, 2024).
- [37] Royal Society of Chemistry, RSC Periodic Table-Hydrogen, Royal Society of Chemistry (2024). https://www.rsc.org/periodic-table/element/1/hydrogen (accessed October 10, 2024).
- [38] F. Ausfelder, A. Bazzanella, Hydrogen in the Chemical Industry, in: Hydrogen Science and Engineering: Materials, Processes, Systems and Technology, Wiley, 2016: pp. 19–40. https://doi.org/10.1002/9783527674268.ch02.
- [39] W. Liu, H. Zuo, J. Wang, Q. Xue, B. Ren, F. Yang, The production and application of hydrogen in steel industry, Int J Hydrogen Energy 46 (2021) 10548–10569. https://doi.org/10.1016/j.ijhydene.2020.12.123.
- [40] J.G. Speight, Hydrogen in Refineries, in: Hydrogen Science and Engineering: Materials, Processes, Systems and Technology, Wiley, 2016: pp. 1–18. https://doi.org/10.1002/9783527674268.ch01.
- [41] International Energy Agency (IEA), Global Hydrogen Review 2023, Paris, 2023 https://www.iea.org/reports/global-hydrogen-review-2023 (accessed October 10, 2024).
- [42] European Hydrogen Observatory, Hydrogen Demand, European Commission-Clean Hydrogen Partnership (2024). <a href="https://observatory.clean-hydrogen.europa.eu/hydrogen-landscape/end-use/hydrogen-demand">https://observatory.clean-hydrogen.europa.eu/hydrogen-landscape/end-use/hydrogen-demand</a> (accessed October 10, 2024).
- [43] International Energy Agency (IEA), Global Hydrogen Review 2024, Paris, 2024. https://www.iea.org/reports/global-hydrogen-review-2024 (accessed October 10, 2024).
- [44] W. Grochala, First there was hydrogen, Nat Chem 7 (2015) 264–264. https://doi.org/10.1038/nchem.2186.
- [45] W. Lubitz, W. Tumas, Hydrogen: An Overview, Chem Rev 107 (2007) 3900–3903. https://doi.org/10.1021/cr050200z.
- [46] L. Chen, Z. Qi, S. Zhang, J. Su, G.A. Somorjai, Catalytic hydrogen production from methane: A review on recent progress and prospect, Catalysts 10 (2020). https://doi.org/10.3390/catal10080858.

- [47] O.O. James, B. Chowdhury, M.A. Mesubi, S. Maity, Reflections on the chemistry of the Fischer–Tropsch synthesis, RSC Adv 2 (2012) 7347. <a href="https://doi.org/10.1039/c2ra20519j">https://doi.org/10.1039/c2ra20519j</a>.
- [48] G. Bozzano, F. Manenti, Efficient methanol synthesis: Perspectives, technologies and optimization strategies, Prog Energy Combust Sci 56 (2016) 71–105. <a href="https://doi.org/10.1016/j.pecs.2016.06.001">https://doi.org/10.1016/j.pecs.2016.06.001</a>.
- [49] Y. An, T. Lin, F. Yu, Y. Yang, L. Zhong, M. Wu, Y. Sun, Advances in direct production of value-added chemicals via syngas conversion, Sci China Chem 60 (2017) 887–903. https://doi.org/10.1007/s11426-016-0464-1.
- [50] S. Kasipandi, J.W. Bae, Recent Advances in Direct Synthesis of Value-Added Aromatic Chemicals from Syngas by Cascade Reactions over Bifunctional Catalysts, Advanced Materials 31 (2019). <a href="https://doi.org/10.1002/adma.201803390">https://doi.org/10.1002/adma.201803390</a>.
- [51] Grand View Research Inc, Syngas Market Size, Share & Trends Analysis Report By Production Technology (Steam Reforming, Partial Oxidation), By Feedstock (Natural Gas, Coal), By Gasifier Type, By Application, By Region, And Segment Forecasts, 2024 2030, 2024. <a href="https://www.grandviewresearch.com/industry-analysis/syngas-market-report#:~:text=The%20global%20syngas%20market%20demand,expected%20to%20drive%20market%20growth">https://www.grandviewresearch.com/industry-analysis/syngas-market-report#:~:text=The%20global%20syngas%20market%20demand,expected%20to%20drive%20market%20growth</a>. (accessed November 18, 2024).
- [52] Maximize Market Research PVT. LTD., Syngas Market: Global Industry Analysis and Forecast (2024-2030), 2024. <a href="https://www.maximizemarketresearch.com/market-report/global-syngas-market/68868/">https://www.maximizemarketresearch.com/market-report/global-syngas-market/68868/</a> (accessed November 18, 2024).
- [53] Emergen Research, Syngas Market Size, Share, Trends, By Production Technology (Steam Reforming, Partial Oxidation, Auto-Thermal Reforming, Two-step Reforming, and Biomass Gasification), Gasifier Type, Feedstock, Application, and By Region Forecast to 2030, 2022. <a href="https://www.emergenresearch.com/industry-report/syngas-market">https://www.emergenresearch.com/industry-report/syngas-market</a> (accessed November 18, 2024).
- [54] Mordor Intelligence, Europe Syngas Market Size & Share Analysis Growth Trends & Forecasts (2024 2029), 2024. <a href="https://www.mordorintelligence.com/industry-reports/europe-synthesis-gas-syngas-market-industry">https://www.mordorintelligence.com/industry-reports/europe-synthesis-gas-syngas-market-industry</a> (accessed November 18, 2024).
- [55] Z. Abdin, A. Zafaranloo, A. Rafiee, W. Mérida, W. Lipiński, K.R. Khalilpour, Hydrogen as an energy vector, Renewable and Sustainable Energy Reviews 120 (2020). https://doi.org/10.1016/j.rser.2019.109620.
- [56] T. Capurso, M. Stefanizzi, M. Torresi, S.M. Camporeale, Perspective of the role of hydrogen in the 21st century energy transition, Energy Convers Manag 251 (2022). https://doi.org/10.1016/j.enconman.2021.114898.
- [57] Q. Hassan, A.M. Abdulateef, S.A. Hafedh, A. Al-samari, J. Abdulateef, A.Z. Sameen, H.M. Salman, A.K. Al-Jiboory, S. Wieteska, M. Jaszczur, Renewable energy-to-green hydrogen: A review of main resources routes, processes and evaluation, Int J Hydrogen Energy 48 (2023) 17383–17408. https://doi.org/10.1016/j.ijhydene.2023.01.175.
- [58] United Nations (UN), UN Sustainable Development Goals, UN Department of Economic and Social Affairs (2015). <a href="https://sdgs.un.org/goals">https://sdgs.un.org/goals</a> (accessed October 11, 2024).
- [59] F.P. Martins, S. De-León Almaraz, A.B. Botelho Junior, C. Azzaro-Pantel, P. Parikh, Hydrogen and the sustainable development goals: Synergies and trade-offs, Renewable and Sustainable Energy Reviews 204 (2024) 114796. <a href="https://doi.org/10.1016/j.rser.2024.114796">https://doi.org/10.1016/j.rser.2024.114796</a>.
- [60] M.G. Rasul, M.A. Hazrat, M.A. Sattar, M.I. Jahirul, M.J. Shearer, The future of hydrogen: Challenges on production, storage and applications, Energy Convers Manag 272 (2022). https://doi.org/10.1016/j.enconman.2022.116326.
- [61] N. Mahinpey, A. Farooqui, A. Abdalla, K. Asghari, Power generation from syngas, in: Advances in Synthesis Gas: Methods, Technologies and Applications, Elsevier, 2023: pp. 289–319. https://doi.org/10.1016/B978-0-323-91878-7.00001-0.
- [62] N. Mac Dowell, N. Sunny, N. Brandon, H. Herzog, A.Y. Ku, W. Maas, A. Ramirez, D.M. Reiner, G.N. Sant, N. Shah, The hydrogen economy: A pragmatic path forward, Joule 5 (2021) 2524–2523. https://doi.org/10.1016/j.joule.2021.09.014.

- [63] J.M.M. Arcos, D.M.F. Santos, The Hydrogen Color Spectrum: Techno-Economic Analysis of the Available Technologies for Hydrogen Production, Gases 3 (2023) 25–46. https://doi.org/10.3390/gases3010002.
- [64] R. Moradi, K.M. Groth, Hydrogen storage and delivery: Review of the state of the art technologies and risk and reliability analysis, Int J Hydrogen Energy 44 (2019) 12254–12269. https://doi.org/10.1016/j.ijhydene.2019.03.041.
- [65] M.D. Allendorf, V. Stavila, J.L. Snider, M. Witman, M.E. Bowden, K. Brooks, B.L. Tran, T. Autrey, Challenges to developing materials for the transport and storage of hydrogen, Nat Chem 14 (2022) 1214–1223. https://doi.org/10.1038/s41557-022-01056-2.
- [66] M. Yang, R. Hunger, S. Berrettoni, B. Sprecher, B. Wang, A review of hydrogen storage and transport technologies, Clean Energy 7 (2023) 190–216. <a href="https://doi.org/10.1093/ce/zkad021">https://doi.org/10.1093/ce/zkad021</a>.
- [67] M.S. Ali, M.S. Hossain Khan, R.A. Tuhin, M.A. Kabir, A.K. Azad, O. Farrok, Hydrogen energy storage and transportation challenges, in: Hydrogen Energy Conversion and Management, Elsevier, 2024: pp. 255–287. https://doi.org/10.1016/B978-0-443-15329-7.00001-6.
- [68] I. Théry, J. Gril, J.L. Vernet, L. Meignen, J. Maury, Coal used for Fuel at Two Prehistoric Sites in Southern France: Les Canalettes (Mousterian) and Les Usclades (Mesolithic), J Archaeol Sci 23 (1996) 509–512. https://doi.org/10.1006/jasc.1996.0048.
- [69] M. Qiu, R. Liu, X. Li, L. Du, Q. Ruan, A.M. Pollard, S. Zhang, X. Yuan, F. Liu, G. Li, G. Li, Z. Jiao, J. Luo, S. Chen, X. Yang, Y. Wang, J. Han, F. Chen, G. Dong, Earliest systematic coal exploitation for fuel extended to ~3600 B.P., Sci Adv 9 (2023). https://doi.org/10.1126/sciadv.adh0549.
- [70] E.A. Wrigley, Energy and the English Industrial Revolution, Philosophical Transactions of the Royal Society A: Mathematical, Physical and Engineering Sciences 371 (2013) 20110568. https://doi.org/10.1098/rsta.2011.0568.
- [71] A. Fernihough, K.H. O'Rourke, Coal and the European Industrial Revolution, The Economic Journal 131 (2021) 1135–1149. https://doi.org/10.1093/ej/ueaa117.
- [72] R.U. Ayres, Petroleum and Petrochemicals, in: The History and Future of Technology, Springer International Publishing, Cham, 2021: pp. 199–221. <a href="https://doi.org/10.1007/978-3-030-71393-5\_10">https://doi.org/10.1007/978-3-030-71393-5\_10</a>.
- [73] P.G. Levi, J.M. Cullen, Mapping Global Flows of Chemicals: From Fossil Fuel Feedstocks to Chemical Products, Environ Sci Technol 52 (208) 1725–1734. https://doi.org/10.1021/acs.est.7b04573.
- [74] J. Incer-Valverde, A. Korayem, G. Tsatsaronis, T. Morosuk, "Colors" of hydrogen: Definitions and carbon intensity, Energy Convers Manag 291 (2023). https://doi.org/10.1016/j.enconman.2023.117294.
- [75] IRENA, Hydrogen (IRENA), International Renewable Energy Agency (2023). <a href="https://www.irena.org/Energy-Transition/Technology/Hydrogen#:~:text=As%20at%20the%20end%20of,around%204%25%20comes%20from%20electrolysis">https://www.irena.org/Energy-Transition/Technology/Hydrogen#:~:text=As%20at%20the%20end%20of,around%204%25%20comes%20from%20electrolysis</a> (accessed August 24, 2023).
- [76] J. Rostrup-Nielsen, Steam reforming of hydrocarbons. A historical perspective, in: X. Bao, Y. Xu (Eds.), Stud Surf Sci Catal, Elsevier, 2004: pp. 121–126. <a href="https://doi.org/10.1016/S0167-2991(04)80038-7">https://doi.org/10.1016/S0167-2991(04)80038-7</a>.
- [77] E. Monteiro, P.S.D. Brito, Hydrogen supply chain: Current status and prospects, Energy Storage (2023). <a href="https://doi.org/10.1002/est2.466">https://doi.org/10.1002/est2.466</a>.
- [78] L. Kaiwen, Y. Bin, Z. Tao, Economic analysis of hydrogen production from steam reforming process: A literature review, Energy Sources, Part B: Economics, Planning and Policy 13 (2018) 109–115. https://doi.org/10.1080/15567249.2017.1387619.
- [79] J. Sehested, Sintering of nickel steam-reforming catalysts, J Catal 217 (2003) 417–426. https://doi.org/10.1016/S0021-9517(03)00075-7.
- [80] J. Sehested, Four challenges for nickel steam-reforming catalysts, Catal Today 111 (2006) 103–110. https://doi.org/10.1016/j.cattod.2005.10.002.
- [81] E. Meloni, M. Martino, V. Palma, A short review on Ni based catalysts and related engineering issues for methane steam reforming, Catalysts 10 (2020). https://doi.org/10.3390/catal10030352.

- [82] K. Großmann, P. Treiber, J. Karl, Steam methane reforming at low S/C ratios for power-to-gas applications, Int J Hydrogen Energy 41 (2016) 17784–17792. https://doi.org/10.1016/j.ijhydene.2016.08.007.
- [83] A.A. AL-Dhfeery, A.A. Jassem, Modeling and simulation of an industrial secondary reformer reactor in the fertilizer plants, International Journal of Industrial Chemistry 3 (2012) 1–8. https://doi.org/10.1186/2228-5547-3-14.
- [84] E. Baraj, K. Ciahotný, T. Hlinčík, The water gas shift reaction: Catalysts and reaction mechanism, Fuel 288 (2021) 119817. <a href="https://doi.org/10.1016/j.fuel.2020.119817">https://doi.org/10.1016/j.fuel.2020.119817</a>.
- [85] D.K.S. Ng, K.S. Ng, R.T.L. Ng, Integrated Biorefineries, in: Encyclopedia of Sustainable Technologies, Elsevier, 2017: pp. 299–314. <a href="https://doi.org/10.1016/B978-0-12-409548-9.10138-1">https://doi.org/10.1016/B978-0-12-409548-9.10138-1</a>.
- [86] A. Ozbilen, I. Dincer, M.A. Rosen, Comparative environmental impact and efficiency assessment of selected hydrogen production methods, Environ Impact Assess Rev 42 (2013) 1–9. https://doi.org/10.1016/j.eiar.2013.03.003.
- [87] Z. Xiao, C. Zhang, S. Huang, S. Zhang, X. Tan, Z. Lian, J.J. Zou, X. Zhang, G. Li, D. Wang, A comprehensive review on steam reforming of liquid hydrocarbon fuels: Research advances and Prospects, Fuel 368 (2024). https://doi.org/10.1016/j.fuel.2024.131596.
- [88] A.P.E. York, T. Xiao, M.L.H. Green, Brief overview of the partial oxidation of methane to synthesis gas, Top Catal 22 (2003) 345–358. <a href="https://doi.org/10.1023/A:1023552709642">https://doi.org/10.1023/A:1023552709642</a>.
- [89] Y. Lu, T. Lee, Influence of the Feed Gas Composition on the Fischer-Tropsch Synthesis in Commercial Operations, Journal of Natural Gas Chemistry 16 (2007) 329–341. https://doi.org/10.1016/S1003-9953(08)60001-8.
- [90] I.A. Makaryan, E.A. Salgansky, V.S. Arutyunov, I. V. Sedov, Non-Catalytic Partial Oxidation of Hydrocarbon Gases to Syngas and Hydrogen: A Systematic Review, Energies (Basel) 16 (2023). https://doi.org/10.3390/en16062916.
- [91] C.M. Kalamaras, A.M. Efstathiou, Hydrogen Production Technologies: Current State and Future Developments, Conference Papers in Energy 2013 (2013) 1–9. https://doi.org/10.1155/2013/690627.
- [92] D. Li, R. Xu, Z. Gu, X. Zhu, S. Qing, K. Li, Chemical-Looping Conversion of Methane: A Review, Energy Technology 8 (2020). <a href="https://doi.org/10.1002/ente.201900925">https://doi.org/10.1002/ente.201900925</a>.
- [93] V. LaParola, G. Pantaleo, A. Venezia, Effect of active and inert oxide on catalytic partial oxidation (CPO) of methane over supported Ni catalysts, Inorganica Chim Acta 531 (2022) 120710. <a href="https://doi.org/10.1016/j.ica.2021.120710">https://doi.org/10.1016/j.ica.2021.120710</a>.
- [94] A.P.E. York, T. Xiao, M.L.H. Green, Brief Overview of the Partial Oxidation of Methane to Synthesis Gas, Top Catal 22 (2003) 345–358. <a href="https://doi.org/10.1023/A:1023552709642">https://doi.org/10.1023/A:1023552709642</a>.
- [95] C. Bauer, K. Treyer, C. Antonini, J. Bergerson, M. Gazzani, E. Gencer, J. Gibbins, M. Mazzotti, S.T. McCoy, R. McKenna, R. Pietzcker, A.P. Ravikumar, M.C. Romano, F. Ueckerdt, J. Vente, M. van der Spek, On the climate impacts of blue hydrogen production, Sustain Energy Fuels 6 (2022) 66–75. https://doi.org/10.1039/D1SE01508G.
- [96] A.I. Osman, Catalytic Hydrogen Production from Methane **Partial** Oxidation: Chem Mechanism and Kinetic Study, Eng Technol 43 (2020)641–648. https://doi.org/10.1002/ceat.201900339.
- [97] Y. Gao, J. Jiang, Y. Meng, F. Yan, A. Aihemaiti, A review of recent developments in hydrogen production via biogas dry reforming, Energy Convers Manag 171 (2018) 133–155. https://doi.org/10.1016/j.enconman.2018.05.083.
- [98] Z. Fan, W. Weng, J. Zhou, D. Gu, W. Xiao, Catalytic decomposition of methane to produce hydrogen: A review, Journal of Energy Chemistry 58 (2021) 415–430. https://doi.org/10.1016/j.jechem.2020.10.049.
- [99] M.M. Barroso Quiroga, A.E. Castro Luna, Kinetic Analysis of Rate Data for Dry Reforming of Methane, Ind Eng Chem Res 46 (2007) 5265–5270. https://doi.org/10.1021/ie061645w.
- [100] A. Abdulrasheed, A.A. Jalil, Y. Gambo, M. Ibrahim, H.U. Hambali, M.Y. Shahul Hamid, A review on catalyst development for dry reforming of methane to syngas: Recent advances, Renewable and Sustainable Energy Reviews 108 (2019) 175–193. https://doi.org/10.1016/j.rser.2019.03.054.

- [101] P.A. Argyris, A. Wright, O. Taheri Qazvini, V. Spallina, Dynamic behaviour of integrated chemical looping process with pressure swing adsorption in small scale on-site H<sub>2</sub> and pure CO<sub>2</sub> production, Chemical Engineering Journal 428 (2022). https://doi.org/10.1016/j.cej.2021.132606.
- [102] Y.T. Shah, T.H. Gardner, Dry Reforming of Hydrocarbon Feedstocks, Catalysis Reviews 56 (2014) 476–536. <a href="https://doi.org/10.1080/01614940.2014.946848">https://doi.org/10.1080/01614940.2014.946848</a>.
- [103] P. Gangadharan, K.C. Kanchi, H.H. Lou, Evaluation of the economic and environmental impact of combining dry reforming with steam reforming of methane, Chemical Engineering Research and Design 90 (2012) 1956–1968. <a href="https://doi.org/10.1016/j.cherd.2012.04.008">https://doi.org/10.1016/j.cherd.2012.04.008</a>.
- [104] D.P. Minh, T.J. Siang, D.V.N. Vo, T.S. Phan, C. Ridart, A. Nzihou, D. Grouset, Hydrogen production from biogas reforming: An overview of steam reforming, dry reforming, dual reforming, and trireforming of methane, in: Hydrogen Supply Chain: Design, Deployment and Operation, Elsevier, 2018: pp. 111–166. https://doi.org/10.1016/B978-0-12-811197-0.00004-X.
- [105] W. Li, Z. Zhao, F. Ding, X. Guo, G. Wang, Syngas Production via Steam–CO<sub>2</sub> Dual Reforming of Methane over La-Ni/ZrO<sub>2</sub> Catalyst Prepared by L-Arginine Ligand-Assisted Strategy: Enhanced Activity and Stability, ACS Sustain Chem Eng 3 (2015) 3461–3476. <a href="https://doi.org/10.1021/acssuschemeng.5b01277">https://doi.org/10.1021/acssuschemeng.5b01277</a>.
- [106] H. Al-Megeren, T. Xiao, Natural Gas Dual Reforming Catalyst and Process, in: Advances in Natural Gas Technology, InTech, 2012. <a href="https://doi.org/10.5772/36790">https://doi.org/10.5772/36790</a>.
- [107] R. Chava, H. Mehta, B. Roy, S. Appari, Dual reforming of model biogas for syngas production on Ni/γ-Al<sub>2</sub>O<sub>3</sub> and Ni-C/ZSM-5 cordierite monolith catalysts, Mater Today Proc 76 (2023) 393–397. https://doi.org/10.1016/j.matpr.2022.11.468.
- [108] M. Ji, J. Wang, Review and comparison of various hydrogen production methods based on costs and life cycle impact assessment indicators, Int J Hydrogen Energy 46 (2021) 38612–38635. https://doi.org/10.1016/j.ijhydene.2021.09.142.
- [109] M. Zahedi nezhad, S. Rowwshanzamir, M.H. Eikani, Autothermal reforming of methane to synthesis gas: Modeling and simulation, Int J Hydrogen Energy 34 (2009) 1292–1300. https://doi.org/10.1016/j.ijhydene.2008.11.091.
- [110] Y. Patcharavorachot, M. Wasuleewan, S. Assabumrungrat, A. Arpornwichanop, Analysis of hydrogen production from methane autothermal reformer with a dual catalyst-bed configuration, Theoretical Foundations of Chemical Engineering 46 (2012) 658–665. https://doi.org/10.1134/S0040579512060188.
- [111] S. Assabumrungrat, N. Laosiripojana, FUELS HYDROGEN PRODUCTION | Autothermal Reforming, in: Encyclopedia of Electrochemical Power Sources, Elsevier, 2009: pp. 238–248. https://doi.org/10.1016/B978-044452745-5.00296-3.
- [112] P. Wachter, P. Hödl, J. Raic, C. Gaber, M. Demuth, C. Hochenauer, Towards thermochemical recuperation applying combined steam reforming and partial oxidation of methane: Thermodynamic and experimental considerations, Energy Convers Manag 251 (2022) 114927. <a href="https://doi.org/10.1016/j.enconman.2021.114927">https://doi.org/10.1016/j.enconman.2021.114927</a>.
- [113] M.H.S. Cavalcante, Í.A. Maccari Zelioli, E.É.X. Guimarães Filho, J.M. dos S. Júnior, A.D. Souza Vidotti, A.C. Daltro de Freitas, R. Guirardello, Autothermal Reforming of Methane: A Thermodynamic Study on the Use of Air and Pure Oxygen as Oxidizing Agents in Isothermal and Adiabatic Systems, Methane 2 (2023) 389–403. https://doi.org/10.3390/methane2040026.
- [114] D. Scognamiglio, L. Russo, P.L. Maffettone, L. Salemme, M. Simeone, S. Crescitelli, Modeling Temperature Profiles of a Catalytic Autothermal Methane Reformer with Nickel Catalyst, Ind Eng Chem Res 48 (2009) 1804–1815. <a href="https://doi.org/10.1021/ie800518e">https://doi.org/10.1021/ie800518e</a>.
- [115] M.L. Rodríguez, M.N. Pedernera, D.O. Borio, Oxygen feeding strategies for methane ATR, Int J Hydrogen Energy 47 (2022) 11417–11427. https://doi.org/10.1016/j.ijhydene.2021.12.252.
- [116] E. Necoechea, J. Needels, C. Agba, P. Erickson, Effects of catalyst separation in stratified-bed autothermal reforming of methanol, Int J Hydrogen Energy 46 (2021) 34175–34183. https://doi.org/10.1016/j.ijhydene.2021.08.018.

- [117] A.W.A. Al-Fatlawi, M.A.R. Sadiq Al-Baghdadi, M. Al-Waily, Thermal stress analysis of a reactor used to produce hydrogen from hydrocarbon fuel, Int J Hydrogen Energy 50 (2024) 605–613. https://doi.org/10.1016/j.ijhydene.2023.10.079.
- [118] R. Pinsky, P. Sabharwall, J. Hartvigsen, J. O'Brien, Comparative review of hydrogen production technologies for nuclear hybrid energy systems, Progress in Nuclear Energy 123 (2020) 103317. https://doi.org/10.1016/j.pnucene.2020.103317.
- [119] R.D. Alli, P.A.L. de Souza, M. Mohamedali, L.D. Virla, N. Mahinpey, Tri-reforming of methane for syngas production using Ni catalysts: Current status and future outlook, Catal Today 407 (2023) 107–124. https://doi.org/10.1016/j.cattod.2022.02.006.
- [120] A.J. Majewski, J. Wood, Tri-reforming of methane over Ni@SiO<sub>2</sub> catalyst, Int J Hydrogen Energy 39 (2014) 12578–12585. https://doi.org/10.1016/j.ijhydene.2014.06.071.
- [121] S. Soleimani, M. Lehner, Tri-Reforming of Methane: Thermodynamics, Operating Conditions, Reactor Technology and Efficiency Evaluation—A Review, Energies (Basel) 15 (2022). https://doi.org/10.3390/en15197159.
- [122] X.H. Pham, U.P.M. Ashik, J.I. Hayashi, A. Pérez Alonso, D. Pla, M. Gómez, D. Pham Minh, Review on the catalytic tri-reforming of methane Part II: Catalyst development, Appl Catal A Gen 623 (2021). <a href="https://doi.org/10.1016/j.apcata.2021.118286">https://doi.org/10.1016/j.apcata.2021.118286</a>.
- [123] D. Pham Minh, X.H. Pham, T.J. Siang, D.V. N. Vo, Review on the catalytic tri-reforming of methane Part I: Impact of operating conditions, catalyst deactivation and regeneration, Appl Catal A Gen 621 (2021). <a href="https://doi.org/10.1016/j.apcata.2021.118202">https://doi.org/10.1016/j.apcata.2021.118202</a>.
- [124] C. Song, W. Pan, Tri-reforming of methane: A novel concept for catalytic production of industrially useful synthesis gas with desired H<sub>2</sub>/CO ratios, in: Catal Today, 2004: pp. 463–484. https://doi.org/10.1016/j.cattod.2004.09.054.
- [125] R.W. Breault, Gasification processes old and new: A basic review of the major technologies, Energies (Basel) 3 (2010) 216–240. <a href="https://doi.org/10.3390/en3020216">https://doi.org/10.3390/en3020216</a>.
- [126] J.M. Sánchez-Hervás, G.M. Moya, I. Ortiz-González, Current status of coal gasification, in: New Trends in Coal Conversion, Elsevier, 2019: pp. 175–202. <a href="https://doi.org/10.1016/B978-0-08-102201-6.00007-8">https://doi.org/10.1016/B978-0-08-102201-6.00007-8</a>.
- [127] N. Crnomarkovic, B. Repic, R. Mladenovic, O. Neskovic, M. Veljkovic, Experimental investigation of role of steam in entrained flow coal gasification, Fuel 86 (2007) 194–202. <a href="https://doi.org/10.1016/j.fuel.2006.06.015">https://doi.org/10.1016/j.fuel.2006.06.015</a>.
- [128] M. Carmo, A. Coralli, D. Das, P.E. V. de Miranda, S.P. de Oliveira, M.R. Harada, D. Hart, L. Osmieri, N.Q. Minh, N.P. Neves Jr., B. Sampson, B.J.M. Sarruf, V. Singh, S. Specchia, R. Steinberger-Wilckens, D. Stolten, A. V. Tchouvelev, H. Uchida, Application of Hydrogen Combustion for Electrical and Motive Power Generation, in: P.E. V. de Miranda (Ed.), Science and Engineering of Hydrogen-Based Energy Technologies, Elsevier, 2019: pp. 259–278. <a href="https://doi.org/10.1016/B978-0-12-814251-6.00005-8">https://doi.org/10.1016/B978-0-12-814251-6.00005-8</a>.
- [129] C. Lan, Q. Lyu, Y. Qie, M. Jiang, X. Liu, S. Zhang, Thermodynamic and kinetic behaviors of coal gasification, Thermochim Acta 666 (2018) 174–180. <a href="https://doi.org/10.1016/j.tca.2018.06.019">https://doi.org/10.1016/j.tca.2018.06.019</a>.
- [130] R. Hotchkiss, Coal gasification technologies, Proceedings of the Institution of Mechanical Engineers, Part A: Journal of Power and Energy 217 (2003) 27–33. https://doi.org/10.1243/095765003321148664.
- [131] F. Dai, S. Zhang, Y. Luo, K. Wang, Y. Liu, X. Ji, Recent Progress on Hydrogen-Rich Syngas Production from Coal Gasification, Processes 11 (2023). <a href="https://doi.org/10.3390/pr11061765">https://doi.org/10.3390/pr11061765</a>.
- [132] F. Emun, M. Gadalla, T. Majozi, D. Boer, Integrated gasification combined cycle (IGCC) process simulation and optimization, Comput Chem Eng 34 (2010) 331–338. <a href="https://doi.org/10.1016/j.compchemeng.2009.04.007">https://doi.org/10.1016/j.compchemeng.2009.04.007</a>.
- [133] K.S. Weil, Coal gasification and IGCC technology: A brief primer, Proceedings of Institution of Civil Engineers: Energy 163 (2010) 7–16. https://doi.org/10.1680/ener.2010.163.1.7.

- [134] R. Kothari, D. Buddhi, R.L. Sawhney, Comparison of environmental and economic aspects of various hydrogen production methods, Renewable and Sustainable Energy Reviews 12 (2008) 553–563. https://doi.org/10.1016/j.rser.2006.07.012.
- [135] I. Dincer, C. Acar, Review and evaluation of hydrogen production methods for better sustainability, Alternative Energy and Ecology (ISJAEE) (2016) 14–36. <a href="https://doi.org/10.15518/isjaee.2016.11-12.014-036">https://doi.org/10.15518/isjaee.2016.11-12.014-036</a>.
- [136] C. Higman, S. Tam, Advances in coal gasification, hydrogenation, and gas treating for the production of chemicals and fuels, Chem Rev 114 (2014) 1673–1708. <a href="https://doi.org/10.1021/cr400202m">https://doi.org/10.1021/cr400202m</a>.
- [137] A. Midilli, H. Kucuk, M.E. Topal, U. Akbulut, I. Dincer, A comprehensive review on hydrogen production from coal gasification: Challenges and Opportunities, Int J Hydrogen Energy 46 (2021) 25385–25412. <a href="https://doi.org/10.1016/j.ijhydene.2021.05.088">https://doi.org/10.1016/j.ijhydene.2021.05.088</a>.
- [138] Q. Ji, S. Tabassum, S. Hena, C.G. Silva, G. Yu, Z. Zhang, A review on the coal gasification wastewater treatment technologies: past, present and future outlook, J Clean Prod 126 (2016) 38–55. https://doi.org/10.1016/j.jclepro.2016.02.147.
- [139] S.J. Yoon, J. Goo Lee, Syngas Production from Coal through Microwave Plasma Gasification: Influence of Oxygen, Steam, and Coal Particle Size, Energy & Fuels 26 (2012) 524–529. https://doi.org/10.1021/ef2013584.
- [140] Z. Chen, L. Gao, W. Han, L. Zhang, Energy and exergy analyses of coal gasification with supercritical water and O<sub>2</sub>-H<sub>2</sub>O, Appl Therm Eng 148 (2019) 57–63. https://doi.org/10.1016/j.applthermaleng.2018.10.050.
- [141] S. Lavis, M. Mostade, Underground coal gasification, in: The Coal Handbook, Elsevier, 2023: pp. 323–337. <a href="https://doi.org/10.1016/B978-0-12-824328-2.00010-8">https://doi.org/10.1016/B978-0-12-824328-2.00010-8</a>.
- [142] L. Jiang, D. Xue, Z. Wei, Z. Chen, M. Mirzayev, Y. Chen, S. Chen, Coal decarbonization: A state-of-the-art review of enhanced hydrogen production in underground coal gasification, Energy Reviews 1 (2022). https://doi.org/10.1016/j.enrev.2022.100004.
- [143] M. Green, Recent developments and current position of underground coal gasification, Proceedings of the Institution of Mechanical Engineers, Part A: Journal of Power and Energy 232 (2018) 39–46. https://doi.org/10.1177/0957650917718772.
- [144] K. Kostúr, M. Laciak, M. Durdan, Some influences of Underground Coal Gasification on the environment, Sustainability (Switzerland) 10 (2018). https://doi.org/10.3390/su10051512.
- [145] Y. Sun, G. Wang, Y. Wang, N. Zhang, Z. Zhu, Managing Innovation: Accelerating the Development of Clean Coal Technology, Frontiers of Engineering Management 2 (2015) 86. <a href="https://doi.org/10.15302/J-FEM-2015013">https://doi.org/10.15302/J-FEM-2015013</a>.
- [146] A.G. Olabi, A. saleh bahri, A.A. Abdelghafar, A. Baroutaji, E.T. Sayed, A.H. Alami, H. Rezk, M.A. Abdelkareem, Large-vscale hydrogen production and storage technologies: Current status and future directions, Int J Hydrogen Energy 46 (2021) 23498–23528. <a href="https://doi.org/10.1016/j.ijhydene.2020.10.110">https://doi.org/10.1016/j.ijhydene.2020.10.110</a>.
- [147] S. Roussanaly, R. Anantharaman, C. Fu, Low-carbon footprint hydrogen production from natural gas: A techno-economic analysis of carbon capture and storage from steam-methane reforming, Chem Eng Trans 81 (2020) 1015–1020. https://doi.org/10.3303/CET2081170.
- [148] N.S. Alhajeri, M. Dannoun, A. Alrashed, A.Z. Aly, Environmental and economic impacts of increased utilization of natural gas in the electric power generation sector: Evaluating the benefits and trade-offs of fuel switching, J Nat Gas Sci Eng 71 (2019) 102969. <a href="https://doi.org/10.1016/j.jngse.2019.102969">https://doi.org/10.1016/j.jngse.2019.102969</a>.
- [149] W.W. Tso, C.D. Demirhan, C.A. Floudas, E.N. Pistikopoulos, Multi-scale energy systems engineering for optimal natural gas utilization, Catal Today 356 (2020) 18–26. https://doi.org/10.1016/j.cattod.2019.09.009.
- [150] B. Dziejarski, R. Krzyżyńska, K. Andersson, Current status of carbon capture, utilization, and storage technologies in the global economy: A survey of technical assessment, Fuel 342 (2023) 127776. https://doi.org/10.1016/j.fuel.2023.127776.

- [151] F.S. AlHumaidan, M. Absi Halabi, M.S. Rana, M. Vinoba, Blue hydrogen: Current status and future technologies, Energy Convers Manag 283 (2023) 116840. https://doi.org/10.1016/j.enconman.2023.116840.
- [152] J. Rosenow, R. Lowes, Will blue hydrogen lock us into fossil fuels forever?, One Earth 4 (2021) 1527–1529. https://doi.org/10.1016/j.oneear.2021.10.018.
- [153] A.O. Oni, K. Anaya, T. Giwa, G. Di Lullo, A. Kumar, Comparative assessment of blue hydrogen from steam methane reforming, autothermal reforming, and natural gas decomposition technologies for natural gas-producing regions, Energy Convers Manag 254 (2022) 115245. <a href="https://doi.org/10.1016/j.enconman.2022.115245">https://doi.org/10.1016/j.enconman.2022.115245</a>.
- [154] J. Pettersen, R. Steeneveldt, D. Grainger, T. Scott, L. Holst, E.S. Hamborg, Blue hydrogen must be done properly, Energy Sci Eng 10 (2022) 3220–3236. https://doi.org/10.1002/ese3.1232.
- [155] D.A. Tetteh, S. Salehi, The Blue Hydrogen Economy: A Promising Option for the Near-to-Mid-Term Energy Transition, J Energy Resour Technol 145 (2023). <a href="https://doi.org/10.1115/1.4055205">https://doi.org/10.1115/1.4055205</a>.
- [156] M. Noussan, P.P. Raimondi, R. Scita, M. Hafner, The Role of Green and Blue Hydrogen in the Energy Transition—A Technological and Geopolitical Perspective, Sustainability 13 (2020) 298. <a href="https://doi.org/10.3390/su13010298">https://doi.org/10.3390/su13010298</a>.
- [157] R.W. Howarth, M.Z. Jacobson, How green is blue hydrogen?, Energy Sci Eng 9 (2021) 1676–1687. https://doi.org/10.1002/ese3.956.
- [158] D. Schlissel, A. Juhn, Blue Hydrogen: Not Clean, Not Low Carbon, Not a Solution, Lakewood, 2023. <a href="https://ieefa.org/resources/blue-hydrogen-not-clean-not-low-carbon-not-solution">https://ieefa.org/resources/blue-hydrogen-not-clean-not-low-carbon-not-solution</a> (accessed October 22, 2024).
- [159] J. Incer-Valverde, A. Korayem, G. Tsatsaronis, T. Morosuk, "Colors" of hydrogen: Definitions and carbon intensity, Energy Convers Manag 291 (2023) 117294. https://doi.org/10.1016/j.enconman.2023.117294.
- [160] H.F. Abbas, W.M.A. Wan Daud, Hydrogen production by methane decomposition: A review, Int J Hydrogen Energy 35 (2010) 1160–1190. https://doi.org/10.1016/j.ijhydene.2009.11.036.
- [161] A.M. De Groote, G.F. Froment, The role of coke formation in catalytic partial oxidation for synthesis gas production, Catal Today 37 (1997) 309–329. <a href="https://doi.org/10.1016/S0920-5861(97)00013-8">https://doi.org/10.1016/S0920-5861(97)00013-8</a>.
- [162] O. Muraza, A. Galadima, A review on coke management during dry reforming of methane, Int J Energy Res 39 (2015) 1196–1216. https://doi.org/10.1002/er.3295.
- [163] Z. Shakor, A. Alasseel, E. Al-Shafei, The structure of deposited coke on hydrocracking and reforming catalysts: Coke deactivation and kinetics, Can J Chem Eng 102 (2024) 2876–2891. https://doi.org/10.1002/cjce.25222.
- [164] J. Diab, L. Fulcheri, V. Hessel, V. Rohani, M. Frenklach, Why turquoise hydrogen will Be a game changer for the energy transition, Int J Hydrogen Energy 47 (2022) 25831–25848. <a href="https://doi.org/10.1016/j.ijhydene.2022.05.299">https://doi.org/10.1016/j.ijhydene.2022.05.299</a>.
- [165] T.I. Korányi, M. Németh, A. Beck, A. Horváth, Recent Advances in Methane Pyrolysis: Turquoise Hydrogen with Solid Carbon Production, Energies (Basel) 15 (2022). https://doi.org/10.3390/en15176342.
- [166] A.M. Amin, E. Croiset, W. Epling, Review of methane catalytic cracking for hydrogen production, Int J Hydrogen Energy 36 (2011) 2904–2935. <a href="https://doi.org/10.1016/j.ijhydene.2010.11.035">https://doi.org/10.1016/j.ijhydene.2010.11.035</a>.
- [167] C.Q. Pham, T.J. Siang, P.S. Kumar, Z. Ahmad, L. Xiao, M.B. Bahari, A.N.T. Cao, N. Rajamohan, A.S. Qazaq, A. Kumar, P.L. Show, D.V.N. Vo, Production of hydrogen and value-added carbon materials by catalytic methane decomposition: a review, Environ Chem Lett 20 (2022) 2339–2359. <a href="https://doi.org/10.1007/s10311-022-01449-2">https://doi.org/10.1007/s10311-022-01449-2</a>.
- [168] S. Schneider, S. Bajohr, F. Graf, T. Kolb, State of the Art of Hydrogen Production via Pyrolysis of Natural Gas, ChemBioEng Reviews 7 (2020) 150–158. <a href="https://doi.org/10.1002/cben.202000014">https://doi.org/10.1002/cben.202000014</a>.
- [169] M. Kheirollahivash, F. Rashidi, M.M. Moshrefi, Experimental study and kinetic modeling of methane decomposition in a rotating arc plasma reactor with different cross-sectional areas, Int J Hydrogen Energy 44 (2019) 17460–17469. https://doi.org/10.1016/j.ijhydene.2019.05.011.

- [170] R.B. Raja, R. Sarathi, R. Vinu, Selective Production of Hydrogen and Solid Carbon via Methane Pyrolysis Using a Swirl-Induced Point–Plane Non-thermal Plasma Reactor, Energy and Fuels 36 (2022) 826–836. https://doi.org/10.1021/acs.energyfuels.1c03383.
- [171] M.R. Rahimpour, A. Jahanmiri, M. Mohamadzadeh Shirazi, N. Hooshmand, H. Taghvaei, Combination of non-thermal plasma and heterogeneous catalysis for methane and hexadecane co-cracking: Effect of voltage and catalyst configuration, Chemical Engineering Journal 219 (2013) 245–253. https://doi.org/10.1016/j.cej.2013.01.011.
- [172] M. Wnukowski, Methane Pyrolysis with the Use of Plasma: Review of Plasma Reactors and Process Products, Energies (Basel) 16 (2023). <a href="https://doi.org/10.3390/en16186441">https://doi.org/10.3390/en16186441</a>.
- [173] A. Mašláni, M. Hrabovský, P. Křenek, M. Hlína, S. Raman, V.S. Sikarwar, M. Jeremiáš, Pyrolysis of methane via thermal steam plasma for the production of hydrogen and carbon black, Int J Hydrogen Energy 46 (2021) 1605–1614. https://doi.org/10.1016/j.ijhydene.2020.10.105.
- [174] V. Maslova, R. Nastase, G. Veryasov, N. Nesterenko, E. Fourré, C. Batiot-Dupeyrat, Current status and challenges of plasma and plasma-catalysis for methane coupling: A review, Prog Energy Combust Sci 101 (2024). https://doi.org/10.1016/j.pecs.2023.101096.
- [175] F. Kerscher, A. Stary, S. Gleis, A. Ulrich, H. Klein, H. Spliethoff, Low-carbon hydrogen production via electron beam plasma methane pyrolysis: Techno-economic analysis and carbon footprint assessment, Int J Hydrogen Energy 46 (2021) 19897–19912. https://doi.org/10.1016/j.ijhydene.2021.03.114.
- [176] X. Zhao, B. Joseph, J. Kuhn, S. Ozcan, Biogas Reforming to Syngas: A Review, IScience 23 (2020) 101082. <a href="https://doi.org/10.1016/j.isci.2020.101082">https://doi.org/10.1016/j.isci.2020.101082</a>.
- [177] D.B. Pal, A. Singh, A. Bhatnagar, A review on biomass based hydrogen production technologies, Int J Hydrogen Energy 47 (2022) 1461–1480. <a href="https://doi.org/10.1016/j.ijhydene.2021.10.124">https://doi.org/10.1016/j.ijhydene.2021.10.124</a>.
- [178] V. Singh Yadav, V. R, D. Yadav, Bio-hydrogen production from waste materials: A review, MATEC Web of Conferences 192 (2018) 02020. <a href="https://doi.org/10.1051/matecconf/201819202020">https://doi.org/10.1051/matecconf/201819202020</a>.
- [179] V.G. Nguyen, T.X. Nguyen-Thi, P.Q. Phong Nguyen, V.D. Tran, Ü. Ağbulut, L.H. Nguyen, D. Balasubramanian, W. Tarelko, S. A. Bandh, N.D. Khoa Pham, Recent advances in hydrogen production from biomass waste with a focus on pyrolysis and gasification, Int J Hydrogen Energy 54 (2024) 127–160. <a href="https://doi.org/10.1016/j.ijhydene.2023.05.049">https://doi.org/10.1016/j.ijhydene.2023.05.049</a>.
- [180] K.L. Kenney, W.A. Smith, G.L. Gresham, T.L. Westover, Understanding biomass feedstock variability, Biofuels 4 (2013) 111–127. <a href="https://doi.org/10.4155/bfs.12.83">https://doi.org/10.4155/bfs.12.83</a>.
- [181] C.L. Williams, T.L. Westover, R.M. Emerson, J.S. Tumuluru, C. Li, Sources of Biomass Feedstock Variability and the Potential Impact on Biofuels Production, Bioenergy Res 9 (2016) 1–14. https://doi.org/10.1007/s12155-015-9694-y.
- [182] M. Buffi, M. Prussi, N. Scarlat, Energy and environmental assessment of hydrogen from biomass sources: Challenges and perspectives, Biomass Bioenergy 165 (2022). <a href="https://doi.org/10.1016/j.biombioe.2022.106556">https://doi.org/10.1016/j.biombioe.2022.106556</a>.
- [183] R. Kumar, A. Kumar, A. Pal, Overview of hydrogen production from biogas reforming: Technological advancement, Int J Hydrogen Energy 47 (2022) 34831–34855. <a href="https://doi.org/10.1016/j.ijhydene.2022.08.059">https://doi.org/10.1016/j.ijhydene.2022.08.059</a>.
- [184] M.S. Herdem, M.Y. Sinaki, S. Farhad, F. Hamdullahpur, An overview of the methanol reforming process: Comparison of fuels, catalysts, reformers, and systems, Int J Energy Res 43 (2019) 5076–5105. <a href="https://doi.org/10.1002/er.4440">https://doi.org/10.1002/er.4440</a>.
- [185] C. Quan, Z. Gao, X. Liu, N. Miskolczi, Ethanol steam reforming for hydrogen production under Ni/Ce catalysts, Journal of the Energy Institute 112 (2024) 101446. https://doi.org/10.1016/j.joei.2023.101446.
- [186] F. Qureshi, M. Yusuf, A.A. Pasha, H.W. Khan, B. Imteyaz, K. Irshad, Sustainable and energy efficient hydrogen production via glycerol reforming techniques: A review, Int J Hydrogen Energy 47 (2022) 41397–41420. https://doi.org/10.1016/j.ijhydene.2022.04.010.
- [187] V. Chiodo, S. Maisano, G. Zafarana, F. Urbani, Effect of pollutants on biogas steam reforming, Int J Hydrogen Energy 42 (2017) 1622–1628. https://doi.org/10.1016/j.ijhydene.2016.07.251.

- [188] U. Izquierdo, I. García-García, Á. Gutierrez, J. Arraibi, V. Barrio, J. Cambra, P. Arias, Catalyst Deactivation and Regeneration Processes in Biogas Tri-Reforming Process. The Effect of Hydrogen Sulfide Addition, Catalysts 8 (2018) 12. https://doi.org/10.3390/catal8010012.
- [189] R.-Y. Chein, Y.-C. Chen, W.-H. Chen, Experimental Study on Sulfur Deactivation and Regeneration of Ni-Based Catalyst in Dry Reforming of Biogas, Catalysts 11 (2021) 777. https://doi.org/10.3390/catal11070777.
- [190] P. Frontera, P.L. Antonucci, A. Macario, Focus on Materials for Sulfur-Resistant Catalysts in the Reforming of Biofuels, Catalysts 11 (2021) 1029. <a href="https://doi.org/10.3390/catal11091029">https://doi.org/10.3390/catal11091029</a>.
- [191] J. Wei, M. Wang, F. Wang, X. Song, G. Yu, Y. Liu, H. Vuthaluru, J. Xu, Y. Xu, H. Zhang, S. Zhang, A review on reactivity characteristics and synergy behavior of biomass and coal Co-gasification, Int J Hydrogen Energy 46 (2021) 17116–17132. <a href="https://doi.org/10.1016/j.ijhydene.2021.02.162">https://doi.org/10.1016/j.ijhydene.2021.02.162</a>.
- [192] S. Mishra, R.K. Upadhyay, Review on biomass gasification: Gasifiers, gasifying mediums, and operational parameters, Mater Sci Energy Technol 4 (2021) 329–340. https://doi.org/10.1016/j.mset.2021.08.009.
- [193] W.A. Wan Ab Karim Ghani, R.A. Moghadam, M.A.M. Salleh, A.B. Alias, Air Gasification of Agricultural Waste in a Fluidized Bed Gasifier: Hydrogen Production Performance, Energies (Basel) 2 (2009) 258–268. https://doi.org/10.3390/en20200258.
- [194] I.-H. Hwang, J. Kobayashi, K. Kawamoto, Characterization of products obtained from pyrolysis and steam gasification of wood waste, RDF, and RPF, Waste Management 34 (2014) 402–410. https://doi.org/10.1016/j.wasman.2013.10.009.
- [195] G. Duman, Md.A. Uddin, J. Yanik, Hydrogen production from algal biomass via steam gasification, Bioresour Technol 166 (2014) 24–30. <a href="https://doi.org/10.1016/j.biortech.2014.04.096">https://doi.org/10.1016/j.biortech.2014.04.096</a>.
- [196] N. Couto, V. Silva, E. Monteiro, S. Teixeira, R. Chacartegui, K. Bouziane, P.S.D. Brito, A. Rouboa, Numerical and experimental analysis of municipal solid wastes gasification process, Appl Therm Eng 78 (2015) 185–195. https://doi.org/10.1016/j.applthermaleng.2014.12.036.
- [197] S. Akkache, A.-B. Hernández, G. Teixeira, F. Gelix, N. Roche, J.H. Ferrasse, Co-gasification of wastewater sludge and different feedstock: Feasibility study, Biomass Bioenergy 89 (2016) 201–209. https://doi.org/10.1016/j.biombioe.2016.03.003.
- [198] M.G. Macavei, V.-C. Gheorghe, G. Ionescu, A. Volceanov, R. Pătrașcu, C. Mărculescu, A. Magdziarz, Thermochemical Conversion of Animal-Derived Waste: A Mini-Review with a Focus on Chicken Bone Waste, Processes 12 (2024) 358. <a href="https://doi.org/10.3390/pr12020358">https://doi.org/10.3390/pr12020358</a>.
- [199] W. Zhang, S. Huang, S. Wu, Y. Wu, J. Gao, Ash fusion characteristics and gasification activity during biomasses co-gasification process, Renew Energy 147 (2020) 1584–1594. https://doi.org/10.1016/j.renene.2019.09.058.
- [200] Y. Gao, M. Wang, A. Raheem, F. Wang, J. Wei, D. Xu, X. Song, W. Bao, A. Huang, S. Zhang, H. Zhang, Syngas Production from Biomass Gasification: Influences of Feedstock Properties, Reactor Type, and Reaction Parameters, ACS Omega 8 (2023) 31620–31631. <a href="https://doi.org/10.1021/acsomega.3c03050">https://doi.org/10.1021/acsomega.3c03050</a>.
- [201] D. Sutton, B. Kelleher, J.R.H. Ross, Review of literature on catalysts for biomass gasification, Fuel Processing Technology 73 (2001) 155–173. <a href="https://doi.org/10.1016/S0378-3820(01)00208-9">https://doi.org/10.1016/S0378-3820(01)00208-9</a>.
- [202] Q. He, Q. Guo, K. Umeki, L. Ding, F. Wang, G. Yu, Soot formation during biomass gasification: A critical review, Renewable and Sustainable Energy Reviews 139 (2021) 110710. <a href="https://doi.org/10.1016/j.rser.2021.110710">https://doi.org/10.1016/j.rser.2021.110710</a>.
- [203] M. Cortazar, L. Santamaria, G. Lopez, J. Alvarez, L. Zhang, R. Wang, X. Bi, M. Olazar, A comprehensive review of primary strategies for tar removal in biomass gasification, Energy Convers Manag 276 (2023) 116496. https://doi.org/10.1016/j.enconman.2022.116496.
- [204] S. Yadav, D. Singh, P. Mohanty, P.K. Sarangi, Biochemical and Thermochemical Routes of H<sub>2</sub> Production from Food Waste: A Comparative Review, Chem Eng Technol 46 (2023) 191–203. https://doi.org/10.1002/ceat.202000526.
- [205] F. Qureshi, M. Yusuf, M. Tahir, M. Haq, M.M.I. Mohamed, H. Kamyab, H.-H.T. Nguyen, D.-V.N. Vo, H. Ibrahim, Renewable hydrogen production via biological and thermochemical routes:

- Nanomaterials, economic analysis and challenges, Process Safety and Environmental Protection 179 (2023) 68–88. https://doi.org/10.1016/j.psep.2023.07.075.
- [206] H. Argun, F. Kargi, Bio-hydrogen production by different operational modes of dark and photo-fermentation: An overview, Int J Hydrogen Energy 36 (2011) 7443–7459. https://doi.org/10.1016/j.ijhydene.2011.03.116.
- [207] A. Adessi, R. De Philippis, Hydrogen Production: Photofermentation, in: Microbial Technologies in Advanced Biofuels Production, Springer US, Boston, MA, 2012: pp. 53–75. <a href="https://doi.org/10.1007/978-1-4614-1208-3\_4">https://doi.org/10.1007/978-1-4614-1208-3\_4</a>.
- [208] K. Urbaniec, R.R. Bakker, Biomass residues as raw material for dark hydrogen fermentation A review, Int J Hydrogen Energy 40 (2015) 3648–3658. <a href="https://doi.org/10.1016/j.ijhydene.2015.01.073">https://doi.org/10.1016/j.ijhydene.2015.01.073</a>.
- [209] Z. Zhang, X. Zhou, J. Hu, T. Zhang, S. Zhu, Q. Zhang, Photo-bioreactor structure and light-heat-mass transfer properties in photo-fermentative bio-hydrogen production system: A mini review, Int J Hydrogen Energy 42 (2017) 12143–12152. https://doi.org/10.1016/j.ijhydene.2017.03.111.
- [210] N. Akhlaghi, G. Najafpour-Darzi, A comprehensive review on biological hydrogen production, Int J Hydrogen Energy 45 (2020) 22492–22512. <a href="https://doi.org/10.1016/j.ijhydene.2020.06.182">https://doi.org/10.1016/j.ijhydene.2020.06.182</a>.
- [211] L. Singh, Z.A. Wahid, Methods for enhancing bio-hydrogen production from biological process: A review, Journal of Industrial and Engineering Chemistry 21 (2015) 70–80. https://doi.org/10.1016/j.jiec.2014.05.035.
- [212] J. Baeyens, H. Zhang, J. Nie, L. Appels, R. Dewil, R. Ansart, Y. Deng, Reviewing the potential of bio-hydrogen production by fermentation, Renewable and Sustainable Energy Reviews 131 (2020) 110023. https://doi.org/10.1016/j.rser.2020.110023.
- [213] H. Weingärtner, I. Teermann, U. Borchers, P. Balsaa, H. V. Lutze, T.C. Schmidt, E.U. Franck, G. Wiegand, N. Dahmen, G. Schwedt, F.H. Frimmel, B.C. Gordalla, Water, 1. Properties, Analysis, and Hydrological Cycle, in: Ullmann's Encyclopedia of Industrial Chemistry, Wiley-VCH Verlag GmbH & Co. KGaA, Weinheim, Germany, 2016: pp. 1–40. <a href="https://doi.org/10.1002/14356007.a28-001.pub3">https://doi.org/10.1002/14356007.a28-001.pub3</a>.
- [214] T. Ohta, T. Takahashi, S. Ihara, S. Sato, N. Kamiya, K. Honda, A. Fujishima, T. Watanabe, A. Mitsui, S. Ono, M. Yamaguchi, W.J.D. Escher, Chapter 2-Thermodynamics of water-splitting, in: T. Ohta (Ed.), Solar-Hydrogen Energy Systems, Elsevier, 1979: pp. 25–33. <a href="https://doi.org/10.1016/B978-0-08-022713-9.50008-2">https://doi.org/10.1016/B978-0-08-022713-9.50008-2</a>.
- [215] S. Shiva Kumar, H. Lim, An overview of water electrolysis technologies for green hydrogen production, Energy Reports 8 (2022) 13793–13813. https://doi.org/10.1016/j.egyr.2022.10.127.
- [216] S. Sebbahi, A. Assila, A. Alaoui Belghiti, S. Laasri, S. Kaya, E.K. Hlil, S. Rachidi, A. Hajjaji, A comprehensive review of recent advances in alkaline water electrolysis for hydrogen production, Int J Hydrogen Energy 82 (2024) 583–599. <a href="https://doi.org/10.1016/j.ijhydene.2024.07.428">https://doi.org/10.1016/j.ijhydene.2024.07.428</a>.
- [217] T. Wang, X. Cao, L. Jiao, PEM water electrolysis for hydrogen production: fundamentals, advances, and prospects, Carbon Neutrality 1 (2022). https://doi.org/10.1007/s43979-022-00022-8.
- [218] A. Hauch, R. Küngas, P. Blennow, A.B. Hansen, J.B. Hansen, B. V. Mathiesen, M.B. Mogensen, Recent advances in solid oxide cell technology for electrolysis, Science (1979) 370 (2020). <a href="https://doi.org/10.1126/science.aba6118">https://doi.org/10.1126/science.aba6118</a>.
- [219] I. Vincent, D. Bessarabov, Low cost hydrogen production by anion exchange membrane electrolysis: A review, Renewable and Sustainable Energy Reviews 81 (2018) 1690–1704. https://doi.org/10.1016/j.rser.2017.05.258.
- [220] B. Panigrahy, K. Narayan, B. Ramachandra Rao, Green hydrogen production by water electrolysis: A renewable energy perspective, Mater Today Proc 67 (2022) 1310–1314. <a href="https://doi.org/10.1016/j.matpr.2022.09.254">https://doi.org/10.1016/j.matpr.2022.09.254</a>.
- [221] N. Gerloff, Comparative Life-Cycle-Assessment analysis of three major water electrolysis technologies while applying various energy scenarios for a greener hydrogen production, J Energy Storage 43 (2021) 102759. <a href="https://doi.org/10.1016/j.est.2021.102759">https://doi.org/10.1016/j.est.2021.102759</a>.

- [222] T. Jafari, E. Moharreri, A.S. Amin, R. Miao, W. Song, S.L. Suib, Photocatalytic water splitting The untamed dream: A review of recent advances, Molecules 21 (2016). https://doi.org/10.3390/molecules21070900.
- [223] C.F. Fu, X. Wu, J. Yang, Material Design for Photocatalytic Water Splitting from a Theoretical Perspective, Advanced Materials 30 (2018). <a href="https://doi.org/10.1002/adma.201802106">https://doi.org/10.1002/adma.201802106</a>.
- [224] N. Fajrina, M. Tahir, A critical review in strategies to improve photocatalytic water splitting towards hydrogen production, Int J Hydrogen Energy 44 (2019) 540–577. <a href="https://doi.org/10.1016/j.ijhydene.2018.10.200">https://doi.org/10.1016/j.ijhydene.2018.10.200</a>.
- [225] Y. Ma, L. Lin, T. Takata, T. Hisatomi, K. Domen, A perspective on two pathways of photocatalytic water splitting and their practical application systems, Physical Chemistry Chemical Physics 25 (2023) 6586–6601. <a href="https://doi.org/10.1039/d2cp05427b">https://doi.org/10.1039/d2cp05427b</a>.
- [226] N. Abas, E. Kalair, A. Kalair, Q. ul Hasan, N. Khan, Nature inspired artificial photosynthesis technologies for hydrogen production: Barriers and challenges, Int J Hydrogen Energy 45 (2020) 20787–20799. https://doi.org/10.1016/j.ijhydene.2019.12.010.
- [227] T. Gobbato, G.A. Volpato, A. Sartorel, M. Bonchio, A breath of sunshine: oxygenic photosynthesis by functional molecular architectures, Chem Sci 14 (2023) 12402–12429. https://doi.org/10.1039/d3sc03780k.
- [228] S.I. Allakhverdiev, V. Thavasi, V.D. Kreslavski, S.K. Zharmukhamedov, V. V. Klimov, S. Ramakrishna, D.A. Los, M. Mimuro, H. Nishihara, R. Carpentier, Photosynthetic hydrogen production, Journal of Photochemistry and Photobiology C: Photochemistry Reviews 11 (2010) 101–113. https://doi.org/10.1016/j.jphotochemrev.2010.07.002.
- [229] R.E. Blankenship, Molecular Mechanisms of Photosynthesis, Wiley, 2002. <a href="https://doi.org/10.1002/9780470758472">https://doi.org/10.1002/9780470758472</a>.
- [230] S. Ashitha, S.C. George, Splitting of water: biological and non-biological approaches, in: Handbook of Biofuels, Elsevier, 2022: pp. 453–469. <a href="https://doi.org/10.1016/B978-0-12-822810-4.00023-3">https://doi.org/10.1016/B978-0-12-822810-4.00023-3</a>.
- [231] S. Li, M. Tabatabaei, F. Li, S.H. Ho, A review of green biohydrogen production using anoxygenic photosynthetic bacteria for hydrogen economy: Challenges and opportunities, Int J Hydrogen Energy 54 (2024) 218–238. https://doi.org/10.1016/j.ijhydene.2022.11.014.
- [232] S.I. Allakhverdiev, Photosynthetic and biomimetic hydrogen production, Int J Hydrogen Energy 37 (2012) 8744–8752. https://doi.org/10.1016/j.ijhydene.2012.01.045.
- [233] Q.K. Chen, X.H. Xiang, P. Yan, S.Y. Liu, Enhancing strategies of photosynthetic hydrogen production from microalgae: Differences in hydrogen production between prokaryotic and eukaryotic algae, Bioresour Technol 406 (2024). <a href="https://doi.org/10.1016/j.biortech.2024.131029">https://doi.org/10.1016/j.biortech.2024.131029</a>.
- [234] M.L. Ghirardi, A. Dubini, J. Yu, P.C. Maness, Photobiological hydrogen-producing systems, Chem Soc Rev 38 (2009) 52–61. https://doi.org/10.1039/b718939g.
- [235] T. Ohta, T. Takahashi, S. Ihara, S. Sato, N. Kamiya, K. Honda, A. Fujishima, T. Watanabe, A. Mitsui, S. Ono, M. Yamaguchi, W.J.D. Escher, Chapter 4-Direct thermal decomposition of water, in: T. Ohta (Ed.), Solar-Hydrogen Energy Systems, Elsevier, 1979: pp. 59–79. <a href="https://doi.org/10.1016/B978-0-08-022713-9.50010-0">https://doi.org/10.1016/B978-0-08-022713-9.50010-0</a>.
- [236] S. Baykara, Experimental solar water thermolysis, Int J Hydrogen Energy 29 (2004) 1459–1469. https://doi.org/10.1016/j.ijhydene.2004.02.011.
- [237] S.Z. Baykara, E. Bilgen, An overall assessment of hydrogen production by solar water thermolysis, Int J Hydrogen Energy 14 (1989) 881–891. <a href="https://doi.org/10.1016/0360-3199(89)90075-X">https://doi.org/10.1016/0360-3199(89)90075-X</a>.
- [238] C. Perkins, A.W. Weimer, Likely near-term solar-thermal water splitting technologies, Int J Hydrogen Energy 29 (2004) 1587–1599. https://doi.org/10.1016/j.ijhydene.2004.02.019.
- [239] S.Z. Baykara, Hydrogen production by direct solar thermal decomposition of water, possibilities for improvement of process efficiency, Int J Hydrogen Energy 29 (2004) 1451–1458. <a href="https://doi.org/10.1016/j.ijhydene.2004.02.014">https://doi.org/10.1016/j.ijhydene.2004.02.014</a>.
- [240] O. Oruc, I. Dincer, Assessing the potential of thermochemical water splitting cycles: A bridge towards for clean and sustainable hydrogen generation, Fuel 286 (2021). https://doi.org/10.1016/j.fuel.2020.119325.

- [241] L. Wang, M. Wang, A. Syeda, F. Ye, C. Liu, Y. Tao, C. Chen, B. Liu, Thermocatalytic Hydrogen Production from Water at Boiling Condition, Small 20 (2024). https://doi.org/10.1002/sml1.202400561.
- [242] M. Orfila, M. Linares, R. Molina, J.Á. Botas, R. Sanz, J. Marugán, Perovskite materials for hydrogen production by thermochemical water splitting, Int J Hydrogen Energy 41 (2016) 19329–19338. https://doi.org/10.1016/j.ijhydene.2016.07.041.
- [243] Y. Mao, Y. Gao, W. Dong, H. Wu, Z. Song, X. Zhao, J. Sun, W. Wang, Hydrogen production via a two-step water splitting thermochemical cycle based on metal oxide A review, Appl Energy 267 (2020). https://doi.org/10.1016/j.apenergy.2020.114860.
- [244] D. Oudejans, M. Offidani, A. Constantinou, S. Albonetti, N. Dimitratos, A. Bansode, Comprehensive Review on Two-Step Thermochemical Water Splitting for Hydrogen Production in a Redox Cycle, Energies (Basel) 15 (2022). <a href="https://doi.org/10.3390/en15093044">https://doi.org/10.3390/en15093044</a>.
- [245] F. Safari, I. Dincer, A review and comparative evaluation of thermochemical water splitting cycles for hydrogen production, Energy Convers Manag 205 (2020). https://doi.org/10.1016/j.enconman.2019.112182.
- [246] S. Li, Q. Kang, J. Baeyens, H.L. Zhang, Y.M. Deng, Hydrogen Production: State of Technology, in: IOP Conf Ser Earth Environ Sci, Institute of Physics Publishing, 2020. <a href="https://doi.org/10.1088/1755-1315/544/1/012011">https://doi.org/10.1088/1755-1315/544/1/012011</a>.
- [247] A. Boretti, Which thermochemical water-splitting cycle is more suitable for high-temperature concentrated solar energy?, Int J Hydrogen Energy 47 (2022) 20462–20474. https://doi.org/10.1016/j.ijhydene.2022.04.159.
- [248] R. Pinsky, P. Sabharwall, J. Hartvigsen, J. O'Brien, Comparative review of hydrogen production technologies for nuclear hybrid energy systems, Progress in Nuclear Energy 123 (2020). https://doi.org/10.1016/j.pnucene.2020.103317.
- [249] A. Boretti, Technology Readiness Level of Solar Thermochemical Splitting Cycles, ACS Energy Lett 6 (2021) 1170–1174. https://doi.org/10.1021/acsenergylett.1c00181.
- [250] B.S. Zainal, P.J. Ker, H. Mohamed, H.C. Ong, I.M.R. Fattah, S.M.A. Rahman, L.D. Nghiem, T.M.I. Mahlia, Recent advancement and assessment of green hydrogen production technologies, Renewable and Sustainable Energy Reviews 189 (2024) 113941. https://doi.org/10.1016/j.rser.2023.113941.
- [251] A. Ajanovic, M. Sayer, R. Haas, The economics and the environmental benignity of different colors of hydrogen, Int J Hydrogen Energy 47 (2022) 24136–24154. <a href="https://doi.org/10.1016/j.ijhydene.2022.02.094">https://doi.org/10.1016/j.ijhydene.2022.02.094</a>.
- [252] P. Fernández-Arias, Á. Antón-Sancho, G. Lampropoulos, D. Vergara, Emerging Trends and Challenges in Pink Hydrogen Research, Energies (Basel) 17 (2024) 2291. https://doi.org/10.3390/en17102291.
- [253] O.A. Habeeb, R. Kanthasamy, G.A.M. Ali, S. Sethupathi, R.B.M. Yunus, Hydrogen sulfide emission sources, regulations, and removal techniques: a review, Reviews in Chemical Engineering 34 (2018) 837–854. https://doi.org/10.1515/revce-2017-0004.
- [254] National Center for Biotechnology Information, PubChem Compound Summary for CID 402, Hydrogen Sulfide, PubChem Compound Summary for CID 402, Hydrogen Sulfide (2024). <a href="https://pubchem.ncbi.nlm.nih.gov/compound/Hydrogen-Sulfide">https://pubchem.ncbi.nlm.nih.gov/compound/Hydrogen-Sulfide</a> (accessed October 31, 2024).
- [255] U.W. R. Siagian, H.P.S. Siregar, R.K. Santoso, D.D. Salam, S. Sumarli, A Novel Approach of H<sub>2</sub>S Corrosion Modeling in Oil/Gas Production Pipeline, in: All Days, IPTC, 2014. https://doi.org/10.2523/IPTC-18148-MS.
- [256] S. Nirmal Kumar, S. Appari, B.V.R. Kuncharam, Techniques for Overcoming Sulfur Poisoning of Catalyst Employed in Hydrocarbon Reforming, Catalysis Surveys from Asia 25 (2021) 362–388. https://doi.org/10.1007/s10563-021-09340-w.
- [257] H. Ghahraloud, M. Farsi, M.R. Rahimpour, Modeling and optimization of an industrial Claus process: Thermal and catalytic section, J Taiwan Inst Chem Eng 76 (2017) 1–9. https://doi.org/10.1016/j.jtice.2017.03.005.

- [258] A.G. De Crisci, A. Moniri, Y. Xu, Hydrogen from hydrogen sulfide: towards a more sustainable hydrogen economy, Int J Hydrogen Energy 44 (2019) 1299–1327. https://doi.org/10.1016/j.ijhydene.2018.10.035.
- [259] A.L. Martínez-Salazar, J.A. Melo-Banda, M.A. Coronel-García, P.M. García-Vite, I. Martínez-Salazar, J.M. Domínguez-Esquivel, Technoeconomic analysis of hydrogen production via hydrogen sulfide methane reformation, Int J Hydrogen Energy 44 (2019) 12296–12302. <a href="https://doi.org/10.1016/j.ijhydene.2018.11.023">https://doi.org/10.1016/j.ijhydene.2018.11.023</a>.
- [260] A.L. Martínez-Salazar, J.A. Melo-Banda, A.I. Reyes De La Torre, Y. Salazar-Cerda, M.A. Coronel-García, B. Portales Martínez, V.H. Martínez-Sifuentes, J.M. Domínguez-Esquivel, R. Silva Rodrigo, Hydrogen production by methane reforming with H<sub>2</sub>S using Mo,Cr/ZrO<sub>2</sub>-SBA15 and Mo,Cr/ZrO<sub>2</sub>-La<sub>2</sub>O<sub>3</sub> catalysts, in: Int J Hydrogen Energy, Elsevier Ltd, 2015: pp. 17272–17283. <a href="https://doi.org/10.1016/j.ijhydene.2015.09.154">https://doi.org/10.1016/j.ijhydene.2015.09.154</a>.
- [261] F. Tollini, M. Sponchioni, V. Calemma, D. Moscatelli, Methane Reforming with H<sub>2</sub>S and Sulfur for Hydrogen Production: Thermodynamic Assessment, Energy and Fuels 37 (2023) 11197–11208. https://doi.org/10.1021/acs.energyfuels.3c01237.
- [262] S.M. Ali, I.I.I. Alkhatib, A. AlHajaj, L.F. Vega, How sustainable and profitable are large-scale hydrogen production plants from CH<sub>4</sub> and H<sub>2</sub>S?, J Clean Prod 428 (2023). https://doi.org/10.1016/j.jclepro.2023.139475.
- [263] E. Spatolisano, G. De Guido, L.A. Pellegrini, V. Calemma, A.R. de Angelis, M. Nali, Hydrogen sulphide to hydrogen via H<sub>2</sub>S methane reformation: Thermodynamics and process scheme assessment, Int J Hydrogen Energy 47 (2022) 15612–15623. <a href="https://doi.org/10.1016/j.ijhydene.2022.03.090">https://doi.org/10.1016/j.ijhydene.2022.03.090</a>.
- [264] F. Abdulrahman, Q. Wang, F. Angikath, S.M. Sarathy, Hydrogen sulfide methane reforming: A kinetic modeling and techno-economic analysis study, Int J Hydrogen Energy 67 (2024) 750–759. https://doi.org/10.1016/j.ijhydene.2024.04.213.
- [265] A. Nova, K. Prifti, F. Negri, F. Manenti, Multiscale techno-economic analysis of orange hydrogen synthesis, Energy 282 (2023). <a href="https://doi.org/10.1016/j.energy.2023.128644">https://doi.org/10.1016/j.energy.2023.128644</a>.
- [266] G. Jiang, Z. Yang, F. Zhang, G. Li, Z. Wei, B. Niu, M. Zhao, Z. Zhang, Z. Hao, Thermal Decomposition of H<sub>2</sub>S at Low Temperature on Mo-Containing Catalysts Derived from MAIO (M = Mg, Co, and Ni) Layered Double Hydroxides, Ind Eng Chem Res 62 (2023) 7224–7234. <a href="https://doi.org/10.1021/acs.iecr.2c03735">https://doi.org/10.1021/acs.iecr.2c03735</a>.
- [267] M.Y. Dogan, H.M. Tasdemir, H. Arbag, N. Yasyerli, S. Yasyerli, H<sub>2</sub> production via H<sub>2</sub>S decomposition over activated carbon supported Fe- and W- catalysts, Int J Hydrogen Energy 75 (2024) 483–495. https://doi.org/10.1016/j.ijhydene.2024.02.316.
- [268] H. Aljama, Z. Alaithan, A. Almofleh, Catalytic Conversion of H<sub>2</sub>S to H<sub>2</sub>: Challenges and Catalyst Limitations, Journal of Physical Chemistry C 127 (2023) 9022–9029. https://doi.org/10.1021/acs.jpcc.3c00903.
- [269] S.H. Rajaee Shooshtari, A. Shahsavand, Clean hydrogen energy production via purification of hydrogen sulfide thermolysis products employing supersonic separator, Int J Hydrogen Energy 48 (2023) 38749–38765. https://doi.org/10.1016/j.ijhydene.2023.06.148.
- [270] Y.H. Chan, A.C.M. Loy, K.W. Cheah, S.Y.W. Chai, L.H. Ngu, B.S. How, C. Li, S.S.M. Lock, M.K. Wong, C.L. Yiin, B.L.F. Chin, Z.P. Chan, S.S. Lam, Hydrogen sulfide (H<sub>2</sub>S) conversion to hydrogen (H<sub>2</sub>) and value-added chemicals: Progress, challenges and outlook, Chemical Engineering Journal 458 (2023). <a href="https://doi.org/10.1016/j.cej.2023.141398">https://doi.org/10.1016/j.cej.2023.141398</a>.
- [271] L. Zhao, Y. Wang, X. Li, A. Wang, C. Song, Y. Hu, Hydrogen production via decomposition of hydrogen sulfide by synergy of non-thermal plasma and semiconductor catalysis, Int J Hydrogen Energy 38 (2013) 14415–14423. https://doi.org/10.1016/j.ijhydene.2013.09.008.
- [272] R. Gautam, S. Kumar, S. Upadhyayula, A comprehensive review on recent breakthroughs in hydrogen production from hydrogen sulfide decomposition: Harnessing the power of plasma, Renewable and Sustainable Energy Reviews 202 (2024). https://doi.org/10.1016/j.rser.2024.114735.

- [273] M. Luo, J. Zhou, W. Xu, J. Chen, M. Xiang, K. Peng, Development of composite microwave catalysts (ABS<sub>x</sub>/CNTs, A = Co, B = Ni, Mo) for the highly effective direct decomposition of H<sub>2</sub>S into H<sub>2</sub> and S, Fuel 281 (2020). https://doi.org/10.1016/j.fuel.2020.118729.
- [274] K. Jangam, Y.Y. Chen, L. Qin, L.S. Fan, Perspectives on reactive separation and removal of hydrogen sulfide, Chemical Engineering Science: X 11 (2021). <a href="https://doi.org/10.1016/j.cesx.2021.100105">https://doi.org/10.1016/j.cesx.2021.100105</a>.
- [275] Y. Ma, X. Jin, Y. Hu, Q. Huang, Z. Wang, Recovery of Hydrogen and Sulfur by Electrolysis of Ionized H<sub>2</sub>S in an Amine-Containing Organic Electrolyte with Highly Temperature-Dependent Sulfur Solubility, Energy and Fuels 34 (2020) 7756–7762. https://doi.org/10.1021/acs.energyfuels.0c01161.
- [276] M. Kumar, T.C. Nagaiah, Pure hydrogen and sulfur production from H<sub>2</sub>S by an electrochemical approach using a NiCu-MoS<sub>2</sub> catalyst, J Mater Chem A Mater 10 (2022) 13031–13041. https://doi.org/10.1039/d2ta02751h.
- [277] K. Kim, C. Lee, Recent progress in electrochemical hydrogen sulfide splitting: Strategies for enabling Sulfur-tolerant anodic reactions, Chemical Engineering Journal 469 (2023). https://doi.org/10.1016/j.cej.2023.143861.
- [278] M. Han, X. Zhang, S. Hassan, A. Al-Yousef, Advancement and Prospective of Hydrogen Generation from Hydrogen Sulfide Via Electrolysis Decomposition Approaches, in: SPE Middle East Oil and Gas Show and Conference, MEOS, Proceedings, Society of Petroleum Engineers (SPE), 2023. <a href="https://doi.org/10.2118/213245-MS">https://doi.org/10.2118/213245-MS</a>.
- [279] M. Velazquez-Rizo, A.C. Cavazos Sepulveda, Low-temperature direct electrochemical splitting of H<sub>2</sub>S, Frontiers in Chemical Engineering 4 (2022). <a href="https://doi.org/10.3389/fceng.2022.1087435">https://doi.org/10.3389/fceng.2022.1087435</a>.
- [280] Z. Yu, Z. Deng, Y. Li, X. Wang, Advances in Electrocatalyst Design and Mechanism for Sulfide Oxidation Reaction in Hydrogen Sulfide Splitting, Adv Funct Mater (2024). <a href="https://doi.org/10.1002/adfm.202403435">https://doi.org/10.1002/adfm.202403435</a>.
- [281] H. Huang, J. Shang, Y. Yu, K.H. Chung, Recovery of hydrogen from hydrogen sulfide by indirect electrolysis process, Int J Hydrogen Energy 44 (2019) 5108–5113. https://doi.org/10.1016/j.ijhydene.2018.11.010.
- [282] G. Ma, H. Yan, J. Shi, X. Zong, Z. Lei, C. Li, Direct splitting of H<sub>2</sub>S into H<sub>2</sub> and S on CdS-based photocatalyst under visible light irradiation, J Catal 260 (2008) 134–140. https://doi.org/10.1016/j.jcat.2008.09.017.
- [283] S. Yu, Y. Zhou, Photochemical Decomposition of Hydrogen Sulfide, in: Advanced Catalytic Materials Photocatalysis and Other Current Trends, InTech, 2016: p. 493. <a href="https://doi.org/10.5772/61823">https://doi.org/10.5772/61823</a>.
- [284] M. Dan, S. Yu, Y. Li, S. Wei, J. Xiang, Y. Zhou, Hydrogen sulfide conversion: How to capture hydrogen and sulfur by photocatalysis, Journal of Photochemistry and Photobiology C: Photochemistry Reviews 42 (2020). <a href="https://doi.org/10.1016/j.jphotochemrev.2019.100339">https://doi.org/10.1016/j.jphotochemrev.2019.100339</a>.
- [285] H. Oladipo, A. Yusuf, S. Al Jitan, G. Palmisano, Overview and challenges of the photolytic and photocatalytic splitting of H<sub>2</sub>S, Catal Today 380 (2021) 125–137. https://doi.org/10.1016/j.cattod.2021.03.021.
- [286] H. Oladipo, A. Yusuf, K. Al-Ali, G. Palmisano, Techno-Economic Evaluation of Photocatalytic H<sub>2</sub>S Splitting, Energy Technology 9 (2021). <a href="https://doi.org/10.1002/ente.202100163">https://doi.org/10.1002/ente.202100163</a>.
- [287] A.A. Oladipo, R. Vaziri, Z.M. Mizwari, A.O. Ifebajo, In<sub>2</sub>S<sub>3</sub>/AgIO<sub>3</sub> photoanode coupled I<sup>-</sup>/I<sub>3</sub><sup>-</sup> cyclic redox system for solar-electrocatalytic recovery of H<sub>2</sub> and S from toxic H<sub>2</sub>S, Int J Hydrogen Energy 45 (2020) 15831–15840. https://doi.org/10.1016/j.ijhydene.2019.06.192.
- [288] V.J. Aimikhe, O.E. Eyankware, Recent Advances in White Hydrogen Exploration and Production: A Mini Review, Journal of Energy Research and Reviews 13 (2023) 64–79. https://doi.org/10.9734/jenrr/2023/v13i4272.
- [289] E. Ohtani, The role of water in Earth's mantle, Natl Sci Rev 7 (2020) 224–232. https://doi.org/10.1093/nsr/nwz071.
- [290] S.P. Gregory, M.J. Barnett, L.P. Field, A.E. Milodowski, Subsurface microbial hydrogen cycling: Natural occurrence and implications for industry, Microorganisms 7 (2019). https://doi.org/10.3390/microorganisms7020053.

- [291] F. Klein, J.D. Tarnas, W. Bach, Abiotic sources of molecular hydrogen on earth, Elements 16 (2020) 19–24. https://doi.org/10.2138/GSELEMENTS.16.1.19.
- [292] Q. Williams, R.J. Hemley, Hydrogen in the deep Earth, Annu Rev Earth Planet Sci 29 (2001) 365–418. https://doi.org/10.1146/annurev.earth.29.1.365.
- [293] L. Yuan, G. Steinle-Neumann, Hydrogen distribution between the Earth's inner and outer core, Earth Planet Sci Lett 609 (2023). <a href="https://doi.org/10.1016/j.epsl.2023.118084">https://doi.org/10.1016/j.epsl.2023.118084</a>.
- [294] T.M. McCollom, W. Bach, Thermodynamic constraints on hydrogen generation during serpentinization of ultramafic rocks, Geochim Cosmochim Acta 73 (2009) 856–875. <a href="https://doi.org/10.1016/j.gca.2008.10.032">https://doi.org/10.1016/j.gca.2008.10.032</a>.
- [295] T. Hirose, S. Kawagucci, K. Suzuki, Mechanoradical H<sub>2</sub> generation during simulated faulting: Implications for an earthquake-driven subsurface biosphere, Geophys Res Lett 38 (2011). https://doi.org/10.1029/2011GL048850.
- [296] A. Aiuppa, Y. Moussallam, Hydrogen and hydrogen sulphide in volcanic gases: abundance, processes, and atmospheric fluxes, Comptes Rendus. Géoscience 356 (2023) 1–23. https://doi.org/10.5802/crgeos.235.
- [297] L. Truche, G. Joubert, M. Dargent, P. Martz, M. Cathelineau, T. Rigaudier, D. Quirt, Clay minerals trap hydrogen in the Earth's crust: Evidence from the Cigar Lake uranium deposit, Athabasca, Earth Planet Sci Lett 493 (2018) 186–197. https://doi.org/10.1016/j.epsl.2018.04.038.
- [298] E. Hand, Hidden hydrogen, Science (1979) 379 (2023) 630–636. https://doi.org/10.1126/science.adh1477.
- [299] X. Yang, H. Keppler, Y. Li, Molecular hydrogen in mantle minerals, Geochem Perspect Lett 2 (2016) 160–168. https://doi.org/10.7185/geochemlet.1616.
- [300] O. Maiga, E. Deville, J. Laval, A. Prinzhofer, A.B. Diallo, Characterization of the spontaneously recharging natural hydrogen reservoirs of Bourakebougou in Mali, Sci Rep 13 (2023). https://doi.org/10.1038/s41598-023-38977-y.
- [301] O. Maiga, E. Deville, J. Laval, A. Prinzhofer, A.B. Diallo, Trapping processes of large volumes of natural hydrogen in the subsurface: The emblematic case of the Bourakebougou H<sub>2</sub> field in Mali, Int J Hydrogen Energy 50 (2024) 640–647. https://doi.org/10.1016/j.ijhydene.2023.10.131.
- [302] N. Lefeuvre, L. Truche, F. V. Donzé, F. Gal, J. Tremosa, R.A. Fakoury, S. Calassou, E.C. Gaucher, Natural hydrogen migration along thrust faults in foothill basins: The North Pyrenean Frontal Thrust case study, Applied Geochemistry 145 (2022). <a href="https://doi.org/10.1016/j.apgeochem.2022.105396">https://doi.org/10.1016/j.apgeochem.2022.105396</a>.
- [303] S. Séjourné, F.-A. Comeau, M.L. Moreira dos Santos, G. Bordeleau, M. Claprood, P. Mouge, V. Mulliez, M. Malo, B. Giroux, E. Gloaguen, J. Raymond, Potential for natural hydrogen in Quebec (Canada): a first review, Frontiers in Geochemistry 2 (2024). https://doi.org/10.3389/fgeoc.2024.1351631.
- [304] K. Saidy, M. Fawad, S.A. Whattam, A.A. Al-Shuhail, A.A. Al-Shuhail, M. Campos, F.A. Sulistyohariyanto, Unlocking the H<sub>2</sub> potential in Saudi Arabia: Exploring serpentinites as a source of H<sub>2</sub> production, Int J Hydrogen Energy 89 (2024) 1482–1491. <a href="https://doi.org/10.1016/j.ijhydene.2024.09.256">https://doi.org/10.1016/j.ijhydene.2024.09.256</a>.
- [305] L. Wang, Z. Jin, Q. Liu, K. Liu, Q. Meng, X. Huang, Y. Su, Q. Zhang, The occurrence pattern of natural hydrogen in the Songliao Basin, P.R. China: Insights on natural hydrogen exploration, Int J Hydrogen Energy 50 (2024) 261–275. <a href="https://doi.org/10.1016/j.ijhydene.2023.08.237">https://doi.org/10.1016/j.ijhydene.2023.08.237</a>.
- [306] E. Frery, L. Langhi, M. Maison, I. Moretti, Natural hydrogen seeps identified in the North Perth Basin, Western Australia, Int J Hydrogen Energy 46 (2021) 31158–31173. https://doi.org/10.1016/j.ijhydene.2021.07.023.
- [307] A. Prinzhofer, I. Moretti, J. Françolin, C. Pacheco, A. D'Agostino, J. Werly, F. Rupin, Natural hydrogen continuous emission from sedimentary basins: The example of a Brazilian H<sub>2</sub>-emitting structure, Int J Hydrogen Energy 44 (2019) 5676–5685. <a href="https://doi.org/10.1016/j.ijhydene.2019.01.119">https://doi.org/10.1016/j.ijhydene.2019.01.119</a>.

- [308] L. Truche, F.-V. Donzé, E. Goskolli, B. Muceku, C. Loisy, C. Monnin, H. Dutoit, A. Cerepi, A deep reservoir for hydrogen drives intense degassing in the Bulqizë ophiolite, Science (1979) 383 (2024) 618–621. https://doi.org/10.1126/science.adk9099.
- [309] N. Larin, V. Zgonnik, S. Rodina, E. Deville, A. Prinzhofer, V.N. Larin, Natural Molecular Hydrogen Seepage Associated with Surficial, Rounded Depressions on the European Craton in Russia, Natural Resources Research 24 (2015) 369–383. <a href="https://doi.org/10.1007/s11053-014-9257-5">https://doi.org/10.1007/s11053-014-9257-5</a>.
- [310] V. Zgonnik, V. Beaumont, E. Deville, N. Larin, D. Pillot, K.M. Farrell, Evidence for natural molecular hydrogen seepage associated with Carolina bays (surficial, ovoid depressions on the Atlantic Coastal Plain, Province of the USA), Prog Earth Planet Sci 2 (2015) 31. <a href="https://doi.org/10.1186/s40645-015-0062-5">https://doi.org/10.1186/s40645-015-0062-5</a>.
- [311] L. Stalker, A. Talukder, J. Strand, M. Josh, M. Faiz, Gold (hydrogen) rush: risks and uncertainties in exploring for naturally occurring hydrogen, The APPEA Journal 62 (2022) 361–380. https://doi.org/10.1071/AJ21130.
- [312] E.C. Gaucher, New perspectives in the industrial exploration for native hydrogen, Elements 16 (2020) 8–9. <a href="https://doi.org/10.2138/gselements.16.1.8">https://doi.org/10.2138/gselements.16.1.8</a>.
- [313] D. Knez, O.A.M. Zamani, Up-to-Date Status of Geoscience in the Field of Natural Hydrogen with Consideration of Petroleum Issues, Energies (Basel) 16 (2023). <a href="https://doi.org/10.3390/en16186580">https://doi.org/10.3390/en16186580</a>.
- [314] F. Osselin, C. Soulaine, C. Fauguerolles, E.C. Gaucher, B. Scaillet, M. Pichavant, Orange hydrogen is the new green, Nat Geosci 15 (2022) 765–769. https://doi.org/10.1038/s41561-022-01043-9.
- [315] E.C. Gaucher, The place of natural hydrogen in the energy transition: A position paper, European Geologist (2023) 5–9. https://doi.org/10.5281/zenodo.8108239.
- [316] D. Li, R. Xu, Z. Gu, X. Zhu, S. Qing, K. Li, Chemical-Looping Conversion of Methane: A Review, Energy Technology 8 (2020). <a href="https://doi.org/10.1002/ente.201900925">https://doi.org/10.1002/ente.201900925</a>.
- [317] J. Adánez, A. Abad, Chemical-looping combustion: Status and research needs, Proceedings of the Combustion Institute 37 (2019) 4303–4317. <a href="https://doi.org/10.1016/j.proci.2018.09.002">https://doi.org/10.1016/j.proci.2018.09.002</a>.
- [318] O. Palone, L. Cedola, D. Borello, C.N. Markides, Decarbonizing power and fuels production by chemical looping processes: Systematic review and future perspectives, Appl Therm Eng 254 (2024) 123844. https://doi.org/10.1016/j.applthermaleng.2024.123844.
- [319] Q. Guo, Y. Cheng, Y. Liu, W. Jia, H.-J. Ryu, Coal Chemical Looping Gasification for Syngas Generation Using an Iron-Based Oxygen Carrier, Ind Eng Chem Res 53 (2014) 78–86. https://doi.org/10.1021/ie401568x.
- [320] A. Goel, E.M. Moghaddam, W. Liu, C. He, J. Konttinen, Biomass chemical looping gasification for high-quality syngas: A critical review and technological outlooks, Energy Convers Manag 268 (2022) 116020. <a href="https://doi.org/10.1016/j.enconman.2022.116020">https://doi.org/10.1016/j.enconman.2022.116020</a>.
- [321] J. Bofhàr-Nordenkampf, T. Pröll, P. Kolbitsch, H. Hofbauer, Chemical Looping Autothermal Reforming at a 120 kW Pilot Rig, in: Proceedings of the 20th International Conference on Fluidized Bed Combustion, Springer Berlin Heidelberg, Berlin, Heidelberg, 2009: pp. 603–607. <a href="https://doi.org/10.1007/978-3-642-02682-9">https://doi.org/10.1007/978-3-642-02682-9</a> 91.
- [322] T. Pröll, P. Kolbitsch, J. Bolhàr-Nordenkampf, H. Hofbauer, Chemical Looping Pilot Plant Results Using a Nickel-Based Oxygen Carrier, Oil & Gas Science and Technology Revue d'IFP Energies Nouvelles 66 (2011) 173–180. <a href="https://doi.org/10.2516/ogst/2010036">https://doi.org/10.2516/ogst/2010036</a>.
- [323] A. Cabello, T. Mendiara, A. Abad, M.T. Izquierdo, F. García-Labiano, Production of hydrogen by chemical looping reforming of methane and biogas using a reactive and durable Cu-based oxygen carrier, Fuel 322 (2022) 124250. <a href="https://doi.org/10.1016/j.fuel.2022.124250">https://doi.org/10.1016/j.fuel.2022.124250</a>.
- [324] K. Anaya, A. Olufemi Oni, A. Kumar, Investigating the techno-economic and environmental performance of chemical looping technology for hydrogen production, Sustainable Energy Technologies and Assessments 56 (2023). https://doi.org/10.1016/j.seta.2022.103008.
- [325] P.A. Argyris, J. Wong, A. Wright, L.M.C. Pereira, V. Spallina, Reducing the cost of low-carbon hydrogen production via emerging chemical looping process, Energy Convers Manag 277 (2023). https://doi.org/10.1016/j.enconman.2022.116581.

- [326] S. Luo, L. Zeng, L.S. Fan, Chemical Looping Technology: Oxygen Carrier Characteristics, Annu Rev Chem Biomol Eng 6 (2015) 53–75. https://doi.org/10.1146/annurev-chembioeng-060713-040334.
- [327] L. Protasova, F. Snijkers, Recent developments in oxygen carrier materials for hydrogen production via chemical looping processes, Fuel 181 (2016) 75–93. <a href="https://doi.org/10.1016/j.fuel.2016.04.110">https://doi.org/10.1016/j.fuel.2016.04.110</a>.
- [328] K. Li, H. Wang, Y. Wei, Syngas generation from methane using a chemical-looping concept: A review of oxygen carriers, J Chem (2013). <a href="https://doi.org/10.1155/2013/294817">https://doi.org/10.1155/2013/294817</a>.
- [329] W. Chang, Y. Hu, W. Xu, C. Huang, H. Chen, J. He, Y. Han, Y. Zhu, X. Ma, X. Wang, Recent Advances of Oxygen Carriers for Hydrogen Production via Chemical Looping Water-Splitting, Catalysts 13 (2023). <a href="https://doi.org/10.3390/catal13020279">https://doi.org/10.3390/catal13020279</a>.
- [330] G. Liu, G. Lisak, Cu-based oxygen carriers for chemical looping processes: Opportunities and challenges, Fuel 342 (2023). <a href="https://doi.org/10.1016/j.fuel.2023.127828">https://doi.org/10.1016/j.fuel.2023.127828</a>.
- [331] F. Abild-Pedersen, O. Lytken, J. Engbæk, G. Nielsen, I. Chorkendorff, J.K. Nørskov, Methane activation on Ni(111): Effects of poisons and step defects, Surf Sci 590 (2005) 127–137. https://doi.org/10.1016/j.susc.2005.05.057.
- [332] M. Tian, C. Wang, Y. Han, X. Wang, Recent Advances of Oxygen Carriers for Chemical Looping Reforming of Methane, ChemCatChem 13 (2021) 1615–1637. <a href="https://doi.org/10.1002/cctc.202001481">https://doi.org/10.1002/cctc.202001481</a>.
- [333] M. Zhu, Y. Song, S. Chen, M. Li, L. Zhang, W. Xiang, Chemical looping dry reforming of methane with hydrogen generation on Fe<sub>2</sub>O<sub>3</sub>/Al<sub>2</sub>O<sub>3</sub> oxygen carrier, Chemical Engineering Journal 368 (2019) 812–823. <a href="https://doi.org/10.1016/j.cej.2019.02.197">https://doi.org/10.1016/j.cej.2019.02.197</a>.
- [334] S. Chuayboon, S. Abanades, S. Rodat, Stepwise Solar Methane Reforming and Water-Splitting via Lattice Oxygen Transfer in Iron and Cerium Oxides, Energy Technology 8 (2020). https://doi.org/10.1002/ente.201900415.
- [335] D. Li, R. Xu, X. Li, Z. Li, X. Zhu, K. Li, Chemical Looping Conversion of Gaseous and Liquid Fuels for Chemical Production: A Review, Energy and Fuels 34 (2020) 5381–5413. https://doi.org/10.1021/acs.energyfuels.0c01006.
- [336] M.A. Peña, J.L.G. Fierro, Chemical Structures and Performance of Perovskite Oxides, Chem Rev 101 (2001) 1981–2018. https://doi.org/10.1021/cr980129f.
- [337] T. Dawa, B. Sajjadi, Exploring the potential of perovskite structures for chemical looping technology: A state-of-the-art review, Fuel Processing Technology 253 (2024). <a href="https://doi.org/10.1016/j.fuproc.2023.108022">https://doi.org/10.1016/j.fuproc.2023.108022</a>.
- [338] Y. Li, M. Chen, L. Jiang, D. Tian, K. Li, Perovskites as oxygen storage materials for chemical looping partial oxidation and reforming of methane, Physical Chemistry Chemical Physics 26 (2023) 1516–1540. https://doi.org/10.1039/d3cp04626e.
- [339] M. Qasim, M. Ayoub, N.A. Ghazali, A. Aqsha, M. Ameen, Recent Advances and Development of Various Oxygen Carriers for the Chemical Looping Combustion Process: A Review, Ind Eng Chem Res 60 (2021) 8621–8641. <a href="https://doi.org/10.1021/acs.iecr.1c01111">https://doi.org/10.1021/acs.iecr.1c01111</a>.
- [340] Z. Sarshar, F. Kleitz, S. Kaliaguine, Novel oxygen carriers for chemical looping combustion: La<sub>1-x</sub>Ce<sub>x</sub>BO<sub>3</sub> (B = Co, Mn) perovskites synthesized by reactive grinding and nanocasting, Energy Environ Sci 4 (2011) 4258. https://doi.org/10.1039/c1ee01716k.
- [341] L. Liu, Z. Li, Y. Wang, Z. Li, Y. Larring, N. Cai, Industry-scale production of a perovskite oxide as oxygen carrier material in chemical looping, Chemical Engineering Journal 431 (2022) 134006. https://doi.org/10.1016/j.cej.2021.134006.
- [342] X. Li, Z. Li, C. Lu, D. Li, Z. Li, J. Gao, J. Wei, K. Li, Enhanced performance of LaFeO<sub>3</sub> oxygen carriers by NiO for chemical looping partial oxidation of methane, Fuel Processing Technology 236 (2022). https://doi.org/10.1016/j.fuproc.2022.107396.
- [343] D. Cao, C. Luo, F. Wu, L. Zhang, X. Li, Screening loaded perovskite oxygen carriers for chemical looping steam methane reforming, J Environ Chem Eng 10 (2022) 107315. https://doi.org/10.1016/j.jece.2022.107315.

- [344] Z. Bian, Z. Wang, B. Jiang, P. Hongmanorom, W. Zhong, S. Kawi, A review on perovskite catalysts for reforming of methane to hydrogen production, Renewable and Sustainable Energy Reviews 134 (2020) 110291. https://doi.org/10.1016/j.rser.2020.110291.
- [345] M. Tang, L. Xu, M. Fan, Progress in oxygen carrier development of methane-based chemical-looping reforming: A review, Appl Energy 151 (2015) 143–156. https://doi.org/10.1016/j.apenergy.2015.04.017.
- [346] K. Wang, X. Yuan, W. Liang, S. Yao, J. Li, C. Wang, G. Yue, Red mud-based perovskite oxygen carrier preparation for chemical looping gasification of municipal sludge, Waste Management 177 (2024) 169–176. https://doi.org/10.1016/j.wasman.2024.01.042.
- [347] J.J. Torrez-Herrera, S.A. Korili, A. Gil, Progress in the synthesis and applications of hexaaluminate-based catalysts, Catal Rev Sci Eng 64 (2022) 592–630. https://doi.org/10.1080/01614940.2020.1831756.
- [348] K. Skrbek, O. Jankovský, M. Lojka, F. Antončík, V. Bartůněk, Synthesis of nanosized LaFeAl<sub>11</sub>O<sub>19</sub> hexaaluminate by mixed metal glycerolate method, Ceram Int 47 (2021) 29653–29659. https://doi.org/10.1016/j.ceramint.2021.07.135.
- [349] Y. Zhu, R. Liu, X. Sun, X. Ma, X. Wang, H. Tian, Metal modified hexaaluminates for syngas generation and CO<sub>2</sub> utilization via chemical looping, Int J Hydrogen Energy 44 (2019) 10218–10231. https://doi.org/10.1016/j.ijhydene.2019.02.187.
- [350] M. Tian, X. Wang, X. Liu, A. Wang, T. Zhang, Fe-substituted Ba-hexaaluminates oxygen carrier for carbon dioxide capture by chemical looping combustion of methane, AIChE Journal 62 (2016) 792–801. https://doi.org/10.1002/aic.15135.
- [351] X. Sun, L. Zhu, W. Zhao, F. Li, X. Chen, Ni-Fe bimetallic hexaaluminate for efficient reduction of O<sub>2</sub>-containing CO<sub>2</sub> via chemical looping, Chemical Engineering Journal 441 (2022) 136071. https://doi.org/10.1016/j.cej.2022.136071.
- [352] Q. Yang, L. Chen, N. Jin, Y. Zhu, J. He, P. Zhao, C. Huang, L. Wei, X. Ma, X. Wang, Boosted carbon resistance of ceria-hexaaluminate by in-situ formed CeFe<sub>x</sub>Al<sub>1-x</sub>O<sub>3</sub> as oxygen pool for chemical looping dry reforming of methane, Appl Catal B 330 (2023) 122636. <a href="https://doi.org/10.1016/j.apcatb.2023.122636">https://doi.org/10.1016/j.apcatb.2023.122636</a>.
- [353] M. Tian, X.D. Wang, T. Zhang, Hexaaluminates: a review of the structure, synthesis and catalytic performance, Catal Sci Technol 6 (2016) 1984–2004. https://doi.org/10.1039/C5CY02077H.
- [354] A. Trovarelli, Catalytic Properties of Ceria and CeO<sub>2</sub>-Containing Materials, Catalysis Reviews 38 (1996) 439–520. <a href="https://doi.org/10.1080/01614949608006464">https://doi.org/10.1080/01614949608006464</a>.
- [355] T. Montini, M. Melchionna, M. Monai, P. Fornasiero, Fundamentals and Catalytic Applications of CeO<sub>2</sub>-Based Materials, Chem Rev 116 (2016) 5987–6041. https://doi.org/10.1021/acs.chemrev.5b00603.
- [356] P. Li, X. Chen, Y. Li, J.W. Schwank, A review on oxygen storage capacity of CeO<sub>2</sub>-based materials: Influence factors, measurement techniques, and applications in reactions related to catalytic automotive emissions control, Catal Today (2019) 90–115. <a href="https://doi.org/10.1016/j.cattod.2018.05.059">https://doi.org/10.1016/j.cattod.2018.05.059</a>.
- [357] Z.Q. Huang, T. Zhang, C.R. Chang, J. Li, Dynamic Frustrated Lewis Pairs on Ceria for Direct Nonoxidative Coupling of Methane, ACS Catal 9 (2019) 5523–5536. https://doi.org/10.1021/acscatal.9b00838.
- [358] E.G. Maulidanti, M. Awaji, K. Asami, Low temperature oxidative coupling of methane over cerium oxide based catalyst, Gas Science and Engineering 116 (2023). <a href="https://doi.org/10.1016/j.jgsce.2023.205057">https://doi.org/10.1016/j.jgsce.2023.205057</a>.
- [359] W.Z. Yu, M.Y. Wu, W.W. Wang, C.J. Jia, In Situ Generation of the Surface Oxygen Vacancies in a Copper-Ceria Catalyst for the Water-Gas Shift Reaction, Langmuir 37 (2021) 10499–10509. https://doi.org/10.1021/acs.langmuir.1c01428.
- [360] P. Ebrahimi, A. Kumar, M. Khraisheh, A Review of CeO<sub>2</sub> Supported Catalysts for CO<sub>2</sub> Reduction to CO through the Reverse Water Gas Shift Reaction, Catalysts 12 (2022). https://doi.org/10.3390/catal12101101.

- [361] A. Trovarelli, C. de Leitenburg, M. Boaro, G. Dolcetti, The utilization of ceria in industrial catalysis, Catal Today 50 (1999) 353–367. <a href="https://doi.org/10.1016/S0920-5861(98)00515-X">https://doi.org/10.1016/S0920-5861(98)00515-X</a>.
- [362] M. Kurian, Cerium oxide based materials for water treatment-A review, J Environ Chem Eng 8 (2020). <a href="https://doi.org/10.1016/j.jece.2020.104439">https://doi.org/10.1016/j.jece.2020.104439</a>.
- [363] L. Lei, Y. Wang, Z. Zhang, J. An, F. Wang, Transformations of Biomass, Its Derivatives, and Downstream Chemicals over Ceria Catalysts, ACS Catal 10 (2020) 8788–8814. https://doi.org/10.1021/acscatal.0c01900.
- [364] M. Stoian, V. Rogé, L. Lazar, T. Maurer, J.C. Védrine, I.C. Marcu, I. Fechete, Total oxidation of methane on oxide and mixed oxide ceria-containing catalysts, Catalysts 11 (2021). https://doi.org/10.3390/catal11040427.
- [365] A.C. Chien, N.J. Ye, C.W. Huang, I.H. Tseng, Studies of nickel/samarium-doped ceria for catalytic partial oxidation of methane and effect of oxygen vacancy, Catalysts 11 (2021). https://doi.org/10.3390/catal11060731.
- [366] H. Wang, L. Wang, Q. Luo, J. Zhang, C. Wang, X. Ge, W. Zhang, F.S. Xiao, Two-dimensional manganese oxide on ceria for the catalytic partial oxidation of hydrocarbons, Chemical Synthesis 2 (2022). <a href="https://doi.org/10.20517/cs.2022.02">https://doi.org/10.20517/cs.2022.02</a>.
- [367] D. Khurana, N. Dahiya, S. Negi, A. Bordoloi, M. Ali Haider, R. Bal, T.S. Khan, Improving the Coke Resistance of Ni-Ceria Catalysts for Partial Oxidation of Methane to Syngas: Experimental and Computational Study, Chem Asian J 18 (2023). https://doi.org/10.1002/asia.202201298.
- [368] L.G. Moura, R.P. Borges, F.B. Noronha, C.E. Hori, Steam reforming of liquefied petroleum gas using catalysts supported on ceria-silica, Int J Hydrogen Energy 46 (2021) 1801–1814. https://doi.org/10.1016/j.ijhydene.2020.10.021.
- [369] W.N. Manan, W.N.R. Wan Isahak, Z. Yaakob, CeO<sub>2</sub>-Based Heterogeneous Catalysts in Dry Reforming Methane and Steam Reforming Methane: A Short Review, Catalysts 12 (2022). https://doi.org/10.3390/catal12050452.
- [370] L.P. Teh, H.D. Setiabudi, S.N. Timmiati, M.A.A. Aziz, N.H.R. Annuar, N.N. Ruslan, Recent progress in ceria-based catalysts for the dry reforming of methane: A review, Chem Eng Sci 242 (2021). https://doi.org/10.1016/j.ces.2021.116606.
- [371] Y.G. Kim, Y. Lee, N. Lee, M. Soh, D. Kim, T. Hyeon, Ceria-Based Therapeutic Antioxidants for Biomedical Applications, Advanced Materials 36 (2024). https://doi.org/10.1002/adma.202210819.
- [372] A. Vijayan, S. Ramadoss, N. Sisubalan, M. Gnanaraj, K. Chandrasekaran, V. Kokkarachedu, Cerium Oxide Nanoparticles for Biomedical Applications, in: V. Kokkarachedu, R. Sadiku (Eds.), Nanoparticles in Modern Antimicrobial and Antiviral Applications. Nanotechnology in the Life Sciences (NALIS)., 1st ed., Springer Cham, 2024: pp. 175–200. <a href="https://doi.org/10.1007/978-3-031-50093-0">https://doi.org/10.1007/978-3-031-50093-0</a> 8.
- [373] H. Okamoto, Ce-O (Cerium-Oxygen), J Phase Equilibria Diffus 29 (2008) 545–547. https://doi.org/10.1007/s11669-008-9392-y.
- [374] R. Schmitt, A. Nenning, O. Kraynis, R. Korobko, A.I. Frenkel, I. Lubomirsky, S.M. Haile, J.L.M. Rupp, A review of defect structure and chemistry in ceria and its solid solutions, Chem Soc Rev 49 (2020) 554–592. <a href="https://doi.org/10.1039/c9cs00588a">https://doi.org/10.1039/c9cs00588a</a>.
- [375] S. Ackermann, J.R. Scheffe, A. Steinfeld, Diffusion of oxygen in ceria at elevated temperatures and its application to H<sub>2</sub>O/CO<sub>2</sub> splitting thermochemical redox cycles, Journal of Physical Chemistry C 118 (2014) 5216–5225. https://doi.org/10.1021/jp500755t.
- [376] T. Nagata, K. Miyajima, R.A. Hardy, G.F. Metha, F. Mafuné, Reactivity of oxygen deficient cerium oxide clusters with small gaseous molecules, Journal of Physical Chemistry A 119 (2015) 5545–5552. https://doi.org/10.1021/acs.jpca.5b02816.
- [377] G.B. Haxel, J.B. Hedrick, G.J. Orris, U.S. Geological Survey Fact Sheet 087-02. Rare Earth Elements—Critical Resources for High Technology, U.S. Department of the Interior (2002). https://pubs.usgs.gov/fs/2002/fs087-02 (accessed November 29, 2024).
- [378] E. Allahkarami, B. Rezai, A literature review of cerium recovery from different aqueous solutions, J Environ Chem Eng 9 (2021). <a href="https://doi.org/10.1016/j.jece.2020.104956">https://doi.org/10.1016/j.jece.2020.104956</a>.

- [379] Y. Chen, B. Zheng, What happens after the rare earth crisis: A systematic literature review, Sustainability (Switzerland) 11 (2019). https://doi.org/10.3390/su11051288.
- [380] M. Jaganmohan, Forecast of cerium oxide price globally 2009-2030, Statista (2024). <a href="https://www.statista.com/statistics/450146/global-reo-cerium-oxide-price-forecast/#:~:text=The%20price%20of%20the%20rare,U.S.%20dollars%20per%20metric%20ton.">https://www.statista.com/statistics/450146/global-reo-cerium-oxide-price-forecast/#:~:text=The%20price%20of%20the%20rare,U.S.%20dollars%20per%20metric%20ton.</a> (accessed November 29, 2024).
- [381] F. Wulandari, Nickel Price Forecast: Will the Downtrend Continue in 2025?, Technopedia (2024). <a href="https://www.techopedia.com/investing/nickel-price-forecast">https://www.techopedia.com/investing/nickel-price-forecast</a> (accessed November 30, 2024).
- [382] F. Wulandari, Copper Price Forecast 2024, 2025, 2030: Will the Red Metal's Bull Run Continue?, Technopedia (2024). <a href="https://www.techopedia.com/investing/copper-price-forecast">https://www.techopedia.com/investing/copper-price-forecast</a> (accessed November 30, 2024).
- [383] K. Otsuka, M. Hatano, A. Morikawa, Decomposition of water by cerium oxide of δ-phase, Inorganica Chim Acta 109 (1985) 193–197. <a href="https://doi.org/10.1016/S0020-1693(00)81768-5">https://doi.org/10.1016/S0020-1693(00)81768-5</a>.
- [384] D. Uxa, L. Dörrer, M. Schulz, N. Knoblauch, P. Fielitz, M. Roeb, M. Schmücker, G. Borchardt, Investigation of CO<sub>2</sub> Splitting on Ceria-Based Redox Materials for Low-Temperature Solar Thermochemical Cycling with Oxygen Isotope Exchange Experiments, Processes 11 (2023). <a href="https://doi.org/10.3390/pr11010109">https://doi.org/10.3390/pr11010109</a>.
- [385] N. Gokon, S. Sagawa, T. Kodama, Comparative study of activity of cerium oxide at thermal reduction temperatures of 1300-1550 C for solar thermochemical two-step water-splitting cycle, Int J Hydrogen Energy 38 (2013) 14402–14414. <a href="https://doi.org/10.1016/j.ijhydene.2013.08.108">https://doi.org/10.1016/j.ijhydene.2013.08.108</a>.
- [386] K. Otsuka, Y. Wang, E. Sunada, I. Yamanaka, Direct Partial Oxidation of Methane to Synthesis Gas by Cerium Oxide, J Catal 175 (1998) 152–160. <a href="https://doi.org/10.1006/jcat.1998.1985">https://doi.org/10.1006/jcat.1998.1985</a>.
- [387] A. Storione, M. Minelli, F. Doghieri, E. Landi, F. Miccio, Thermodynamic study on the feasibility of a new combined chemical looping process for syngas production, Chem Eng Trans 86 (2021) 1267–1272. https://doi.org/10.3303/CET2186212.
- [388] K. Otsuka, E. Sunada, T. Ushiyama, I. Yamanaka, The production of synthesis gas by the redox of cerium oxide, (1997) 531–536. <a href="https://doi.org/10.1016/S0167-2991(97)80386-2">https://doi.org/10.1016/S0167-2991(97)80386-2</a>.
- [389] E. Ramírez-Cabrera, A. Atkinson, D. Chadwick, Reactivity of ceria, Gd- and Nb-doped ceria to methane, Appl Catal B 36 (2002) 193–206. https://doi.org/10.1016/S0926-3373(01)00299-5.
- [390] H.H. Jeong, J.H. Kwak, G.Y. Han, K.J. Yoon, Stepwise production of syngas and hydrogen through methane reforming and water splitting by using a cerium oxide redox system, Int J Hydrogen Energy 36 (2011) 15221–15230. https://doi.org/10.1016/j.ijhydene.2011.08.079.
- [391] X. Zhu, H. Wang, Y. Wei, K. Li, X. Cheng, Hydrogen and syngas production from two-step steam reforming of methane using CeO<sub>2</sub> as oxygen carrier, Journal of Natural Gas Chemistry 20 (2011) 281–286. <a href="https://doi.org/10.1016/S1003-9953(10)60185-5">https://doi.org/10.1016/S1003-9953(10)60185-5</a>.
- [392] C.G. Rotaru, G. Postole, M. Florea, F. Matei-Rutkovska, V.I. Pârvulescu, P. Gelin, Dry reforming of methane on ceria prepared by modified precipitation route, Appl Catal A Gen 494 (2015) 29–40. https://doi.org/10.1016/j.apcata.2015.01.024.
- [393] F. Matei-Rutkovska, G. Postole, C.G. Rotaru, M. Florea, V.I. Pârvulescu, P. Gelin, Synthesis of ceria nanopowders by microwave-assisted hydrothermal method for dry reforming of methane, Int J Hydrogen Energy 41 (2016) 2512–2525. https://doi.org/10.1016/j.ijhydene.2015.12.097.
- [394] M.M. Nair, S. Abanades, Tailoring Hybrid Nonstoichiometric Ceria Redox Cycle for Combined Solar Methane Reforming and Thermochemical Conversion of H<sub>2</sub>O/CO<sub>2</sub>, Energy and Fuels 30 (2016) 6050–6058. <a href="https://doi.org/10.1021/acs.energyfuels.6b01063">https://doi.org/10.1021/acs.energyfuels.6b01063</a>.
- [395] X. Gao, A. Vidal, A. Bayon, R. Bader, J. Hinkley, W. Lipiński, A. Tricoli, Efficient ceria nanostructures for enhanced solar fuel production: Via high-temperature thermochemical redox cycles, J Mater Chem A Mater 4 (2016) 9614–9624. https://doi.org/10.1039/c6ta02187e.
- [396] M. Welte, K. Warren, J.R. Scheffe, A. Steinfeld, Combined Ceria Reduction and Methane Reforming in a Solar-Driven Particle-Transport Reactor, Ind Eng Chem Res 56 (2017) 10300–10308. https://doi.org/10.1021/acs.iecr.7b02738.

- [397] A. Riaz, M.U. Ali, W. Lipiński, A. Lowe, Enhanced oxygen exchange capacity in nano-structured vanadia-ceria multi-phase oxygen carriers for solar thermal fuel production, J Mater Chem A Mater 7 (2019) 27347–27360. https://doi.org/10.1039/c9ta06471k.
- [398] K.J. Warren, R.J. Carrillo, B. Greek, C.M. Hill, J.R. Scheffe, Solar Reactor Demonstration of Efficient and Selective Syngas Production via Chemical-Looping Dry Reforming of Methane over Ceria, Energy Technology 8 (2020). <a href="https://doi.org/10.1002/ente.202000053">https://doi.org/10.1002/ente.202000053</a>.
- [399] S. Chuayboon, S. Abanades, S. Rodat, Solar chemical looping reforming of methane combined with isothermal H<sub>2</sub>O/CO<sub>2</sub> splitting using ceria oxygen carrier for syngas production, Journal of Energy Chemistry 41 (2020) 60–72. https://doi.org/10.1016/j.jechem.2019.05.004.
- [400] S. Chuayboon, S. Abanades, S. Rodat, Stepwise Solar Methane Reforming and Water-Splitting via Lattice Oxygen Transfer in Iron and Cerium Oxides, Energy Technology 8 (2020). https://doi.org/10.1002/ente.201900415.
- [401] A. Haeussler, S. Chuayboon, S. Abanades, Solar redox cycling of ceria in a monolithic reactor for two-step H<sub>2</sub>O/CO<sub>2</sub> splitting: Isothermal methane-induced reduction versus temperature-swing cycle, in: AIP Conf Proc, American Institute of Physics Inc., 2020. https://doi.org/10.1063/5.0028582.
- [402] A. Farooqui, A. Bose, M. Boaro, J. Llorca, M. Santarelli, Assessment of integration of methane-reduced ceria chemical looping CO<sub>2</sub>/H<sub>2</sub>O splitting cycle to an oxy-fired power plant, Int J Hydrogen Energy 45 (2020) 6184–6206. https://doi.org/10.1016/j.ijhydene.2019.12.182.
- [403] A. Riaz, F. Kremer, T. Kim, S. Sattayaporn, T. Tsuzuki, W. Lipiński, A. Lowe, Experimental demonstration of vanadium-doped nanostructured ceria for enhanced solar thermochemical syngas production, Nano Energy 81 (2021). <a href="https://doi.org/10.1016/j.nanoen.2020.105639">https://doi.org/10.1016/j.nanoen.2020.105639</a>.
- [404] F. Miccio, E. Landi, A.N. Murri, M. Minelli, F. Doghieri, A. Storione, Fluidized bed reforming of methane by chemical looping with cerium oxide oxygen carriers, Chemical Engineering Research and Design 191 (2023) 568–577. https://doi.org/10.1016/j.cherd.2023.02.007.
- [405] A.J. Carrillo, L. Navarrete, M. Laqdiem, M. Balaguer, J.M. Serra, Boosting methane partial oxidation on ceria through exsolution of robust Ru nanoparticles, Mater Adv 2 (2021) 2924–2934. https://doi.org/10.1039/d1ma00044f.
- [406] D. Kang, M. Lee, H.S. Lim, J.W. Lee, Chemical looping partial oxidation of methane with CO<sub>2</sub> utilization on the ceria-enhanced mesoporous Fe<sub>2</sub>O<sub>3</sub> oxygen carrier, Fuel 215 (2018) 787–798. https://doi.org/10.1016/j.fuel.2017.11.106.
- [407] F.R. García-García, I.S. Metcalfe, Chemical looping dry reforming of methane using mixed oxides of iron and cerium: Operation window, Catal Commun 160 (2021). https://doi.org/10.1016/j.catcom.2021.106356.
- [408] W. Zhang, L. Zhang, S. Pei, J. Wang, D. Liu, X. Ma, M. Fan, L. Xu, Rational design and reduction kinetics of efficient Ce-Co oxygen carriers for chemical looping reforming of methane, Fuel 345 (2023). <a href="https://doi.org/10.1016/j.fuel.2023.128208">https://doi.org/10.1016/j.fuel.2023.128208</a>.
- [409] X. Zhang, J. Wang, Z. Song, X. Zhao, J. Sun, Y. Mao, W. Wang, Co<sub>3</sub>O<sub>4</sub>-CeO<sub>2</sub> for enhanced syngas by low-temperature methane conversion with CO<sub>2</sub> utilization via a catalytic chemical looping process, Fuel Processing Technology 245 (2023). https://doi.org/10.1016/j.fuproc.2023.107741.
- [410] A. Löfberg, J. Guerrero-Caballero, T. Kane, A. Rubbens, L. Jalowiecki-Duhamel, Ni/CeO<sub>2</sub> based catalysts as oxygen vectors for the chemical looping dry reforming of methane for syngas production, Appl Catal B 212 (2017) 159–174. <a href="https://doi.org/10.1016/j.apcatb.2017.04.048">https://doi.org/10.1016/j.apcatb.2017.04.048</a>.
- [411] C. Hill, R. Robbins, P. Furler, S. Ackermann, J. Scheffe, Kinetic investigation of solar chemical looping reforming of methane over Ni-CeO<sub>2</sub> at low temperature, Sustain Energy Fuels 7 (2022) 574–584. https://doi.org/10.1039/d2se01452a.
- [412] J. Guerrero-Caballero, T. Kane, N. Haidar, L. Jalowiecki-Duhamel, A. Löfberg, Ni, Co, Fe supported on Ceria and Zr doped Ceria as oxygen carriers for chemical looping dry reforming of methane, Catal Today 333 (2019) 251–258. https://doi.org/10.1016/j.cattod.2018.11.064.
- [413] H. Lu, X. Shi, M. Costa, C. Huang, Carcinogenic effect of nickel compounds, Mol Cell Biochem 279 (2005) 45–67. <a href="https://doi.org/10.1007/s11010-005-8215-2">https://doi.org/10.1007/s11010-005-8215-2</a>.

- [414] D. Kunii, O. Levenspiel, Chapter 1 Introduction, in: Fluidization Engineering, 2nd ed., Butterworth-Heinemann, Elsevier, Newton (MA), 1991: pp. 1–13. <a href="https://doi.org/10.1016/B978-0-08-050664-7.50007-X">https://doi.org/10.1016/B978-0-08-050664-7.50007-X</a>.
- [415] A. Ugwu, A. Zaabout, S. Amini, An advancement in CO<sub>2</sub> utilization through novel gas switching dry reforming, International Journal of Greenhouse Gas Control 90 (2019) 102791. https://doi.org/10.1016/j.ijggc.2019.102791.
- [416] J. Francisco Morgado, S. Cloete, J. Morud, T. Gurker, S. Amini, Modelling study of two chemical looping reforming reactor configurations: looping vs. switching, Powder Technol 316 (2017) 599–613. https://doi.org/10.1016/j.powtec.2016.11.059.
- [417] X. Cheng, Z. Xu, L. Jiang, M. Zheng, Z. Gu, D. Tian, K. Li, H. Wang, Self-regulation of bed temperature field of the fixed-bed reactor unit by composite-filled oxygen carriers for chemical looping combustion of methane, Chemical Engineering Journal 481 (2024). https://doi.org/10.1016/j.cej.2023.148396.
- [418] Z. Zhou, L. Han, G.M. Bollas, Overview of chemical-looping reduction in fixed bed and fluidized bed reactors focused on oxygen carrier utilization and reactor efficiency, Aerosol Air Qual Res 14 (2014) 559–571. <a href="https://doi.org/10.4209/aaqr.2013.06.0198">https://doi.org/10.4209/aaqr.2013.06.0198</a>.
- [419] S. Cloete, F. Gallucci, M. van Sint Annaland, S. Amini, Gas Switching as a Practical Alternative for Scaleup of Chemical Looping Combustion, Energy Technology 4 (2016) 1286–1298. https://doi.org/10.1002/ente.201600027.
- [420] Z. Gao, D. Wu, F. Yin, L. Sun, D. Zeng, R. Xiao, Thermodynamic and kinetic analysis on the biomass syngas fueled chemical looping hydrogen generation process in fixed bed reactor, Energy 298 (2024). <a href="https://doi.org/10.1016/j.energy.2024.131308">https://doi.org/10.1016/j.energy.2024.131308</a>.
- [421] J. Koornneef, M. Junginger, A. Faaij, Development of fluidized bed combustion-An overview of trends, performance and cost, Prog Energy Combust Sci 33 (2007) 19–55. https://doi.org/10.1016/j.pecs.2006.07.001.
- [422] D. Kunii, Levenspiel Octave, Chapter 3 Fluidization and Mapping of Regimes, in: Fluidization Engineering, 2nd ed., Butterworth-Heinemann, Elsevier, Newton (MA), 1991: pp. 61–94. https://doi.org/10.1016/B978-0-08-050664-7.50009-3.
- [423] J. Aronsson, E. Krymarys, V. Stenberg, T. Mattisson, A. Lyngfelt, M. Rydén, Improved Gas-Solids Mass Transfer in Fluidized Beds: Confined Fluidization in Chemical-Looping Combustion, Energy and Fuels 33 (2019) 4442–4453. <a href="https://doi.org/10.1021/acs.energyfuels.9b00508">https://doi.org/10.1021/acs.energyfuels.9b00508</a>.
- [424] N. Galinsky, S. Bayham, E. Monazam, R.W. Breault, Oxygen Carrier Structure and Attrition, in: Handbook of Chemical Looping Technology, 1st ed., Wiley, 2018: pp. 263–301. https://doi.org/10.1002/9783527809332.ch9.
- [425] C. Arnaiz del Pozo, S. Cloete, J.H. Cloete, Á. Jiménez Álvaro, S. Amini, The potential of chemical looping combustion using the gas switching concept to eliminate the energy penalty of CO<sub>2</sub> capture, International Journal of Greenhouse Gas Control 83 (2019) 265–281. <a href="https://doi.org/10.1016/j.ijggc.2019.01.018">https://doi.org/10.1016/j.ijggc.2019.01.018</a>.
- [426] A. Ugwu, C. Arnaiz del Pozo, A. Zaabout, S.M. Nazir, N.U. Kalendar, S. Cloete, S. Szima, S. Fogarasi, F. Donat, G. van Diest, J.H. Cloete, Á. Jiménez Álvaro, K. Albertsen, A.M. Cormos, C.C. Cormos, S. Amini, Gas switching technology: Economic attractiveness for chemical looping applications and scale up experience to 50 kWth, International Journal of Greenhouse Gas Control 114 (2022). <a href="https://doi.org/10.1016/j.ijggc.2022.103593">https://doi.org/10.1016/j.ijggc.2022.103593</a>.
- [427] J.W. Chew, W.C.Q. LaMarche, R.A. Cocco, 100 years of scaling up fluidized bed and circulating fluidized bed reactors, Powder Technol 409 (2022). https://doi.org/10.1016/j.powtec.2022.117813.
- [428] M. Osman, A. Zaabout, S. Cloete, S. Amini, Mapping the operating performance of a novel internally circulating fluidized bed reactor applied to chemical looping combustion, Fuel Processing Technology 197 (2020). <a href="https://doi.org/10.1016/j.fuproc.2019.106183">https://doi.org/10.1016/j.fuproc.2019.106183</a>.
- [429] M.N. Khan, T. Shamim, Techno-economic assessment of a plant based on a three reactor chemical looping reforming system, Int J Hydrogen Energy 41 (2016) 22677–22688. https://doi.org/10.1016/j.ijhydene.2016.09.016.

- [430] S.M. Nazir, J.F. Morgado, O. Bolland, R. Quinta-Ferreira, S. Amini, Techno-economic assessment of chemical looping reforming of natural gas for hydrogen production and power generation with integrated CO<sub>2</sub> capture, International Journal of Greenhouse Gas Control 78 (2018) 7–20. <a href="https://doi.org/10.1016/j.ijggc.2018.07.022">https://doi.org/10.1016/j.ijggc.2018.07.022</a>.
- [431] M.N. Khan, T. Shamim, Techno-economic assessment of a chemical looping reforming combined cycle plant with iron and tungsten based oxygen carriers, Int J Hydrogen Energy 44 (2019) 11525–11534. https://doi.org/10.1016/j.ijhydene.2019.03.109.
- [432] V. Spallina, G. Motamedi, F. Gallucci, M. van Sint Annaland, Techno-economic assessment of an integrated high pressure chemical-looping process with packed-bed reactors in large scale hydrogen and methanol production, International Journal of Greenhouse Gas Control 88 (2019) 71–84. <a href="https://doi.org/10.1016/j.ijggc.2019.05.026">https://doi.org/10.1016/j.ijggc.2019.05.026</a>.
- [433] O. Palone, G.G. Gagliardi, M. Mechelli, L. Cedola, D. Borello, Techno-economic analysis of sustainable methanol and ammonia production by chemical looping hydrogen generation from waste plastic, Energy Convers Manag 292 (2023) 117389. https://doi.org/10.1016/j.enconman.2023.117389.
- [434] H.C. Mantripragada, G. Veser, Intensifying chemical looping dry reforming: Process modeling and systems analysis, Journal of CO<sub>2</sub> Utilization 49 (2021). <a href="https://doi.org/10.1016/j.jcou.2021.101555">https://doi.org/10.1016/j.jcou.2021.101555</a>.
- [435] H.C. Mantripragada, G. Veser, Hydrogen production via chemical looping dry reforming of methane: Process modeling and systems analysis, AIChE Journal 68 (2022). https://doi.org/10.1002/aic.17612.
- [436] Y. Wang, Y. Zheng, Y. Wang, K. Li, Y. Wang, L. Jiang, X. Zhu, Y. Wei, H. Wang, Syngas production modified by oxygen vacancies over CeO<sub>2</sub>-ZrO<sub>2</sub>-CuO oxygen carrier via chemical looping reforming of methane, Appl Surf Sci 481 (2019) 151–160. https://doi.org/10.1016/j.apsusc.2019.03.050.
- [437] J.F.W. Bowles, Oxides, in: Encyclopedia of Geology, Elsevier, 2021: pp. 428–441. https://doi.org/10.1016/B978-0-08-102908-4.00185-5.
- [438] N. Koleli, A. Demir, Chapter 11-Chromite, Environmental Materials and Waste. Resource Recovery and Pollution Prevention (2016) 245–263. https://doi.org/10.1016/B978-0-12-803837-6.00011-1.
- [439] F. Nurjaman, S. Subandrio, D. Ferdian, B. Suharno, Effect of basicity on beneficiated chromite sand smelting process using submerged arc furnace, Proceedings of the International Seminar on Metallurgy and Materials (ISMM2017): Metallurgy and Advanced Material Technology for Sustainable Development (2018) 020009. https://doi.org/10.1063/1.5038291.
- [440] H. Zhang, Y. Lei, A.J. Kropf, G. Zhang, J.W. Elam, J.T. Miller, F. Sollberger, F. Ribeiro, M.C. Akatay, E.A. Stach, J.A. Dumesic, C.L. Marshall, Enhancing the stability of copper chromite catalysts for the selective hydrogenation of furfural using ALD overcoating, J Catal 317 (2014) 284–292. <a href="https://doi.org/10.1016/j.jcat.2014.07.007">https://doi.org/10.1016/j.jcat.2014.07.007</a>.
- [441] C.D.V. Prasad, P. Kanakaraju, R. Vinu, A.P. Deshpande, Synthesis of HHTPB by partial hydrogenation of HTPB using copper chromite as a catalyst, Propellants, Explosives, Pyrotechnics 49 (2024). <a href="https://doi.org/10.1002/prep.202300339">https://doi.org/10.1002/prep.202300339</a>.
- [442] J. Chen, W. Shi, J. Li, Catalytic combustion of methane over cerium-doped cobalt chromite catalysts, Catal Today 175 (2011) 216–222. <a href="https://doi.org/10.1016/j.cattod.2011.03.061">https://doi.org/10.1016/j.cattod.2011.03.061</a>.
- [443] P. Zhao, M. Ehara, A. Satsuma, S. Sakaki, Theoretical Study of the Propene Combustion Catalysis of Chromite Spinels: Reaction Mechanism and Relation between the Activity and Electronic Structure of Spinels, The Journal of Physical Chemistry C 125 (2021) 25983–26002. <a href="https://doi.org/10.1021/acs.jpcc.1c06760">https://doi.org/10.1021/acs.jpcc.1c06760</a>.
- [444] H. Ueda, Y. Matsui, Y. Sawaki, Abiotic Methane Generation via CO<sub>2</sub> Hydrogenation With Natural Chromitite Under Hydrothermal Conditions, Geochemistry, Geophysics, Geosystems 22 (2021). https://doi.org/10.1029/2020GC009533.
- [445] S. Das, A. Biswas, J. Bhattacharya, C.S. Tiwary, M. Paliwal, Utilization of laterite ore as an oxygen carrier in chemical looping reforming of methane for syngas production, Int J Hydrogen Energy 48 (2023) 19411–19421. https://doi.org/10.1016/j.ijhydene.2023.02.054.

- [446] S. Das, F. Eden, M. Paliwal, Syngas production through multi-cycle chemical looping of chromite mines waste: A sustainable approach to mitigate CO<sub>2</sub> emissions, J Clean Prod 420 (2023) 138412. https://doi.org/10.1016/j.jclepro.2023.138412.
- [447] Z. Zhao, Redox kinetics study for chemical-looping combustion, water and CO<sub>2</sub> splitting using nickel and cerium-based oxygen carrier, Ph. D. Thesis, Massachusetts Institute of Technology, 2016. <a href="http://hdl.handle.net/1721.1/106783">http://hdl.handle.net/1721.1/106783</a> (accessed December 9, 2024).
- [448] D. Knapp, T. Ziegler, Methane dissociation on the ceria (111) surface, Journal of Physical Chemistry C 112 (2008) 17311–17318. <a href="https://doi.org/10.1021/jp8039862">https://doi.org/10.1021/jp8039862</a>.
- [449] C.S.T. Peraça, K.F. Andriani, M.J. Piotrowski, J.L.F. Da Silva, Ab Initio Investigation of CH<sub>4</sub> Dehydrogenation on a (CeO<sub>2</sub>)<sub>10</sub> Cluster, Journal of Physical Chemistry C 126 (2022) 11937–11948. https://doi.org/10.1021/acs.jpcc.2c02038.
- [450] H. Arunachalam, G. Pozzato, M.A. Hoffman, S. Onori, Modeling the thermal and soot oxidation dynamics inside a ceria-coated gasoline particulate filter, Control Eng Pract 94 (2020). https://doi.org/10.1016/j.conengprac.2019.104199.
- [451] Aspentech, Aspen Adsorption, Aspentech (2024). <a href="https://www.aspentech.com/en/products/engineering/aspen-adsorption-and-aspen-chromatography">https://www.aspentech.com/en/products/engineering/aspen-adsorption-and-aspen-chromatography</a> (accessed December 9, 2024).
- [452] C.G. Visconti, Alumina: A Key-Component of Structured Catalysts for Process Intensification, Transactions of the Indian Ceramic Society 71 (2012) 123–136. https://doi.org/10.1080/0371750X.2012.738481.
- [453] F. Miccio, M. Mazzocchi, M. Boscherini, A. Storione, M. Minelli, F. Doghieri, The Trade-Off between Combustion and Partial Oxidation during Chemical Looping Conversion of Methane, Energies (Basel) 17 (2024) 2764. <a href="https://doi.org/10.3390/en17112764">https://doi.org/10.3390/en17112764</a>.
- [454] A. Storione, M. Boscherini, F. Miccio, E. Landi, M. Minelli, F. Doghieri, Improvement of Process Conditions for H<sub>2</sub> Production by Chemical Looping Reforming, Energies (Basel) 17 (2024) 1544. https://doi.org/10.3390/en17071544.
- [455] Z. Wu, Y. Cheng, F. Tao, L. Daemen, G.S. Foo, L. Nguyen, X. Zhang, A. Beste, A.J. Ramirez-Cuesta, Direct Neutron Spectroscopy Observation of Cerium Hydride Species on a Cerium Oxide Catalyst, J Am Chem Soc 139 (2017) 9721–9727. https://doi.org/10.1021/jacs.7b05492.
- [456] Z. Li, K. Werner, L. Chen, A. Jia, K. Qian, J.Q. Zhong, R. You, L. Wu, L. Zhang, H. Pan, X.P. Wu, X.Q. Gong, S. Shaikhutdinov, W. Huang, H.J. Freund, Interaction of Hydrogen with Ceria: Hydroxylation, Reduction, and Hydride Formation on the Surface and in the Bulk, Chemistry A European Journal 27 (2021) 5268–5276. https://doi.org/10.1002/chem.202005374.
- [457] Q. Zhou, H. Akber, A. Zhao, F. Yang, Z. Liu, Interaction of Water with Ceria Thin Film, ChemCatChem 15 (2023). <a href="https://doi.org/10.1002/cctc.202300318">https://doi.org/10.1002/cctc.202300318</a>.
- [458] C. Wang, C.-C. Wei, L. Wan, C.-L. Lin, J.-D. Tsai, Association of exposure to hydrocarbon air pollution with the incidence of atopic dermatitis in children, Ital J Pediatr 47 (2021) 202. https://doi.org/10.1186/s13052-021-01157-7.
- [459] J.-W. Kwon, H.-W. Park, W.J. Kim, M.-G. Kim, S.-J. Lee, Exposure to volatile organic compounds and airway inflammation, Environmental Health 17 (2018) 65. <a href="https://doi.org/10.1186/s12940-018-0410-1">https://doi.org/10.1186/s12940-018-0410-1</a>.
- [460] K.L. Alford, N. Kumar, Pulmonary Health Effects of Indoor Volatile Organic Compounds—A Meta-Analysis, Int J Environ Res Public Health 18 (2021) 1578. <a href="https://doi.org/10.3390/ijerph18041578">https://doi.org/10.3390/ijerph18041578</a>.
- [461] Z. Khorrami, M. Pourkhosravani, M. Rezapour, K. Etemad, S.M. Taghavi-Shahri, N. Künzli, H. Amini, N. Khanjani, Multiple air pollutant exposure and lung cancer in Tehran, Iran, Sci Rep 11 (2021) 9239. https://doi.org/10.1038/s41598-021-88643-4.
- [462] C.P. Rennix, M.M. Quinn, P.J. Amoroso, E.A. Eisen, D.H. Wegman, Risk of breast cancer among enlisted Army women occupationally exposed to volatile organic compounds, Am J Ind Med 48 (2005) 157–167. <a href="https://doi.org/10.1002/ajim.20201">https://doi.org/10.1002/ajim.20201</a>.

- [463] A. Khan, H. Kanwal, S. Bibi, S. Mushtaq, A. Khan, Y.H. Khan, T.H. Mallhi, Volatile Organic Compounds and Neurological Disorders: From Exposure to Preventive Interventions, in: 2021: pp. 201–230. https://doi.org/10.1007/978-3-030-66376-6 10.
- [464] R. Montero-Montoya, R. López-Vargas, O. Arellano-Aguilar, Volatile Organic Compounds in Air: Sources, Distribution, Exposure and Associated Illnesses in Children, Ann Glob Health 84 (2018) 225–238. <a href="https://doi.org/10.29024/aogh.910">https://doi.org/10.29024/aogh.910</a>.
- [465] A.L. Lang, J.I. Beier, Interaction of volatile organic compounds and underlying liver disease: a new paradigm for risk, Biol Chem 399 (2018) 1237–1248. <a href="https://doi.org/10.1515/hsz-2017-0324">https://doi.org/10.1515/hsz-2017-0324</a>.
- [466] X. Zhou, X. Zhou, C. Wang, H. Zhou, Environmental and human health impacts of volatile organic compounds: A perspective review, Chemosphere 313 (2023) 137489. <a href="https://doi.org/10.1016/j.chemosphere.2022.137489">https://doi.org/10.1016/j.chemosphere.2022.137489</a>.
- [467] K. Zhang, L. Li, L. Huang, Y. Wang, J. Huo, Y. Duan, Y. Wang, Q. Fu, The impact of volatile organic compounds on ozone formation in the suburban area of Shanghai, Atmos Environ 232 (2020) 117511. https://doi.org/10.1016/j.atmosenv.2020.117511.
- [468] E. Cetin, M. Odabasi, R. Seyfioglu, Ambient volatile organic compound (VOC) concentrations around a petrochemical complex and a petroleum refinery, Science of The Total Environment 312 (2003) 103–112. https://doi.org/10.1016/S0048-9697(03)00197-9.
- [469] G.H. Pandya, A.G. Gavane, A.D. Bhanarkar, V.K. Kondawar, Concentrations of volatile organic compounds (VOCs) at an oil refinery, International Journal of Environmental Studies 63 (2006) 337–351. https://doi.org/10.1080/00207230500241918.
- [470] D. Hoyt, L.H. Raun, Measured and estimated benzene and volatile organic carbon (VOC) emissions at a major U.S. refinery/chemical plant: Comparison and prioritization, J Air Waste Manage Assoc 65 (2015) 1020–1031. <a href="https://doi.org/10.1080/10962247.2015.1058304">https://doi.org/10.1080/10962247.2015.1058304</a>.
- [471] G. You, S. Lu, Z. Jin, J. Ren, R. Sun, J. Li, W. Hou, S. Xie, Emission Factors and Source Profiles of Volatile Organic Compounds in the Petroleum Refining Industry through On-Site Measurement from Multiple Refineries, Environ Sci Technol Lett 11 (2024) 230–236. <a href="https://doi.org/10.1021/acs.estlett.4c00036">https://doi.org/10.1021/acs.estlett.4c00036</a>.
- [472] L. Barregard, E. Holmberg, G. Sallsten, Leukaemia incidence in people living close to an oil refinery, Environ Res 109 (2009) 985–990. https://doi.org/10.1016/j.envres.2009.09.001.
- [473] C.-K. Lin, Y.-T. Hsu, D.C. Christiani, H.-Y. Hung, R.-T. Lin, Risks and burden of lung cancer incidence for residential petrochemical industrial complexes: A meta-analysis and application, Environ Int 121 (2018) 404–414. <a href="https://doi.org/10.1016/j.envint.2018.09.018">https://doi.org/10.1016/j.envint.2018.09.018</a>.
- [474] G. Axelsson, L. Barregard, E. Holmberg, G. Sallsten, Cancer incidence in a petrochemical industry area in Sweden, Science of The Total Environment 408 (2010) 4482–4487. https://doi.org/10.1016/j.scitotenv.2010.06.028.
- [475] M.S. Sebastián, B. Armstrong, J.A. Córdoba, C. Stephens, Exposures and cancer incidence near oil fields in the Amazon basin of Ecuador, Occup Environ Med 58 (2001) 517–522. https://doi.org/10.1136/oem.58.8.517.
- [476] S.B. Williams, Y. Shan, U. Jazzar, P.S. Kerr, I. Okereke, V.S. Klimberg, D.S. Tyler, N. Putluri, D.S. Lopez, J.D. Prochaska, C. Elferink, J.G. Baillargeon, Y.-F. Kuo, H.B. Mehta, Proximity to Oil Refineries and Risk of Cancer: A Population-Based Analysis, JNCI Cancer Spectr 4 (2020). <a href="https://doi.org/10.1093/jncics/pkaa088">https://doi.org/10.1093/jncics/pkaa088</a>.
- [477] J.L. Domingo, M. Marquès, M. Nadal, M. Schuhmacher, Health risks for the population living near petrochemical industrial complexes. 1. Cancer risks: A review of the scientific literature, Environ Res 186 (2020) 109495. <a href="https://doi.org/10.1016/j.envres.2020.109495">https://doi.org/10.1016/j.envres.2020.109495</a>.
- [478] Z. Zhang, X. Yan, F. Gao, P. Thai, H. Wang, D. Chen, L. Zhou, D. Gong, Q. Li, L. Morawska, B. Wang, Emission and health risk assessment of volatile organic compounds in various processes of a petroleum refinery in the Pearl River Delta, China, Environmental Pollution 238 (2018) 452–461. <a href="https://doi.org/10.1016/j.envpol.2018.03.054">https://doi.org/10.1016/j.envpol.2018.03.054</a>.
- [479] F.M. Onyije, B. Hosseini, K. Togawa, J. Schüz, A. Olsson, Cancer Incidence and Mortality among Petroleum Industry Workers and Residents Living in Oil Producing Communities: A Systematic

- Review and Meta-Analysis, Int J Environ Res Public Health 18 (2021) 4343. https://doi.org/10.3390/ijerph18084343.
- [480] E.M. Andersson, L. Barregard, M. Akerstrom, G. Sallsten, B. Järvholm, R.I. Nilsson, Cancer incidence in Swedish oil refinery workers exposed to benzene, Int J Hyg Environ Health 261 (2024) 114420. <a href="https://doi.org/10.1016/j.ijheh.2024.114420">https://doi.org/10.1016/j.ijheh.2024.114420</a>.
- [481] Veronico, L. Kristin, Y. Hartanto, A. Indarto, Surface cover method to reduce evaporation rate of crude oil, IOP Conf Ser Mater Sci Eng 823 (2020) 012012. <a href="https://doi.org/10.1088/1757-899X/823/1/012012">https://doi.org/10.1088/1757-899X/823/1/012012</a>.
- [482] D. Lv, S. Lu, X. Tan, M. Shao, S. Xie, L. Wang, Source profiles, emission factors and associated contributions to secondary pollution of volatile organic compounds (VOCs) emitted from a local petroleum refinery in Shandong, Environmental Pollution 274 (2021) 116589. <a href="https://doi.org/10.1016/j.envpol.2021.116589">https://doi.org/10.1016/j.envpol.2021.116589</a>.
- [483] S. Saikomol, S. Thepanondh, W. Laowagul, Emission losses and dispersion of volatile organic compounds from tank farm of petroleum refinery complex, J Environ Health Sci Eng 17 (2019) 561–570. https://doi.org/10.1007/s40201-019-00370-1.
- [484] M. Invernizzi, S. Sironi, Odour emission rate estimation methods for hydrocarbon storage tanks, Chem Eng Trans 85 (2021) 67–72. <a href="https://doi.org/10.3303/CET2185012">https://doi.org/10.3303/CET2185012</a>.
- [485] F.M. Howari, Evaporation losses and dispersion of volatile organic compounds from tank farms, Environ Monit Assess 187 (2015). https://doi.org/10.1007/s10661-015-4456-z.
- [486] M. Tamaddoni, R. Sotudeh-Gharebagh, S. Nario, M. Hajihosseinzadeh, N. Mostoufi, Experimental study of the VOC emitted from crude oil tankers, Process Safety and Environmental Protection 92 (2014) 929–937. https://doi.org/10.1016/j.psep.2013.10.005.
- [487] C.A. Haldera, G.S. Van Gorp, N.S. Hatoum, T.M. Warne, Gasoline Vapor Exposures. Part I. Characterization of Workplace Exposures, Am Ind Hyg Assoc J 47 (1986) 164–172. https://doi.org/10.1080/15298668691389522.
- [488] G. Tironi, G.J. Nebel, R.L. Williams, Measurement of Vapor Exposure During Gasoline Refueling, in: SAE International Congress and Exposition, 1986. <a href="https://doi.org/10.4271/860087">https://doi.org/10.4271/860087</a>.
- [489] R. Rota, S. Frattini, S. Astori, R. Paludetto, Emissions from Fixed-Roof Storage Tanks: Modeling and Experiments, Ind Eng Chem Res 40 (2001) 5847–5857. <a href="https://doi.org/10.1021/ie010111m">https://doi.org/10.1021/ie010111m</a>.
- [490] S.S. Virdi, L.Y. Lee, C. Li, A.K. Dev, Simulation of VOC Emission During Loading Operations in a Crude Oil Tanker, International Journal of Maritime Engineering 163 (2021). <a href="https://doi.org/10.3940/rina.ijme.2021.a1.603">https://doi.org/10.3940/rina.ijme.2021.a1.603</a>.
- [491] S.B. Barbeş, A.C. Badea, V. Iordache, Volatile organic compounds losses simulation during storage of gasoline, in: IOP Conf Ser Earth Environ Sci, Institute of Physics, 2023. https://doi.org/10.1088/1755-1315/1185/1/012009.
- [492] A. Maxwell, A. Lawal, Petroleum Product Storage Tank, Design and Loss Control Management, in: All Days, SPE, 2016: pp. 4–6. https://doi.org/10.2118/183615-MS.
- [493] S. Chen, K. Lin, A. Pan, T.C. Ho, Y. Zhu, C.Y. Tso, Study of a passive radiative cooling coating on chemical storage tanks for evaporative loss control, Renew Energy 211 (2023) 326–335. https://doi.org/10.1016/j.renene.2023.04.141.
- [494] P. Rao, S. Ankam, M. Ansari, A.G. Gavane, A. Kumar, V.I. Pandit, P. Nema, Monitoring of hydrocarbon emissions in a petroleum refinery, Environ Monit Assess 108 (2005) 123–132. https://doi.org/10.1007/s10661-005-3961-x.
- [495] C.S. Ooi, W. Keng Ngui, K.H. Hui, H. Lim, M.S. Leong, Review of Underground Storage Tank Condition Monitoring Techniques, MATEC Web of Conferences 255 (2019). https://doi.org/10.1051/matecconf/20192.
- [496] D.K. Stone, S.K. Lynch, R.F. Pandullo, L.B. Evans, W.M. Vatavuk, Flares. Part I: Flaring technologies for controlling VOC-containing waste streams, J Air Waste Manage Assoc 42 (1992) 333–340. https://doi.org/10.1080/10473289.1992.10466996.

- [497] S. Ge, Q. Xu, J. Zhao, S. Wang, T. Ho, X. Lun, Q. Wang, Comprehensive study on air-quality impacts from chemical plant flare emissions under planned or emergency shutdown operations†, Atmos Pollut Res 15 (2024). https://doi.org/10.1016/j.apr.2024.102084.
- [498] New Jersey Department of Environmental Protection-Bureau of Discharge Prevention, Guide to Vapor Recovery Units (VRU), 1998. <a href="https://doi.org/10.7282/T3DJ5DNQ">https://doi.org/10.7282/T3DJ5DNQ</a>.
- [499] F.I. Khan, A. Kr. Ghoshal, Removal of Volatile Organic Compounds from polluted air, J Loss Prev Process Ind 13 (2000) 527–545. <a href="https://doi.org/10.1016/S0950-4230(00)00007-3">https://doi.org/10.1016/S0950-4230(00)00007-3</a>.
- [500] G. Sagun, S. Wiley, J. Barbour, S.K. Lynch, W.R. Pelt, W.M. Vatavuk, Section 3-VOC control; Section 3.1-VOC Recapture Controls; Chapter 2-Refrigerated Condensers, in: EPA/452/B-02-001 EPA Air Pollution Control Cost Manual, 6th ed., United States Environmental Protection Agency-Office of Air Quality Planning and Standards, 2002. <a href="https://nepis.epa.gov/Exe/ZyNET.exe/910118CI.TXT?ZyActionD=ZyDocument&Client=EPA&Index=2000+Thru+2005&Docs=&Query=&Time=&EndTime=&SearchMethod=1&TocRestrict=n&Toc=&TocEntry=&QField=&QFieldYear=&QFieldMonth=&QFieldDay=&IntQFieldOp=0&ExtQFieldOp=0&XmlQuery=&File=D%3A%5Czyfiles%5CIndex%20Data%5C00thru05%5CTxt%5C00000029%5C910118CI.txt&User=ANONYMOUS&Password=anonymous&SortMethod=h%7C-&MaximumDocuments=1&FuzzyDegree=0&ImageQuality=r75g8/r75g8/x150y150g16/i425&Display=hpfr&DefSeekPage=x&SearchBack=ZyActionL&Back=ZyActionS&BackDesc=Results%20page&MaximumPages=1&ZyEntry=1&SeekPage=x&ZyPURL#">hpfr&DefSeekPage=x&SearchBack=ZyActionL&Back=ZyActionS&BackDesc=Results%20page&MaximumPages=1&ZyEntry=1&SeekPage=x&ZyPURL#</a> (accessed December 18, 2024).
- [501] R.F. Dunn, M.M. El-Halwagi, Selection of optimal VOC-condensation systems, Waste Management 14 (1994) 103–113. <a href="https://doi.org/10.1016/0956-053X(94)90003-5">https://doi.org/10.1016/0956-053X(94)90003-5</a>.
- [502] H. Xu, X. Xi, X. Xu, J. Guo, L. Chen, W. Ji, J. Wang, Development of a volatile organic compounds cryogenic condensation recovery system cooled by liquid nitrogen, IOP Conf Ser Mater Sci Eng 1240 (2022) 012098. https://doi.org/10.1088/1757-899x/1240/1/012098.
- [503] H. Wang, H. Guo, Y. Zhao, X. Dong, M. Gong, Thermodynamic analysis of a petroleum volatile organic compounds (VOCs) condensation recovery system combined with mixed-refrigerant refrigeration, International Journal of Refrigeration 116 (2020) 23–35. <a href="https://doi.org/10.1016/j.ijrefrig.2020.03.011">https://doi.org/10.1016/j.ijrefrig.2020.03.011</a>.
- [504] G.T. Sameshima, J.D. Eisenwasser, Cryogenic recovery of VOC emissions, in: Industrial Solvent Recycling Conference, U. S. Department of Energy-Office of Industrial Technologies, Sand Diego, 1991: pp. 297–315. <a href="https://p2infohouse.org/ref/29/28031.pdf">https://p2infohouse.org/ref/29/28031.pdf</a> (accessed December 19, 2024).
- [505] V.G. Shram, N.N. Lysyannikova, Yu.N. Bezborodov, M.A. Kovaleva, O.Yu. Moroz, T.Y. Matkerimov, Cryogenic Vapor Recovery Unit for Light Fractions of Hydrocarbon Fuel, Chemical and Petroleum Engineering 57 (2021) 317–321. https://doi.org/10.1007/s10556-021-00936-7.
- [506] L. Shi, W. Huang, Sensitivity analysis and optimization for gasoline vapor condensation recovery, Process Safety and Environmental Protection 92 (2014) 807–814. https://doi.org/10.1016/j.psep.2013.03.003.
- [507] Q. Jiang, Q. Zhu, W. Duan, S. Wan, T. Guo, H. Li, H. Feng, W. Du, J. Gu, Thermodynamic design and experimental study of a condensation recovery system for VOCs, Appl Therm Eng 236 (2024). https://doi.org/10.1016/j.applthermaleng.2023.121822.
- [508] F.I. Khan, A. Kr. Ghoshal, Removal of Volatile Organic Compounds from polluted air, J Loss Prev Process Ind 13 (2000) 527–545. https://doi.org/10.1016/S0950-4230(00)00007-3.
- [509] C.Z. Liang, T.S. Chung, J.Y. Lai, A review of polymeric composite membranes for gas separation and energy production, Prog Polym Sci 97 (2019). https://doi.org/10.1016/j.progpolymsci.2019.06.001.
- [510] Y.Y. Choi, J.H. Kim, K.W. Chun, Evaluating the possibility of utilizing hollow fiber membranes for recovering VOC generated by oil tankers, Journal of Marine Engineering and Technology 20 (2021) 278–287. https://doi.org/10.1080/20464177.2019.1572058.
- [511] X. Zhao, Y. Chen, Q. Ding, T. Xiao, X. Yang, High-Performance Silicone Membranes for VOC/N<sub>2</sub> Separation: A New Crosslinking Strategy via Octyl-Grafted Poly(hydromethylsiloxane), Ind Eng Chem Res 62 (2023) 13974–13987. https://doi.org/10.1021/acs.iecr.3c01940.

- [512] Y.M. Shirke, Y.J. Yu, J.W. Chung, S.J. Cho, S.J. Kwon, S.U. Hong, J.D. Jeon, Hydrophobic hollow fiber composite membranes based on hexadecyl-modified SiO<sub>2</sub> nanoparticles for toluene separation, J Environ Chem Eng 12 (2024). https://doi.org/10.1016/j.jece.2023.111819.
- [513] A. Iulianelli, E. Drioli, Membrane engineering: Latest advancements in gas separation and pretreatment processes, petrochemical industry and refinery, and future perspectives in emerging applications, Fuel Processing Technology 206 (2020). https://doi.org/10.1016/j.fuproc.2020.106464.
- [514] G. Gan, S. Fan, X. Li, Z. Zhang, Z. Hao, Adsorption and membrane separation for removal and recovery of volatile organic compounds, J Environ Sci (China) 123 (2023) 96–115. <a href="https://doi.org/10.1016/j.jes.2022.02.006">https://doi.org/10.1016/j.jes.2022.02.006</a>.
- [515] G.B. Evans, R. Nelson, Applications of Vapor Recovery to Crude Oil Production, in: SPE Automation Symposium, SPE, 1968. <a href="https://doi.org/10.2118/2089-MS">https://doi.org/10.2118/2089-MS</a>.
- [516] C. Pirola, M. Mattia, Purification of air from volatile organic compounds by countercurrent liquid gas mass transfer absorption process, International Journal of Thermofluids 9 (2021). https://doi.org/10.1016/j.ijft.2020.100060.
- [517] Ö. Yildirim, A.A. Kiss, N. Hüser, K. Leßmann, E.Y. Kenig, Reactive absorption in chemical process industry: A review on current activities, Chemical Engineering Journal 213 (2012) 371–391. https://doi.org/10.1016/j.cej.2012.09.121.
- [518] R. Tatin, L. Moura, N. Dietrich, S. Baig, G. Hébrard, Physical absorption of volatile organic compounds by spraying emulsion in a spray tower: Experiments and modelling, Chemical Engineering Research and Design 104 (2015) 409–415. <a href="https://doi.org/10.1016/j.cherd.2015.08.030">https://doi.org/10.1016/j.cherd.2015.08.030</a>.
- [519] A.S. Rodriguez Castillo, P.F. Biard, S. Guihéneuf, L. Paquin, A. Amrane, A. Couvert, Assessment of VOC absorption in hydrophobic ionic liquids: Measurement of partition and diffusion coefficients and simulation of a packed column, Chemical Engineering Journal 360 (2019) 1416–1426. <a href="https://doi.org/10.1016/j.cej.2018.10.146">https://doi.org/10.1016/j.cej.2018.10.146</a>.
- [520] Y. Li, H. Chang, H. Yan, S. Tian, P.G. Jessop, Reversible Absorption of Volatile Organic Compounds by Switchable-Hydrophilicity Solvents: A Case Study of Toluene with N, N-Dimethylcyclohexylamine, ACS Omega 6 (2021) 253–264. <a href="https://doi.org/10.1021/acsomega.0c04443">https://doi.org/10.1021/acsomega.0c04443</a>.
- [521] P. Makoś-Chełstowska, VOCs absorption from gas streams using deep eutectic solvents A review, J Hazard Mater 448 (2023). https://doi.org/10.1016/j.jhazmat.2023.130957.
- [522] H. Abdelli, F. Colonna, E. Tunisia, Gas condensate recovery technologies in ENI Tunisia fields, in: All Days, Offshore Mediterranean Conference and Exhibition, Ravenna, 2011: pp. 1–16. <a href="https://onepetro.org/OMCONF/proceedings/OMC11/All-OMC11/OMC-2011-017/1158">https://onepetro.org/OMCONF/proceedings/OMC11/All-OMC11/OMC-2011-017/1158</a> (accessed December 20, 2024).
- [523] W. Huang, L. Shi, Methods for the control of oil vapour emissions, International Journal of Oil, Gas and Coal Technology 6 (2013) 271. <a href="https://doi.org/10.1504/IJOGCT.2013.052238">https://doi.org/10.1504/IJOGCT.2013.052238</a>.
- [524] X. Li, L. Zhang, Z. Yang, P. Wang, Y. Yan, J. Ran, Adsorption materials for volatile organic compounds (VOCs) and the key factors for VOCs adsorption process: A review, Sep Purif Technol 235 (2020). <a href="https://doi.org/10.1016/j.seppur.2019.116213">https://doi.org/10.1016/j.seppur.2019.116213</a>.
- [525] L. Zhu, D. Shen, K.H. Luo, A critical review on VOCs adsorption by different porous materials: Species, mechanisms and modification methods, J Hazard Mater 389 (2020). https://doi.org/10.1016/j.jhazmat.2020.122102.
- [526] P. Dwivedi, V. Gaur, A. Sharma, N. Verma, Comparative study of removal of volatile organic compounds by cryogenic condensation and adsorption by activated carbon fiber, Sep Purif Technol 39 (2004) 23–37. <a href="https://doi.org/10.1016/j.seppur.2003.12.016">https://doi.org/10.1016/j.seppur.2003.12.016</a>.
- [527] M. Králik, Adsorption, chemisorption, and catalysis, Chemical Papers 68 (2014) 1625–1638. https://doi.org/10.2478/s11696-014-0624-9.
- [528] J. Pei, J.S. Zhang, Critical review of catalytic oxidization and chemisorption methods for indoor formaldehyde removal, HVAC and R Research 17 (2011) 476–503. https://doi.org/10.1080/10789669.2011.587587.

- [529] Q. Ye, Y. Chen, Y. Li, R. Jin, Q. Geng, S. Chen, Management of typical VOCs in air with adsorbents: status and challenges, Dalton Transactions 52 (2023) 12169–12184. https://doi.org/10.1039/d3dt01930f.
- [530] B. Barker, Activated Carbon in Vapour Recovery Units, Tank Storage Magazine 13 (2017). <a href="https://24198570.fs1.hubspotusercontent-na1.net/hubfs/24198570/TSM\_feb-mar-2017-Activated-Carbon-3.pdf">https://24198570.fs1.hubspotusercontent-na1.net/hubfs/24198570/TSM\_feb-mar-2017-Activated-Carbon-3.pdf</a> (accessed December 20, 2024).
- [531] X. Zhang, B. Gao, A.E. Creamer, C. Cao, Y. Li, Adsorption of VOCs onto engineered carbon materials: A review, J Hazard Mater 338 (2017) 102–123. https://doi.org/10.1016/j.jhazmat.2017.05.013.
- [532] K. Isinkaralar, Optimal preparation of low-cost activated carbon: the enhanced mechanism of interaction and performance studies for volatile organic compounds (VOCs) capture, Biomass Convers Biorefin (2023). <a href="https://doi.org/10.1007/s13399-023-05159-9">https://doi.org/10.1007/s13399-023-05159-9</a>.
- [533] K. Isinkaralar, Multi-component volatile organic compounds (VOCs) treatment nexus: High-performance of activated carbon derived from residual agroforestry biomass, International Journal of Environmental Science and Technology 21 (2024) 925–938. <a href="https://doi.org/10.1007/s13762-023-05202-2">https://doi.org/10.1007/s13762-023-05202-2</a>.
- [534] X. Yang, H. Zhong, W. Zhang, Y. Liu, N. Sun, R. Kuang, C. Wang, A. Zhan, J. Zhang, Q. Tang, Z. Li, Progress in Adsorptive Removal of Volatile Organic Compounds by Zeolites, Aerosol Air Qual Res 23 (2023). <a href="https://doi.org/10.4209/aaqr.220442">https://doi.org/10.4209/aaqr.220442</a>.
- [535] T.N. Tu, T.M. Pham, Q.H. Nguyen, N.T. Tran, V.N. Le, L.H. Ngo, K. Chang, J. Kim, Metal-organic frameworks for aromatic-based VOC capture, Sep Purif Technol 333 (2024). https://doi.org/10.1016/j.seppur.2023.125883.
- [536] H. Sui, H. Liu, P. An, L. He, X. Li, S. Cong, Application of silica gel in removing high concentrations toluene vapor by adsorption and desorption process, J Taiwan Inst Chem Eng 74 (2017) 218–224. https://doi.org/10.1016/j.jtice.2017.02.019.
- [537] C.A. Grande, Advances in Pressure Swing Adsorption for Gas Separation, ISRN Chemical Engineering 2012 (2012) 1–13. <a href="https://doi.org/10.5402/2012/982934">https://doi.org/10.5402/2012/982934</a>.
- [538] Y. Shen, W. Shi, D. Zhang, P. Na, Z. Tang, Recovery of light hydrocarbons from natural gas by vacuum pressure swing adsorption process, J Nat Gas Sci Eng 68 (2019). https://doi.org/10.1016/j.jngse.2019.05.008.
- [539] J. Bonjour, J.B. Chalfen, F. Meunier, Temperature swing adsorption process with indirect cooling and heating, Ind Eng Chem Res 41 (2002) 5802–5811. <a href="https://doi.org/10.1021/ie011011j">https://doi.org/10.1021/ie011011j</a>.
- [540] R. Zhao, L. Liu, L. Zhao, S. Deng, S. Li, Y. Zhang, H. Li, Techno-economic analysis of carbon capture from a coal-fired power plant integrating solar-assisted pressure-temperature swing adsorption (PTSA), J Clean Prod 214 (2019) 440–451. https://doi.org/10.1016/j.jclepro.2018.12.316.
- [541] Y. Li, Y. Shen, Z. Niu, J. Tian, D. Zhang, Z. Tang, W. Li, Process analysis of temperature swing adsorption and temperature vacuum swing adsorption in VOCs recovery from activated carbon, Chin J Chem Eng 53 (2023) 346–360. https://doi.org/10.1016/j.cjche.2022.01.029.
- [542] A.K. Ghoshal, S.D. Manjare, Selection of appropriate adsorption technique for recovery of VOCs: an analysis, 2002. www.elsevier.com/locate/jlp.
- [543] D.J. Pezolt, S.J. Collick, H.A. Johnson, L.A. Robbins, Pressure swing adsorption for VOC recovery at gasoline loading terminals, Environmental Progress 16 (1997) 16–19. <a href="https://doi.org/10.1002/ep.3300160115">https://doi.org/10.1002/ep.3300160115</a>.
- [544] K. Chue, Y.-K. Park, J.-K. Jeon, Development of Adsorption Buffer and Pressure Swing Adsorption (PSA) Unit for Gasoline Vapor Recovery, Korean J. Chem. Eng. 21, 676–679 (2004). https://doi.org/10.1007/BF02705504.
- [545] V.K. Gupta, N. Verma, Removal of volatile organic compounds by cryogenic condensation followed by adsorption, Chem Eng Sci 57 (2002) 2679–2696. <a href="https://doi.org/10.1016/S0009-2509(02)00158-6">https://doi.org/10.1016/S0009-2509(02)00158-6</a>.

- [546] J. Liang, L. Sun, C. Cheng, K. Wang, T. Zhu, T. Li, Advancing gasoline vapor recovery in oil depots: Integrating cooling and adsorption technologies, Energy 313 (2024). https://doi.org/10.1016/j.energy.2024.133823.
- [547] B. Belaissaoui, Y. Le Moullec, E. Favre, Energy efficiency of a hybrid membrane/condensation process for VOC (Volatile Organic Compounds) recovery from air: A generic approach, Energy 95 (2016) 291–302. <a href="https://doi.org/10.1016/j.energy.2015.12.006">https://doi.org/10.1016/j.energy.2015.12.006</a>.
- [548] D. Roizard, F. Lapicque, E. Favre, C. Roizard, Potentials of pervaporation to assist VOCs' recovery by liquid absorption, Chem Eng Sci 64 (2009) 1927–1935. <a href="https://doi.org/10.1016/j.ces.2009.01.014">https://doi.org/10.1016/j.ces.2009.01.014</a>.
- [549] I.A.A.C. Esteves, J.P.B. Mota, Chapter 9. Novel Hybrid Membrane/Pressure Swing Adsorption Processes for Gas Separation Applications, in: 2011: pp. 245–275. <a href="https://doi.org/10.1039/9781849733472-00245">https://doi.org/10.1039/9781849733472-00245</a>.
- [550] J.C. McGill, W.N. Scott, Adsorption-absorption vapor recovery system, 4066423, 1978. https://patents.google.com/patent/US4066423A/en (accessed December 22, 2024).
- [551] P.E. Kennedy, Absorption-absorption vapor recovery process, 4670028, 1987. https://patents.google.com/patent/US4670028A/en (accessed December 22, 2024).
- [552] W.N. Tuttle, Vapor recovery system, 5480475, 1996. https://patents.google.com/patent/US5480475A/en (accessed December 22, 2024).
- [553] R.G. Hornsby, L. Larrinaga, Installation and Operation of SORBATHENE Solvent Vapor Recovery Units to Recover and Recycle Volatile Organic Compounds at Operating Sites Within the Dow Chemical Company, in: SAE Technical Paper 950242, Detroit, 1995. <a href="https://doi.org/10.4271/950242">https://doi.org/10.4271/950242</a>.
- [554] M. Douglas LeVan, G. Carta, Section 16-Adsorption and Ion Exchange, in: D.W. Green, R.H. Perry (Eds.), Perry's Chemical Engineers' Handbook, 8th ed., McGraw-Hill, New York, Chicago, San Francisco, Lisbon, London, Madrid, Mexico City, Milan, New Delhi, San Juan, Seoul, Singapore, Sydney, Toronto, 2008. <a href="https://www.accessengineeringlibrary.com/content/book/9780071422949/toc-chapter/chapter16/section/section1">https://www.accessengineeringlibrary.com/content/book/9780071422949/toc-chapter16/section/section1</a> (accessed December 23, 2024).
- [555] M.-G. Olivier, R. Jadot, Adsorption of Light Hydrocarbons and Carbon Dioxide on Silica Gel, J Chem Eng Data 42 (1997) 230–233. <a href="https://doi.org/10.1021/je960200j">https://doi.org/10.1021/je960200j</a>.
- [556] E. Díaz, S. Ordóñez, A. Vega, J. Coca, Adsorption characterisation of different volatile organic compounds over alumina, zeolites and activated carbon using inverse gas chromatography, J Chromatogr A 1049 (2004) 139–146. <a href="https://doi.org/10.1016/j.chroma.2004.07.061">https://doi.org/10.1016/j.chroma.2004.07.061</a>.
- [557] P. Ye, Z. Fang, B. Su, H. Xing, Y. Yang, Y. Su, Q. Ren, Adsorption of propylene and ethylene on 15 activated carbons, J Chem Eng Data 55 (2010) 5669–5672. https://doi.org/10.1021/je100601n.
- [558] R. Zhang, Y. Shen, Z. Tang, W. Li, D. Zhang, A Review of Numerical Research on the Pressure Swing Adsorption Process, Processes 10 (2022). <a href="https://doi.org/10.3390/pr10050812">https://doi.org/10.3390/pr10050812</a>.
- [559] J.W. Chen, J.A. Buege, F.L. Cunningham, J.I. Northam, Scale-up of Column Adsorption Process by Computer Simulation, Industrial & Engineering Chemistry Process Design and Development 7 (1968) 26–31. https://doi.org/10.1021/i260025a006.
- [560] Y. Chung, B.-K. Na, H.K. Song, Short-cut evaluation of pressure swing adsorption systems, Comput Chem Eng 22 (1998) S637–S640. <a href="https://doi.org/10.1016/S0098-1354(98)00113-6">https://doi.org/10.1016/S0098-1354(98)00113-6</a>.
- [561] S. Nilchan, C.C. Pantelides, On the Optimisation of Periodic Adsorption Processes, Adsorption 4 (1998) 113–147. <a href="https://doi.org/10.1023/A:1008823102106">https://doi.org/10.1023/A:1008823102106</a>.
- [562] F.A. Da Silva, J.A. Silva, A.E. Rodrigues, A General Package for the Simulation of Cyclic Adsorption Processes, Adsorption 5 (1999) 229–244. <a href="https://doi.org/10.1023/A:1008974908427">https://doi.org/10.1023/A:1008974908427</a>.
- [563] A. Agarwal, L.T. Biegler, S.E. Zitney, Simulation and optimization of pressure swing adsorption systems using reduced-order modeling, Ind Eng Chem Res 48 (2009) 2327–2343. https://doi.org/10.1021/ie071416p.
- [564] M. Kheimi, S.K. Salamah, Simulation of temperature swing adsorption process to purify hydrogen for fuel cell uses by SAPO34 as adsorbent, Chemosphere 338 (2023). https://doi.org/10.1016/j.chemosphere.2023.139454.

- [565] S. Li, S. Deng, L. Zhao, R. Zhao, M. Lin, Y. Du, Y. Lian, Mathematical modeling and numerical investigation of carbon capture by adsorption: Literature review and case study, Appl Energy 221 (2018) 437–449. https://doi.org/10.1016/j.apenergy.2018.03.093.
- [566] M. Chenu, A. Bouzaza, D. Wolbert, A. Laplanche, Adsorption of volatile organic compounds (voc) mixtures onto activated carbon. experimental study and simulation of multicomponent adsorption, Environmental Technology (United Kingdom) 19 (1998) 1029–1038. <a href="https://doi.org/10.1080/09593331908616760">https://doi.org/10.1080/09593331908616760</a>.
- [567] J.F. Nastaj, B. Ambrozek, J. Rudnicka, Simulation studies of a vacuum and temperature swing adsorption process for the removal of VOC from waste air streams, International Communications in Heat and Mass Transfer 33 (2006) 80–86. https://doi.org/10.1016/j.icheatmasstransfer.2005.08.005.
- [568] M. Davarpanah, Z. Hashisho, D. Crompton, J.E. Anderson, M. Nichols, Modeling VOC adsorption in lab- and industrial-scale fluidized bed adsorbers: Effect of operating parameters and heel build-up, J Hazard Mater 400 (2020). https://doi.org/10.1016/j.jhazmat.2020.123129.
- [569] S. Wang, L. Huang, Y. Zhang, L. Li, X. Lu, A mini-review on the modeling of volatile organic compound adsorption in activated carbons: Equilibrium, dynamics, and heat effects, Chin J Chem Eng 31 (2021) 153–163. https://doi.org/10.1016/j.cjche.2020.11.018.
- [570] Y. Liu, J.A. Ritter, B.K. Kaul, Simulation of gasoline vapor recovery by pressure swing adsorption, Sep Purif Technol 20 (2000) 111–127. https://doi.org/10.1016/S1383-5866(00)00066-6.
- [571] W.Q. Huang, D.F. Cai, J. Bai, L. Shi, Numerical Simulation of Gasoline Vapor Adsorption, Adv Mat Res 518–523 (2012) 2608–2611. https://doi.org/10.4028/www.scientific.net/AMR.518-523.2608.
- [572] A. Mulet, J. García-Reverter, R. Sanjuán, J. Bon, Sorption isosteric heat determination by thermal analysis and sorption isotherms, J Food Sci 64 (1999) 64–68. <a href="https://doi.org/10.1111/j.1365-2621.1999.tb09862.x">https://doi.org/10.1111/j.1365-2621.1999.tb09862.x</a>.
- [573] E.N. Fuller, K. Ensley, J.C. Giddings, Diffusion of halogenated hydrocarbons in helium. The effect of structure on collision cross sections, J Phys Chem 73 (1969) 3679–3685. https://doi.org/10.1021/j100845a020.
- [574] Y. Belmabkhout, G. De Weireld, M. Frère, High-Pressure Adsorption Isotherms of N<sub>2</sub>, CH<sub>4</sub>, O<sub>2</sub>, and Ar on Different Carbonaceous Adsorbents, J Chem Eng Data 49 (2004) 1379–1391. https://doi.org/10.1021/je049900b.
- [575] D. Park, Y. Ju, J.-H. Kim, H. Ahn, C.-H. Lee, Equilibrium and kinetics of nitrous oxide, oxygen and nitrogen adsorption on activated carbon and carbon molecular sieve, Sep Purif Technol 223 (2019) 63–80. <a href="https://doi.org/10.1016/j.seppur.2019.04.051">https://doi.org/10.1016/j.seppur.2019.04.051</a>.
- [576] N. Tzabar, H.J.M. ter Brake, Adsorption isotherms and Sips models of nitrogen, methane, ethane, and propane on commercial activated carbons and polyvinylidene chloride, Adsorption 22 (2016) 901–914. https://doi.org/10.1007/s10450-016-9794-9.
- [577] S.M.W. Wilson, F. Al-Enzi, V.A. Gabriel, F.H. Tezel, Effect of pore size and heterogeneous surface on the adsorption of CO<sub>2</sub>, N<sub>2</sub>, O<sub>2</sub>, and Ar on carbon aerogel, RF aerogel, and activated carbons, Microporous and Mesoporous Materials 322 (2021) 111089. <a href="https://doi.org/10.1016/j.micromeso.2021.111089">https://doi.org/10.1016/j.micromeso.2021.111089</a>.
- [578] F. Birkmann, C. Pasel, M. Luckas, D. Bathen, Adsorption Thermodynamics and Kinetics of Light Hydrocarbons on Microporous Activated Carbon at Low Temperatures, Ind Eng Chem Res 57 (2018) 8023–8035. <a href="https://doi.org/10.1021/acs.iecr.8b00678">https://doi.org/10.1021/acs.iecr.8b00678</a>.
- [579] G.S. Cheripally, A. Mannava, G. Kumar, R. Gupta, P. Saha, B. Mandal, R. Uppaluri, S. Gumma, A.K. Ghoshal, Measurement and Modeling of Adsorption of Lower Hydrocarbons on Activated Carbon, J Chem Eng Data 58 (2013) 1606–1612. https://doi.org/10.1021/je3013217.
- [580] K. Chue, Y.-K. Park, J.-K. Jeon, Development of adsorption buffer and pressure swing adsorption (PSA) unit for gasoline vapor recovery, Korean Journal of Chemical Engineering 21 (2004) 676–679. <a href="https://doi.org/10.1007/BF02705504">https://doi.org/10.1007/BF02705504</a>.
- [581] D.D. Do, X. Hu, P.L.J. Mayfield, Multicomponent adsorption of ethane, n-butane and n-pentane in activated carbon, Gas Separation & Purification 5 (1991) 35–48. <a href="https://doi.org/10.1016/0950-4214(91)80047-9">https://doi.org/10.1016/0950-4214(91)80047-9</a>.

- [582] H.D. Do, D.D. Do, I. Prasetyo, Surface diffusion and adsorption of hydrocarbons in activated carbon, AIChE Journal 47 (2001) 2515–2525. <a href="https://doi.org/10.1002/aic.690471114">https://doi.org/10.1002/aic.690471114</a>.
- [583] U. Eiden, E.U. Schlünder, Adsorption equilibria of pure vapors and their binary mixtures on activated carbon Part I. Single-component equilibria, Chemical Engineering and Processing: Process Intensification 28 (1990) 1–11. <a href="https://doi.org/10.1016/0255-2701(90)85020-5">https://doi.org/10.1016/0255-2701(90)85020-5</a>.
- [584] I.A.A.C. Esteves, M.S.S. Lopes, P.M.C. Nunes, J.P.B. Mota, Adsorption of natural gas and biogas components on activated carbon, Sep Purif Technol 62 (2008) 281–296. https://doi.org/10.1016/j.seppur.2008.01.027.
- [585] E. Fiani, L. Perier-Cambry, G. Thomas, Non-isothermal modelling of hydrocarbon adsorption on a granulated activated carbon, J Therm Anal Calorim 60 (2000) 557–570. <a href="https://doi.org/10.1023/A:1010147005169">https://doi.org/10.1023/A:1010147005169</a>.
- [586] P. Glanz, B. Körner, G.H. Findenegg, Adsorption of Propene and Propane on Graphitized Carbon. II. Analysis of Single Gas and Mixed Gas Isotherms, Adsorption Science & Technology 1 (1984) 183–193. https://doi.org/10.1177/026361748400100301.
- [587] R.J. Grant, M. Manes, S.B. Smith, Adsorption of normal paraffins and sulfur compounds on activated carbon, AIChE Journal 8 (1962) 403–406. <a href="https://doi.org/10.1002/aic.690080328">https://doi.org/10.1002/aic.690080328</a>.
- [588] X. Hu, G.N. Rao, D.D. Do, A mathematical model for multicomponent adsorption, desorption and displacement kinetics of ethane, propane and n-butane on activated carbon, Gas Separation & Purification 7 (1993) 197–206. https://doi.org/10.1016/0950-4214(93)80018-R.
- [589] M. Kuru-Oka, T. Suzuki, T. Nitta, T. Katayama, Adsorption isotherms of hydrocarbons and carbon dioxide on activated fiber carbon., Journal of Chemical Engineering of Japan 17 (1984) 588–592. https://doi.org/10.1252/jcej.17.588.
- [590] S. Kutluay, O. Baytar, Ö. Şahin, Equilibrium, kinetic and thermodynamic studies for dynamic adsorption of benzene in gas phase onto activated carbon produced from elaeagnus angustifolia seeds, J Environ Chem Eng 7 (2019) 102947. <a href="https://doi.org/10.1016/j.jece.2019.102947">https://doi.org/10.1016/j.jece.2019.102947</a>.
- [591] M.-H. Lai, R.Q. Chu, H.-C. Huang, S.-H. Shu, T.-W. Chung, Equilibrium Isotherms of Volatile Alkanes, Alkenes, and Ketones on Activated Carbon, J Chem Eng Data 54 (2009) 2208–2215. https://doi.org/10.1021/je800826d.
- [592] C. Long, Y. Li, W. Yu, A. Li, Removal of benzene and methyl ethyl ketone vapor: Comparison of hypercrosslinked polymeric adsorbent with activated carbon, J Hazard Mater 203–204 (2012) 251–256. <a href="https://doi.org/10.1016/j.jhazmat.2011.12.010">https://doi.org/10.1016/j.jhazmat.2011.12.010</a>.
- [593] A. Malek, S. Farooq, Determination of Equilibrium Isotherms Using Dynamic Column Breakthrough and Constant Flow Equilibrium Desorption, J Chem Eng Data 41 (1996) 25–32. https://doi.org/10.1021/je950178e.
- [594] M.-G. Olivier, K. Berlier, R. Jadot, Adsorption of Butane, 2-Methylpropane, and 1-Butene on Activated Carbon, J Chem Eng Data 39 (1994) 770–773. https://doi.org/10.1021/je00016a029.
- [595] M.-G. Olivier, K. Berlier, J. Bougard, Adsorption of 2-Methylpropene and 1,3-Butadiene on Activated Carbon, J Chem Eng Data 39 (1994) 774–776. <a href="https://doi.org/10.1021/je00016a030">https://doi.org/10.1021/je00016a030</a>.
- [596] M.-G. Olivier, J. Bougard, R. Jadot, Adsorption of propane, propylene and propadiene on activated carbon, Appl Therm Eng 16 (1996) 383–387. <a href="https://doi.org/10.1016/1359-4311(95)00019-4">https://doi.org/10.1016/1359-4311(95)00019-4</a>.
- [597] G. Pigorini, Periodic Behavior of Pressure Swing Adsorption Cycles and Coadsorption of Light and Heavy n-Alkanes on Activated Carbon, Ph. D., University of Virginia, 2000. <a href="https://www.proquest.com/docview/304635569?fromopenview=true&pq-origsite=gscholar&sourcetype=Dissertations%20&%20Theses">https://www.proquest.com/docview/304635569?fromopenview=true&pq-origsite=gscholar&sourcetype=Dissertations%20&%20Theses</a> (accessed December 26, 2024).
- [598] D. Pino, F. Plantier, D. Bessières, Adsorption of Alkanes in the Dense Vapor Phase on a Microporous Activated Carbon, J Chem Eng Data 62 (2017) 1716–1724. https://doi.org/10.1021/acs.jced.7b00175.
- [599] D. Ramirez, S. Qi, M.J. Rood, K.J. Hay, Equilibrium and Heat of Adsorption for Organic Vapors and Activated Carbons, Environ Sci Technol 39 (2005) 5864–5871. https://doi.org/10.1021/es048144r.
- [600] M.E. Ramos, P.R. Bonelli, A.L. Cukierman, M.M.L. Ribeiro Carrott, P.J.M. Carrott, Adsorption of volatile organic compounds onto activated carbon cloths derived from a novel regenerated cellulosic precursor, J Hazard Mater 177 (2010) 175–182. https://doi.org/10.1016/j.jhazmat.2009.12.014.

- [601] B.P. Russel, M. Douglas LeVan, Coadsorption of Organic Compounds and Water Vapor on BPL Activated Carbon. 3. Ethane, Propane, and Mixing Rules, Ind Eng Chem Res 36 (1997) 2380–2389. <a href="https://doi.org/10.1021/ie960533">https://doi.org/10.1021/ie960533</a>+.
- [602] B.B. Saha, A. Chakraborty, S. Koyama, S.-H. Yoon, I. Mochida, M. Kumja, C. Yap, K.C. Ng, Isotherms and thermodynamics for the adsorption of n-butane on pitch based activated carbon, Int J Heat Mass Transf 51 (2008) 1582–1589. https://doi.org/10.1016/j.ijheatmasstransfer.2007.07.031.
- [603] B.J. Schindler, L.C. Buettner, M. Douglas LeVan, Transition to Henry's law in ultra-low concentration adsorption equilibrium for n-pentane on BPL activated carbon, Carbon N Y 46 (2008) 1285–1293. https://doi.org/10.1016/j.carbon.2008.05.001.
- [604] W.G. Shim, J.W. Lee, H. Moon, Equilibrium and Fixed-Bed Adsorption of n-Hexane on Activated Carbon, Sep Sci Technol 38 (2003) 3905–3926. <a href="https://doi.org/10.1081/SS-120024711">https://doi.org/10.1081/SS-120024711</a>.
- [605] K. Wang, Rate and equilibrium studies of benzene and toluene removal by activated carbon, Sep Purif Technol 17 (1999) 53–63. <a href="https://doi.org/10.1016/S1383-5866(99)00027-1">https://doi.org/10.1016/S1383-5866(99)00027-1</a>.
- [606] J. Wu, L. Zhang, C. Long, Q. Zhang, Adsorption Characteristics of Pentane, Hexane, and Heptane: Comparison of Hydrophobic Hypercrosslinked Polymeric Adsorbent with Activated Carbon, J Chem Eng Data 57 (2012) 3426–3433. https://doi.org/10.1021/je300550x.
- [607] J.-H. Yun, D.-K. Choi, Adsorption Isotherms of Benzene and Methylbenzene Vapors on Activated Carbon, J Chem Eng Data 42 (1997) 894–896. https://doi.org/10.1021/je970066i.
- [608] J.-H. Yun, K.-Y. Hwang, D.-K. Choi, Adsorption of Benzene and Toluene Vapors on Activated Carbon Fiber at 298, 323, and 348 K, J Chem Eng Data 43 (1998) 843–845. https://doi.org/10.1021/je980069a.
- [609] W. Zhu, J.C. Groen, F. Kapteijn, J.A. Moulijn, Adsorption of Butane Isomers and SF<sub>6</sub> on Kureha Activated Carbon: 1. Equilibrium, Langmuir 20 (2004) 5277–5284. https://doi.org/10.1021/la030264+.
- [610] S. Schmittmann, C. Pasel, M. Luckas, D. Bathen, Adsorption of Light Alkanes and Alkenes on Activated Carbon and Zeolite 13X at Low Temperatures, J Chem Eng Data 65 (2020) 706–716. https://doi.org/10.1021/acs.jced.9b00948.
- [611] H. Sui, H. Liu, P. An, L. He, X. Li, S. Cong, Application of silica gel in removing high concentrations toluene vapor by adsorption and desorption process, J Taiwan Inst Chem Eng 74 (2017) 218–224. https://doi.org/10.1016/j.jtice.2017.02.019.
- [612] P. Brea, J.A. Delgado, V.I. Águeda, P. Gutiérrez, M.A. Uguina, Multicomponent adsorption of H<sub>2</sub>, CH<sub>4</sub>, CO and CO<sub>2</sub> in zeolites NaX, CaX and MgX. Evaluation of performance in PSA cycles for hydrogen purification, Microporous and Mesoporous Materials 286 (2019) 187–198. <a href="https://doi.org/10.1016/j.micromeso.2019.05.021">https://doi.org/10.1016/j.micromeso.2019.05.021</a>.
- [613] O.M. Dzhigit, A.V. Kiselev, T.A. Rachmanova, Henry's constants, isotherms and heats of adsorption of some hydrocarbons in zeolites of faujasite type with different content of sodium cations, Zeolites 4 (1984) 389–397. <a href="https://doi.org/10.1016/0144-2449(84)90017-4">https://doi.org/10.1016/0144-2449(84)90017-4</a>.
- [614] N. Lamia, L. Wolff, P. Leflaive, P. Sá Gomes, C.A. Grande, A.E. Rodrigues, Propane/Propylene Separation by Simulated Moving Bed I. Adsorption of Propane, Propylene and Isobutane in Pellets of 13X Zeolite, Sep Sci Technol 42 (2007) 2539–2566. https://doi.org/10.1080/01496390701515219.
- [615] K. Li, E.M. Kennedy, S.Z. Chen, Adsorption of n-Butane and n-Heptane on 5A Zeolite, Sep Sci Technol 33 (1998) 1571–1584. <a href="https://doi.org/10.1080/01496399808545065">https://doi.org/10.1080/01496399808545065</a>.
- [616] F. Miano, Adsorption of hydrocarbon vapour mixtures onto zeolite 5A, Colloids Surf A Physicochem Eng Asp 110 (1996) 95–104. <a href="https://doi.org/10.1016/0927-7757(95)03439-0">https://doi.org/10.1016/0927-7757(95)03439-0</a>.
- [617] G.-M. Nam, B.-M. Jeong, S.-H. Kang, B.-K. Lee, D.-K. Choi, Equilibrium Isotherms of CH<sub>4</sub>, C<sub>2</sub>H<sub>6</sub>, C<sub>2</sub>H<sub>4</sub>, N<sub>2</sub>, and H<sub>2</sub> on Zeolite 5A Using a Static Volumetric Method, J Chem Eng Data 50 (2005) 72–76. https://doi.org/10.1021/je0498309.
- [618] Y. Park, Y. Ju, D. Park, C.-H. Lee, Adsorption equilibria and kinetics of six pure gases on pelletized zeolite 13X up to 1.0 MPa: CO<sub>2</sub>, CO, N<sub>2</sub>, CH<sub>4</sub>, Ar and H<sub>2</sub>, Chemical Engineering Journal 292 (2016) 348–365. <a href="https://doi.org/10.1016/j.cej.2016.02.046">https://doi.org/10.1016/j.cej.2016.02.046</a>.

- [619] F. Romá, J.L. Riccardo, A.J. Ramirez-Pastor, Statistical Thermodynamics Models for Polyatomic Adsorbates: Application to Adsorption of n-paraffins in 5A Zeolite, Langmuir 21 (2005) 2454–2459. https://doi.org/10.1021/la0473207.
- [620] H. Sun, B. Shen, J. Liu, Adsorption Equilibrium of n-Paraffins on Binderless 5A Zeolite, Pet Sci Technol 28 (2010) 103–111. https://doi.org/10.1080/10916460903066205.
- [621] A.P. Vavlitis, D.M. Ruthven, K.F. Loughlin, Sorption of N-pentane, N-octane, and N-decane in 5A zeolite crystals, J Colloid Interface Sci 84 (1981) 526–531. <a href="https://doi.org/10.1016/0021-9797(81)90242-3">https://doi.org/10.1016/0021-9797(81)90242-3</a>.
- [622] K.G. Wynnyk, B. Hojjati, R.A. Marriott, High-Pressure Sour Gas and Water Adsorption on Zeolite 13X, Ind Eng Chem Res (2018) acs.iecr.8b03317. https://doi.org/10.1021/acs.iecr.8b03317.
- [623] M.A. Garazi, P.M. Haure, D.E. Resasco, n-Hexane sorption in pelletized 5A zeolite, Industrial & Engineering Chemistry Process Design and Development 25 (1986) 290–293. https://doi.org/10.1021/i200032a047.
- [624] O. Golubyatnikov, E. Akulinin, Application of the Dubinin–Radushkevich–Astakhov equation to calculate gases isotherms on zeolite adsorbents (on example of H<sub>2</sub>, CO<sub>2</sub>, CO, CH<sub>4</sub>, N<sub>2</sub> adsorption on 13X and 5A), Sep Sci Technol 57 (2022) 2871–2884. <a href="https://doi.org/10.1080/01496395.2022.2084108">https://doi.org/10.1080/01496395.2022.2084108</a>.
- [625] C.A. Grande, C. Gigola, A.E. Rodrigues, Adsorption of Propane and Propylene in Pellets and Crystals of 5A Zeolite, Ind Eng Chem Res 41 (2002) 85–92. https://doi.org/10.1021/ie010494o.
- [626] A. Kondor, A. Dallos, Adsorption isotherms of some alkyl aromatic hydrocarbons and surface energies on partially dealuminated Y faujasite zeolite by inverse gas chromatography, J Chromatogr A 1362 (2014) 250–261. https://doi.org/10.1016/j.chroma.2014.08.047.
- [627] F.A. Da Silva, A.E. Rodrigues, Adsorption Equilibria and Kinetics for Propylene and Propane over 13X and 4A Zeolite Pellets, Ind Eng Chem Res 38 (1999) 2051–2057. <a href="https://doi.org/10.1021/ie980640z">https://doi.org/10.1021/ie980640z</a>.
- [628] L. Song, Z. Sun, L. Duan, J. Gui, G.S. McDougall, Adsorption and diffusion properties of hydrocarbons in zeolites, Microporous and Mesoporous Materials 104 (2007) 115–128. https://doi.org/10.1016/j.micromeso.2007.01.015.
- [629] P.S. Bárcia, J.A.C. Silva, A.E. Rodrigues, Adsorption equilibrium and kinetics of branched hexane isomers in pellets of BETA zeolite, Microporous and Mesoporous Materials 79 (2005) 145–163. https://doi.org/10.1016/j.micromeso.2004.10.037.
- [630] K. Chung, D. Park, K.-M. Kim, C.-H. Lee, Adsorption equilibria and kinetics of ethane and ethylene on zeolite 13X pellets, Microporous and Mesoporous Materials 343 (2022) 112199. https://doi.org/10.1016/j.micromeso.2022.112199.
- [631] I.H. Doetsch, D.M. Ruthven, K.F. Loughlin, Sorption and Diffusion of n-Heptane in 5A Zeolite, Can J Chem 52 (1974) 2717–2724. <a href="https://doi.org/10.1139/v74-396">https://doi.org/10.1139/v74-396</a>.
- [632] C.A. Grande, C. Gigola, A.E. Rodrigues, Propane–Propylene Binary Adsorption on Zeolite 4A, Adsorption 9 (2003) 321–329. https://doi.org/10.1023/A:1026223914143.
- [633] J.-J. Kim, S.-J. Lim, H. Ahn, C.-H. Lee, Adsorption equilibria and kinetics of propane and propylene on zeolite 13X pellets, Microporous and Mesoporous Materials 274 (2019) 286–298. <a href="https://doi.org/10.1016/j.micromeso.2018.07.039">https://doi.org/10.1016/j.micromeso.2018.07.039</a>.
- [634] M. Mofarahi, A. Bakhtyari, Experimental Investigation and Thermodynamic Modeling of CH<sub>4</sub>/N<sub>2</sub> Adsorption on Zeolite 13X, J Chem Eng Data 60 (2015) 683–696. https://doi.org/10.1021/je5008235.
- [635] F. Gholipour, M. Mofarahi, Adsorption equilibrium of methane and carbon dioxide on zeolite 13X: Experimental and thermodynamic modeling, J Supercrit Fluids 111 (2016) 47–54. https://doi.org/10.1016/j.supflu.2016.01.008.
- [636] D.M. Ruthven, R.I. Derrah, Sorption in Davison 5A molecular sieves, Can J Chem Eng 50 (1972) 743–747. https://doi.org/10.1002/cjce.5450500611.
- [637] J.A.C. Silva, A.E. Rodrigues, Fixed-Bed Adsorption of n-Pentane/Isopentane Mixtures in Pellets of 5A Zeolite, Ind Eng Chem Res 36 (1997) 3769–3777. <a href="https://doi.org/10.1021/ie9701581">https://doi.org/10.1021/ie9701581</a>.

- [638] G.R. Youngquist, J.L. Allen, J. Eisenberg, Adsorption of Hydrocarbons by Synthetic Zeolites, Product R&D 10 (1971) 308–314. https://doi.org/10.1021/i360039a011.
- [639] T.A. Al-Sahhaf, E.D. Sloan, A.L. Hines, Application of the modified potential theory to the adsorption of hydrocarbon vapors on silica gel, Industrial & Engineering Chemistry Process Design and Development 20 (1981) 658–662. <a href="https://doi.org/10.1021/i200015a013">https://doi.org/10.1021/i200015a013</a>.
- [640] P.E. Eberly, Kinetics of n-butane adsorption on various particle sizes of silica gel by gas-solid chromatography, Journal of Applied Chemistry 14 (1964) 330–337. <a href="https://doi.org/10.1002/jctb.5010140804">https://doi.org/10.1002/jctb.5010140804</a>.
- [641] M.-G. Olivier, R. Jadot, Adsorption of Light Hydrocarbons and Carbon Dioxide on Silica Gel, J Chem Eng Data 42 (1997) 230–233. <a href="https://doi.org/10.1021/je960200j">https://doi.org/10.1021/je960200j</a>.
- [642] K.G. Wynnyk, B. Hojjati, R.A. Marriott, Sour Gas and Water Adsorption on Common High-Pressure Desiccant Materials: Zeolite 3A, Zeolite 4A, and Silica Gel, J Chem Eng Data 64 (2019) 3156–3163. https://doi.org/10.1021/acs.jced.9b00233.
- [643] A.R. Paniego, J.M. Guil, Adsorption of paraffins on a silica gel correlation of equilibrium data, J Colloid Interface Sci 57 (1976) 166–174. https://doi.org/10.1016/0021-9797(76)90186-7.
- [644] W.K. Lewis, E.R. Gilliland, B. Chertow, W.P. Cadogan, Pure Gas Isotherms, Ind Eng Chem 42 (1950) 1326–1332. <a href="https://doi.org/10.1021/ie50487a023">https://doi.org/10.1021/ie50487a023</a>.
- [645] M.A. Hernández, J.A. Velasco, M. Asomoza, S. Solís, F. Rojas, V.H. Lara, Adsorption of Benzene, Toluene, and p-Xylene on Microporous SiO<sub>2</sub>, Ind Eng Chem Res 43 (2004) 1779–1787. https://doi.org/10.1021/ie0204888.
- [646] A. V. Kislev, Y.S. Nikitin, R.S. Petrova, K.D. Shcherbakova, Y.I. Yashin, Effect of Pore Size of Silica Gels on the Separation of Hydrocarbons., Anal Chem 36 (1964) 1526–1533. https://doi.org/10.1021/ac60214a027.
- [647] P. Goyal, M.J. Purdue, S. Farooq, Adsorption and Diffusion of N<sub>2</sub> and CO<sub>2</sub> and Their Mixture on Silica Gel, Ind Eng Chem Res 58 (2019) 19611–19622. <a href="https://doi.org/10.1021/acs.iecr.9b02685">https://doi.org/10.1021/acs.iecr.9b02685</a>.
- [648] C.A. Grande, A.E. Rodrigues, Adsorption Equilibria and Kinetics of Propane and Propylene in Silica Gel, Ind Eng Chem Res 40 (2001) 1686–1693. <a href="https://doi.org/10.1021/ie000901g">https://doi.org/10.1021/ie000901g</a>.
- [649] J. Shen, J.M. Smith, Adsorption Isotherms for Benzene-Hexane Mixtures, Industrial & Engineering Chemistry Fundamentals 7 (1968) 100–105. https://doi.org/10.1021/i160025a018.
- [650] S.Z. Qiao, S.K. Bhatia, D. Nicholson, Study of Hexane Adsorption in Nanoporous MCM-41 Silica, Langmuir 20 (2004) 389–395. https://doi.org/10.1021/la0353430.
- [651] D. Kunii, Levenspiel Octave, Chapter 3 Fluidization and Mapping of Regimes, in: Fluidization Engineering, 2nd ed., Butterworth-Heinemann, Elsevier, Newton (MA), 1991: pp. 61–94. https://doi.org/10.1016/B978-0-08-050664-7.50009-3.
- [652] C.W. Skarstrom, Method and apparatus for fractionating gaseous mixtures by adsorption, US2944627A, 1960. <a href="https://patents.google.com/patent/US2944627A/en">https://patents.google.com/patent/US2944627A/en</a> (accessed December 28, 2024).
- [653] J. Huang, B. Zhang, W. Huang, Z. Zhu, F. Tao, Q. Wang, Z. Huang, J. Zhu, X. Zhang, L. Zhang, Research on the general technical standards of the gasoline vapor recovery unit set, E3S Web of Conferences 118 (2019) 02017. https://doi.org/10.1051/e3sconf/201911802017.

Borsa di dottorato del Programma Operativo Nazionale Ricerca e Innovazione 2014-2020 (CCI 2014IT16M2OP005), risorse FSE REACT-EU, Azione IV.4 "Dottorati e contratti di ricerca su tematiche dell'innovazione" e Azione IV.5 "Dottorati su tematiche Green." CUP: J35F21003150006